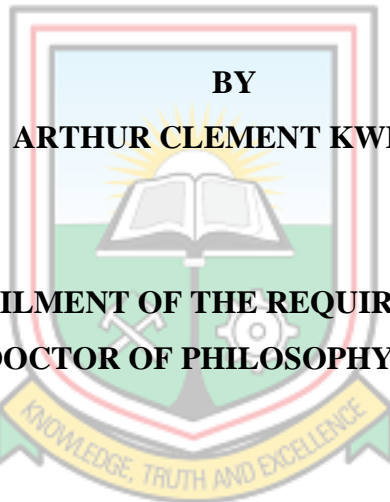# UNIVERSITY OF MINES AND TECHNOLOGY (UMaT), TARKWA

FACULTY OF MINERAL RESOURCES TECHNOLOGY
DEPARTMENT OF MINING ENGINEERING

A PhD THESIS ENTITLED

BLAST-INDUCED GROUND VIBRATION AND AIR OVERPRESSURE PREDICTION USING ARTIFICIAL INTELLIGENCE TECHNIQUES

BY

ARTHUR CLEMENT KWEKU

SUBMITTED IN FULFILMENT OF THE REQUIREMENT FOR THE AWARD OF THE DEGREE OF DOCTOR OF PHILOSOPHY IN MINING ENGINEERING

THESIS SUPERVISORS

ASSOC PROF VICTOR AMOAKO TEMENG

&

DR YAO YEVENYO ZIGGAH

TARKWA, GHANA

MAY 2019

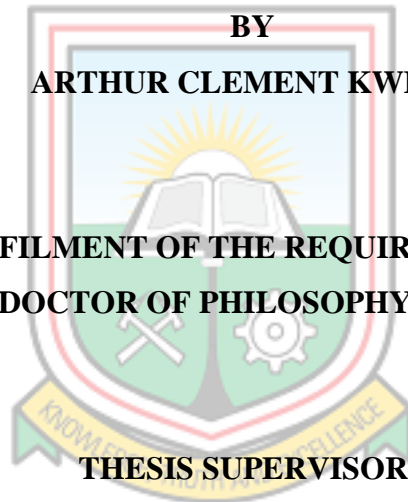# UNIVERSITY OF MINES AND TECHNOLOGY (UMaT), TARKWA

FACULTY OF MINERAL RESOURCES TECHNOLOGY
DEPARTMENT OF MINING ENGINEERING

A PhD THESIS ENTITLED

BLAST-INDUCED GROUND VIBRATION AND AIR OVERPRESSURE PREDICTION USING ARTIFICIAL INTELLIGENCE TECHNIQUES

BY
ARTHUR CLEMENT KWEKU

SUBMITTED IN FULFILMENT OF THE REQUIREMENT FOR THE AWARD OF THE DEGREE OF DOCTOR OF PHILOSOPHY IN MINING ENGINEERING

THESIS SUPERVISORS

…………………………………………………..

ASSOC PROF VICTOR AMOAKO TEMENG
&

………………………………………………......

DR YAO YEVENYO ZIGGAH

TARKWA, GHANA
MAY 2019

DECLARATION

I declare that this thesis is my own work. It is being submitted for the degree of Doctor of Philosophy in Mining Engineering in the University of Mines and Technology (UMaT), Tarkwa. It has not been submitted for any degree or examination in any other University.

…………………………………………

(Signature of candidate)

………. day of …………...……………………… (year) ……………

ABSTRACT

Blast-induced ground vibration and air overpressure are considered as the most important environmental hazards of mining and can damage structures such as buildings, dams and pit slopes. Review of previous studies has shown that some empirical and Artificial Intelligence (AI) models have been proposed to estimate blast-induced ground vibrations and air overpressure. Notable AI techniques applied in prediction of blast-induced ground vibration include Backpropagation Neural Network (BPNN), Radial Basis Function Neural Network (RBFNN), Generalised Regression Neural Network (GRNN), Group Method of Data Handling (GMDH), Support Vector Machine (SVM) and Extreme Learning Machine (ELM). In this study, five techniques, namely Wavelet Neural Network (WNN), Multivariate Adaptive Regression Splines (MARS), Least Square Support Vector Machine (LS-SVM), Relevance Vector Machines (RVM) and Gaussian Process Regression (GPR) are proposed to predict blast-induced ground vibration using 210 blast data sets from Ghana Manganese Company Limited (GMC). Out of the data sets, 130 blast data sets were used to train the models and the remaining 80 to test the developed models. For comparison purpose and ascertaining the suitability of the proposed methods, four empirical techniques (United State Bureau of Mines, Langefors and Kilhstrom, Ambrasey-Hendron and Indian Standard) were also employed. With regards to the air overpressure, BPNN, GMDH, GPR and SVM are the only AI methods applied and captured in the literature. This study therefore tested the capability and applicability of some AI methods, namely RBFNN, GRNN, LS-SVM, RVM, ELM, WNN and MARS, that are yet to be explored in the prediction of air overpressure. To accomplish this task, air overpressure data sets from Newmont Golden Ridge Limited, Akyem Mine was used. In all, 98 data sets were used for the model construction and 73 data sets were used to independently assess the performance of the models formulated. Two empirical predictors, the general predictor model and 'Newmont Model', were utilised for the purpose of comparison. In the blast-induced ground vibration interpretations, the statistical results revealed that, four out of the five newly tested AI techniques (LS-SVM, WNN, MARS and GPR) could produce good ground vibration predictions comparing to the AI benchmark methods of BPNN, RNFNN and GRNN. Hence, LS-SVM, WNN, MARS and GPR have been proposed to be used as suitable alternative tools to predict blast-induced ground vibration. In comparing all methods applied, the proposed LS-SVM was the most accurate on the basis of the statistical analyses carried out

in this study and thus the selected model for predicting blast-induced ground vibration at Ghana Manganese Company Limited. In the air overpressure prediction interpretations, it was found that four out of the seven methods (GRNN, RBFNN, RVM, and MARS) tested produced comparable and satisfactory results as the widely used BPNN, GPR and SVM and thus could serve as suitable alternatives to the prediction of air overpressure. However, it was found on the basis of the statistical analyses carried out that, the BPNN was the selected model for the prediction of air overpressure for Newmont Golden Ridge Limited, Akyem Mine. The overall analyses of the study showed that the AI techniques are superior in predicting both blast-induced ground vibration and air overpressure to the empirical predictors usually employed in most mining and civil engineering industries. To this end, a user-friendly AI-based software package was developed on the MATLAB platform and can be used in the industry for prior prediction of the blast-induced ground vibration and air overpressure based on the blast design in the mining industry.

DEDICATION

I dedicated this work to
the Almighty God, Jesus Christ and the Holy Spirit
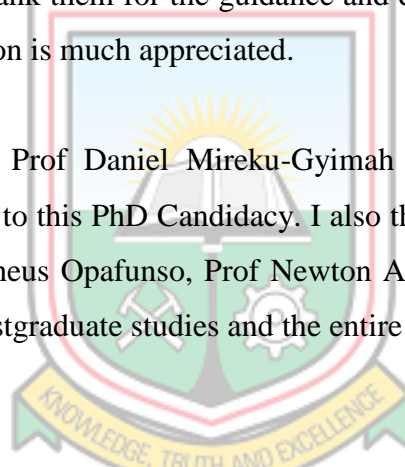*You have done it all.*

ACKNOWLEDGEMENTS

TABLE OF CONTENTS

LIST OF FIGURES

LIST OF TABLES

CHAPTER 1

INTRODUCTION

1.1   Background of Study

In hard rock mines, the in situ rock mass is broken down into fragments by the use of explosives placed into drill holes in a process termed as blasting. When the explosives detonate, the pressure generated shatters the rock near the hole and generates stress waves that travel outside at velocities of 3000 – 5000 m/s. The leading front of the stress which is compressive in nature is closely followed by tensile stresses that are responsible for the rock fragmentation (Bhandari, 1997). According to Elevli and Arpaz (2010), a well-designed blast system will efficiently utilise the explosive energy generated by the detonation of the explosive to result in optimum fragmentation and displacement of rock mass. They however stated that, no matter how well a blast is designed, only a small portion of the energy will be utilised for the fragmentation. That is, only 20 – 30% of explosive energy is utilised for fragmenting the rock and the rest wasted away in the form of ground vibration, air overpressure, noise, fly rock, back breaks, etc. (Rai and Singh, 2004; Mohamed, 2011; Ghasemi *et al*., 2013; Monjezi *et al*., 2010a; Hasanipanah *et al*., 2016a; Hasanipanah *et al*., 2017a; Hasanipanah *et al*., 2017b).

It is agreeable that the safety of workers, environment and surrounding communities of a mine are the primary concerns of the mining industry. Therefore, implementing a ground vibration and air overpressure system to monitor the emitted vibrations and air overpressure due to blasting operations is a rational approach to ensure that they are within safe limits as specified by the mining regulations of a country. This is because ground vibration and air overpressure are among the blasting outcomes that could lead to adverse environmental effects on surrounding structures and humans. With respect to structures, it can result in the creation of cracks and eventually lead to structural damages. With respect to humans, it may be a source of nuisance. In line with that, many research works have been done to develop prediction models to predict ground vibration and air overpressure over the years (Faradonbeh *et al*., 2016; Murmu *et al*., 2018 and Bui *et al*., 2019). The essence is to provide the blast designer *a priori* knowledge of ground vibration levels and air overpressure per blast design before the actual blasting operation is carried out.

1

Review of previous studies have shown that the prediction models range from empirical, statistical through to the use of artificial intelligence in recent years (Armaghani *et al*., 2015a; Sheykhi *et al*., 2018; Murmu *et al*., 2018;). Moreover, the review identified that the artificial intelligence technology is a suitable computational tool for predicting ground vibration and air overpressure. It should be noted that in the Ghanaian mining industries, the empirical models are the most widely used to predict blasting outcomes of ground vibration and air overpressure. In view of that, the study considered two key mining companies namely, Ghana Manganese Company Limited and Newmont Golden Ridge Limited, Akyem in Ghana as study areas, for evaluating the suitability of the artificial intelligence techniques in predicting blast-induced ground vibration and air overpressure respectively.

The Newmont Golden Ridge Limited, Akyem is an open pit mine located in the Birim North District of the Eastern Region of Ghana, the seventh biggest gold producing country in the world. The mine is wholly owned and operated by Newmont Mining Cooperation and commenced production in October 2013. It is Newmont's second mining operation in Ghana after the Ahafo Gold mine in the Brong Ahafo Region. The Akyem mine site covers a total area of 1 903 ha, of which 74 ha is in the Ajenjua Bepo Forest Reserve. Newmont received mining lease for the project in 2010 and developed it with an estimated investment of $ 950 million. Mining activities at the site started in August 2012. Newmont Golden Ridge Limited uses drill and blast to fragment the in situ rock mass (Anon., 2015).

The Akyem mine has three monitoring stations in each of its neighbouring towns namely, Afosu, New Abirem and Aduasena. The Afosu station is the nearest to the East Pit of the mine and hence has the potential of recording occurrences of ground vibration and air overpressure levels beyond the threshold. Newmont uses JKSim Blast software which is based on a form of Ambraseys – Hendron model to predict air overpressure. The Mine has recorded variations in the predicted levels as against the real levels recorded at the station. Hence, the need for accurate prediction of air overpressure in order to control and minimise their occurrences.

Ghana Manganese Company Limited is also an open pit mine located at Nsuta-Wassa, in the Tarkwa Nsuaem Municipality (TNM) of the Western Region of Ghana. The Mine is

about 304 km by road from Accra and about 63 km by road from the regional capital, Takoradi. The mine employs drill and blast techniques to fragment the in situ rock mass.

Since ground vibration and air overpressure are adverse impacts of blasting outcomes on the neighbouring mining communities, the two understudied mines are keen on accurately predicting these levels in order to control and minimise their impact on the environment.

1.2   Statement of Problem

Blast-induced ground vibration and air overpressure are the most important and undesirable environmental impacts of blasting outcomes which may cause severe damage to nearby residents and structures. Modelling and prediction of such outcomes is important for controlling and eliminating associated environmental problems (Ghasemi *et al*., 2013 and Armaghani *et al.,* 2015a). According to Ghasemi *et al.* (2013), different indicators have been proposed to measure and evaluate ground vibration. Among these indicators are the peak particle velocity (PPV) and peak particle displacement (PPD). The PPV has been used frequently in different standards and has been found to be a reliable indicator for the evaluation and prediction of ground vibration.

Over the years, many studies have been carried out leading to the development of empirical models for the prediction of ground vibration (Duvall and Petkof, 1959, Langefors and Kihlstrom, 1963; Davies *et al.*, 1964; Ambraseys and Hendron, 1968; Ghosh and Daemen, 1983; Gupta *et al*., 1987; Roy, 1991; Rai and Singh, 2004). With respect to air overpressure, several empirical equations have also been used for prediction (Holmberg and Person, 1979; NAASRA, 1983; Olofsson, 1990; Persson *et al*., 1994). It is important to note that these empirical predictor models are basically based on two parameters, maximum charge per delay and distance from blast site to monitoring point, excluding other effective parameters (Ghasemi *et al.*, 2013). This makes them fully not suitable to predict ground vibration and air overpressure since a large number of parameters influence the level of vibration or air overpressure with these parameters being complexly interrelated.

In order to address these weaknesses of the empirical models, many researchers over recent years have tried to develop new models based on artificial intelligence techniques. The notable techniques captured in literature include: artificial neural networks (ANN), fuzzy

logic, adaptive neuro-fuzzy inference systems (ANFIS), classification and regression tree (CART) support vector machine (SVM), extreme learning machines (ELM), hybrid intelligent models, group method of data handling (GMDH) and genetic expression programming (GEP) (Akeil, 2004; Iphar *et al*., 2008; Khandelwal *et al*., 2011; Mohamed, 2011; Khandelwal, 2011; Fişne *et al*., 2011; Mohamadnejad *et al*., 2012; Mohamad *et al*., 2012; Ghasemi *et al*., 2013; Monjezi *et al*., 2013; Armaghani *et al.,* 2015a; Dindarloo, 2015; Tiile, 2016; Ghoraba *et al*., 2016; Hasanipanah *et al*., 2016b; Taheri *et al*., 2017; Hasanipanah *et al*., 2017c; Mokfi *et al*., 2018; Jiang *et al*., 2018; Mojtahedi *et al*., 2019). Information gathered from these studies indicate that artificial intelligence techniques are able to predict PPV and air overpressure at higher level of accuracy as compared to empirical and statistical techniques (Armaghani *et al.,* 2015a; Ghoraba *et al*., 2016; Tiile 2016).

There are however a number of artificial intelligence techniques which are yet to be explored in predicting blast-induced ground vibration and air overpressure. This thesis therefore seeks to introduce new artificial intelligence modelling tools for predicting blast-induced ground vibration and air overpressure in the Ghanaian mining industry.

1.3   Research Questions

The research sought to answer the following questions:
  i.   Can the proposed novel artificial intelligence models be used as a supplementary tool for predicting ground vibration and air overpressure?
  ii.   How do the proposed artificial intelligence methods compare to the popularly used empirical models?

1.4   Objectives of the Thesis

The objectives of this research are to:
  i.   propose novel artificial intelligence models for both blast-induced ground vibration and air overpressure prediction;
  ii.   develop empirical models for both blast-induced ground vibration and air overpressure prediction for comparison;
  iii. select an appropriate model for blast-induced ground vibration and air overpressure prediction in the study areas; and

iv.   develop a blast-induced ground vibration and air overpressure artificial intelligence-based software.

1.5   Methods Used

The following methods were used for the research:

i.   Review of relevant literature on blast-induced ground vibration and air overpressure

ii.   Field visits to Ghana Manganese Company Limited and the Newmont, Akyem Mine for data collection;

iii.   Development of the artificial intelligence models for both blast-induced ground vibration and air overpressure prediction using MATLAB program;

iv.   Development of the empirical models for both blast-induced ground vibration and air overpressure prediction using regression analysis; and

v.   Comparative analysis of the prediction results from the various models using various Statistical Performance Indicators.

1.6   Contribution to Knowledge/Science

The following contributions have been made to knowledge/science:

i.   This study has developed five novel artificial intelligence techniques for predicting blast-induced ground vibration. However, four out of these five techniques were capable of producing accurate predictions and hence have been proposed for predicting blast-induced ground vibration. The proposed methods include: Least Square Support Vector Machines (LSSVM), Wavelet Neural Network (WNN), Multivariate Adaptive Regression Splines (MARS), and Gaussian Process Regression (GPR).

ii.   This study has developed seven novel artificial intelligence techniques for predicting air overpressure. However, four out of these seven techniques were capable of producing accurate predictions and hence have been proposed for predicting air overpressure. The proposed approaches are Generalised Regression Neural Network (GRNN), Radial Basis Function Neural Network (RBFNN), Relevance Vector Machines (RVM) and Multivariate Adaptive Regression Splines (MARS).

iii. The study has introduced the application of artificial intelligence techniques in the prediction of ground vibration and air overpressure in some Ghanaian mines.

iv. The study has developed a ground vibration and air overpressure artificial intelligence-based software for Ghana Manganese Company Limited and Newmont Golden Ridge Limited, Akyem Mine operations.

1.7 Organisation of Thesis

This thesis is organised into seven chapters. Chapter 1 contains the general introduction to the research. In Chapter 2, relevant information about the study areas is presented. Chapter 3 contains relevant literature about the research topic. Chapter 4 is on materials and methods; In this chapter, the data collected for the thesis are presented, the various press models are developed using the data collected, ground vibration and air overpressure are predicted using the various models and the model performance are compared. Chapter 5 contains the results and discussion on ground vibration prediction analysis. Chapter 6 also contains results and discussions on air overpressure prediction analysis. This thesis then concludes with Chapter 7, being on conclusions and recommendations.
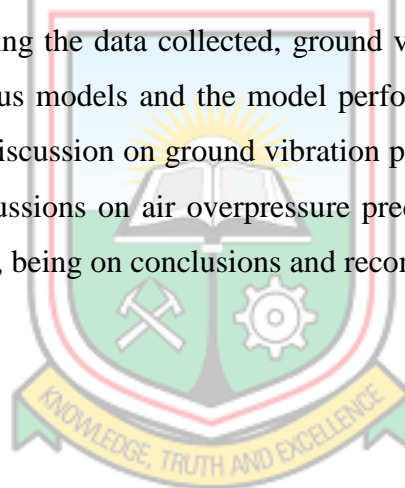
CHAPTER 2

RELEVANT INFORMATION ABOUT THE STUDY AREAS

2.1   Introduction

This study was carried out at Ghana Manganese Company Limited (GMC), Nsuta and Newmont Golden Ridge Limited (NGRL), Akyem Mine and hence this Chapter gives relevant information of these mines, which includes: brief history, the locations, accessibility of the mines, geology, mineralogy of the ore deposits, production operations, mineral processing and environmental issues.

2.2   Brief Information about Ghana Manganese Company Limited

2.2.1   History and Ownership of Ghana Manganese Company Limited

In 1914, the manganese deposits of Nsuta were discovered by Sir Albert Ernest Kitson during the construction of the Western Rail Line. The Fanti Consolidated Mines Limited, the concessionaire, formed the Wassaw Exploration Syndicate and started mining operations in 1916. The African Manganese Company Limited, a subsidiary of Union Carbide Corporation, USA, was established in 1923 to operate the mine (Kamara, 2014).

In the early seventies, negotiations took place between the Government of Ghana and Union Carbide on the possibility of acquisition. In 1973, all assets and liabilities of the company were taken over by the Government of Ghana. The Ghana National Manganese Corporation (GNMC) was founded, which assumed responsibility for the running of the mine and sales of manganese ore on behalf of the Ghana Government for 22 years (Appianing, 2013).

In line with the general policy of national economic recovery and privatisation of state owned enterprises, Ghana International Manganese Corporation (GIMC) acquired the mine in November, 1995 and Ghana Manganese Limited (GMC) was established to run the mine from 1996 to present (Apalangya, 2014).

2.2.2 The Location and Accessibility of Ghana Manganese Company Limited

The Mine is located in Nsuta, in the Wassaw West Municipal Assembly of the Western Region of Ghana and is situated on latitude 5° 16″ North and longitude 1° 59″ West in the south-western Ghana. It is located about 89 km northwest from the port of Takoradi and about 6.5 km south from Tarkwa (Appianing, 2013). Figure 2.1 shows the location of Ghana Manganese Company Limited, the study area on the map of Ghana.
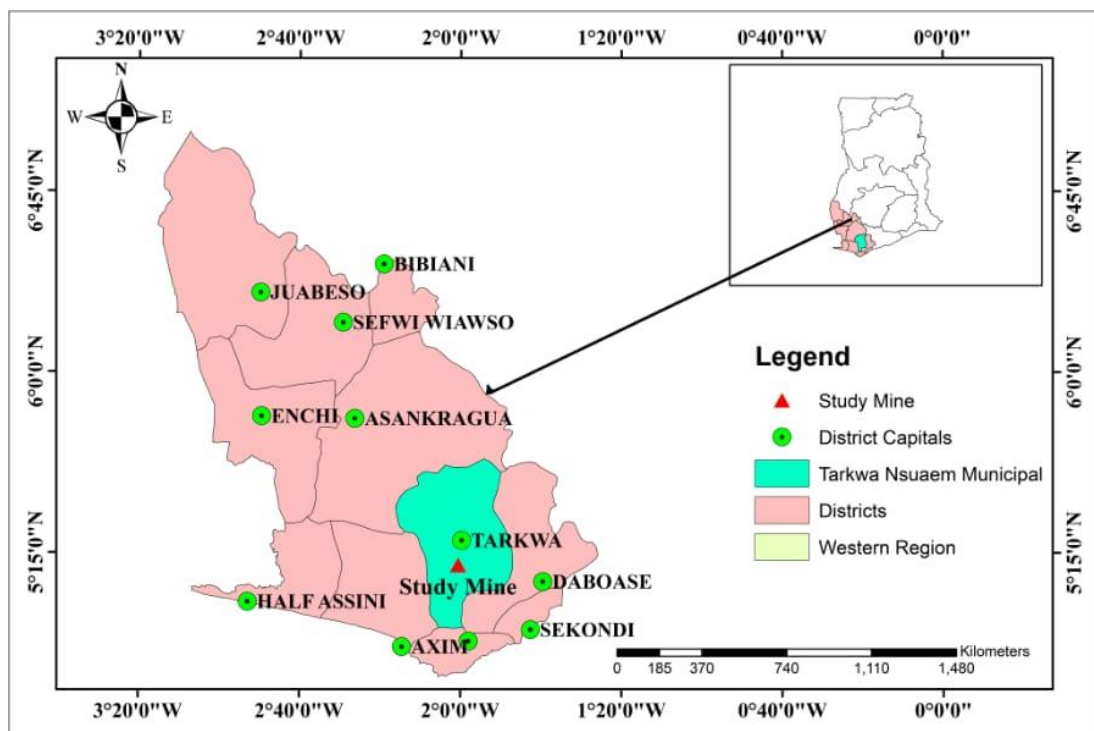
Figure 2.1 Location of Study Mine on the Map of Ghana

2.2.3 Climate of Ghana Manganese Company Limited

The Mine site lies in the tropical humid rainforest zone in the Western Region. According to a study made by Amegbey *et al*. (2016) on the rainfall pattern from January 2009 to December 2013 on the Mine site, the rainfall pattern averaged 117.3 mm per month indicating a high rainfall zone.

According to Amegbey *et al*. (2016), there are two main rainfall seasons on the mine site; the period May to July with rainfall values ranging from 179.2 mm to 195.9 mm and the period September to December with rainfall values ranging from 141.8 mm to 179.9 mm.

However, the maximum rainfall of 296.5 mm was recorded in June, followed by 195.9 mm in July and 210.7 mm in October respectively.

The dry seasons on the mine site were noted in December and January with respective rainfall values 54.3 mm and 62.97 mm followed by August and February with rainfall values of 78.9 mm and 80.3 mm respectively (Amegbey et al., 2016). Temperature varies between 18 ºC during cold nights and 35 ºC on hot days.

2.2.4   Geological Setting of Ghana Manganese Company Limited

According to Nyame (2011), the Nsuta manganese deposit occurs in Palaeoproterozoic Birimian Supergroup at the eastern portion of the West African craton. The manganese deposit occupies five hills designated A, B, C, D and E, which are oriented along two lines with bearing between N15ºE and N20ºE. These hills have been traced for about 4 km and are connected by saddles. Some of the hills are divided into two parts, namely the north and south crest. Hills A, B, C are along the eastern line and are 60 m – 90 m above the surrounding area, whilst Hills D and E form the western line (Appianing, 2013). These hills were formed from the weathering of volcanic tuff and argillite, which contains the manganese horizon, compared to the surrounding mass of greenstone (Kamara, 2014).

2.2.5   Geology of Ghana Manganese Company Limited

The manganese at the Nsuta Mine area are part of the belt which includes known manganese and gold mineralisation near the margin of the Tarkwaian geosynclines which are underlain by rocks of complex folded Upper Birimian (Kamara, 2014). Although the system as a whole consists of "green stones", the Nsuta hills consist of a thick series of interbedded green tuffs and thin argillaceous horizon (Apalangya, 2014).

The mine is characterised by three main types of rock formations which are Greenstones, Turbidites (Metatuffs) and the Manganiferous horizon. The greenstones and Meta tuffs are the host rocks whilst the Manganiferous horizon is the ore deposit. The manganese ore comes in different types based on the rate of weathering and alteration. These include: detrital ore, the oxide ore, carbonate-oxide ore (carbox) and the manganese carbonate ore (Appianing, 2013). Figure 2.2 shows the geological map of Ghana Manganese Company

Limited (study area). Stratigraphically, the rocks of the mine have been subdivided into units as shown in Table 2.1.
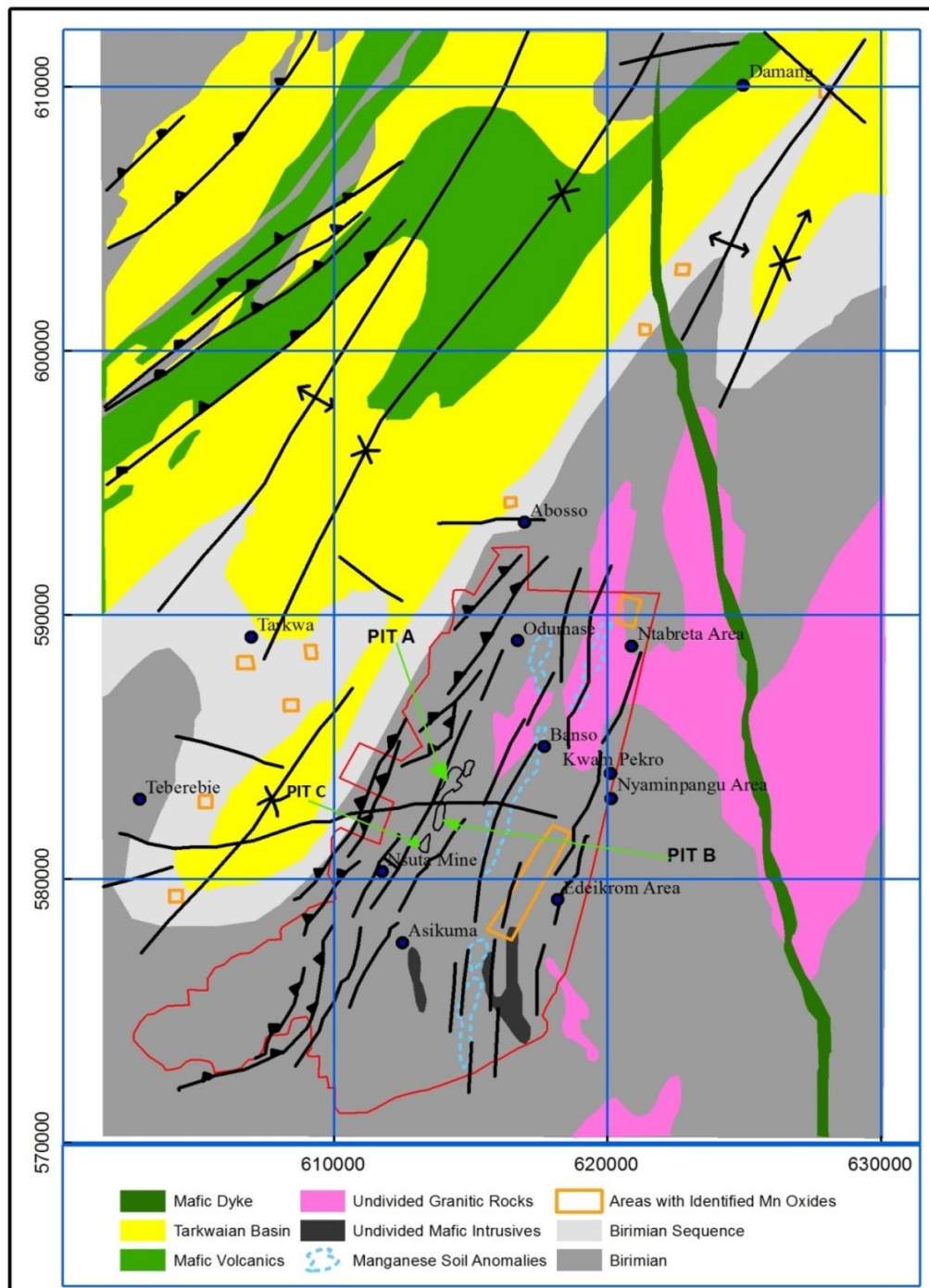
Figure 2.2 Geological Map of the Study Area

Table 2.1 Major Stratigraphic Units of the Mine Area

Age	Unit	Geology	Thickness (m)
Recent	Detrital	Rounded boulder; lateritic clays	Variables
Post Birimian	Intrusive	Metamorphosed gabbros, diorites and granite	Variables
Birimian	Metavolcanic Rocks (Greenstones)	Mafic and intermediate metalavas	460 – 660
	Upper Argillaceous Metatuffs	Bedded sequence of grey lithic sediments, dark grey metatuffs and metalavas	150
	Manganeferous Horizon	Mn-oxide and carbonates	50 – 60
	Lower Argillaceous Metatuffs	Lower sequence of bedded and interlayed lithics sediments, dark grey metatuffs and metalavas	50 – 90
	Basal Lower Greenstones	Metamorphosed volcanic flow rocks	460 – 600

(Source: Appianing, 2013)

The main structure of the deposit is anticlinal with north-northeast (NNE) pitch and an axial plane declined to the east. Both limbs of the anticline dip eastwards and this isoclinal folding is a feature of the Upper Birimian in this area. Beds to the east of Hill D have moderate to steep dips to the east but beds in the western flanks of Hill D dip west (Apalangya, 2014).

2.2.6   Production Operation at Ghana Manganese Company

The mine has three open pits, namely: Pit A; Pit B and Pit C. The Pit C is where active mining is currently going on. The Pit C is subdivided into: C South West (CSW); C South East (CSE); C Central West (CCW); C Central East (CCE); and C North (CN). The major mining operations carried out by GMC are rock fragmentation by conventional drill and blast techniques and followed by loading and hauling of the fragmented rocks. These operations are planned ahead of production to provide the required tonnage at the lowest

cost. The consolidated manganese carbonate ore is what is currently being mined by GMC. (Kamara, 2014).

Drilling operations

The drilling operation at GMC has been contracted to Rock Sure International. The company currently has nine Sandvik Pantera DP1500i drill rigs on site with seven of them in operation at Pit C. The operational rigs are: Rig 08, Rig 10, Rig 11, Rig 12, Rig 13, Rig 14 and Rig 16. Drilled holes have diameters of 115 mm with average depth of 10 m. The drill pattern adopted by GMC is the staggered pattern (Apalangya, 2014). The drill pattern parameters are shown in Table 2.2.

Table 2.2 Parameters of Drill Pattern

Material	Burden (m)	Spacing (m)	Depth (m)	Sub-drill (m)
Ore	3.5	3.5	10.0	1.0
Waste (Hard)	3.5	3.5	10.0	1.0
Waste (Semi-hard)	3.5	3.5	10.0	1.0

(Source: Apalangya, 2014)

The Planning Department provides the layout while the Survey Department marks the patterns on the ground. The depth of each drill hole is written on a cardboard and placed near the hole. The orange reflective cones are placed around the drilling area to prevent vehicles moving on the marked area. Sacks are placed on the collar of each hole to pluck the holes to prevent loose materials or rock fragments to enter and block the holes after they have been drilled. During drilling, the holes depths are measured by off-setters with measuring tapes having weights tied to their bottom to make sure the drill holes are drilled to the required depths (Apalangya, 2014).

Blasting operations

GMC conducts its own blasting operations with Maxam International supplying explosives and accessories. Before the charging process begins, the depths of the drill holes are measured by the blasting crew to ascertain the correct depth of the holes. Over drilled holes

are backfilled while short or blocked holes re-drilled to the right depths. Priming is done using a 250 g Pentolite booster and a 500 ms down the hole and either a 25 ms or 42 ms DDX non-electronic (NONEL) detonator for firing. The bulk explosives used for the column charge is the Emulsion EX 7000. A 3 m stemming height is applied at GMC with stemming material of 15 mm blended with 20 mm to ensure effective confinement. The NONEL MS firing method is used at GMC. The surface connectors used for the trunk line connections include 17 ms, 42 ms and 67 ms (Apalangya, 2014).

Load and haul operations

The mine practices selective mining in its ore extraction. Blasted ore above plant feed cut-off grade is delineated on plan by the Geology Department as ore and marked out by surveyors in pit for mining. The load and haul operations of the mine have been contracted to Rocksure International and African Mining Services (AMS). The O & K excavators (RH30s, RH40s and RH90s) are used to load the ore into Volvo AD35, Komatsu HD 465 and CAT 777F rear dump trucks. The O & K RH90 excavators are matched with CAT 777F trucks, the O & K RH40 excavators are matched with Komatsu HD 465 trucks while the O & K RH30 excavators are matched with Volvo AD35 trucks. An average of 4 to 5 passes of the excavator bucket fills the trucks. Loaded materials are then hauled either to the crusher or the waste dump (Apalangya, 2014).

2.2.7   Mineral Processing at Ghana Manganese Company Limited

Manganese carbonate ore, which is the main product produced by GMC, is processed by crushing to aggregates of 100 mm, 40 mm and 20 mm, which are designated as lumps, logs and fines respectively. The plant has a crushing capacity of 300 metric tons per hour. The finished product from the plant is stockpiled and further conveyed to the port in Takoradi from where it is shipped overseas (Apalangya, 2014).

2.2.8   Environmental Issues at Ghana Manganese Company Limited

Over the years GMC has put in prudent measures to meet the environmental requirements and regulations of Ghana. The Management of GMC has adopted an environmental policy statement to clearly demonstrate the company's commitment to environmental protection

and enlightened operational practice. Nevertheless, mining has impact on the environment in terms of air pollution, noise, ground vibration and air overpressure etc. The environmental policy has been adopted to minimise these environmental impact issues.

Air pollution

According to Apalangya (2014), the predominant air pollutants produced by GMC operation is dust emitted from loading and hauling, blasting, drilling, vehicular motion and crushing operations. Dust monitoring is carried out in certain areas of the mine and other neighbouring communities to the mine. The mitigating techniques employed by Management to minimise the production of dust are by:

i.   The use of water bowsers to suppress dust generated by haulage trucks and other vehicles along the haul roads;

ii.   The installation of dust collectors on drill rigs and where necessary, the use of water mixed with mud;

iii. The processing plant is fitted with water sprinkling systems to suppress dust emanating from crushing; and

iv.   Monitoring of dust emission using dust emission equipment.

Noise

The main sources of noise are from the mining and processing operations. The sources of noise in the mining operations are from drilling, blasting, loading and hauling and vehicular motions. To mitigate the effects, drill rigs are fitted with silencers, where applicable, and drilling in pits during the night close to the communities is avoided. The processing plant is fitted with rubber rollers to reduce noise. Also, personnel in working areas where there is noise, are mandated to put on ear plucks (Apalangya, 2014).

Ground vibration and air overpressure

Blast-induced ground vibration and air overpressure are environment impacts and can cause damages to buildings and other man-made structures and can be a nuisance to people. blast-induced ground vibration and air overpressure are monitored using 3000 EZ Plus portable seismograph as shown in Figure 2.3. If the monitored levels go beyond regulatory standard

of 2 mm/s for blast-induced ground vibration and 117 dB for air overpressure, measures are quickly taken to address the situation. This is done by conducting an investigation to ascertain the possible causes of these high levels so as to prevent future occurrences. The blast-induced ground vibration is constantly being monitored to enable further redesign of drilling parameters that will give maximum cost benefit (Apalangya, 2014).

Figure 2.3 A 300 EZ Plus Portable Seismograph

2.3 Brief Information about Newmont Golden Ridge Limited

2.3.1 History and Ownership of Newmont Golden Ridge Limited

The Newmont Golden Ridge Limited (NGRL), Akyem is an open pit mine located in the Birim North District of the Eastern Region of Ghana, the seventh biggest gold producing country in the world (Gupta, 2013). The mine is wholly owned and operated by Newmont Mining Cooperation and commenced production in October 2013. It is Newmont's second mining operation in Ghana after the Ahafo Gold mine in the Brong Ahafo Region. Newmont received mining lease for the project in 2010 and developed it with an estimated investment of $ 950 million. Mining activities at the site started in August 2012. The mine employs 1 300 workers and contractors drawn mostly from the communities within the mining area. The estimated mine life of the Akyem open pit is 16 years (Arthur, 2015).

2.3.2   The Location and Accessibility of Newmont Golden Ridge Limited

The mine is located approximately 3 kilometres west of the district capital New Abirem, 133 kilometres west of Koforidua the regional capital, and 180 kilometres northwest of Accra (Kaba, 2013).

It is also accessed by the main Accra-Kumasi highway at Abepotia near Nkawkaw and travelling south via Inter-Regional Road 3 to New Abirem (approximately 40 km) (Arthur, 2015). Figure 2.4 shows the location of NGRL on the map of Ghana.
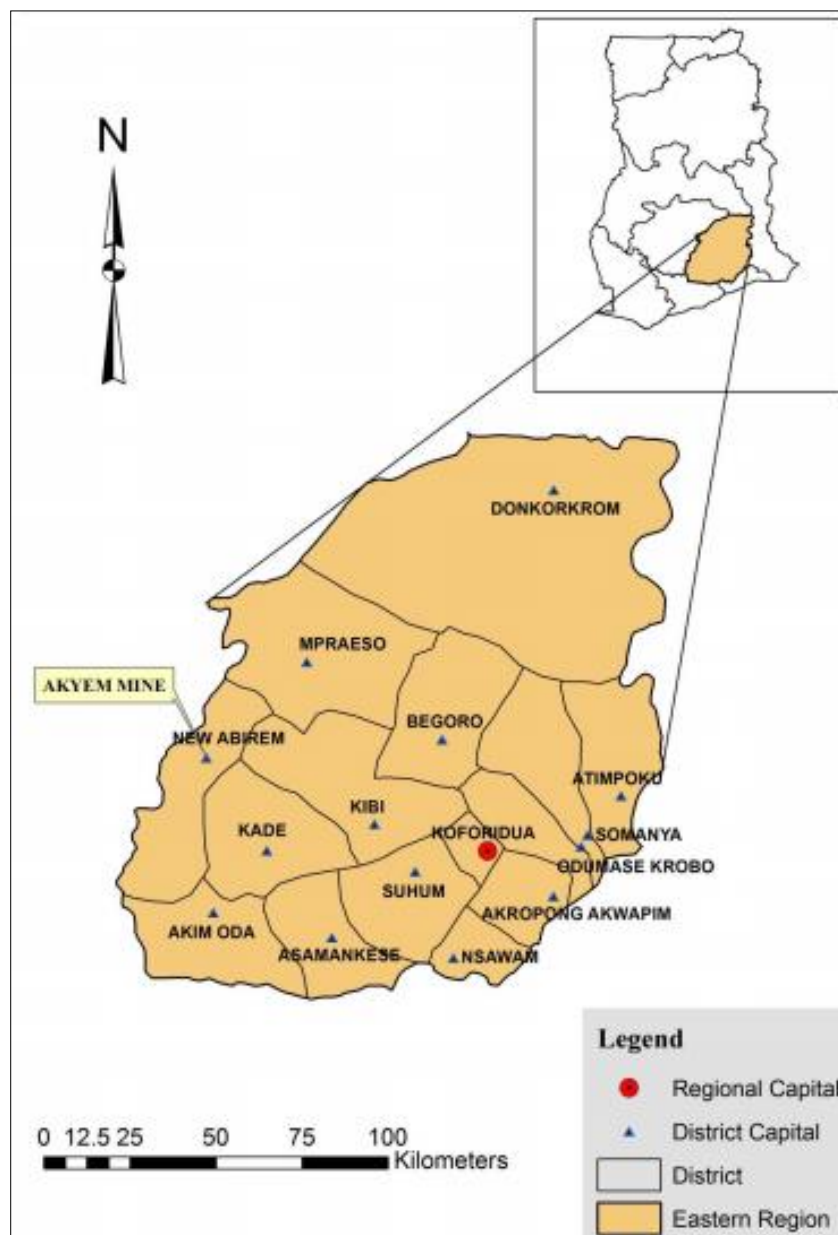
Figure 2.4 Map Showing the Location of NGRL, Akyem Mine (Source: Arthur, 2015)

16

2.3.3   Geological Setting of Newmont Golden Ridge Limited

Northeast trending belts of folded, metamorphosed volcanic and sedimentary rocks of the early Proterozoic underlay the mining area. The southeast side of the mining area is underlain by rocks of the Birimian Supergroup. In this Region, Birimian terrain comprises northeast trending belts of volcanic and volcanoclastic material separated by broad turbidite-dominated sedimentary basins. Tarkwaian sediments consisting of conglomerate, sandstone, and phyllite unconformably overlay Birimian volcanic belts in the north-western portion of the mining area as shown in Figure 2.5.

2.3.4   Mineralisation of Newmont Golden Ridge Limited

The Akyem deposit is developed at the northern end and along the southeast margin of the Ashanti Greenstone Belt. The Ashanti Greenstone Belt is one of five Palaeoproterozoic Birimian tholeiitic to acidic composition volcanic belts in Ghana located in Birimian rocks near the contact of metavolcanic (i.e., mafic volcanic) and overlying metasedimentary (i.e., greywacke) units. A stratigraphic section of the geological units associated with the Akyem deposit is shown on Figure 2.6. The Akyem deposit is localized in the hanging wall of a regional fault trending northeast 70 degrees parallel to regional structures, and dipping 60 degrees to the southeast, parallel to the foliation developed in the Birimian host rock. The fault shows evidence of thrust, strike slip, and normal movement. The planar fault structure displays mylonitic to bracciated texture. Zones of graphitic rubble suggest the fault was likely reactivated over time.

Associated joints around the fault are often filled with quartz veins. The graphite-bearing, mylonitic fault zone ranges from 1 to 15 meters thick. The fault structure defines a sharp base to the mineralisation of the deposit. Ore above the fault ranges from 10 to 100 m in thickness. The deposit is developed over approximately 2 500 m in strike length (along the fault) and the ore has been delineated to a depth of about 400 m down the fault structure (Anon., 2015).
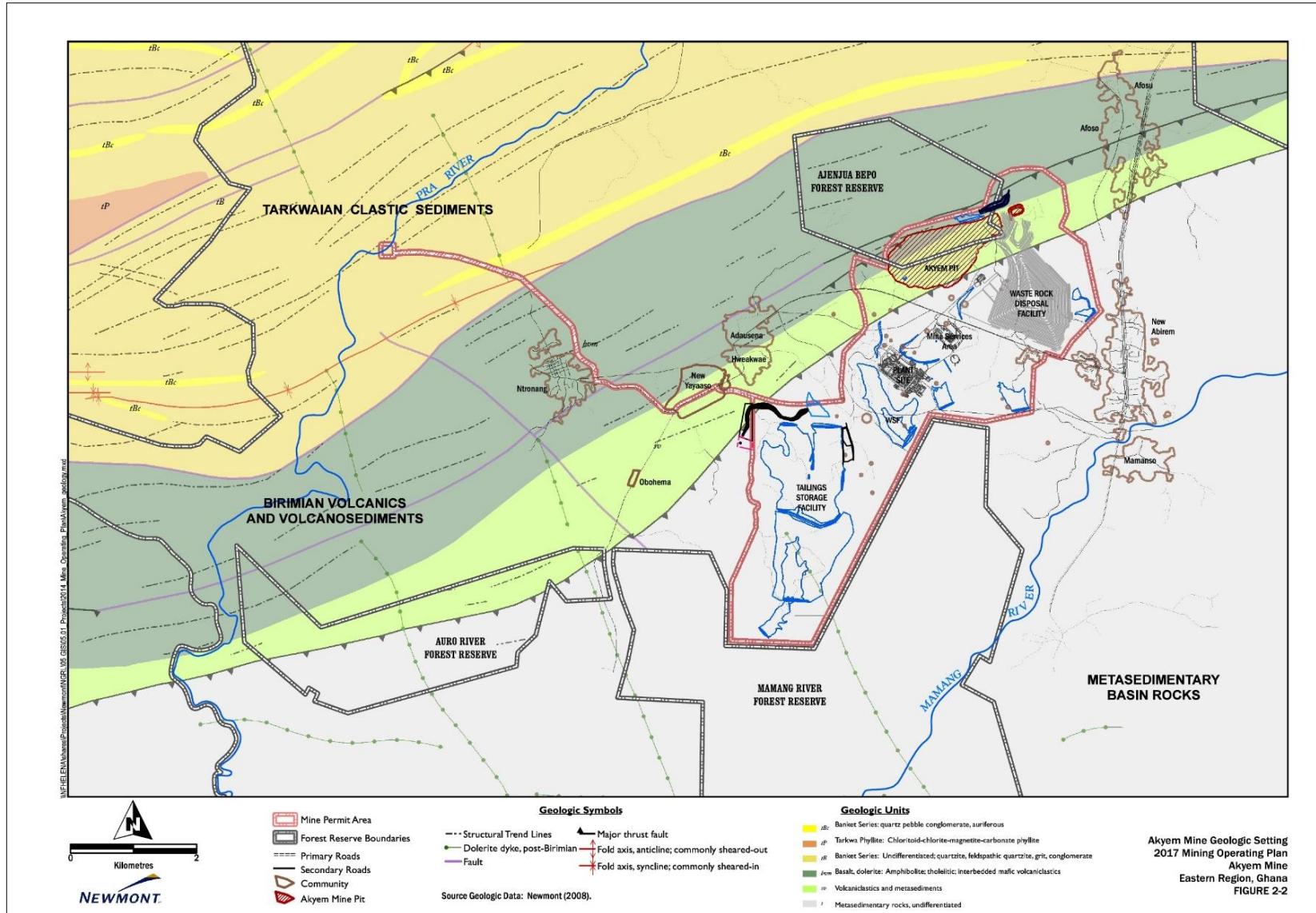
Figure 2.5 Geological Setting of NGRL Akyem Mine

18
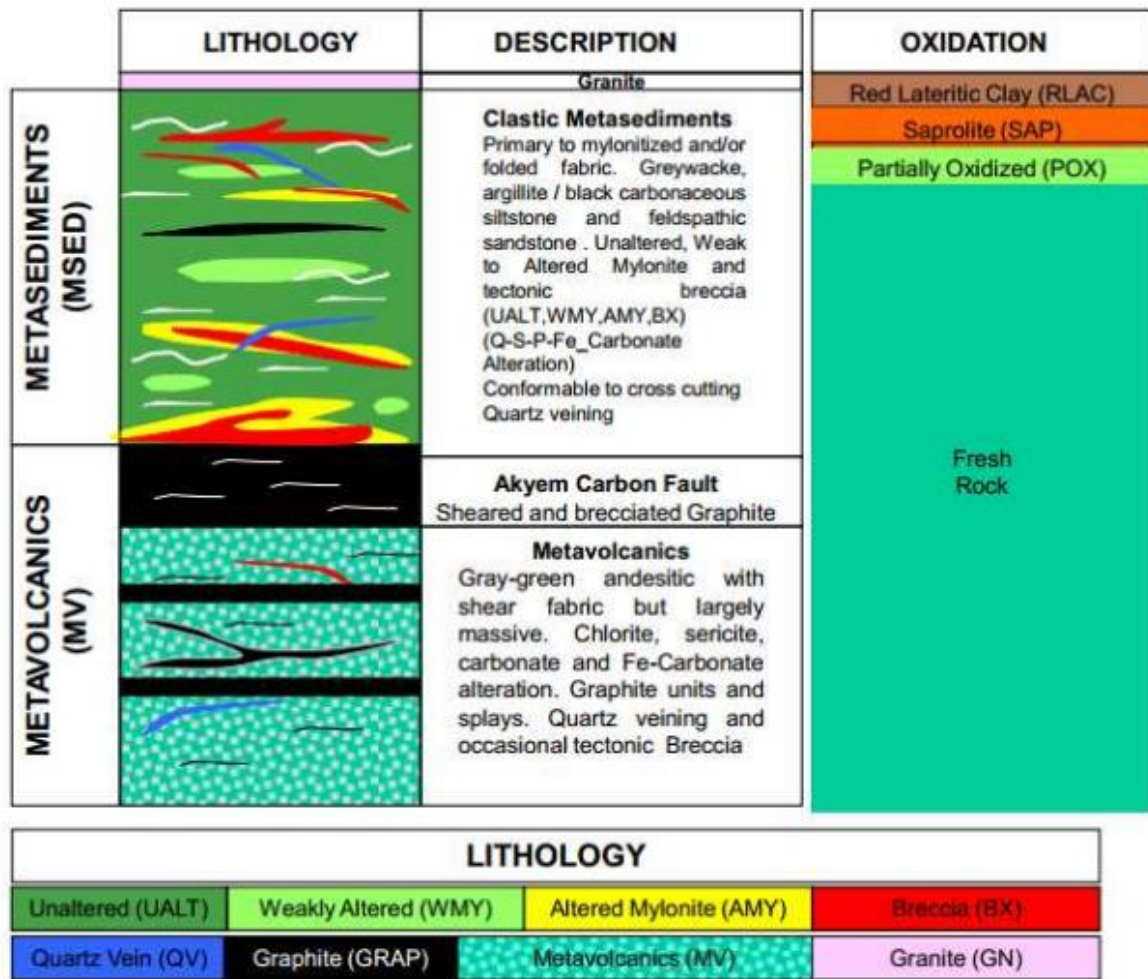
Figure 2.6 A Stratigraphic Section of the Geological Units Associated with the Akyem Deposit (Source: Kaba, 2013)

2.3.5   Production Operations at Newmont Golden Ridge Limited

The mine has two pits, namely: East Pit and the Main Pit. The major mining operations carried out at NGRL are ground fragmentation by conventional drill and blast techniques and loading and hauling of the fragmented rocks. These operations are planned ahead of production to provide the required tonnage at the lowest cost.

Drilling

The Mine has eight (8) Atlas Copco drill rigs, six of which utilise a drill bit diameter of 165 mm for drilling production holes and while the other two (2) utilise a 115 mm diameter drill bit for drilling presplit holes.

The drill pattern employed by NGRL is the staggered drill pattern with burden and spacing in the ore of 4 m × 4 m and 4.5 m × 4.5 m for the waste. The drilled holes are normally of depth of 9 m with sub-drill of 1 m. Prior to drilling, the drill hole pattern is planned and printed out for the drill and blast supervisors whilst the holes data are exported from the 3D Minesight into the Leica jigsaw software to be used by the drill rigs. This is to enable the drill rig operators to navigate and drill the patterns on the working bench without the need of a surveyor to mark out the drill patterns.

Blasting

Blasting of hard rock involves the use of explosives for the disintegration of in situ rocks. The explosives used in blasting are supplied by Orica Mining Service, a contractor of Newmont, Akyem. The main explosive used is emulsion, which is prepared by Orica and supplied to the pit to be discharged into the blast hole by the use of a Mobile Manufacturing Unit (MMU). Other explosives used in blasting include, booster-410 g; surface connectors, shock tube lead in line; 15 m Unitronics (UT 500); 4.2 m × 500 ms in hole detonators; 12 m × 500 ms in hole detonators and harness Wire (UT 600).

Load and haul operations

The mine has four Liebherr 994B excavators of which two are backhoe and two shovels for loading. The mine has nineteen 785 Caterpillar rear dump trucks, each of which has a capacity of 134 tonnes, for hauling waste to the waste dump or ore to the crusher or stockpile.

2.3.6   Mineral Processing at Newmont Golden Ridge Limited

The Akyem gold processing plant has the capacity to treat 8.8 million tonnes of ore a year, including both run-of-mine (ROM) primary ore and oxide ore. The processing facilities at the plant include primary and secondary crushers, a semi- autogenous grinding (SAG) mill, hydrocyclones, a ball mill, leach-feed thickening tanks, a Carbon-in-Leach (CIL) circuit, a cyanide recovery circuit, carbon recovery systems and a refining facility to produce gold (Anon., 2017a).

The essential chemicals and reagents used by the processing facility include: lime; sodium cyanide; caustic; hydrochloric acid; activated carbon; hydrogen peroxide and flocculants. Tailings from the processing plant are transported to the nearby tailings storage facility via an above ground pipe placed in a high-density polythene lined trench (Anon., 2017a).

2.3.7 Environmental Issues at Newmont Golden Ridge Limited

The Management of NGRL has adopted environmental programmes to clearly demonstrate the company's commitment to environmental protection and enlightened operational practice to meet the environment requirements and regulations in Ghana.

Ambient air quality monitoring

Air quality monitoring programme has been instituted by NGRL to ensure compliance with Ghana standards and verify adequacy of mitigation measures in accordance with the Site-Wide Air Quality Monitoring Plan. The programme continues to monitor particulate matter 10 micrometres (PM_{10}), total suspended particle (TSP), nitrogen oxides (NO_x) and sulphur oxides (SO_x) in the mine area and surrounding communities.

The mine continues to operate dust minimisation and collection systems at ore transfer points, conveyor systems, and ore crushing circuits. The mine controls fugitive dust emissions through daily direct water application on the roads in the mine area during dry conditions. It also continues to enforce vehicle speed limits to reduce dust generation associated with vehicular traffic as prescribed in the Akyem Mine Traffic Management Plan.

Noise, ground vibration and air overpressure monitoring

The mine has instituted the noise monitoring programme to ensure compliance with Environmental Protection Agency (EPA) standards. It also maintains the vibration and air overpressure monitoring programme to ensure values do not exceed the standard set by the Ghanaian Mineral and Mining (Explosives) Regulation, 2012 (L.I. 2177), Sub section 199 of 2.0 millimetres per second and 117 decibels (dB), respectively. The mine conducts weekly blast process review meetings to assess noise and vibration impacts of blasting events from the preceding week to better manage blasting activities planned for the

proceeding week. The review focuses on what went well with the blast(s) and what went wrong, and if appropriate changes may be recommended to improve on any lapses.

The mine has three monitoring stations in each of its neighbouring towns namely, Afosu, New Abirem and Aduasena. Figure 2.7 shows the monitoring instrument at the New Abirem monitoring station.

Figure 2.7 An Instantel Minimate Plus Seismic Monitor

CHAPTER 3

LITERATURE REVIEW

3.1   Blast-Induced Ground Vibration

When an explosive is blasted in a blasthole, the chemical reaction evolves a huge quantity of gas which generate energy. This energy starts propagating away in a radial direction. Initially the intensity of the energy is so high that matter near the walls of the blastholes are crushed and displaced radially. When the intensity of energy decreases, the energy continues to travel through the rock as an elastic ground vibration (Gokhale, 2011).

Olofsson (1990), therefore defined blast-induced ground vibration as seismic movements in the ground. According to him, blast-induced ground vibrations are complicated type of seismic waves and consist of the P-wave, which is also called the primary wave or compression wave as shown in Figure 3.1. This wave is the fastest wave through the ground. The particles in the wave move in the same direction as the propagation of the wave. The density of the material will change when the wave passes. The second kind of wave is the S-wave, which is also called the secondary or shear wave as shown in Figure 3.1. It moves through the medium at right angle to the wave propagation but slower than the P-wave. The S-wave changes the shape of the material but not the density. The last kind is the R-wave which stands for Rayleigh wave as shown in Figure 3.2. It is a surface wave that fades fast with depth. It propagates more slowly than the P and S waves and the particles move elliptically in the vertical plane and in the same direction as the propagation.

3.1.1   Measurement of Blast-Induced Ground Vibration

The measurement of blast-induced ground vibration is done by use of blasting seismographs. The seismograph consists of a transducer or a geophone connected to a processor to collect and analyse the signals. The displacement, particle velocity, particle acceleration and frequency of blast-induced ground vibration can be measured. According to Nicholson (2005), the peak particle velocity correlates with damage more closely than peak displacement or peak acceleration. Hence Peak Particle Velocity is used in assessing blast-induced ground vibration.
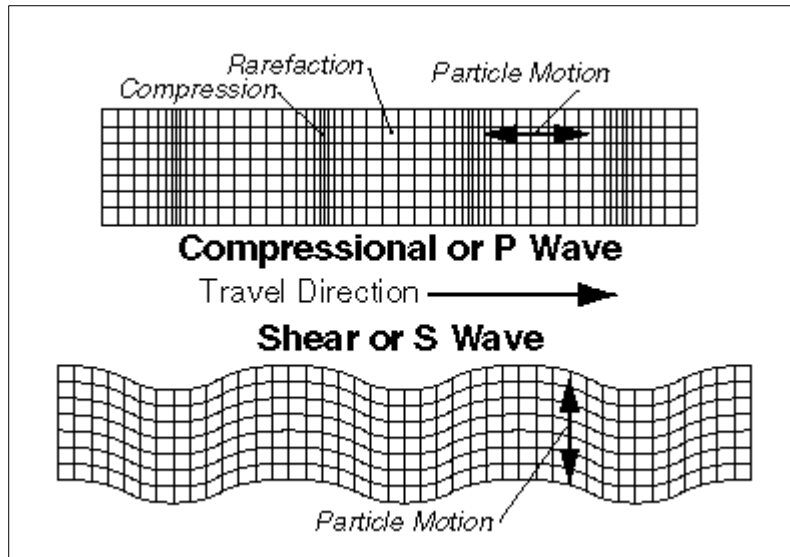
Figure 3.1 P Wave and S Wave (Source: Anon., 2017b)
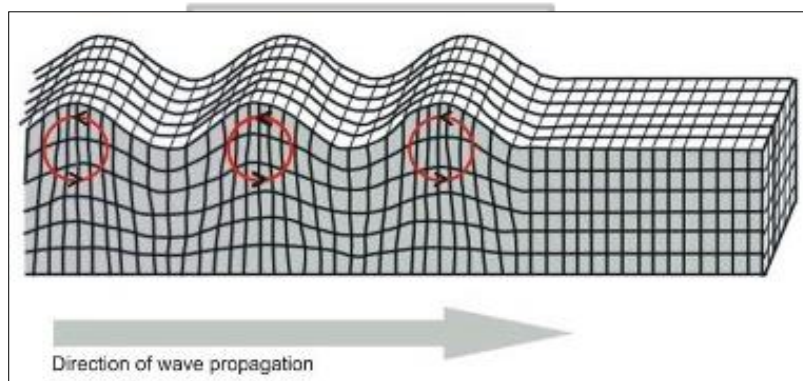
Figure 3.2 Rayleigh Wave (Source: Anon., 2014)

The triaxial geophone of the blasting seismograph contains three mutually perpendicular transducers, each consisting of a spring-loaded moving mass system located within a moving coil to record the three mutually perpendicular components of the motion of the ground particles due to the passage of blasting vibration. These components are: longitudinal (radial) (x); transverse (y), and vertical (z).

The particle velocity at a point is the vector sum of the three components at the same instant of time as shown in Equation (3.1).

$$\text{Particle Velocity} = \sqrt{v_x^2 + v_y^2 + v_z^2} \qquad (3.1)$$

The peak value, known as the Peak Vector Sum (PVS) or Peak Particle Velocity (PPV), is the highest value of the vector sums. The Peak Particle Velocity is the velocity of motion of a particle on or in the ground induced by the passing of the blast vibration waves and is not the velocity of the waves through the ground (Richards and Moore, 2012).

3.1.2   Factors Affecting Blast-induced Ground Vibration

The intensity of blast-induced ground vibration depends on two main groups of parameters, namely controllable and uncontrollable parameters as given in Table 3.1 (Khandelwal and Singh, 2009; Ghasemi *et al*., 2013; Hasanipanah *et al*., 2015; Amiri *et al*., 2016; Fouladgar *et al*., 2017; Hasanipanah *et al*., 2018). The controllable parameters are those that can be changed by the blasting engineers whereas the uncontrollable parameters cannot be changed by the blast engineers (Hasanipanah *et al*., 2018).

Table 3.1 Factors that Affect Blast-Induced Ground Vibration

Controllable Parameters		Uncontrollable Parameters
Blast Design Parameters	Explosive Parameters	Geotechnical and Geomechanical Parameters
Hole depth	Explosive type	Rock mass strength
Hole diameter	Maximum charge per delay	Ground water condition
Bench height	Total charge	Discontinuity frequency
Burden	Powder factor	Bedding plane
Spacing	Velocity of detonation (VOD)	Discontinuities (Faults)
Stemming	Delay time	
sub-drilling	Direction of initiation	
No. of holes and rows		
Hole Inclination		

(Source: Murmu *et al*., 2018)

3.1.3   Prediction of Blast-Induced Ground Vibration

Over the years, attempts have been made to relate the contributing factors of blast-induced ground vibration particle motion to the measured PPV. This led to the development of many

empirical models presented in Table 3.2. As these methods have been extensively applied throughout the scientific literature, Table 3.2 provides only a summary of the modelling method and a description of terms in the related equations.

Table 3.2 Summary of Various PPV Empirical Predictors

Modelling Method	Reference	Equation	Description
USBM	Duvall and Petkof (1959)	$PPV = k\left(D/\sqrt{Q}\right)^{-\beta}$	PPV is the peak particle velocity, D is the distance from the blast face to the monitoring station (m), Q is the cooperating charge (kg), k, β, A, α and n are the site specific constants to be determined.
Langefor-Kihlstrom	Langefors and Kihlstrom (1963)	$PPV = k\left(Q^{1/2}/D^{3/4}\right)^{\beta}$	
General Predictor	Davies *et al*. (1964)	$PPV = k.D^{-\beta}.Q^{A}$	
Ambrasey-Hendron	Ambraseys and Hendron (1968)	$PPV = k\left(D/\sqrt[3]{Q}\right)^{-\beta}$	
Indian Standard	Indian Standard Institute (1973)	$PPV = k\left(Q/D^{2/3}\right)^{\beta}$	
Ghosh-Daemen 1	Ghosh and Daemen (1983)	$PPV = k\left(D/\sqrt{Q}\right)^{-\beta}.e^{-\alpha.D}$	
Ghosh-Daemen 2	Ghosh and Daemen (1983)	$PPV = k\left(D/\sqrt[3]{Q}\right)^{-\beta}.e^{-\alpha.D}$	
Gupta *et al*.	Gupta *et al*. (1987)	$PPV = k\left(D/\sqrt{Q}\right)^{-\beta}.e^{-\alpha.(D/Q)}$	
CMRI Predictor	Roy (1991)	$PPV = n + k\left(D/\sqrt{Q}\right)^{-1}$	
Rai-Singh	Rai and Singh (2004)	$PPV = k.D^{-\beta}.Q^{A}.e^{-\alpha.D}$	

These empirical models have been applied to predict blast-induced ground vibration in Ghana (Amegbey and Afum, 2015; Bansah *et al*., 2016). The empirical models employed in this thesis are: The USBM model, the Langefors-Kihlstrom model, the Ambreseys-Hedron model and the Indian Standard model. These empirical equations were selected because most studies (Khandelwal and Singh, 2006; Mohamadnejad *et al*., 2012; Saadat *et al*., 2014; Armaghani *et al*., 2014; Tiile, 2016; Ragam and Nimaje, 2018) conducted in the area of the application of artificial intelligence techniques in the prediction of blast–induced

ground vibration have compared the developed methods to these four empirical equations, making them the most widely used empirical equation. They are consequently also the empirical equations adopted by the Ghanaian mining industry for blast-induced ground vibration prediction.

3.1.4   Ways of Minimising Blast-Induced Ground Vibration

Thomas and Goldfarb (2005) listed out various factors to be considered in minimising the intensity of blast-induced ground vibrations. They stated that using a computer software such as Alpha-blast to analyse the effect of different timing sequence can help change the intensity of ground vibrations and shift the frequency of the vibrations to a higher range. Another way they stated was to minimise the charge weight per delay. They explained that small charges will generate vibrations with higher frequencies and smaller amplitudes while large charges will generate vibrations with low frequencies and large amplitudes, hence the need to use a smaller charge. They also stated that a longer blast will produce a longer period of ground vibrations hence the duration of the vibration is another factor to be considered in minimising blast-induced ground vibration. Other factors stated by them include:

i.   Using appropriate burden and spacing.
ii. Selection of the appropriate powder factor. A powder factor which is too low can result in lower vibrations than predicted and a too large powder factor will result in high levels of ground vibration due to the volume of explosives.

3.2   Air Overpressure

Air overpressure on the other hand are pressure waves that are created in the atmosphere after blasting. These waves are compressed in nature and travel through the air in a similar fashion to blast waves travelling through the ground (Thomas and Goldfarb, 2005). According to Olofsson (1990), the intensity of the pressure depends on the size of the charge and on the degree of confinement. The maximum pressure is known as the peak air overpressure. The air shock waves are within a wide range of frequencies typically between 0.1 Hz and 200 Hz. When the frequencies range from 20 Hz and above, they are audible and termed as noise but when the frequencies are under 20 Hz, they become inaudible and are termed as concussion. The lower, inaudible frequencies are damped more slowly than the higher, audible and cause overpressure over greater distances. These low frequencies can

occasionally cause direct damage of structures but can more commonly induce higher frequency vibrations which are noticed as noise on windows, doors, crockery. Under such circumstances, it is impossible to determine whether the ground vibration or air shock wave is being perceived without monitoring the blast.

3.2.1 Sources of Air Overpressure

During blasting operations, air overpressure waves are generally generated from four main sources, namely (Armaghani *et al.*, 2015b):

  i.   Air pressure pulse (APP): the rock displacement at bench face as the blast progresses.
  ii. Gas release pulse (GRP): generated by the gas escapes through rock fractures.
  iii. Rock pressure pulse (RPP): caused by vibration of ground.
  iv. Stemming release pulse (SRP): produced by the gas escapes from blast-hole once the stemming is ejected

3.2.2 Factors Affecting Air Overpressure

According to Sawmliana *et al.* (2007), there are both controllable and uncontrollable factors that affect the intensity of the air overpressure. The controllable factors include:

  i.   Maximum charge weight per delay;
  ii. Depth of burial of the charges;
  iii. Exposure of detonating materials on the ground surface;
  iv. Volume of displaced rock; and
  v.   Delay interval and orientation.

The uncontrollable factors also include:

  i.   Atmospheric condition; and
  ii. Topography.

They also stated that among the controllable factors, the maximum charge per delay is the most predominating factor followed by depth of burial of charge.

3.2.3 Measurement of Air Overpressure

Air overpressure is measured as units of pressure in millibar (mbar). The units, decibel (dB) and kiloPascal (kPa) are also used. The decibel unit is expressed in Equation (3.2) as:

$$dB = 20\log\frac{P}{P_o} \hspace{4cm} (3.2)$$

where, P is the measured pressure; P_o is the reference pressure of 0.00002 Pa.

Popularly used air overpressure prediction models

The most widely used form of prediction equation of air overpressure is Equation (3.3) (Gokhale, 2011; Armaghani *et al.*, 2015b):

$$AOp = H\left(\frac{D}{\sqrt[3]{Q}}\right)^{-\beta} \hspace{3cm} (3.3)$$

where AOp is air overpressure in decibel; D is distance in meters; Q is the weight of explosive in kilogram; H and β are site constants.
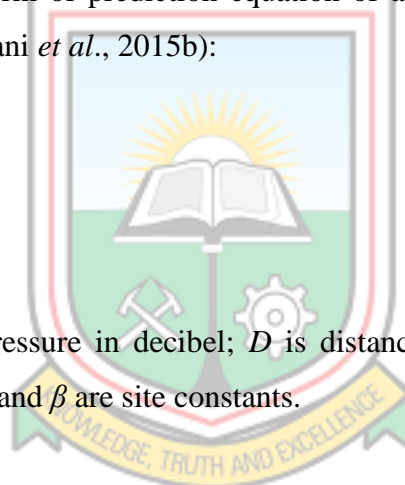
However, air overpressure predictive models have been developed over the years (Holmberg and Person, 1979; NAASRA, 1983; Olofsson, 1990; Persson *et al.*, 1994).

3.2.4 Ways of Minimising Air Overpressure

In order to minimise air overpressure, the following must be done (Anon., 2018a)
  i.   Use sufficient stem length (at least 0.7 times the burden).
  ii. Use an angular, crushed-rock product of the correct size distribution appropriate for the hole diameter.
  iii. Check the free faces for excessive fracturing from back break and the presence of mud seams or voids and load the front row of holes accordingly.

iv.   Conduct blasting in the afternoon when temperature inversions are least likely to persist. Contact a local airport to find out the elevation of the cloud ceiling.

v.   Blast when wind conditions are favourable (e.g., either in directions away from structures or at low velocities).

vi.   Use non-electric, shock-tube initiation systems instead of detonating cord.

3.3   Artificial Intelligence Techniques

The artificial intelligence (AI) is a new technique with a flexible mathematical structure that is capable of identifying complex non-linear relationships between input and output data when compared with other classical modelling techniques (Najah *et al*., 2011). The AI techniques found in literature for prediction modelling include: support vector regression (SVR), support vector machines (SVM), least square support vector machines (LSSVM), classification and regression tree (CART), extreme learning machines, Gaussian process regression (GPR), multivariate adaptive regression splines (MARS), fuzzy logic, artificial neural networks (ANN), generalised regression neural network (GRNN), radial basis function neural network (RBFNN), wavelet neural network (WNN), functional network, adaptive neuro-fuzzy inference systems (ANFIS), genetic algorithm (GA), particle swarm optimisation (PSO), ant colony algorithm (ACA), gene expression programming (GEP), bee colony algorithm (BCA), cuckoo search algorithm (CSA), imperialist competitive algorithm (ICA) etc.
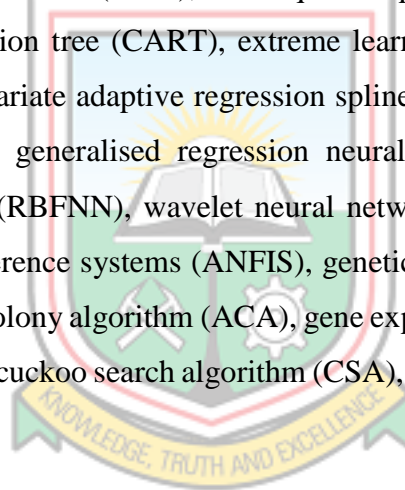
3.3.1   Essence of Prediction Using Artificial Intelligence Techniques

In recent years, many researches have tried to develop new models using AI techniques for the prediction of blast-induced ground vibration and air overpressure. The introduction of these AI techniques as an alternative predictor for ground and air vibration is due to the empirical predictor models not being fully suitable to predict these vibrations (Ghasemi *et al*., 2013). The reason being, the empirical predictor models are basically based on two parameters, maximum charge per delay and distance from blast site to monitoring point, excluding other effective parameters (Table 3.1) which influence the intensity of ground vibration vibrations (Ghasemi *et al*., 2013). Besides, blast-induced ground vibration is a complex phenomenon with highly nonlinear variable interactions which cannot be adequately modelled using closed-form mathematical equations (Table 3.2) (Dehghani and

Ataee-Pour, 2011; Dindarloo, 2015). Additionally, Dindarloo (2015) is of the view that lack of generalisability is a common phenomenon inherent in the empirical prediction models (Table 3.2) because of the number of input parameters considered.

Generally, the obtained results by previous researchers show that AI techniques are able to predict PPV and air overpressure with higher level of accuracy compared to empirical and statistical techniques (Armaghani *et al*., 2015a; Armaghani *et al*., 2015b; Ghoraba *et al*., 2016; Tiile, 2016). These techniques have been found to outperform the empirical predictors due to their ability to learn, adapt and generalise well to the data set introduced to them without *a priori* knowledge of the mathematical association between input and output parameters. Thus, they have the ability to model correctly the complex nonlinear and dynamic system interactions of the blast design, explosive, geotechnical and geomechanical parameters. The soft computing techniques also have the capability to tolerate imprecision, uncertainty, approximate reasoning and partial truth to achieve tractability and robustness on simulating human thinking to match up with reality (Zadeh, 1994).

3.3.2   Review of Application of Artificial Intelligence in Blast-Induced Ground Vibration Prediction

It is noteworthy that literature is replete with the application of the various AI techniques in the prediction of blast-induced ground vibration. For example, authors such as: Singh (2004) applied ANN to predict blast-induced ground vibration. To check the accuracy of the ANN model, a multivariate regression analysis (MVRA) model was also developed. In constructing the various models, input parameters of hole depth, number of holes, burden, spacing, stemming column height, mass of charge per delay, and horizontal and radial distance from the blast location were considered whereas frequency of blast vibration was the output parameter. The results obtained revealed that the ANN predictions of ground vibrations agreed adequately with actual data and gave significantly lower errors relative to the predictions from a MVRA model.

Singh and Singh (2005) applied ANN to predict blast-induced ground vibration. To provide an inspection of the reliability and accuracy of the ANN model, a multivariate regression analysis (MVRA) model was also developed. In constructing the various models, hole diameter, number of holes, depth, burden, spacing, stemming, charge per delay, horizontal

31

distance and radial distance were considered as the input parameters, whereas the frequency of the blast-induced ground vibration was the output parameter. The prediction results obtained revealed that, the ANN provided a better correlation between the observed and predicted frequency. Moreover, the ANN model, had a lower error range of 0.6 – 19% whereas the MVRA model had an error range of 0.5 – 47%.

Khandelwal and Singh (2006) applied ANN to predict blast-induced ground vibration. To check the accuracy of the ANN model, a multivariate regression analysis (MVRA) mode was also developed. In that regard, authors used 150 and 20 blast data sets to develop and test the ANN and MVRA models respectively. In constructing the models, hole diameter, average hole depth, average burden, average spacing, average charge length, average explosive per hole, distance of monitoring point from blasting face, blastability index, Young's modulus, Poisson's ratio, P-wave velocity, velocity of detonation of explosive and density of explosive were considered as input parameters whereas PPV was the output parameter. The prediction results obtained showed the superiority of ANN in predicting blast-induced ground vibration compare with the MVRA model. The reason being, the ANN had a correlation coefficient (R) value of 0.9994 and mean absolute percentage error (MAPE) value of 4.74 whereas the MVRA model had R value of 0.4971 and MAPE value of 343.98.

Khandelwal and Singh (2007) developed a three-layer feed forward backpropagation neural network (BPNN) model to predict blast-induced ground vibration in Dharapani Magnesite Mine, India. To check the accuracy of the BPNN model, empirical equation models of USBM, Ambraseys–Hendron, Langefors–Kihlstrom and Indian Standard were also developed. In that regard, authors used 150 and 20 blast data sets to develop and test the various predictive models respectively. In constructing the models, maximum charge per delay and distance from the blast face to the monitoring point were the considered input parameters whereas PPV was the output parameter. The predicted PPV obtained on testing data sets in comparison with the measured showed the greater capability of the ANN model at predicting blast-induced ground vibration than the empirical models.

Iphar *et al*. (2008) applied adaptive neuro-fuzzy inference system (ANFIS) to predict blast induced ground vibration using blasting events from Magnesite Incorporated Company (MAS), Turkey. To check the performance of the ANFIS model, a simple regression model

based on the USBM was also developed. In that regard, a total of 44 blasting dataset of which 35 blasting data sets (80%) were used in the model development and the remaining 20% (9 records) were used to independently ascertain the performance of various developed models. In constructing the various predictive modes, authors considered, distance between the shot and the station and maximum charge per delay as the input parameters with PPV as the output parameter. Using variance accounted for (VAF), root mean square error (RMSE) and standard error of estimation and R as the performance indices, the obtained results on the testing dataset showed that, the ANFIS model with VAF value of 98.79, RMSE value of 0.78, standard error of estimation value of 0.80 and correlation value of 0.99 was more accurate at predicting blast-induced ground vibration than the regression model (VAF value of 80.57, RMSE value of 3.19, standard error of estimation value of 3.17 and correlation value of 0.90).

Mohamed (2009) applied ANN to predict blast-induced ground vibration at Assiut Cement Company (ACC). Three ANN models based on the number of input parameters used were developed. These models are: one-single-input model, two-input model and large number of input model. To ascertain the performance of the ANN models, a conventional scaling law predictor was developed. In that regard a total of 124 data sets were used to develop the models whereas 25 new data sets were used to test and validate the developed models. In the case of one-single-input model, the author used scaled distance as the only input, whereas the two-input model had distance and the maximum explosives/delay as the input parameters. The large number of input model consisted of 15 input parameters, namely: hole diameter, burden distance, spacing distance, bench height, hole inclination, maximum explosives/delay, total explosives/blast, explosive density, rock density, porosity, compressive strength, modulus of elasticity, measuring distance, velocity of detonation, propagation wave velocity. The prediction results obtained on the testing data sets showed that the large number of input ANN model gave better prediction than the two-input ANN model and one-single-input ANN model in that order. Also, the ANN models in general outperformed the conventional scaling law predictor.

Khandelwal and Singh (2009) developed and applied a three-layer, feed-forward backpropagation neural network to predict blast-induced ground vibration at Jayant opencast mine of Northern Coalfields Limited (NCL), India. To check the performance of the ANN model, a multivariate regression analysis (MVRA) model and empirical models

of USBM, Langefors–Kihlstrom, General predictor, Ambraseys–Hendron, Bureau of Indian Standard, Ghosh–Daemen predictor and CMRI predictor were developed. In that regard, a total of 174 data sets were collected of which 154 data sets were used to develop the various models whereas the remaining 20 data sets were used to test and evaluate the developed models. In constructing the ANN and MVRA model, authors considered hole depth, burden, spacing, maximum charge per delay, distance of monitoring point from blasting face, compressive strength/tensile strength, young's modulus, poisson's ratio and p-wave velocity as input parameters with PPV as output parameter. Using coefficient of determination (R^2) and mean absolute error (MAE) as statistical measure of performance indices, the obtained prediction on the testing dataset indicated that the ANN model was superior at predicting blast-induced ground vibration than the MVRA and empirical predictors. The reason is that it had the highest R^2 of 0.9864 and lowest MAE of 0.196379.

Khandelwal (2010) applied support vector machines (SVM) to predict blast-induced ground vibration at Jayant opencast mine of Northern Coalfields Limited (NCL), India. To check the performance of the ANN model, a multivariate regression analysis (MVRA) model and empirical models of USBM, Langefors–Kihlstrom, General predictor, Ambraseys–Hendron, Bureau of Indian Standard, Ghosh–Daemen predictor and CMRI predictor were developed. In that regard, a total of 174 data sets were collected of which 154 data sets were used to develop the various models and the remaining 20 data sets were used to test and evaluate the developed models. In constructing the various models, the author considered maximum charge per delay and distance of monitoring point from blasting face as input parameters with PPV as output parameter. Using R^2 and MAE as statistical measure of performance indices, the prediction obtained on the testing dataset indicated that the SVM model was superior at predicting blast-induced ground vibration than the MVRA and empirical predictors. The reason is that it had the highest R^2 of 0.960 and lowest MAE of 0.257.

Khandelwal *et al*. (2010) applied support vector machine (SVM) for the prediction of blast induced ground vibration at Magnesite mine of Pithoragarh, India. For comparison purposes and to investigate the suitability of the SVM model, conventional predictor equations of USBM, Langefors-Kihlstrom, Ambraseys-Hendron and Indian Standard were also developed. In that regard, a total of 170 blast vibrations data sets were recorded from the study area. Out of 170 data sets, 150 were used to develop (train) the various predictive

models, whereas 20 new randomly selected data sets were used to test the developed models. In constructing the SVM and empirical models, maximum charge per delay and distance between blast face to monitoring point were considered as input parameters with PPV being the output parameter. Statistical results based on R^2 and MAE revealed that, SVM was more accurate in predicting PPV than the conventional predictor equations. The reason being it had the higest R^2 values (0.955) and lowest MAE value (0.226)

Amnieh *et al*. (2010) applied backpropagation neural network to predict blasting vibrations in Sarcheshmeh copper mine. In their study, the input parameters considered were: charge weight per delay, distance from blast point, the height of stemming column and the number of drill hole-rows. PPV was considered as the output parameter for the network. The network was trained using 4 hidden layers and 23 training data sets. The first hidden layer has 20 neurons with the three having 17, 15 and 10 neurons respectively. The Tan-sigmoid transfer function was employed for hidden layers and the linear transfer function was used for the output layer that generated PPV. Levenberg-Marquardt algorithm was used as the training function. Six additional data sets were used to test the trained neural network. The correlation coefficient of the predicted PPV and the actual PPV of the six-additional data sets was 0.99355. The average relative error obtained was 6.77%.

In Monjezi *et al*. (2010b), multilayer perceptron neural network (MPNN), the radial basis function neural network (RBFNN) and the generalised regression neural network (GRNN) were applied to predict blast-induced ground vibration at Sarcheshmeh Copper Mine. The input parameters that were considered include: The distance from the blasting location (m); maximum charge per delay (kg); burden/spacing ratio; number of holes per delay (m); UCS (mpa); and delay per rows. A total of 269 data sets were used in the development of these various type of ANN models. Out of these 269 data sets, 242 data sets were used for training, 27 data sets were used for testing. They found out that the Multilayer Perceptron Neural Network was a better predictor than the other ANN models with a RMSE of 0.031 and R^2 of 0.954.

Kamali and Ataei (2010) applied ANN to predict blast-induced ground vibration in Karoun III power plant and dam. To check the performance of the ANN model, a multivariate regression analysis (MVRA) model, empirical equation models of USBM, Langfors–Kihlstrom, General predictor, Ambrasey-Hendron, Bureau of Indian Standard, Ghosh–

Daemen, CMRI were also developed. A total of 28 data sets were collected from which 20 datasets were used to develop (train) the various models whereas the additional 8 data sets were used to validate the developed models. In constructing the ANN and the MVRA model, authors considered maximum charge per delay, total charge per round, distance from blast, direction of blasting, blast hole length, number of blast holes, total delay in millisecond, number of delay intervals, average specific charge as input parameters with PPV being the output parameter. Using R^2 and mean square error (MSE) as the statistical evaluator of the performance of the developed models, the obtained results based on the validation data sets revealed that, the ANN, MVRA model and CMRI (best empirical model) had the R^2 values of 0.98, 0.94 and 0.92 respectively. Also, the ANN, MVRA model and CMRI (best empirical model) had the MSE values of 9.19, 5443.67 and 60.44 respectively. They thus, concluded that the ANN model was superior in predicting blast-induced ground vibration than the MVRA and empirical models.

Khandelwal (2011) developed and applied support vector machine (SVM) approach to predict blast induced ground vibration at three different opencast coal mines namely, PK OCP-III, GDK OCP-II, and JVR OCP-I of Sinagreni Collieries Company Limited (SCCL), Andhra Pradesh, India. For comparison purposes and to investigate the suitability of the SVM model, conventional predictor equations of USBM, Langefors-Kihlstrom, Ambraseys-Hendron, Indian Standard and CMRI predictors were also developed. A total of 150 blast vibrations data sets were recorded from the study area. Out of 150 data sets, 120 were used to develop (train) the various predictive models, whereas 30 new randomly selected data sets were used to test the developed models. In constructing the SVM and empirical models, maximum charge per delay and distance between blast face to monitoring point were considered as input parameters with PPV being the output parameter. Statistical results based on R^2 and MAE revealed that, SVM was more accurate in predicting PPV than the conventional predictor equations. The reason being it had the highest R^2 values (0.9644) and lowest MAE value (0.227).

In Khandelwal *et al.* (2011), a three-layer feed forward backpropagation neural network model with 2-5-1 architecture was developed to predict ground vibration due to blasting. The input parameters considered for this model were explosive charge per delay and distance from the blast face to the monitoring point. This model was trained and tested using 130 experimental and monitored blast records. Twenty additional blast data were used to

validate the model and compare the model to conventional vibration predictors. The model comparison indices – coefficient of determination and root mean square error, indicated that the prediction performance of the ANN model was higher than the conventional vibration predictors.

Monjezi *et al*. (2011) applied ANN to predict blast-induced ground vibration in the Siahbisheh project, Iran. To provide a comprehensive assessment of the reliability and accuracy of the developed model, empirical models of USBM, Langefors–Kihlstrom, Ambraseys–Hendron, Bureau of Indian Standard, CMRI predictor as well as a multivariate regression analysis (MVRA) model were developed. To achieve that aim, a total of 182 blast vibration records were monitored, from which 162 data sets were used construct the various models, whereas the remaining 20 data sets were used to test the developed models. In constructing the ANN and MVRA models, maximum charge per delay, distance of monitoring point from blasting face, stemming and hole depth were taken as input parameters, whereas PPV was considered as an output parameter. Their prediction results on the testing data sets revealed that, a four layered ANN model with structure 4-10-5-1 was more accurate and reliable at predicting blast-induced ground vibration than the MVRA and empirical models collectively.

Fişne *et al*. (2011) applied fuzzy logic (FL) to predict blast-induced ground vibration using blast data from Akdaglar Quarry, Istanbul, Turkey. To check the performance of the fuzzy logic model, a statistical model based on the USBM was also developed. Using a total of 33 blasting events for the validation of the various predictive models, authors found out that on the basis of computed VAF, RMSE, standard error of estimation and correlation, the fuzzy logic model with VAF value of 0.91, RMSE value of 5.31, standard error of estimation value of 5.07 and correlation value of 0.96 was more accurate at predicting blast-induced ground vibration than the statistical model (VAF value of 0.59, RMSE value of 11.32, standard error of estimation value of 11.54 and correlation value of 0.82).

Mohamed (2011) applied ANN and fuzzy logic to predict blast-induced ground vibration in Assiut Cement Company. For comparison purposes, a traditional regression model was developed. In that regard, a total of 136 dataset were collected and used to develop (train) the predictor models. Twenty-six new dataset were collected to independently test the developed models. In constructing the models, charge weight per delay and distance from

blast-face to monitoring station were used by authors as input parameters. The authors used VAF and RMSE as statistical performance indicators for the various models. The results obtained based on the testing data sets revelated that, the fuzzy logic and ANN models were more accurate at predicting AOp than the traditional regression model. Also, the authors found out that, the fuzzy logic model performed slightly better than the ANN model. These assertions were made because, values of 87.00% and 0.17 were obtained for VAF and RMSE respectively by fuzzy logic model. Values of 78.39% and 0.21 were obtained for VAF and RMSE respectively by ANN model whereas values of 3.23% and 0.45 were obtained for VAF and RMSE respectively by traditional regression model.

Dehghani and Ataee-Pour (2011) applied ANN to predict blast-induced ground vibration at Sarcheshmeh copper mine located in Iran. A total of 116 blasting events were collected to develop (train) the ANN model whereas 17 additional blasting events were used to test the developed ANN model. Authors used nine input parameters of burden, spacing. delay between rows, powder factor, number of rows in each blast, distance of monitoring point from blasting face, maximum hole per delay, charge per delay and point load index with PPV being the output parameter were used to construct the ANN model. The obtained prediction results demonstrated that, an ANN with 9-25-1 topology (9 inputs, 25 neurons in hidden layer and 1 output) was found to be optimum for prediction of PPV.

Verma and Singh (2011) applied genetic algorithm (GA) optimisation technique to predict blast-induced ground vibration using dataset from Karusia mines. To ascertain the predictive capability of the GA model, a three-layer feed forward BPNN, empirical equations and a multivariate regression analysis model were also developed. To achieve that aim, a total of 127 blast data sets were used to develop the GA model and the other predictive models. Ten (10) additional data sets were used to independently test the performance of the various predictive models. The considered input parameters to the development of the models include: burden, spacing, hole depth, stemming, maximum charge per delay, total charge and distance from source. Using MAPE as the criteria for evaluating performance, the obtained prediction results revealed that the GA model was more effective and accurate at predicting blast-induced ground vibration than the conventional empirical equations and PBNN. That assertion was made because the GA model had the lowest MAPE of 0.088.

Shuran and Shujin (2011) developed a backpropagation neural network to predict blast-induced ground vibration. In providing a better inspection of the reliability and accuracy of the BPNN model, a linear regression statistics (LRS) model was also developed. A total of 134 dataset were used to develop (train) the BPNN and LRS models whereas 10 data sets were used independently to assess the performance of the developed models. Explosives weight per delay, largest horizontal distance and height were the input parameters that were considered in constructing the various predictive models. The obtained prediction results showed that the BPNN was more reliable and accurate at predicting blast-induced ground vibration as it had an average prediction error of 5.7%. The LRS model on the other hand, had an average prediction error of 20.7%.

Álvarez-Vigil *et al*. (2012) applied ANN to predict blast-induced ground vibration. To inspect the accuracy and reliability of the ANN model, a multilinear regression model was also developed. In constructing the various models, input parameters of RMR, blast-control point relative arrangement, distance from blast to control point, blast hole diameter, blast hole length, spacing between blast holes, burden, instantaneous charge, total charge, number of blast holes, explosive detonation velocity were considered. The prediction results obtained showed that the ANN model had a lower mean relative error of 0.65 and higher correlation coefficient of 0.98 whereas, the MLR model had a mean relative error of 2.77 and a correlation coefficient of 0.50. Thus, the ANN model was more accurate at predicting blast-induced ground vibration than the MLR model.

Mohamad *et al*. (2012) applied ANN to predict blast-induced ground vibration. In checking the reliability and accuracy of the ANN model, empirical models of USBM, Ambrasey-Hendron and Ground Empirical (General predictor) were also developed. The obtained prediction results showed that the ANN model was superior in predicting blast-induced ground vibration to the empirical equation models.

Mohamadnejad *et al*. (2012) applied support vector machines (SVM) to predict blast-induced ground vibration using blast data from two limestone quarries. The maximum charge per delay and the distance between the blast face and monitoring point were the input parameters used in the study with PPV being the output parameter. To ascertain the performance of SVM, empirical models of Thoenen and Windes, Langefors and Kilhstrom, Ambraseys and Hendron, Indian standard Institute, Roy and Rai *et al* were also developed.

Twenty-six (26) blast data was used in the development and testing of the various methods applied in the study. Based on the performance criterion of R^2, it was found out that, the developed SVM model outperformed the empirical models by having a R^2 value of 0.944.

Mohammadnejad *et al*. (2012) applied general regression neural network (GRNN) and support vector machine (SVM) to predict blast-induced ground vibration at Masjed Soleiman dam, Iran. Empirical models of USBM, Langerfors-Kihlstrom, Ambrasey-Hendron, Indian standard and Central Mining Research Institute (CMRI) models were also developed to provide a better inspection of the suitability and accuracy of the GRNN and SVM models at predicting blast-induced ground vibration. A random selection of 25 dataset were used to construct and train the various models whereas 12 data sets were also randomly selected to test the developed models. Input parameters of maximum charge per delay and distance were considered as input parameters and PPV was the output parameter. The obtained prediction results revealed that the SVM model was more accurate in predicting the blast-induced ground vibration than the GRNN model and empirical models in decreasing order of performance.

Ghasemi *et al*. (2013) developed and applied a fuzzy logic (FL) model to predict blast-induced ground vibration in Sarcheshmeh copper mine, Iran. To provide a better assessment of the accuracy of the FL model, empirical models of USBM, Langefors–Kihlstrom, General predictor, Ambraseys–Hendron, Indian Standard, Ghosh–Daemen 1, Ghosh–Daemen 2, Gupta *et al*., CMRI predictor, Rai–Singh as well as a multivariate regression (MVR) model were developed. To do that, a total of 120 blasting events were collected, from which 90 data sets representing 90% of the entire data sets and the remaining 30 data sets were used for developing the various models and testing the developed models respectively. In constructing the FL and MVR models, authors considered burden, spacing, stemming, number of holes per delay, maximum charge per delay, distance from blast location to monitoring point as input parameters whereas PPV was the output parameter. For the empirical models, input parameters of maximum charge per delay and distance from blast location to monitoring point were considered. Using R^2, VAF (%), RMSE and MAPE as the statistical measures of model performance, the results obtained based on the testing dataset showed that the FL model was superior and most accurate at predicting blast-induced ground vibration among the list of models. The reason being that the FL model had the

highest R^2 and VAF values of 94.59% and 94.59% respectively and lowest RMSE and MAPE values of 2.73 and 23.25 respectively.

Ataei and Kamali (2013) applied adaptive neuro-fuzzy inference system (ANFIS) to predict blast-induced ground vibration in Karoun 3 power plant and dam, Iran. To assess the reliability and accuracy of the ANFIS model, an empirical model of USBM was also developed. A total of 29 data sets were collected, from which 23 data sets representing 80% of the entire data sets were used to develop (train) the ANFIS and USBM models, whereas the remaining 6 data sets were used to test the developed models. In constructing the various models, maximum charge per delay and distance from blast site were used as the input parameters whereas PPV was the output parameter. The obtained results based on the testing dataset showed that the ANFIS model had better correlation between predicted and measured PPV than the USBM model and thus, the ANFIS model was superior at predicting blast-induced ground vibration than the USBM.

Monjezi *et al*. (2013) applied artificial neutral network (ANN) to predict blast-induced ground vibration. To ascertain the predictive strength of the ANN model, empirical models of USBM, Ambraseys-Hendron, General predictor, Indian Standard and CMRI were also developed. For that reason, a total of 20 blast vibration record were monitored from which 16 data sets were used for developing (training) the ANN model while the remaining 4 data sets were used for validating and comparing the ANN model and the results of the empirical models. In constructing the ANN model, input parameters of total charge, maximum charge per delay and distance between shot point and monitoring station were used with PPV serving as the output parameter. Using coefficient of determination, MAPE, VARE, MEDAE, VAF and RMSE as the statistical performance indices, the obtained prediction results showed the superiority of ANN model in predicting blast-induced ground vibration to the empirical models.

Kostić *et al*. (2013) applied artificial neural network (ANN) to predict blast-induced ground vibration at the limestone quarry "Suva Vrelá" near Kosjerić, which is located in the western part of Serbia. To ascertain the predictive performance of the ANN model, empirical models of USBM, Langefors-Kihlstrom, General predictor, Ambraseys-Hendron and CMRI were also developed. A total of 33 blast data sets were collected, from which 22 data sets representing 65% of the total blast data sets were used for developing and training the

various predictive models whereas the remaining 11 data sets were used for testing and validating the developed models. In constructing the ANN models, authors used total charge, maximum charge per delay, distance from blasting source, average hole depth as input parameters with PPV serving as the output parameter. The prediction results obtained based on the testing data revealed that the ANN model was more accurate at predicting blast-induced ground vibration than the empirical predictor equations.

Görgülü *et al*. (2013) applied ANN to predict blast-induced ground vibration at Tülü boron open pit mine. For comparison purposes, five empirical models based on different propagation direction were developed. In the development of the ANN model, distance, maximum charge per delay, number of holes, hole depth, stemming, spacing, burden, RMR, resistivity, and the P- and S-wave velocities were used as input parameters. Comparing the obtained prediction results using R^2 showed that, the ANN was more accurate at predicting PPV than the five empirical models. This assertion was made because, the ANN had R^2 value of 0.94 whereas the five empirical equation models had R^2 values between 0.43 and 0.86.

Saadat *et al*. (2014) applied artificial neural network to predict blast-induced ground vibration of the Gol-E-Gohar iron mine in Iran. The input parameters that were considered include: the maximum charge per delay, distance from blasting face to monitoring point, stemming height and hole depth. The output parameter was PPV. Sixty nine (69) data sets were used to train and test the ANN model developed. The performance indices selected to ascertain the performance of the developed model were R^2 and MSE. From their work, a network with architecture 4-11-5-1 with R^2 of 0.957 and MSE of 0.000722 was found to be optimum. This means that two hidden layers with neurons of 11 and 5 were used. A USBM model, Langerfors-Kihlstrom model, bureau of Indian standard model and a multiple linear regression model were developed to predict PPV using the same 69 data sets. They found out that the ANN gave the highest R^2 and lowest RMSE of 0.957 and 8.796 respectively.

Xue and Yang (2014) applied general regression neural network to predict blast-induced ground vibration. To provide an inspection of the accuracy and reliability of the GRNN model, an ANN model as well as a multivariate regression analysis model were also developed. In that regard, a total of 20 data sets were used for model development (15 data sets) and testing (5 data sets). In constructing the models, hole diameter, average hole depth,

42

average burden, average spacing, average charge length, average explosive per hole, distance of monitoring point from blasting face, blastability index, Young's modulus, Poisson's ratio, P-wave velocity, velocity of detonation of explosive and density of explosive. The obtained results based on the testing data set showed that, the GRNN was superior at predicting blast-induced ground vibration to the ANN and the MVRA models.

Armaghani *et al*. (2014) developed and applied a PSO-based ANN for the prediction of blast-induced ground vibration as well as blast-induced flyrock at three granite quarry sites in Malaysia. Empirical models of USBM, General predictor, Indian Standard, Ghosh Daemen and CMRI for ground vibration prediction and Lundborg predictor for flyrock prediction were also developed for comparison. In that regard, 44 data sets were collected with hole diameter, hole depth, charge per delay. spacing, burden, stemming, powder factor, rock density, sub-drilling and number of rows serving as the input parameters and flyrock distance and PPV as the output parameters. 20% of the data sets (9 data sets) were used as the testing data sets. The prediction results based on the testing dataset showed that the proposed PSO-based ANN model was highly able to predict flyrock distance and blast-induced ground vibration as it produced predicted values very close to the measured values that the empirical models applied in their study.

Vasović *et al*. (2014) developed and applied a three-layer feed forward backpropagation neural network to predict blast-induced ground vibration. For comparison purposes, conventional empirical predictors of USBM, Langefors–Kihlstrom, general predictor, Ambraseys– Hendron, and CMRI were also developed. In constructing the ANN model, input parameters of total charge, maximum charge per delay and distance from the explosive charge to monitoring station were considered. Also, 16 data sets representing 50% of the whole data set were used to training the ANN model, 25% (8 data sets) for validation and 25% (8 data sets) for testing. The developed ANN model had the structure [3-6-1], indicating three input, six neurons in the hidden layer and one output. Using the R as the statistical indicator of performance measure, the obtained results on testing data sets with R value of 0.89978 for the ANN model whereas the empirical predictors had R values in the range 0.87–0.88 with the exception of Ambraseys– Hendron (0.69).

Lapčević *et al*. (2014) applied artificial neural network to predict blast-induced ground vibration. To check the performance of the ANN model, five empirical predictor models of

USBM, Langefors-Kihlstrom, General predictor, Ambraseys-Hendron and CMRI were developed. A total of 42 data sets were collected, 21 of which was used to train the ANN model, 7 for validation and 13 for testing the developed ANN model. In developing the ANN model, input parameters of total charge, maximum charge per delay, distance from blasting shot, charge per hole, delay time were considered with PPV values serving as the output parameter. Using MAPE, variance absolute relative error (VARE), median absolute error (MEDAE) and VAF, authors found out that ANN model outperformed the empirical model by having the lowest MAPE, VARE and MEDAE values of 16.38, 16.07, 110.885 respectively and the highest VAF value of 91.17%.

Parida and Mishra (2015) developed and applied ANN for the prediction of blast-induced ground vibration using blasting data from iron an ore mine in Indian. Multiple linear regression (MLR) and empirical models of USBM, Ambraseys-Hendron, Langefors-Kihlstrom, Indian Standard and CMRI were also developed in their study to ascertain the predictive strength of the ANN model. A total of 9 blasting data sets were used to develop and test the developed models. The input parameters that were considered include: the maximum charge per delay and distance from blasting face to monitoring point with measured PPV being the output parameter. Using R^2 and RMSE as the performance indices, their work revealed that a network with architecture 2-5-1 with R^2 of 0.898 and RMSE of 0.908 was found to be outperform the MLR and the empirical models.

Armaghani *et al*. (2015a) applied ANFIS and ANN to predict blast-induced ground vibration in ISB granite quarry, Johor, Malaysia. To ascertain the suitability of these AI techniques, conventional empirical equation of USBM, Langefors–Kihlstrom, General predictor, Indian Standard, Ghosh–Daemen predictor and CMRI were also developed. To achieve that aim, a total of 109 blast data sets were collected. Maximum charge per delay and distance between monitoring point and blast-face were considered as inputs to the various models whereas, PPV served as the output parameter. Out of the 109 data sets, 87 data sets representing 80% were used to adequately develop the various predictive models. The remaining 22 data sets were used to test the performance of the developed models. Using R^2, RMSE and VAF as model performance indices, the prediction results showed that the ANFIS model had superior predictive capability to the ANN model which in turn was more accurate than the empirical models. This is because the ANFIS and ANN model had the high R^2 values of 0.973 and 0.949 respectively, VAF values of 97.345 and 94.895

respectively and low RMSE values 0.987 and 1.372 respectively in comparison to the empirical models.

Hasanipanah *et al.* (2015) developed and applied support vector machines (SVM) to predict blast-induced ground vibration using blasting data from Bakhtiari Dam, Iran. To investigate the applicability of the SVM model for blast-induced ground vibration, empirical models of USBM, Ambraseys-Hendron, Davies *et al.* and Indian Standard were also developed and utilised. In that regard, a total of 80 blasting dataset were collected from the study area. Authors also considered the maximum charge per delay and distance from blasting face to monitoring point as the input parameters and PPV as output parameter to the various predictive models. In the analysis procedure of their study, the authors used 60 data sets for the development of the various models whereas the remaining 20 data sets were used to test the developed models. They applied performance indices of VAF, VARE, RMSE, median absolute error (MEDAE), MAPE, Nash and Sutcliffe (NS) and R^2. The obtained results based on the performance indices showed that the SVM model provided the highest performance capacity in predicting PPV in comparison with the applied empirical equations.

In Hajihassani *et al.* (2015), a hybrid model of an ANN and a PSO was developed and applied to predict ground vibration induced by blasting at Hulu Langat granite quarry site, Malaysia. To check the performance of the PSO-based ANN, several conventional empirical equations were also developed. Eighty-eight (88) data sets collected from the mine site were used to develop the various models. Hole depth, maximum charge per delay, burden to spacing ratio, stemming length, sub-drilling, powder factor, RQD, distance between the free face and the monitoring point, and number of holes were used as input parameters, while PPV values were set as output parameters. The prediction results showed that the PSO-based ANN model was more accurate at predicting than the empirical approaches.

Görgülü *et al.* (2015) conducted a study to investigate the effects of blasting design parameters and rock properties on blast-induced ground vibration and to develop estimation models with higher reliability for the evaluation of these vibrations. In that regard ANN and multiple regression analysis (MRA) models were developed. In developing these models, the authors used distance from blasting point, maximum charge per delay, number of drill holes, hole depth, burden, spacing, stemming, resistivity, P-wave and S wave velocities as input parameters whereas measured PPV values were used as the output parameter. The

obtained prediction results showed that the ANN model had a R^2 value of 0.976 and thus had a higher reliability and prediction capability than the MRA model which had a poor R^2 value of 0.45.

Ghoraba *et al*. (2016) applied empirical, ANN and ANFIS to predict blast-induced ground vibration in Gol-E-Gohar Iron mine, Iran. To achieve their aim, a total of 115 blasting dataset were monitored and collected from the mine, 80% (92 data sets) of which were used to develop the various predictive models whereas the remaining 20% (23 data sets) were independently used to assess the performance of the developed models. The various predictive models had distance from the blast-face and maximum charge per delay as their input parameters with peak particle velocity (PPV) as their output parameter. The authors then adopted RMSE, VAF and R^2 to evaluate the accuracy of the various developed models. The obtained results on the testing data sets showed that, the ANFIS model was superior in predicting blast-induced ground vibration than the ANN and the empirical model. This was because, the ANFIS model had the highest R^2 value of 0.952 while the R^2 values of 0.888 and 0.749 were obtained by the ANN and empirical models respectively.

Tiile (2016) developed a three-layer feed forward back propagation neural network (BPNN) model to predict blast-induced ground vibration in a gold mine in Ghana. To check the accuracy of the BPNN model, empirical models of USBM, Ambraseys–Hendron, Langefors–Kihlstrom and Indian Standard as well as a multivariate regression analysis (MVRA) model, were developed. The author used a total of 180 data sets, from which 126 representing 70% of the entire blasting data sets were used to develop (train) the various models. Twenty-seven (27) representing 15% of the entire blasting data sets were used as the validation data sets while the remaining 27 data sets were used to test the developed models. In constructing the BPNN model, maximum charge per delay, distance from blast to monitoring point, hole depth, stemming length, hole diameter, powder factor and spacing to burden ratio were the considered input parameters whereas PPV was the output parameter. The obtained predicted PPV on testing data sets in comparison with the measured showed the greater capability of the ANN model at predicting blast-induced ground vibration than the empirical models.

Monjezi *et al*. (2016) applied the gene expression programming (GEP) to predict blast-induced ground vibration using blasting data sets from Chadormalu iron mine, Iran. To check the predictive capability of the GEP model, a modified USBM, USBM, Ambraseys-Hendron, Langefors-Kihlstrom and Indian Standard as well as Linear and non-linear multiple regression models were developed. The authors used 35 blasting data sets for the training and testing of the developed models. Using model performance evaluation criteria of R^2, RMSE and VAF, it was found out that the GEP model had the highest predictive capability relative to the other predictive models. This is because it had the highest R^2 and VAF values of 0.918 and 90.879% respectively and the lowest RMSE value of 2.321.

In Amiri *et al*. (2016), a novel combination of artificial neural network (ANN) and K-nearest neighbors (KNN) models was developed and applied to predict blast-induced ground vibration using 81 data sets from the Shur river dam, Iran. To check the performance of the ANN-KNN model, a pre-developed ANN as well as the empirical equation USBM, was developed to predict blast-induced ground vibration. In constructing the predictive models applied in their study, maximum charge per delay (MC) and distance between blast face and monitoring station (D) were used as input parameters, peak particle velocity (PPV), serving as the output parameter. Sixty-one (61) data sets out of the 75 were used as training data sets to develop and train the various predictive models whereas the remaining 20 data sets were used to test the performance of the developed models. Using R^2, RMSE and VAF as the statistical performance measures of the various predictive models, the prediction results revealed that, the ANN-KNN had the highest R^2 and VAF values and lowest RMSE values in blast-induced ground vibration prediction. The ANN-KNN model was then followed by the pre-developed ANN and then the USBM models in that order.

Faradonbeh *et al*. (2016) developed and applied gene expression programming (GEP) model to predict blast-induced ground vibration using blast data from a quarry in Malaysia. To check the performance of the GEP model, a nonlinear multiple regression (NLMR) model was also developed. In that regard a total of 102 blast dataset were collected from the quarry site. Burden-to-spacing ratio, hole depth, stemming, powder factor, maximum charge per delay and the distance from the blast face were considered as input parameters in the construction of the GEP model. The authors used 20 data sets representing 20% of the total data sets for testing and validation purposes whereas the remaining 80% (82 data sets) was used to GEP and NLMR models. Considering testing data sets, values of 0.874, 87.107,

0.851 and 0.963 were obtained for R^2, VAF, MAE, and RMSE, respectively, by the GEP model, whereas values of 0.790, 69.261, 1.221 and 1.498 were obtained for R^2, VAF, MAE, and RMSE, respectively, by the NLMR technique. This obtained results indicate higher degree of prediction accuracy by the GEP model.

In Hasanipanah *et al*. (2017c), a classification and regression tree (CART) model was developed to predict blast induced ground vibration at Miduk copper mine, Iran. They also developed a multiple regression model and empirical models of USBM, Davies *et al*. (1964), Ghosh and Daemen (1983) and Gupta *et al*. (1987) to serve as comparators to the CART model. A total of 86 blasting events were used in the development and testing of the various models with distance between blast-face and monitoring station (m) and maximum charge used per delay (kg) being the input parameters. Sixty-nine (69) data sets, representing 80% of whole data sets were selected randomly to train the model and the remaining 17 data sets were used to evaluate the performance of the developed models. Using R^2, NS, RMSE as the statistical performance measure, it was found out that the CART technique with a R^2 of 0.95, NS of 0.17 and RMSE of 0.17 outperformed the empirical and multiple regression models and hence was superior in predicting blast-induced ground vibration to the empirical and multiple regression models.

Shahnazar *et al*. (2017) proposed a hybrid model of adaptive neuro-fuzzy inference system (ANFIS) optimised by particle swarm optimization (PSO) to predict blast-induced ground vibration in Pengerang granite quarry, Malaysia. To check the performance of the PSOANFIS model, ANFIS and USBM models were also developed. To achieve their aim, a total of 81 data sets were monitored and collected. Sixty-five (65) of which were used to construct the various predictive models. The remaining 16 data sets were used to test the performance of the developed models. Maximum charge per delay (kg) and distance between monitoring station and blasting-point were the input parameters considered for the development of the aforementioned models. Using VAF, mean absolute bias error (MABE) and median absolute error (MEDAE) as model performance indices, the prediction results showed that the PSO-ANFIS model had superior predictive capability in comparison to ANFIS and empirical models. This is because the PSO-ANFIS model had the highest VAF values of 98.35% and the lowest MABE and MEDAE of 0.78 and 0.58 respectively.

Taheri *et al*. (2017) proposed a combination of artificial bee colony (ABC) and artificial neural network (ANN) for the prediction of blast-induced ground vibration at Miduk copper mine, Iran. They also developed ANN and empirical models of USBM, Ambrasey-Hendron, Davies *et al*. (1964) and Indian Standard, to evaluate the accuracy of the proposed ABC-ANN model. Maximum charge per delay (kg) and distance between monitoring station and blasting-point were the input parameters considered for the development of the aforementioned models. A total of 89 data events were used in the development (training) and testing the various models under consideration. Training was done using 71 of the 89 data sets whereas the remaining 18 data sets were used to independently test the developed models. Based on the statistical assessment of the prediction results using RMSE, MAPE and R^2, it was found out that the ABC-ANN model had the lowest RMSE and MAPE of 0.22 and 4.36 respectively and the highest R^2 value of 0.92. It was concluded that the ABCANN model is comparatively better at prediction of PPV than ANN and empirical models.

Fouladgar *et al*. (2017) proposed a novel swarm intelligence algorithm based on cuckoo search (NSICS) to create a precise equation for predicting the blast-induced ground vibration in Miduk copper mine, Iran. To check the accuracy of the NSICS model, empirical models of USBM, Ambraseys–Hendron, Langefors–Kihlstrom, Davies *et al*., Roy, Gupta, and Rai-Singh were also developed. To develop the various predictive models, 85 blasting data sets were considered with maximum charge used per delay and distance between blast face and monitoring station being the input parameters. Using the R^2 and RMSE as the performance indices for the various predictive models, the obtained results showed that the NSICS had the highest R^2 value and lowest RMSE value followed by Rai-Singh, then Gupta, Roy, Davies *et al*., Langefors–Kihlstrom, Ambraseys–Hendron, USBM in that order.

Chandar *et al*. (2017) applied ANN to predict blast-induced ground vibration in three different mines. For comparison purposes, a USBM based predictor, multilinear regression (MLR), nonlinear regression (NLR) models were developed for each mine. In that regard, a total of 168 data sets were collected from the three mines. In the development of the various models, maximum charge per delay, distance and scaled distance were used as input parameters whereas PPV was used as the output parameter. Using R^2 as the statistical performance index, the obtained results showed that, in relation to the data from three mines, the ANN model was able to accurately predict blast-induced ground vibration better than

the predictor equation, multilinear regression (MLR), nonlinear regression (NLR) models as it had the highest R^2 values.

Xue *et al*. (2017) developed and applied ANFIS to predict blast-induced ground vibration. A total of 25 data sets were selected. The first 20 of which were used to train the ANFIS model whereas the remaining five (5) were used to test the developed ANFIS model. Hole depth, burden, spacing, stemming, maximum charge per delay, total charge and distance, were considered as the input parameters to the ANFIS model, whereas the PPV was used as the output parameter. Prediction results based on the testing dataset showed that the ANFIS model was 100% accurate at predicting the PPV. Indicating that, the ANFIS model is a good tool to predict blast-induced ground vibration.

Hasanipanah *et al*. (2017d) developed and applied an AI model based on particle swarm optimization (PSO) approach to predict blast-ground vibration in Shur River dam region, Iran. In constructing the PSO model, two forms of PSO models which are PSO-linear and PSO-power were developed. A total of 80 data sets were collected for the model development and testing. In developing the PSO models, maximum charge weight per delay and distance between blast-point and monitoring station were used as the input parameters and peak particle velocity (PPV) as the output parameter. To ascertain the predictive strength of the PSO models, multiple linear regression model (MLR) and USBM equation were also developed. Using R^2, RMSE, VARE and NS as the statistical measures of accuracy, the obtained prediction results revealed that the PSO power model was more accurate at predicting blast-induced ground vibration than the PSO linear, MLR and USBM models in that order. The reason being, the PSO linear had the highest R^2 and NS values of 0.934 and 0.94 respectively and lowest RMSE and VARE values of 0.24 and 0.13 respectively.

In Faradonbeh and Monjezi (2017), an optimised gene expression programming (GEP) model using cuckoo optimisation algorithm (COA) was developed to predict blast induced ground vibration with blast data from Gol-E-Gohar iron mine, Iran. In the first step of their work, a gene programming model was developed. Capacity of the GEP model was checked by developing non-linear multiple regression (NLMR) model and five conventional equations. To achieve that aim, a total of 115 blast data were used for the development and testing of the various predictive models, with burden, spacing, stemming, hole-depth, hole

50

diameter, powder factor, maximum charge per delay and distance from the blast face serving as the input parameters to the models while measured PPV was the output parameter. In analysing the performance of the developed models, authors applied the R^2, RMSE, and MAE. The obtained results showed that, the superiority of the GEP in estimating blast-induced ground vibration, as it had the highest R^2 value of 0.874 and lowest RMSE and MAE values of 6.732 and 5.164 respectively. In the second step of their work, eight different strategies based on COA were proposed to optimize blasting patterns. This was aimed at optimising the GEP model in estimating blast-induced ground vibration. Their final results revealed that, introduction of the COA model greatly reduced the PPV values.

Jiang *et al*. (2018) developed and applied ANFIS to predict blast-induced ground vibration in Shur River Dam area, Iran. In ascertaining the performance of the ANFIS model, a linear regression model was also developed. For their work, a total of 90 blast data sets were collected from the site for the development and testing of the predictive models with maximum charge weight per delay and distance between blast-point and monitoring station serving as the input parameters. Comparison of the prediction results using the R^2, RMSE and VAF, revealed the higher prediction accuracy by ANFIS model than the linear regression model. The reason being the ANFIS model had R^2, RMSE and VAF values of 0.983, 0.241 and 98.3 respectively whereas the linear regression model had R^2, RMSE and VAF values of 0.876, 0.0.577 and 87.6 respectively.

In Hasanipanah *et al*. (2018), a new hybrid model of fuzzy system (FS) designed by imperialistic competitive algorithm (ICA) is proposed and applied for the prediction of blast-induced ground vibration resulting from blasting at Miduk copper mine, Iran. To check the predictive capability of the novel FS-ICA model, empirical models of USBM, Ambraseys-Hendron, Langefors-Kihlstrom and Indian Standards were also developed. To achieve their aim, a total of 50 data sets were monitored and collected. Forty (40) of which was used to construct FS-ICA and empirical models. The remaining 10 data sets were used to independently ascertain the performance of the various predictive models. Maximum charge per delay (kg) and distance between monitoring station and blasting-point were the input parameters considered for the development of the aforementioned models. Using R^2, RMSE and VAF as model performance indices, the prediction results showed that the FSICA model had superior predictive capability in comparison to the empirical models.

This is because the FS-ICA model had the highest R^2 and VAF values of 0.94 and 94.2% respectively and the lowest RMSE of 0.22.

Armaghani, *et al*. (2018), investigated the potential of imperialist competitive algorithm (ICA) in predicting blast-induced ground vibration at three quarry sites, namely Ulu Tiram, Pengerang and Masai in Malaysia. In constructing the ICA model, two forms of ICA model which are ICA -power and ICA-quadratic were developed. To ascertain the predictive capability of the ICA models, empirical equations models of USBM, Langefors-Kihlstrom, Roy and Rai-Singh were also developed. To achieve that aim, a total of 73 data sets were used. In developing the various predictive models, maximum charge weight used per delay (W) and the distance between blasting sites and monitoring stations (D) were used as input parameters whereas measured PPV values were set as output parameters. Using R^2 and RMSE as the statistical performance measures of the accuracy of the ICA and empirical models, the obtained results indicated that the ICA-quadratic model with R^2 of 0.94 and RMSE of 0.37 was more accurate at predicting blast-induced ground vibration than the ICApower and empirical models.

Sheykhi *et al*. (2018) proposed a novel hybrid model of support vector regression (SVR) and fuzzy C-means clustering (FCM) for the estimation of blast-induced ground vibration. To check the performance of the SVR-FCM model, comparator models of SVR (without data clustering) and USBM (with and without data clustering) were also developed. In that regard, a total of 120 data sets were collected from Sarcheshmeh copper mine, Iran. A traintest technique was adopted to develop and check the performance of the developed models. To that aim, 102 data sets representing 85% of the entire data sets were used to develop the models. The remaining 18 data sets served as an independent assessor of the developed models. The input parameters considered in the model development were maximum charge per delay and distance from blast location to monitoring point, even though 6 input parameters were collected. Using RMSE, VAF, and R^2 as the statistical indicators of model performance, the obtained results showed that, the FCM-SVR outperformed the SVR, FCMUSBM and USBM in that order. The reason being that, it had the highest R^2 and VAF (%) of 0.853 and 85.25 respectively and lowest RMSE of 1.80.

Ragam and Nimaje (2018) developed a three-layer feed-forward back-propagation multilayer perception neural network to predict blast-induced ground vibration in an Iron

ore mine in India. To provide an inspection of the efficiency and accuracy of the developed ANN model, seven conventional predictor models of USBM, Ambraseys–Hendron, Langefors–Kihlstrom, general predictor, Ghosh–Daemen predictor, cardiac magnetic resonance imaging (CMRI) predictor, Bureau of Indian Standards, as well as multiple linear regression (MLR) model were also developed to predict blast-induced ground vibration. A total of 25 blasting data sets were collected, from which 20 data sets were used to develop (train) the various models. The remaining 5 data sets were used to test the performance of the developed models. In constructing the ANN and MLR models, the authors considered distance from blast face, maximum charge per delay, spacing, burden, hole depth and the number of holes as the input parameters with PPV as output. Using R^2 and RMSE as the statistical measure of model's performance, the obtained results based on the testing data sets revealed that the developed ANN model with structure 6-10-1 (6 inputs, 10 neurons in hidden layer and 1 output) can predict the PPV more efficiently and accurately than the empirical predictors and MLR model. The reason being, the ANN had the highest R^2 value of 0.9971 and lowest RMSE value of 0.08133.

Iramina *et al*. (2018) applied ANN to predict blast-induced ground vibration at a Brazilian mining site. For comparison purposes, empirical attenuation (AE) equation based on USBM approach was also developed. Also, empirical equations as based on the Geological Strength Index (GSI) and Rock Quality Designation (RQD) were applied to predict blast-induced ground vibration. In the development of the ANN model, three input parameters: maximum charge per delay, distance and total charge of explosives were considered. Using RMSE as the statistical performance indicator, the obtained results showed that, the ANN had the lowest RMSE of 3.25. This was followed by the AE equation with a RMSE of 3.63, then the GSI approach (4.36) and RQD approach (7.81). These obtained valued indicated that the ANN was best at predicting blast-induced ground vibration than the other predictive methods applied in their study.

In Zhongya and Xiaoguang (2018), novel ANN methods optimised by dimensionality reduction of Factor Analysis and Mean Impact Value (FA-MIV) were proposed to predict blast-induced ground vibration. In their study, predictive models of BPNN (with and without FA-MIV), Extreme learning machine (ELM) (with and without FA-MIV) and multivariate regression analysis (MVRA) (with and without FA-MIV), were developed and applied. To achieve their aim, a total of 108 data sets were collected, 98 of which were used

to develop the various models and the remaining 10 data sets were used to test the developed models. To construct the various models, the authors considered maximum amount of charge at one time, total amount of charge, horizontal distance, elevation difference, front row resist line, presplit penetration ratio, integrity coefficient, angle of minimum resistance line to measured point and detonation velocity. Also using the FA-MIV approach, the dimensions of the input parameters were reduced to 6 factors of which 4 factors were used as new inputs to the models with FA-MIV. Using R^2 and mean absolute error (MAE) as the statistical performance indicators for the various predictive models, the obtained results showed that the ELM with using FA-MIV had the highest R^2 and MAE values of 0.9603 and 0.2161 respectively. That was followed by the ELM without using FA-MIV, then BPNN with FA-MIV, BPNN without using FA-MIV, MVRA with FA-MIV and MVRA without using FA-MIV. This indicated that per their study, ELM with FA-MIV was most accurate at predicting blast-induced ground vibration than the other predictive models.

Mokfi *et al*. (2018) applied group method of data handling (GMDH) as a novel approach to predict blast-induced ground vibration from a quarry in Penang, Malaysia. For comparison purpose, gene expression programming (GEP) and non-linear multiple regression (NLMR) models were also developed for blast-induced ground vibration prediction. A total of 102 blasting events were monitored and collected from the quarry. Eighty-two (82) representing 80% of the whole data sets were used to train the GMDH model whereas the remaining 20% (20 data sets) were used to test the trained model. In constructing the GMDH model, authors selected stemming length, powder factor, burden to spacing ratio, distance from the blast face, blast-hole depth and maximum charge per delay as the input parameters, with PPV values as the output parameter. Using R^2, RMSE, MAE and VAF as statistical evaluator of model performance, the obtained results on testing dataset indicated that the GMDH model had superior predictive capability in comparison to the GEP and NLMR models. This is because the values of R^2, RMSE, MAE and VAF by GMDH model were 0.911, 0.889, 0.68 and 90.52 respectively. From the GEP model, the values of R^2, RMSE, MAE and VAF were 0.874, 0.963 and 0.851, 87.107 respectively. Finally, from the NLMR model, the values of R^2, RMSE, MAE and VAF were 0.790, 1.498 and 1.221, 69.261 respectively.

Shahri and Asheghi, (2018) developed and applied two different ANN-based models (multilayer perceptron (MLP) and generalized feed forward neural network (GFNN)) to predict blast-induced ground vibration at Masjed Soleyman Earth Dam, Iran. To check the

performance of the MLP and GFNN models, empirical models of Ambrasey-Hendron, Nicholas *et al.*, Roy, Langefors-Kihlstrom, Davies *et al.* and Indian Standard were also developed. For that aim, a total of 37 data sets were used to develop the various models. Randomly selected data sets were used to independently test the performance of the developed models. In constructing MLP and GFNN models, maximum charge per delay, distance and total charge were used as input parameters whereas PPV was used as the output parameter. Using MAPE, VAF, RMSE, mean squared deviation (MSD), mean absolute deviation (MAD), R^2, and absolute error (AE) as the statistical criteria for ascertaining the accuracy of the various developed models, the obtained results showed that the ANN-based models of MLP and GFNN were able to predict blast-induced ground vibration than the empirical models, with the GFNN being the most accurate.

Table 3.3 shows a summary of AI techniques used for blast-induced ground vibration Prediction

Table 3.3 Summary of some Research Works Conducted on Blast-Induced Ground Vibration Modelling and Prediction

Researchers	Techniques
Singh, 2004; Singh and Singh, 2005; Khandelwal and Singh, 2006; Khandelwal and Singh, 2007; Mohamed, 2009; Khandelwal and Singh, 2009; Amnieh *et al.*, 2010; Kamali and Ataei, 2010; Monjezi *et al.*, 2010b; Khandelwal *et al.*, 2011; Verma and Singh, 2011; Monjezi *et al.*, 2011; Dehghani and Ataee-pour, 2011; Shuran and Shujin, 2011; Álvarez-Vigil *et al.*, 2012; Mohamad *et al.*, 2012; Monjezi *et al.*, 2013; Kostić *et al.*, 2013; Görgülü *et al.*, 2013; Saadat *et al.*, 2014; Xue and Yang, 2014; Vasović *et al.*, 2014; Lapčević *et al.*, 2014; Parida and Mishra, 2015; Görgülü *et al.*, 2015; Tiile, 2016; Chandar *et al.*, 2017; Ragam and Nimaje, 2018; Iramina, *et al.*, 2018; Shahri and Asheghi, 2018; Mokfi *et al.*, 2018	ANN (BPNN, GRNN, RBFNN, GMDH)

Table 3.3 Continued

Iphar *et al*., 2008; Mohammed, 2011; Fişne *et al*., 2011; Ghasemi *et al*., 2013; Ataei and Kamali, 2013; Armaghani *et al*., 2015a; Ghoraba *et al*., 2016; Xue *et al*., 2017; Jiang *et al*., 2018;	FL, ANFIS
Khandelwal, 2010; Khandelwal *et al* 2010; Khandelwal, 2011; Mohamadnejad *et al*., 2012, Mohammadnejad *et al*., 2012; Hasanipanah *et al*., 2015; Sheykhi *et al*., 2018	SVM, SVR
Hasanipanah *et al*., 2017c	Decision Tree: CART
Monjezi *et al*., 2016; Faradonbeh *et al*., 2016; Faradonbeh and Monjezi, 2017; Fouladgar *et al*., 2017; Hasanipanah *et al*., 2017d; Armaghani, *et al*., 2018	Optimisation: GEP, COA, ICA, PSO, CS
Armaghani *et al*., 2014; Hajihassani *et al*., 2015; Amiri *et al*., 2016; Shahnazar *et al*., 2017; Taheri *et al*., 2017; Hasanipanah *et al*., 2018; Zhongya and Xiaoguang, 2018	Hybrid Models: BPNN-FA-MIV, ELM-FA-MIV, PSO-ANN, FL-ICA, ANN-KNN, PSO-ANFIS, ABC-ANN

NB: artificial neural network (ANN), adaptive neuro-fuzzy inference system (ANFIS), support vector machine (SVM), radial basis function neural network (RBFNN), generalised regression neural network (GRNN), fuzzy logic (FL), extreme learning machines (ELM), particle swarm optimisation (PSO), classification and regression tree (CART), group method of data handling (GMDH), support vector regression (SVR), genetic expression programming (GEP), imperialist competitive algorithm (ICA), cuckoo optimisation algorithm (COA), artificial bee colony (ABC), K-nearest neighbors (KNN), cuckoo search (CS).

3.3.3 Review of Application of Artificial Intelligence in Air Overpressure Prediction

Khandewal and Singh (2005) applied ANN to predict AOp using blasting data from three limestone mines, namely: Gujarat Ambuja Cement, Raipur, Dalla Limestone Mine, Mirzapur, and Magnesite Mine, Pithoragarh. For comparison purposes, a generalised predictor equation and multivariate regression analysis (MVRA) models were also developed. A total of 56 data sets were collected from the three mines, of which 41 data sets were used to construct the various models and the remaining 25 data sets were used to independently assess the performance of the dataset. In constructing the models, authors used maximum charge per delay and distance from blast face to monitoring point as the input parameters. Using *R* and MAPE as the statistical performance indicators for the

various predictive models, the obtained results indicated that the ANN model with R of 0.9574 and MAPE of 2.7437 on testing data sets was most accurate at predicting AOp compared with generalised predictor equation and MVRA models.

Sawmliana *et al*. (2007) applied ANN to predict blast induced air overpressure. The input parameters that were considered include: maximum charge weight per delay, distance of measurement, depth of burial of charge and total charge fired in a round of blast. A total of 95 AOP data sets from these four mines were used in the ANN model. Out of these 95 data sets, 70 data sets, 25 data sets were used for training, validating the developed artificial network model respectively. The 70 data sets for training the ANN model were also used to develop a generalised predictor equation. 15 data sets were selected to test the developed ANN model and the generalised predictor equation. They found out that the air overpressure predicted by ANN was closer to the measured values than those predicted by the generalised equation with a percentage error of 2.05 for the ANN and 5.97 for the generalised equation.

In Kandelwal and Kandar (2011), SVM was applied to predict air overpressure using blast events from three limestone mines in Iran. In their study, maximum charge per delay and distance from blast-face to monitoring station were the input parameters considered in the development of the SVM model. A total of 75 blast events were used for the training and validation of the SVM and a generalised predictor equation, which was used as a tool for comparison. The obtained results based on R^2 and MAPE revealed the superiority of the SVM in predicting AOp as it had a higher R^2 value of 0.855 and MAPE value of 2.10 whereas the generalised predictor equation had an R^2 value of 0.587 and MAPE value of 4.15.

Mohamed (2011) applied ANN and fuzzy logic (FL) to predict AOp in Assiut Cement Company. For comparison purposes, a traditional regression model was developed. In that regard, a total of 136 data sets were collected and used to develop (train) the predictor models. Twenty-six (26) new data sets were collected to independently test the developed models. In constructing the models, charge weight per delay and distance from blast-face to monitoring station were used by authors as input parameters. Authors used VAF and RMSE as statistical performance indicators for the various models. The obtained results based on the testing data sets revelated that, the FL and ANN models were more accurate at predicting

AOp than the traditional regression model. Also, the authors found out that, the fuzzy logic model performed slightly better than the ANN model. These assertions were made because, values of 99.95% and 2.71 were obtained for VAF and RMSE respectively by Fuzzy logic model. Values of 99.94% and 2.90 were obtained for VAF and RMSE respectively by ANN model whereas values of 99.83% and 4.92 were obtained for VAF and RMSE respectively by traditional regression model.

In Hajihassani *et al*. (2014), a novel hybrid AI model of ANN and particle swarm optimisation (ANN-PSO) was developed to predict air overpressure using blast events from four granite quarry sites in Malaysia. For the development of this hybrid model, nine input parameters of hole depth, powder factor, maximum charge per delay, stemming length, burden, spacing, rock quality designation (RQD), number of holes and the distance between blast face and monitoring point with the measured AOp being the output parameter. A total of 62 blast events were used in the training and validation of the trained hybrid PSO-based ANN model. Several empirical formulas were also developed using the same data events to provide a comprehensive assessment of the performance of the hybrid PSO-based ANN model. Prediction results showed that the values of AOp predicted by PSO-based ANN model were much closer to the measured AOp relative to the empirical formulas. This indicates the superiority of the PSO-based ANN model in predicting AOp than the other predictive methods and hence, it was concluded that the PSO-based ANN model is an applicable tool to predict AOp with high degree of accuracy.

In Hajihassani *et al*. (2015), a hybrid model of an ANN and a PSO algorithm was developed and applied to predict air overpressure induced by blasting at Hulu Langat granite quarry site, Malaysia. To check the performance of the PSO-based ANN, several conventional empirical equations were also developed. Eighty-eight (88) data sets collected from the mine site were used to develop the various models. Hole depth, maximum charge per delay, burden-to-spacing ratio, stemming length, sub-drilling, powder factor, RQD, distance between the free face and the monitoring point, and number of holes were used as input parameters, while AOp values were set as output parameter. The prediction results showed that the PSO-based ANN model was more accurate at predicting AOp that the empirical approaches.

Armaghani *et al*. (2015b) developed and applied adaptive neuro-fuzzy inference system (ANFIS) for the prediction of blast-induced air overpressure using blast data from three quarry sites in Malaysia. To check the performance of the ANFIS model, a pre-developed ANN and multiple regression models were also constructed for comparison. In that regard a total of 128 blasting events were monitored and collected from the sites for the development of the various predictive models, with maximum charge per delay, powder factor, burden to spacing ratio, stemming length, and distance between monitoring station and blast face serving as input parameters. Using R^2, RMSE, VAF as the performance indices for all 128 data sets, the obtained results showed that the ANFIS model was superior at predicting AOp as it had the highest R^2 and VAF values of 0.971 and 97.110 respectively and lowest RMSE value of 2.329 in comparison to the other predictive models.

In Armaghani *et al*. (2015c), a novel model of artificial neural network (ANN) optimised by the imperialist competitive algorithm (ICA) was proposed and applied to predict AOp at Harapan Ramai granite quarry site, Malaysia. For comparison purposes, BPNN and generalised predictor equation (GPE) model were also developed. In that regard, 95 blasting data were collected from the site to develop and test the developed models. Input parameters of hole depth, burden, spacing, stemming, maximum charge per delay and distance from the blast-face were considered by the authors, in developing the various models. The obtained results showed that the hybrid ICA-ANN model was more accurate and reliable in predicting AOp than the BPNN and GPE models, as it had the highest R value of 0.984.

Tiile (2016) developed a three-layer feed forward back propagation neural network (BPNN) model to predict AOp in a gold mine in Ghana. To check the accuracy of the BPNN model, empirical model of General predictor as well as a multivariate regression analysis (MVRA) model, were developed. The author used a total of 180 data sets, from which 126 representing 70% of the entire blasting data sets were used to develop (train) the various models. Twenty-seven (27) representing 15% of the entire blasting data sets were used as the validation data sets while the remaining 27 data sets were used to test the developed models. In constructing the BPNN model, maximum charge per delay, distance from blast to monitoring point, hole depth, stemming length, hole diameter, powder factor and spacing to burden ratio were the considered input parameters whereas AOp was the output parameter. The obtained predicted AOp on testing data sets in comparison with the

measured showed the greater capability of the ANN model at predicting AOp than the empirical models.

In Armaghani *et al*. (2016), three non-linear methods of ICA-ANN, ANN and empirical were applied to predict air overpressure in Shur river dam, Iran. A total of 70 data sets were monitored and collected to develop the various predictive models. Maximum charge per delay (kg) and distance between monitoring station and blasting-point were the input parameters considered for the development of the aforementioned models. Using R^2, RMSE and VAF as model performance indices, the testing dataset prediction results indicated that the ICA-ANN model had superior predictive capability in comparison to the ANN and empirical models. This is because the ICA-ANN model had the highest R^2 value of 0.961 whereas R^2 values of 0.886 and 0.882 were obtained for the ANN and empirical methods respectively.

In Mohamad *et al*. (2016), three non-linear methods of empirical, ANN and a hybrid model of genetic algorithm (GA)–ANN were developed and applied to predict air overpressure in Hulu Langat granite quarry site, Malaysia. To achieve that aim, 76 blasting data sets with hole depth, maximum charge per delay, burden, spacing, stemming length, powder factor, and distance from the blast-face as inputs parameters were collected for the mine site. However, in their study, maximum charge per delay and distance from the blast-face were considered as input parameters to the developed models with measured AOp values serving as the output parameter. Fifteen 15 data sets representing 20% of entire data sets were selected randomly as testing data sets, whereas the remaining 61 data sets were used to develop 5 models of each non-linear method. Using R^2, RMSE and VAF as statistical evaluator of model performance, the testing dataset prediction results indicated that the GAANN model had superior predictive capability in comparison to the ANN and empirical models. This is because the GA-ANN model had the highest R^2 value of 0.974 whereas R^2 values of 0.902 and 0.782 were obtained for the ANN and empirical methods respectively.

In Hasanipanah *et al*. (2016a), several non-linear models of ANN, fuzzy systems (FS), ANFIS, empirical models were developed and applied to predict air overpressure using 77 blasting data sets from Miduk copper mine, Iran. The input parameters considered for the development of the various predictive models were the maximum charge per delay and

distance between blast face and monitoring point with the measured AOp values being the output parameter. Sixty-two (62) data sets representing 80% of the total blasting data sets were used to develop and train the various predictive models with remaining 15 (20%) data sets for testing the developed predictive models. During the modelling process, the authors chose 5 different data sets randomly from the total dataset to develop 5 different models for each non-linear model considered in their study. Using the testing data sets, the comparison results based on R^2, VAF and RMSE revealed that, the ANFIS provided highest performance capacity in prediction of AOp. This was followed by the fuzzy systems, ANN and empirical models in that order.

In Amiri *et al*. (2016), a novel combination of ANN and K-nearest neighbors (KNN) models was developed and applied to predict air overpressure using 81 data sets from the Shur river dam, Iran. To check the performance of the ANN-KNN model, a pre-developed ANN and an empirical equation presented by USBM, were developed to predict AOp. In constructing the predictive models applied in their study, maximum charge per delay (MC) and distance between blast face and monitoring station (D) were used as input parameters, with measured AOp values serving as the output parameter. Sixty-one (61) data sets out of the 75 were used as training data sets to develop and train the various predictive models whereas the remaining 20 data sets were used to test the performance of the developed models. Using R^2, RMSE and VAF as the statistical performance measures of the various predictive models, the prediction results revealed that, the ANN-KNN had the highest R^2 and VAF values and lowest RMSE values in air overpressure prediction. The ANN-KNN model was then followed by the pre-developed ANN and then the USBM model in that order. They therefore concluded that, that the acceptability, effectiveness and accuracy in predicting AOp of the ANN-KNN model was better in predicting AOp than ANN and USBM equation.

Hasanipanah *et al*. (2017e) proposed a novel hybrid model of particle swarm optimization (PSO) and support vector regression (SVR) for AOp prediction. Various types of PSO-SVR models based on linear (L), quadratic (Q) and radial basis (RBF) kernel function were developed. In order to evaluate the suitability of the proposed PSO-SVR models, a multiple linear regression model was also developed. A total of 83 data sets were used to develop and test the various predictive models with maximum charge per delay and distance between blast face and monitoring point being the input parameters. Development of the various

models was done using 67 out 83 data sets whereas the remaining 16 were used to test the developed models. The prediction results revealed that all three types of PSO-SVR models outperformed the multiple linear regression model with the PSO-SVR-RBF producing more accurate prediction results than the other predictive results. The reason being that, it had the highest R value of 0.996 and lowest RMSE value of 0.45 which were the performance criteria utilised in their study.

In AminShokravi *et al.* (2018), PSO and ANN models were developed and applied to predict AOp at Shur river dam area, Iran. In constructing the PSO model, three forms of PSO model which are PSO-linear, PSO-power and PSO-quadratic were developed. To check the performance of PSO and ANN models, an empirical model presented by USBM was also developed. To achieve that aim, a total of 80 data sets were utilised for the development and testing of the aforementioned predictive models. Sixty-four (64) data sets were employed in the model development process whereas the remaining 16 data sets were used to independently ascertain the prediction accuracy of the models. Maximum charge per delay, distance between blast face and monitoring point and rock mass rating (RMR) were employed as input parameters for the prediction of the AOp. Using VAF, R^2, mean absolute bias error (MABE) and MSE as the statistical performance measure of the accuracy of the various predictive models, the obtained results indicated the PSO-linear model with R^2 of 0.960, MSE of 4.33, VAF of 95.05 and MABE of 1.67 was more accurate at predicting AOp than the PSO-power, PSO-quadratic, ANN and USBM models in that order. They concluded that, the PSO-based models, especially the PSO-linear model, can be confidently used to predict blast-induced AOp.

Nguyen and Bui (2018) proposed a novel hybrid model of ANN and random forest (RF) to predict AOp using blast data from Nui Beo open-pit coal mine, Vietnam. For comparison purposes, an empirical technique, five ANN and RF models were also developed. To achieve their aim, a total of 114 dataset were collected from the mine site. The maximum explosive charge capacity, monitoring distance, vertical distance, powder factor, burden, spacing, and length of stemming were considered as the input parameters for predicting AOp. Approximately 94 data sets representing 80% of the whole data sets were considered as training dataset to develop the models whereas the remaining 20% (20 data sets) were used to independently assess the performance of the various predictive models. Using R^2,

RMSE and MAE as statistical evaluators of model performance, the testing dataset prediction results indicated that the ANNs-RF model had superior predictive capability in comparison to the ANN and empirical models. This is because the ANNs-RF model had the highest R^2 value of 0.985 and lowest RMSE and MAE values of 0.847 and 0.620 respectively.

Faradonbeh *et al*. (2018) developed and applied genetic programming (GP) and gene expression programming (GEP) to predict AOp due to blasting in Miduk copper mine, Iran. To check the accuracy and reliability of the GP and GEP models, a multiple linear regression (MLR) and three empirical models of National Association of Australian State, McKenzie and USBM were also applied to predict AOp. In that regard, a total of 74 data sets were used to develop (train) the various models whereas a total of 18 data sets were used to test the developed models. Furthermore, maximum charge per delay (MC), distance between the blasting point and monitoring station (D) were used as input parameters whereas AOp was the output parameter. Using R^2, RMSE and MAE as statistical evaluator of model performance, the obtained results based on testing data sets revealed that the GEP was more accurate at predicting AOp than GP, USBM, MLR, National Association of Australian State and McKenzie respectively as it had the highest R^2 (0.941) and VAF (94.12%) and the lowest RMSE (0.06).

Nguyen *et al*. (2018) applied three types of ANN namely: multilayer perceptron neural network (MLP neural nets), Bayesian regularized neural networks (BRNN) and hybrid neural fuzzy inference system (HYFIS), to predict AOp at Deo Nai open-pit coal mine, Vietnam. To achieve that aim, a total of 146 blasting events were collected, of which 118 blasting events representing 80% of the whole dataset were used in constructing the various models and the remaining 20% (28 blasting events) were used to test the developed models. In constructing the models, charge per delay, burden, spacing, length of stemming, powder factor, air humidity, and monitoring distance were selected as input parameters. Using R^2 and RMSE as the performance criteria for the accuracy of the various predictive models, the obtained results indicated the MLP neural nets model with R^2 of 0.961 and RMSE of 2.319 on testing data sets was most accurate at predicting AOp than BRNN and HYFIS models.

In Bui *et al*. (2019), seven AI techniques of random forest, support vector regression, Gaussian process, Bayesian additive regression trees, boosted regression trees, k-nearest neighbors, and artificial neural network (ANN) were developed and applied to predict AOp at Deo Nai open-pit coal mine, Vietnam. To provide an inspection of the accuracy of the AI techniques, an empirical technique was also applied to predict AOp. In that regard, a total of 113 data sets were collected from the study area, from which 97 data sets were used to train (develop) the various predictive models and the remaining 16 data sets were used to independently test the developed models. Using R^2, MAE and RMSE as the performance criteria, the obtained results based on the testing data sets showed that AI techniques provided better performance than the empirical method. Moreover, of the seven AI models, ANN was the most dominant model and the most accurate in predicting AOp.

Gao *et al*. (2019) developed and applied a hybrid model of group method of data handling (GMDH) and genetic algorithm (GA) to predict AOp due to blasting. To achieve this aim, the authors collected a total of 84 data points from the study area from which 67 data sets representing 80% of total data were used for training GMDH-GA. The remaining 17 data points were used to test the developed model. In developing the GMDH-GA models, authors considered maximum charge per delay (MC), distance between the blasting point and monitoring station (D), powder factor (PF) and rock mass rating (RMR) as input parameters whereas AOp value was considered as the output parameter. Using R^2, RMSE and VAF to evaluate the performance of the developed GMDH-GA, it was found out that, the GMDHGA was able to accurately predict AOp as it had a very high R^2 and VAF values of 0.988 and 98.83% respectively and a low RMSE value of 0.915.

Table 3.4 shows a summary of AI techniques used for air overpressure prediction.

3.3.4   Artificial Intelligence Techniques Applied in this Study

This thesis adopted the use of backpropagation neural network (BPNN), generalised regression neural network (GRNN), radial basis function neural network (RBFNN), group method of data handling (GMDH), support vector machines (SVM), and extreme learning machines (ELM), relevance vector machines (RVM), least square support vector machines (LS-SVM), wavelet neural network (WNN), multivariate adaptive regression splines

(MARS) and Gaussian process regression (GPR) for the prediction of blast-induced ground vibration and air overpressure with some techniques being novel as shown in Table 3.5 and Table 3.6.

Table 3.4 Summary of Research Works on Air Overpressure Prediction

Researchers	Techniques
Khandewal and Singh, 2005; Sawmliana *et al*., 2007; Tiile, 2016; Nguyen *et al*., 2018	ANN (MLPNN, BRNN, HYFIS)
Kandelwal and Kandar, 2011	SVM
Mohammed, 2011; Armaghani *et al*., 2015b; Hasanipanah *et al*., 2016a	FL, ANFIS
Faradonbeh *et al*., 2018	Optimisation: GP, GEP
Hajihassani *et al*., 2014; Hajihassani *et al*., 2015; Armaghani *et al*., 2015c; Armaghani *et al*., 2016; Mohamad *et al*., 2016; Amiri *et al*., 2016; Hasanipanah *et al*., 2017e; AminShokravi *et al*., 2018; Nguyen and Bui, 2018; Gao *et al*., 2019.	Hybrid Models: ANN-PSO, ICA-ANN, GA-ANN, PSO-SVR; ANN-KNN; ANN-RF, GMDH-GA
Bui *et al*., 2019	RF, SVR, GPR, BART, BRT, KNN, ANN

NB: artificial neural network (ANN), adaptive neuro-fuzzy inference system (ANFIS), support vector machine (SVM), support vector regression (SVR), fuzzy logic (FL), genetic algorithm (GA), Gaussian process regression (GPR), particle swarm optimisation (PSO), group method of data handling (GMDH), genetic programming (GP), genetic expression programming (GEP), K-nearest neighbours (KNN), random forest (RF), imperialist competitive algorithm (ICA), Bayesian additive regression trees (BART) and boosted regression trees (BRT).

Table 3.5 Applied and Proposed AI Techniques for Blast-Induced Ground Vibration Prediction

Applied AI Techniques	Proposed AI Techniques
Backpropagation Neural Network (BPNN)	Least Square Support Vector Machine (LLSVM)
Radial Basis Function Neural Network (RBFNN)	Wavelet Neural Network (WNN)
Generalised Regression Neural Network (GRNN)	Multivariate Adaptive Regression Splines (MARS)
Group Method of Data Handling (GMDH)	Gaussian Process Regression (GPR)
Support Vector Machine (SVM)	Relevance Vector Machine (RVM)
Extreme Learning Machine (ELM)	

Table 3.6 Applied and Proposed AI Techniques for Air Overpressure Prediction

Applied AI Techniques	Proposed AI Techniques
Backpropagation Neural Network (BPNN)	Radial Basis Function Neural Network (RBFNN)
Support Vector Machine (SVM)	Generalised Regression Neural Network (GRNN)
Gaussian Process Regression (GPR)	Least Square Support Vector Machine (LLSVM)
Group Method of Data Handling (GMDH)	Wavelet Neural Network (WNN)
	Multivariate Adaptive Regression Splines (MARS)
	Extreme Learning Machine (ELM)
	Relevance Vector Machine (RVM)

CHAPTER 4

MATERIALS AND METHODS

4.1   Materials

4.1.1   Data Description

The data sets applied in this research was secondary data. For the ground vibration prediction, the modelling was carried out with a total of 210 blast data set acquired from the Mining Department and the Environmental Department of Ghana Manganese Company Limited (GMC). This data set comprised of the following parameters: number of blast holes, cooperating charge (kg), distance from blasting point and monitoring station (m), hole depth (m), powder factor (kg/m^3), burden (m), spacing (m) and peak particle velocity values (PPV) (mm/s). In the development of the various models for blast-induced ground vibration prediction presented in this study, six out of the eight parameters were used. These parameters are the number of blast holes, cooperating charge (kg), the distance from blasting point and monitoring station (m), hole depth (m), powder factor (kg/m^3) and the PPV value for each blast. The burden and spacing were not considered in the modelling and prediction of the ground vibration. This is because the Mine uses the same values for each blast. Table 4.1 outlines the statistical range of different input and output parameters used for the blast-induced ground vibration prediction

Table 4.1 Statistical Description of the Data Sets for Blast-induced Ground Vibration Prediction

Parameters	Unit	Minimum	Maximum	Average	Standard Deviation
Number of blast holes	-	19	355	122.50	52.37
Cooperating charge	kg	11.60	123.49	90.08	19.54
Distance from blasting point to monitoring station	m	573	1500	915.01	234.62
Hole Depth	m	3.73	12.58	10.45	1.14
Powder factor	kg/m^3	0.10	0.97	0.69	0.15
Peak Particle Velocity	mm/s	0.13	1.65	0.79	0.32

The values for the powder factor (kg/m^3), number of blast holes, hole depth (m) and cooperating charge(kg) were obtained from the designed blasting plans. The distance from blasting point to the monitoring station was found out by the use of Global Positioning System (GPS) measurements. Here, the GPS recorded coordinates between the monitoring station and that of the blasting point were used in calculating the distance. The PPV values were monitored and recorded by the help of a 3000 EZ Plus Portable seismograph which has a single geophone (Figure 2.3). The 3000 EZ Plus device is a one channel seismograph. It is worth noting that the monitoring of the ground vibration was done by spiking the geophone on a firm flat terrain near the closest house of the nearest community to the mining pit. The setup of the 3000 EZ Plus Portable seismograph was done at the same location with varying directions depending on the area of the blast.

For the air overpressure prediction, modelling on the other hand, was undertaken using a total of 171 air overpressure records acquired from the Mining Department of Newmont Golden Ridge Limited (NGRL), Akyem Mine. The data set collected was made up of the following: burden (m), spacing (m), stemming length (m), powder factor (kg/m^3), number of blast holes per blast, cooperating charge (kg); distance between blasting point and monitoring station (m) and air overpressure values for each blast (dB). It is worth mentioning that in the development of the various models for air overpressure prediction, five out of the eight parameters were used. The burden, spacing and powder factor were excluded. The reason being the same values are used for each blast by the Mine. Table 4.2 outlines the statistical range of different input and output parameters used for the air overpressure prediction

Table 4.2 Statistical Range of the Data Sets for Air Overpressure Prediction

Parameters	Unit	Minimum	Maximum	Average	Standard Deviation
Number of Blast Hole	-	35	432	236.71	66.70
Stemming Length	m	3.30	4	3.40	0.11
Coorperating Charge	kg	51.09	188.95	143.78	22.99
Distance	m	1072.50	3062.33	2101.67	495.17
AOp	dB	98.80	108.80	104.39	1.97

It is worth mentioning that the number of blast holes, stemming length (m), cooperating charge (kg) and distance from blasting point to the monitoring station values were obtained from the Minesight software that is used by blast engineers for blast designs. The AOp values were monitored and recorded by the use of an Instantel Minimate Plus seismic monitor which has a single geophone and a microphone (see Figure 2.7).

4.2   Methods

4.2.1   Artificial Intelligence Techniques

This research applied eleven (11) artificial intelligence (AI) techniques to develop prediction models for both ground vibration and air overpressure. The AI techniques considered are the Backpropagation Neural Network (BPNN), Radial Basis Function Neural Network (RBFNN), Generalised Regression Neural Network (GRNN), Wavelet Neural Network (WNN), Group Method of Data Handling (GMDH), Multivariate Adaptive Regression Splines (MARS), Support Vector Machines (SVM), Least Square Support Vector Machines (LS-SVM), Relevance Vector Machines (RVM), Extreme Learning Machines (ELM) and Gaussian Process Regression (GPR). All the models' development based on these aforementioned techniques were carried out using MATLAB program. Methodological explanations of the applied AI techniques are presented as follows.

Backpropagation neural network

The Backpropagation Neural Network (BPNN) is one of the widely used AI techniques for ground vibration and overpressure prediction (Amnieh *et al*., 2010; Saadat *et al*. 2014; Sawmliana *et al*., 2007; Monjezi *et al*., 2010b, Khandelwal *et al*., 2011). The BPNN is a feed forward neural network with input, hidden and output layer as shown in Figure 4.1. However, the BPNN is designed to accommodate more than one hidden layer. Among the layers, the input layer receives external input vector $X_j = \left(X_1, X_2, X_3, ..., X_m \right)^{\mathrm{T}}$ which are assigned to individual weights, w_{ij} with a constant bias term, b_i . The weighted inputs are then transmitted to the hidden layer. The inputs to each neuron in the hidden layer is then transformed by a mathematical non-linear activation function. The activation function preferably used are the hyperbolic tangent sigmoid or the logarithmic sigmoid (Dorofki *et*

al., 2012). The output from the hidden layer, Y_i (Equation (4.1)) is then fed as input to the output layer. In the output layer, the input – output transformation is done by linear activation function to produce a final network output, $\hat{y}$ (Equation (4.2)).

$$Y_i = f\left(\sum_{j=1}^{m}\left(w_{ij}X_j + b_i\right)\right) \tag{4.1}$$

where w_{ij} is the weight connecting the input layer to the hidden layer, b_i is the bias term and $f(\ )$ denotes the transfer function used in the hidden layer.

$$\hat{y} = Y_i \tag{4.2}$$
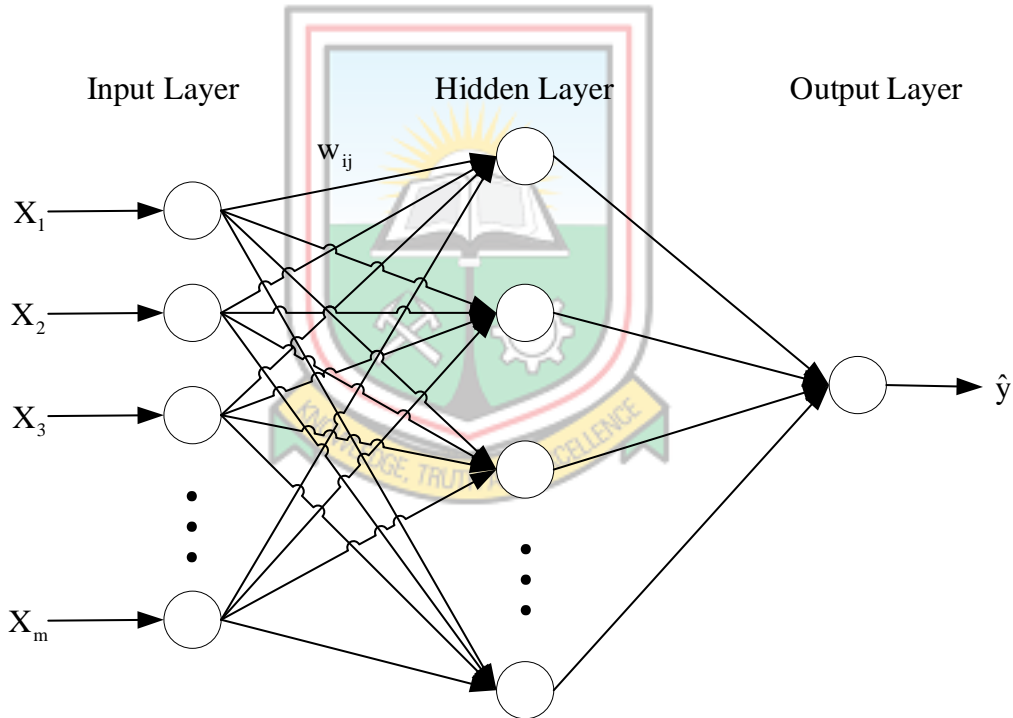
Figure 4.1 BPNN Architecture

The most critical task of designing a BPNN involves the selection of an appropriate training algorithm, transfer function, the number of hidden layers as well as the number of neurons in the hidden layers (Ziggah *et al*., 2016). It has been proven that a BPNN with one hidden layer is sufficient as a universal approximator of any complex problem (Hornik *et al*., 1989; Ziggah *et al*., 2016). Hence, one hidden layer was used in this research.

In this research, the transfer function utilised in the hidden layer for the BPNN model development was the hyperbolic tangent while the linear transfer function was used for the output layer. For the backpropagation training algorithms, Levenberg-Marquardt (Hagan *et al.*, 1996), Bayesian regularization (Foresee and Hagan, 1997) and the scaled conjugate gradient (Møller, 1993) were considered. For each of the training functions, the optimum number of hidden neurons was selected based on an experimental process. That is, the number of hidden neurons that gave the best correlation coefficient as well as the lowest mean squared error (MSE) for both the training and test data set was selected as the optimum, for each training function. The selected architecture for each training function results was then compared to ascertain the best training function and architecture for the BPNN.

It is difficult to know how many iterations will be required before training is stopped hence the maximum number of iterations (number of epoch) is generally set reasonably high (Hagan *et al.*, 1996). If the learning rate is low, then training is more reliable. If the learning rate is high, training may not converge or even diverge. In such situations, the weight changes can be so big that the optimiser overshoots the minimum and makes the loss worse (Surmenok, 2017). A high momentum coefficient can help to increase the speed of convergence of the network. However, setting the momentum coefficient too high can create a risk of overshooting the minimum, which can cause the network to become unstable. A momentum coefficient that is too low cannot reliably avoid local minima, and also can slow the training of the network (Baughman and Liu, 2014). Hence, in this study, the network was trained for 8000 epochs with a learning rate of 0.03 and a momentum coefficient of 0.7 for both the ground vibration and air overpressure modelling. Detailed mathematical treatment on the BPNN can be found in (Hagan *et al.*, 1996; Yegnanarayana, 2005).

Radial basis function neural network

Radial Basis Function Neural Network (RBFNN) is a three-layer feed forward neural network consisting of input layer, a single hidden layer and an output layer. A typical RBFNN architecture of input vector $X_i\left(X_1, X_2, X_3, ..., X_m\right)$, radial basis functions $\left(\varphi_1, \varphi_2, \varphi_3, ..., \varphi_r\right)$, weights $\left(w_1, w_2, w_3, ..., w_r\right)$ and output ($\hat{y}$) is illustrated in Figure 4.2. The input layer serves to transmit inputs from the external environment to the hidden layer

without any weight connections. In each neuron of the hidden layer is a radial basis function which accounts as the non-linear processing element in the hidden layer. There are various types of radial basis functions (Shin and Park, 2000). However, the widely used is the gaussian function (Singla *et al.*, 2007) making it the radial basis function adopted in this study. The Gaussian function responds only to a small input space region where the Gaussian is centred (Poulos *et al.*, 2010). Each neuron then computes a Euclidean distance between each input object and the centre of the Gaussian function. Finding suitable centres for the Gaussian function is required to successfully implement the RBFNN. The Gaussian function is characterised by two parameters, *i.e.* centre, c_j and width parameter σ_j. The computed Euclidean norm is then inserted into the Gaussian function to output net_j as shown in Equation (4.3).

$$net_j = \exp\left(-\frac{\|X_i - c_j\|^2}{2\sigma_j^2}\right) \tag{4.3}$$

where $\|X_i - c_j\|$ is the computed Euclidean distance between X_i and c_j. The input to the output layer is the weighted sum of the outputs of the hidden neurons. This is then processed by a linear function in the output layer to produce the final output, $\hat{y}_k$ of the RBFNN as expressed in Equation (4.4).

$$\hat{y}_k = b_0 + \sum_{j=1}^{r} w_{jk} net_j \tag{4.4}$$

where w_{jk} is the connection weight between the hidden layer and the output layer, b_0 is the bias term and *r* denotes the number of hidden neurons.

The centres, width parameters and a set of weights are adjusted during the training process of RBFNN. This is done with objective function of minimising the mean square error (Equation (4.5)) between the desired output d_k, and the predicted output, y_k.

$$Min \ (MSE) = \frac{1}{N} \sum_{k=1}^{N} \left(d_k - \hat{y}_k \right)^2 \qquad (4.5)$$

where N is the number of observations.
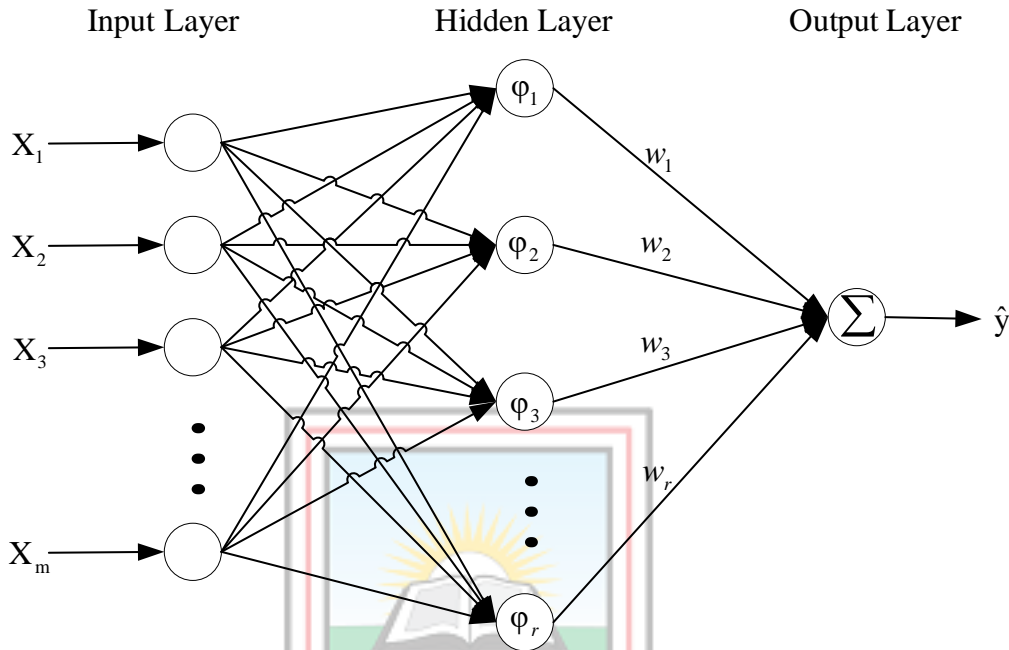
Figure 4.2 RBFNN Architecture

The RBFNN ground vibration and air overpressure was trained using the gradient descent learning algorithm in which the weights are adapted in part to the deviation between the predicted and target outputs. The adjustable parameters that affect the training of the RBFNN are the width parameter and the maximum number of neurons in the hidden layer. Width parameter values of 0.1 to 2 with a step size of 0.1, were investigated for both ground vibration and air overpressure models. The maximum number of neurons of 1 to 20 were also investigated. These range of values for the width parameter and maximum neurons were chosen because the experimental process showed large prediction errors for values beyond them. Hence, the need to settle on the range stipulated for the model building. In choosing the optimum RBFNN architecture, the width value and the maximum number of neurons in the hidden layer that gave the least MSE and largest correlation coefficient in both training and testing data set was selected.

Generalised regression neural network

The Generalised Regression Neural Network (GRNN) is a single pass learning network which consists of the input layer, the pattern layer, the summation layer and the output layer (Figure 4.3). These layers are connected to each other in a feedforward manner. The input layer receives input information and sends to the pattern layer. In the pattern layer, Euclidean distances between each input and stored patterns are calculated. These calculated distances are then fed into a nonlinear activation function. The resulting output is sent to the summation layer. The summation layer consists of the *S*-summation neuron and the *D*-summation neuron. The *S*-summation neuron computes the sum of the weighted outputs of the pattern layer and the *D*-summation neuron calculates the unweighted outputs of the pattern neurons. Finally, the output layer gives the desired estimate, *y(x)* by dividing the output of the *S*-summation neuron by the output of the D-summation neuron as mathematically represented in Equation (4.6) (Specht, 1991).
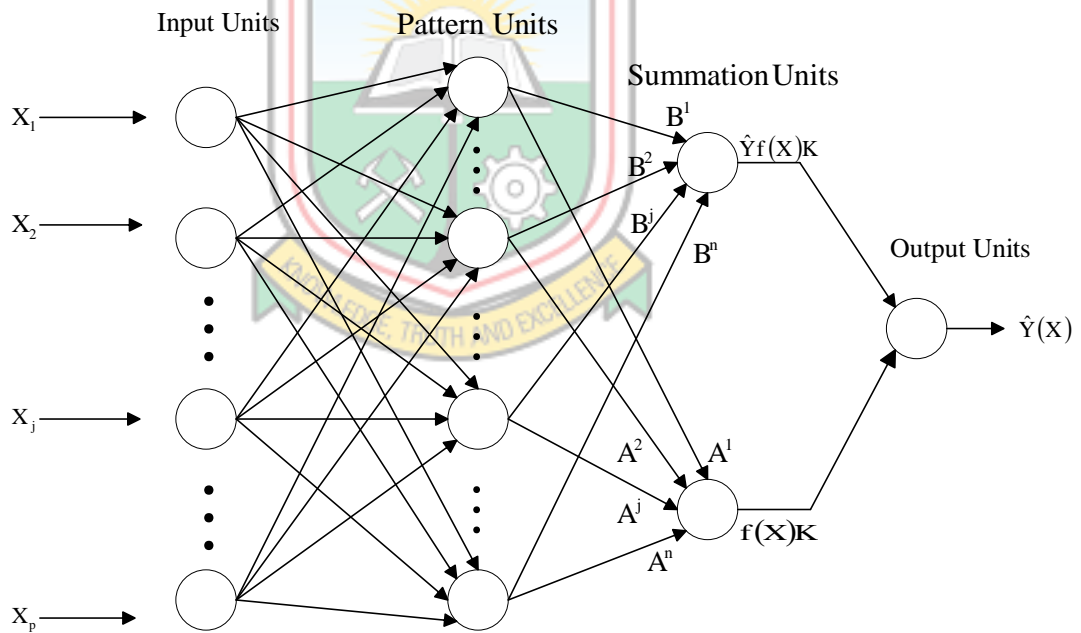
Figure 4.3 GRNN Architecture

$$Y(x) = \frac{\sum\limits_{i=1}^{n} w_i k(x, x_i)}{\sum\limits_{i=1}^{n} k(x, x_i)}$$
(4.6)

where $Y(x)$ is the predicted value of input x, w_i is the activation weight for the pattern layer neurons at i and $k(x, x_i)$ is the radial basis function kernel between input x and training samples, x_i.

In the case of a Gaussian kernel, $k(x, x_i)$ is given in Equation (4.7) as:

$$k\left(x, x_i\right) = e^{-d^2/2\sigma^2} \qquad (4.7)$$

where $d_i = \|x - x_i\|$ is the Euclidean distance between the training samples x_i and the input x and σ is the spread/width parameter. Detailed mathematical description of the GRNN can be found in Specht (1991).

In the GRNN, the adjustable parameters that affect the choice of selecting the optimum GRNN model for both ground vibration and air overpressure prediction is the width parameter. Width parameter values of 0.1 to 1 with a step size of 0.01 were investigated and the value that gave the best correlation coefficient and lowest MSE for both training and testing data sets was chosen as the optimum model.

Wavelet neural network

Wavelet Neural Network (WNN) as proposed by Zhang and Benvenite (1992) is a new class of neural network. It has three layers namely: input, hidden and output layer as shown in Figure 4.4.
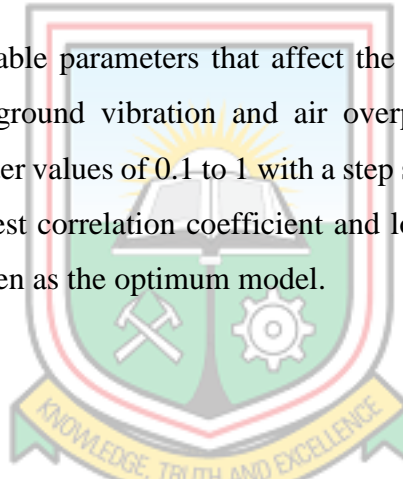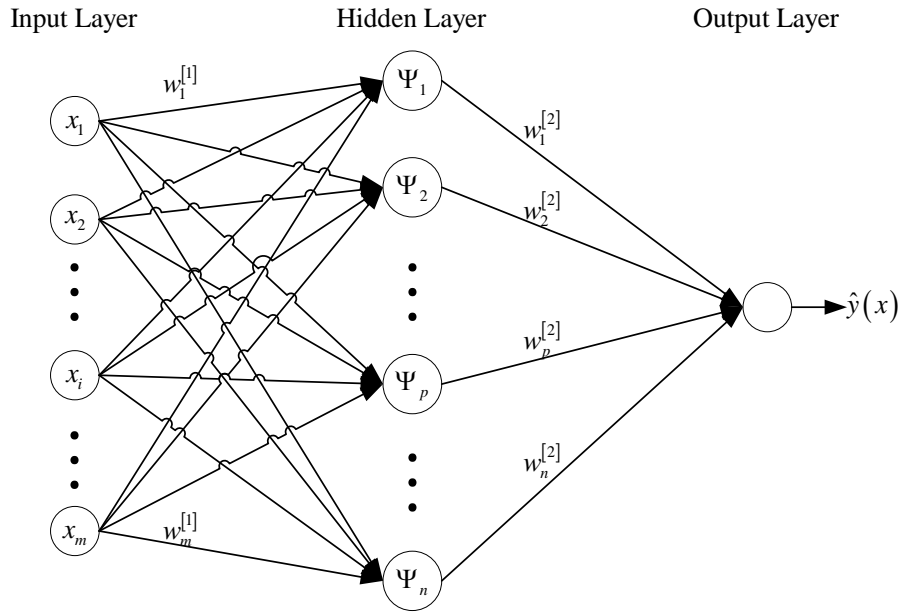
Figure 4.4 WNN Architecture

Its framework was constructed based on Backpropagation Neural Network (BPNN). It however differs from the BPNN in that, it uses wavelet function as the activation function in place of the classic sigmoid function (Wang *et al*., 2013). Given the structure of a WNN with output $\hat{y}(x)$, input vector $\mathrm{x} = (x_1, x_2,...,x_i,...,x_m)$ and *n* number of mother wavelets as shown in Figure 4.4. The inputs are sent to the hidden layer by weighted connections. In the hidden layer, the inputs are processed by a set of wavelet basis functions created by translating and dilating the mother wavelet ψ. According to Alexandridis and. Zapranis (2013), three mother wavelets namely Gaussian, Mexican Hat and the Morlet are usually recommended. The output of the hidden layer, $\Psi_{a,b}(u)$ is given in Equation (4.8).

$$\Psi_{a,b}(u) = \prod_{i=1}^{n} \psi\left(\frac{u - b_i}{a_i}\right) \tag{4.8}$$

where *u* (Equation (4.9)) is the weighted inputs, *a* and *b* are the dilation and translation parameters of the mother wavelet, ψ respectively.

$$u = \sum_{i=1}^{m} x_i w_i^{[1]} \tag{4.9}$$

The output of the hidden layer is then multiplied by connection weights between the hidden and output layer. This serves as input to the output layer. The output of the WNN $\hat{y}(x)$ is given in Equation (4.10).

$$\hat{y}(x) = \sum_{j=1}^{n} w_j^{[2]} \Psi_{a,b}(u) \tag{4.10}$$

It is worth noting that $w_i^{[2]}$, $w_j^{[2]}$, a_i and b_i are the parameters adjusted during the training phase of the WNN development. During the training process, each iteration aims to minimise the error between the actual output $f(x)$ and predicted output $\hat{y}(x)$. The algorithm widely employed to achieve this aim is the back-propagation algorithm (Equation (4.11)).

$$e = \frac{1}{2}\left(f(x) - \hat{y}(x)\right)^2 \tag{4.11}$$

In the development of the WNN model, the Mexican hat wavelet function was used as the activation function in the hidden layer. This is because in comparison to the other mother wavelet functions, the Mexican hat is computationally more efficient and can be differentiated analytically (Jiang and Adeli, 2005). Five inputs and one output variables which were used in this study served as the input and output pattern to the WNN respectively. However, the optimum number of wavelons in the hidden layer was estimated by a sequential trial and error procedure. In view of that 1 to 20 wavelons were experimented. The optimum number of wavelons was selected based on the correlation coefficient and MSE criteria.

Group method of data handling

Group Method of Data Handling (GMDH) technique, developed by Ivakhnenko (1970) is a type of feed forward neural network for modelling non-linear, unstructured and complex systems (Mofki *et al.*, 2018). The technique is a multilayer network comprised of a group of quadratic neurons that are arranged in a special structure to map a given set of input variables into their corresponding target variables. GMDH has the ability to automatically

learn the underlying, complex relations that dominate the system variables in other to select the optimal network structure. This makes the GMDH have a good generalisation ability and can fit the complexity of non-linear systems with a relatively simple and numerically stable network. The GMDH approach is characterised by inductive self-organising procedure used for obtaining multi-parametric model with the feasible variants. This allows the researcher to build models of complex systems without making assumptions about the internal workings. GMDH uses a multilayer network of second order of the Kolmogorov-Gabor polynomial (Equation (4.12)) to define the complex nonlinear relationships among the considered inputs and outputs of a system (Assaleh *et al*., 2013).

$$\hat{y} = a_0 + a_1 x_i + a_2 x_j + a_3 x_i x_j + a_4 x_i^2 + a_5 x_j^2 \tag{4.12}$$

where $\hat{y}$ is the predicted output, a is the vector of the coefficient of the polynomial function, x_i and x_j are the input variables.

It is worth noting that, the number of neurons in a subsequent layer can be excessively large as the number of inputs to the preceding layer becomes large. Such, a neuron selection criterion per layer based on minimising the mean square error ε (Equation (4.13)) between the observed output y_k and predicted output $\hat{y}_k$ is used to keep the network complexity feasible (Assaleh *et al*., 2013).

$$\varepsilon = \frac{1}{N} \sum_{k=1}^{N} \left(y_k - \hat{y}_k \right)^2 \leftarrow \min \tag{4.13}$$

where N is the number of observations.

A GMDH architecture with five inputs and three layers and selected and unselected neurons is shown in Figure 4.5.

| Input Layer | Layer 1 | Layer 2 | Layer 3 | Output Layer |

● Selected

○ Unselected
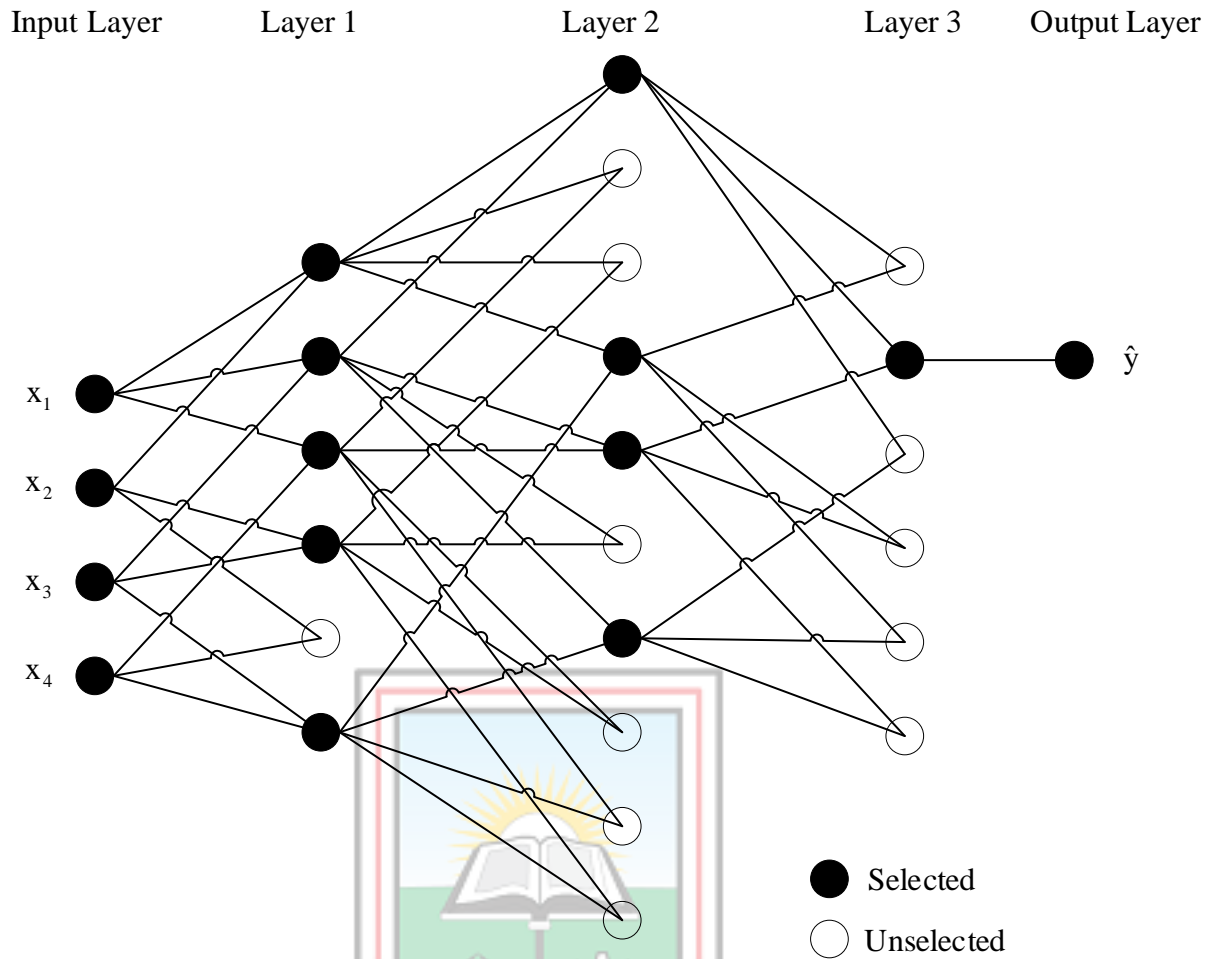
Figure 4.5 GMDH Architecture

Multivariate adaptive regression splines

Multivariate adaptive regression splines (MARS) introduced by Friedman (1991) is a multivariate nonparametric technique. The MARS model does not require any *a priori* assumptions about the underlying functional relationship between input and output variables. That is, the MARS is capable of automatically mapping nonlinear relationship between input and output variables. This relation is uncovered from a set of coefficients and piecewise polynomials of degree *q* (basis functions) that are entirely derived from the regression data (*x, y*). Moreover, the MARS model has the ability to automatically determine both variable selection and functional form, resulting in an explanatory predictive model. The development of this approach has been mainly influenced by recursive partition and adaptive regression splines method. Mathematically, the MARS model can be expressed in Equation (4.14) as:

$$\hat{y} = c_o + \sum_{m=1}^{M} c_m B_m(x) \tag{4.14}$$

where $\hat{y}$ is the dependent variable predicted by the MARS model, c_o is a constant, $B_m(x)$ is the mth basis function, which may be a single spline basis functions and c_m is the coefficient of the mth basis function.

In the model construction phase, the MARS uses a two-step procedure, that is a forward-stepwise regression selection and a backward-stepwise deletion strategy. In the forward process, the MARS starts with a constant in the initial model and iteratively adds pairs of basis functions that will result in the lowest training error to improve the model. This forward stepwise selection of basis function mostly leads to a very complex and overfitted model. Such a forward model, although fits the data well, has poor generalisation abilities when independent data set is introduced to it. To overcome such a problem, the least contributing basis functions are removed one at a time using a backward stepwise deletion strategy. The final MARS model is therefore obtained using the generalised cross-validation (GCV) criteria. The MARS model with the least GCV (Equation (4.15)) error is the optimum.

$$GCV(B) = \frac{\frac{1}{N} \sum_{i=1}^{N} \left[y_i - \hat{f}_B(x_i) \right]^2}{\left[1 - \frac{C(B)}{N} \right]^2} \tag{4.15}$$

where N is the total number of observations of the training data y_i and $\hat{f}_B(x_i)$ are the observed and predicted training output values. $C(B)$ given in Equation (4.16) is a complexity penalty that increases with the number of basis functions in the model.

$$C(B) = (C+1) + d.B \tag{4.16}$$

where B is the number of non-constant basis functions in the MARS model which is proportional to the number of nonlinear basis function parameters, d is a cost for each basis

function optimisation and it is regarded as a smoothing parameter of the process. Larger values of d will lead to fewer knots being placed resulting in smoother function estimates (Friedman, 1991). Detailed mathematical background and theory on MARS can be found in Friedman (1991).

In this study, three different MARS models based on different order of interactions: zero order (no interaction between predictor variables), first order (possible interaction between predictor variables up to two linear members) and second order (interaction between predictor variables up to three linear members) were developed. This was done to determine the optimal MARS model that could accurately predict the ground vibration. In the forward phase of building the MARS model, 20 basis functions were applied. After the forward model was formed, the backward elimination procedure was carried out to remove needless basis functions.

Support vector machine

Similar to the other AI techniques, the Support Vector Machine (SVM) can be used for solving both classification and regression problems with the latter being the main focus of this study. According to Malakar *et al.* (2018), the structure of the SVM is not determined *a priori*. Input vectors supporting the model structure are selected through a model training process. Given a set of training data with input vector $x = (x_1, x_2, ..., x_M)$ with their corresponding target value *f*, an SVM estimator on regression *f(x)* is expressed in Equation (4.17) as:

$$f(x) = w \cdot \phi(x) + b \qquad (4.17)$$

where $w = (w_1, w_2, ..., w_M)$ is a weight vector, $\phi(x) = (\phi(x_1), ..., \phi(x_k))$ is the basis function vector denoting a set of non-linear transformations and *b* is the bias term. The nonlinear basis function $\phi(x)$ maps the *M*-dimensional input vector from a low-dimensional space into a higher dimensional feature space.

It is noteworthy that the objective of SVM is to determine the optimal separating hyperplane that maximises the margin of the training data. In order to obtain a solution to Equation (4.17) so as to find the optimal hyperplane, a quadratic optimisation problem (Equation (4.18)) subject to the constraints in Equation (4.19) with an ε-insensitivity loss function is introduced.

$$\underset{w,b,\xi,\xi^*}{\min \text{imise}} \quad \frac{1}{2}\|w\|^2 + C\sum_{j=1}^{M}\left(\xi_j + \xi_j^*\right) \tag{4.18}$$

$$\text{Subject to} \begin{cases} y_j - w^{\mathrm{T}}\phi\left(x_j\right) - b \leq \varepsilon + \xi_j \\ w^{\mathrm{T}}\phi\left(x_j\right) + b - y_j \leq \varepsilon + \xi_j^* \\ \xi_j, \xi_j^* \geq 0 \end{cases} j = 1, 2, \dots, M \tag{4.19}$$

where ξ and ξ^* are the slack variables that penalises the training errors by the loss function over the error tolerance, ε and C is the positive trade-off parameter that determines the degree of the empirical error in the optimisation. Equation (4.18) subject to Equation (4.19) is usually solved in a dual form (Equation (4.21) subject to Equation (4.22)) using the Lagrangian function and Lagrangian multipliers as defined in Equation (4.20).

$$L = \frac{1}{2}\|w\|^2 + C\left(\sum_{j=1}^{m}\xi_j^* + \sum_{j=1}^{m}\xi_j\right) - \sum_{j=1}^{m}\alpha_j^*\left(y_j - w^T\phi\left(x_j\right) - b + \varepsilon + \xi_j^*\right)$$

$$- \sum_{j=1}^{m}\alpha_j\left(w^T\phi\left(x_j\right) + b - y_j + \varepsilon + \xi_j\right) - \sum_{j=1}^{m}\left(\gamma_j^*\xi_j^* + \gamma_j\xi_j\right) \tag{4.20}$$

where L is the Lagrangian and $\gamma_j, \gamma_j^*, \alpha_j, \alpha_j^*$ are the Lagrange multipliers. It is noteworthy that, the solution of Equation (4.18) must satisfy the Karush-Kuhn-Tucker (KKT) conditions. The input vectors that have nonzero Lagrangian multipliers under the KKT condition support the structure of the estimator and are called support vectors. The architecture of SVM is shown in Figure 4.6.

$$\text{maximise} \quad -\frac{1}{2}\sum_{j,k}^{m}\left(\alpha_j - \alpha_j^*\right)\left(\alpha_k - \alpha_k^*\right)N_{jk} - \varepsilon\sum_{j}^{m}\left(\alpha_j - \alpha_j^*\right) + \sum_{j}^{m}y_j\left(\alpha_j - \alpha_j^*\right) \tag{4.21}$$

$$\text{subject} \begin{cases} \sum_{j}^{m}\left(\alpha_{j}-\alpha_{j}^{*}\right)=0 \\ \alpha_{j},\alpha_{j}^{*}\in[0,C] \end{cases} \qquad (4.22)$$

where $N_{jk}=K\left(x_{j},x_{k}\right)=\phi\left(x_{j}\right)^{T}\phi(x_{k})$ is the kernel trick (Mercer theorem). It is worth noting that the dual variables in Equation (4.20) must satisfy the positivity constraints that $\gamma_{j},\gamma_{j}^{*},\alpha_{j},\alpha_{j}^{*}\geq0.$ The α_{j} and α_{j}^{*} are then computed and the optimum weight vector (w) of the function estimation model hyperplane is given by Equation (4.23) as:

$$w=\sum_{j}^{m}\left(\alpha_{j}-\alpha_{j}^{*}\right)\phi\left(x_{j}\right) \qquad (4.23)$$

Therefore, the SVM estimator on regression applied for this study can be expressed in Equation (4.24) as:

$$f\left(x\right)=\sum_{j}^{m}\left(\alpha_{j}-\alpha_{j}^{*}\right)K\left(x,x_{j}\right)+b. \qquad (4.24)$$

where $K\left(x,x_{j}\right)$ is the kernel function. In general, the common kernel functions treated by the SVM are the functions with the polynomial, Gaussian radial basis, sigmoid radial basis, exponential radial basis, linear among others (Nanda *et al.*, 2018).

In view of that, the Gaussian kernel, polynomial kernel, sigmoid kernel and linear kernel were applied in this study on the dataset with the objective of selecting the kernel function that maps the training data patterns more effectively. The polynomial kernel function, after several trials, was found to accurately fit the pattern in the training data than the other kernels. The polynomial kernel function is mathematically expressed in Equation (4.25) as:

$$K\left(x_{j},x_{k}\right)=\left(1+x_{j}^{T}x_{k}\right)^{q} \qquad (4.25)$$

Furthermore, in the development of the SVM model, the ε and C values of 0.00000001 and 50 respectively were used.

Input Vector   Support Vector   Kernal Function   Output
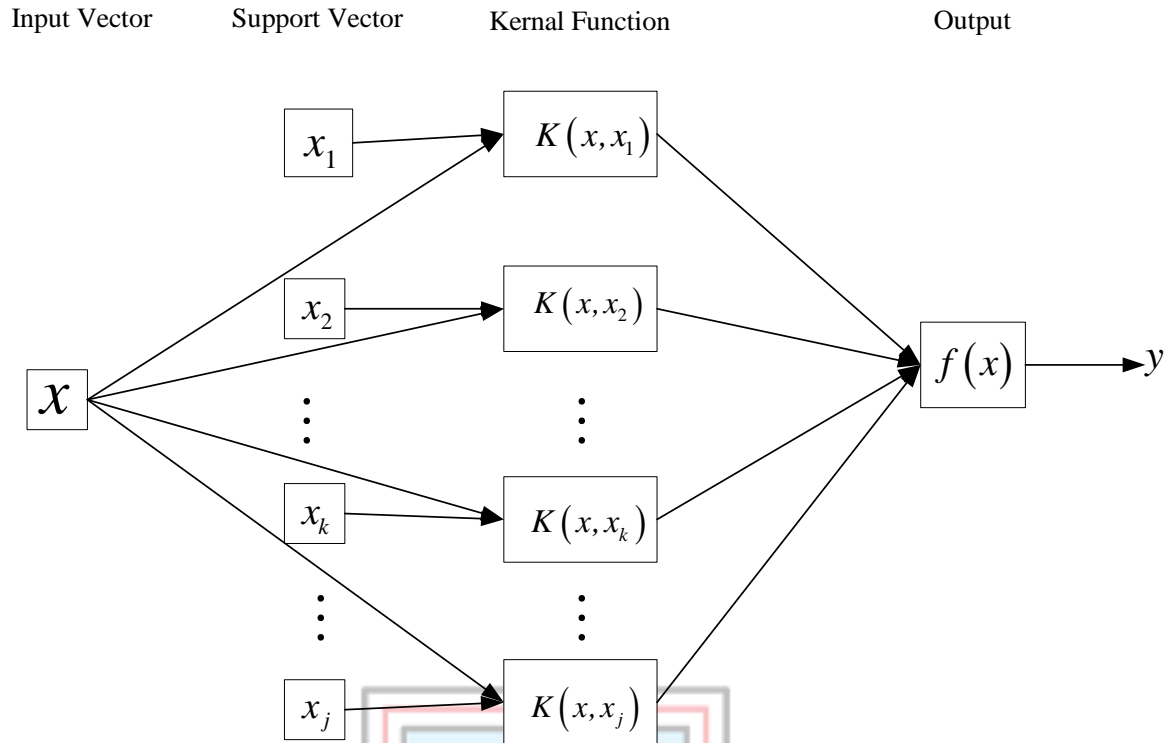
Figure 4.6 SVM Architecture

Least square support vector machine

Least square support vector machines (LS-SVM) proposed by Suyken and Vandewalle (1999) is an alternative formulation of the SVM for classification and regression related problem. In this study, the LS-SVM was formulated as regression technique for the prediction of blast-induced ground vibration and air overpressure. Given a set of N training data $\{x_i, y_i\}_{i=1}^{N}$ with input data $x_i \in R^N$ and corresponding target $y_i \in r$, where R^N is the N-dimensional vector space and r is the one-dimensional vector space. In feature space, the LS-SVM model takes the form of Equation (4.26) as:

$$y(x) = w^T \phi(x) + b \qquad (4.26)$$

where w is the adjustable weight vector, T is the transpose, $\phi(x)$ is the nonlinear mapping that maps the input data into a higher dimensional feature space and b is the scalar threshold.

In line with the structural risk minimisation rule (Suyken *et al.*, 2002), the risk bound is minimised by devising the optimisation problem in Equation (4.27).

84

$$\text{minimise } \frac{1}{2}w^T w + \gamma \frac{1}{2}\sum_{i=1}^{N} e_i^2 \tag{4.27}$$

with the equality constraints (Equation (4.28))

$$y(x) = w^T \phi(x_i) + b + e_i, \quad i = 1, 2, ..., N \tag{4.28}$$

where γ is the regularisation parameter that determines the trade off between the fitting function minimization and flatness, and e_i is the error variable.

In solving Equation (4.27) subject to Equation (4.28), the Lagrangian function L (Equation (4.29)) is used.

$$L(w,b,e,\alpha) = \frac{1}{2}w^T w + \gamma \frac{1}{2}\sum_{i=1}^{N} e_i^2 - \sum_{i=1}^{N} \alpha_i \left[\left(w^T \phi(x) + b \right) + e_m - y_i \right] \tag{4.29}$$

where α_i values are the Lagrange multipliers. The condition of optimality of Equation (4.29) was met by finding the partial derivative of L with respect to each variable as provided by Equation (4.30).

$$\frac{\partial L}{\partial w} = 0 \Rightarrow w = \sum_{i=1}^{N} \alpha_i \phi(x_i)$$

$$\frac{\partial L}{\partial b} = 0 \Rightarrow \sum_{i=1}^{N} \alpha_i = 0$$

$$\frac{\partial L}{\partial e_i} = 0 \Rightarrow \alpha_i = \gamma e_i, \forall i = 1, 2, ..., N \tag{4.30}$$

$$\frac{\partial L}{\partial \alpha_i} = 0 \Rightarrow y_i = w^T \phi(x_i) + b + e_i, \forall i = 1, 2, ..., N$$

Eliminating w and e parameters the linear Karush-Kuhn-Tucker (KKT) system given by Equation (4.31) is obtained instead of quadratic programming (Suyken et al., 2002).

$$\begin{bmatrix} 0 & 1_N^T \\ 1_N^T & \Omega + \gamma^{-1} I_N \end{bmatrix} \begin{bmatrix} b \\ \alpha \end{bmatrix} = \begin{bmatrix} 0 \\ Y \end{bmatrix} \tag{4.31}$$

with $Y = [y_1,..., y_N]^T$, $1_N = [1,...,1]^T$ and $\alpha = [\alpha_1,...,\alpha_N]^T$. Here, I_N is an $N \times N$ identity matric and Ω is the kernel matrix defined by Equation (4.32)

$$\Omega_{ij} = \phi(x_i)^T \phi(x_j) = K(x_i, x_j) \tag{4.32}$$

The radial basis function has been used as the kernel function in this analysis. The radial basis function is given in Equation (4.33) as:

$$K(x_i, x_j) = exp\left\{ -\frac{(x_i - x_j)(x_i - x_j)^T}{2\sigma^2} \right\}, \quad i = 1,..., N \tag{4.33}$$

where σ is the width parameter of the radial basis function kernel.

Equation (4.31) which is a linear equation set corresponding to an optimisation can provide the values of α and b. Thus, the predictive output for LS-SVM is defined in Equation (4.34) as:

$$y(x) = \sum_{i=1}^{N} \alpha_i K(x_i, x_j) + b \tag{4.34}$$

It is noteworthy that the design parameters that affect the development of the LS-SVM are the γ (Equation (4.27)) and σ^2 (Equation 4.33). Hence in this study, the optimum values of these parameters were found iteratively.

Relevance vector machine

The Relevance Vector Machine (RVM) is a Bayesian sparse kernel model that introduces *a prior* distribution over the model weights that are governed by a set of hyper-parameters (Hu and Tse, 2013). The concept of RVM propagate from the concept of linear regression models where the value $y_* = f(x_*)$ of a function $f(x)$ needs to be predicted at some arbitrary point x_*, given a set of typically noisy measurement (Hu and Tse, 2013). This linear regression model is denoted in Equation (4.35) as:

$$y_k = f(x_k) + \varepsilon_k \tag{4.35}$$

where ε_k is the noise component of the measurement. Under the linear model assumption, the function $f(x)$ becomes a linear combination of some known basis function $\phi_k(x)$ as expressed in Equation (4.36).

$$f(x) = \sum_{k=1}^{N} w_k \phi_k(x) \tag{4.36}$$

where $w = (w_1, w_2, ..., w_N)$ is a weight vector. In a vector form, Equation (4.36) can be rewritten into Equation (4.37).

$$y = \Phi w + \varepsilon \tag{4.37}$$

where Φ is $N \times (N+1)$ design matrix, constructed with the kth row vector which is denoted by Equation (4.38) and ε is an additional noise component of the measurement with mean zero and variance σ^2.

$$\Phi_k(x_n) = \left[1, K(x_n, x_1), K(x_n, x_2), ..., K(x_n, x_N) \right] \tag{4.38}$$

In this way, the likelihood of the training data set can be written as (Equation (4.39)):

$$p(y|w, \sigma^2) = (2\pi\sigma^2)^{N-2} \exp\left\{ -\frac{1}{2\sigma^2} \|y - \Phi w\| \right\} \tag{4.39}$$

In the RVM training process, the weight vector w is constrained by putting a zero mean Gaussian prior distribution on it. This is illustrated in Equation (4.40) as:

$$p(w|\alpha) = \prod_{k=1}^{M} N\left(w_k | 0, \alpha_k^{-1} \right) \tag{4.40}$$

where $\alpha_k = (\alpha_1, \alpha_2, ..., \alpha_M)$ is used as a descriptive measure of the inverse variance of each vector w_k.

By Bayes's rule, the posterior probability over all of the unknown parameters can be expressed in Equation (4.41) as:

$$p\left(w, \alpha, \sigma^2 \middle| y\right) = \frac{p\left(y \middle| w, \alpha, \sigma^2\right) p\left(w, \alpha, \sigma^2\right)}{p(y)} \tag{4.41}$$

where p(y) is expressed in Equation (4.42) as

$$p(y) = \iiint p\left(y \middle| w, \alpha, \sigma^2\right) p\left(w, \alpha, \sigma^2\right) dw d\alpha d\sigma^2 \tag{4.42}$$

However, since the normalising integral on Equation (4.42) cannot be executed, the solution of the posterior $p\left(w, \alpha, \sigma^2\right)$ in Equation (4.41) cannot be computed directly. Instead, the posterior is decomposed as shown in Equation (4.43).

$$p\left(w, \alpha, \sigma^2 \middle| y\right) = p\left(w \middle| \alpha, \sigma^2, y\right) p\left(\alpha, \sigma^2 \middle| y\right) \tag{4.43}$$

According to Bayes' rule, the posterior distribution over weights can be expressed in Equation (4.44) as:

$$p\left(w \middle| \alpha, \sigma^2, y\right) = \frac{p\left(y \middle| w, \sigma^2\right) p\left(w \middle| \alpha\right)}{p\left(y \middle| \alpha, \sigma^2\right)} \sim N(m, \Sigma) \tag{4.44}$$

where m (Equation (4.45)) is the mean and Σ (Equation (4.46)) is the covariance.

$$m = \sigma^{-2} \Sigma \Phi^T y \tag{4.45}$$

$$\Sigma = \left(A + \sigma^{-2} \Phi^T \Phi\right)^{-1} \tag{4.46}$$

Here, $A = diag(\alpha) = diag(\alpha_0, \alpha_1, ..., \alpha_N)$. To obtain the marginal likelihood for the hyperparameters, the weights are integrated to obtain the probability distribution over the training targets as expressed in Equation (4.47).

$$p(y|\alpha, \sigma^2) = \int p(y|w, \sigma^2) p(w|\alpha) dw \sim N(0, C) \tag{4.47}$$

where C (Equation (4.48)) is the covariance matrix.

$$C = \sigma^{-2} I + \Phi A^{-1} \Phi^T \tag{4.48}$$

The log probability distribution over the training targets then becomes (Equation (4.49)):

$$\ln p(y|\alpha, \sigma^2) = \frac{N}{2} \ln(\sigma^{-2}) - \frac{1}{2} (\sigma^{-2} y^T y - m^T \Sigma^{-1} m) - \frac{N}{2} \ln(2\pi) + \frac{1}{2} \sum_{k=0}^{N} \ln(\alpha_k) \tag{4.49}$$

Thus, the estimated value of the parameter weights W is given by the mean of the posterior distribution in Equation (4.44), and the hyper-parameters α and σ^2 can be estimated by maximising Equation (4.45). For a new input x_{new}, the probability distribution of the predictor y_{new} is given in Equation (4.50) by:

$$p(y_{new}|x_{new}, \hat{\alpha}, \hat{\sigma}^2) = \int p(y_{new}|x_{new}, w, \hat{\sigma}^2) p(w|y, \hat{\alpha}, \hat{\sigma}^2) dw \sim N(m_{new}, \sigma_{new}^2) \tag{4.50}$$

where the m_{new} (Equation (4.51)) and σ_{new}^2 (Equation (4.52)) are the mean and variance of the predictors respectively.

$$m_{new} = m^T \Phi(x_{new}) \tag{4.51}$$

$$\sigma_{new}^2 = \hat{\sigma}^2 + \Phi(x_{new})^T \Sigma \Phi(x_{new}) \tag{4.52}$$

It is worth mentioning that the adjustable parameter that affects the development of the RVM model is the width parameter (σ) of the Gaussian kernel which was applied in this

study. In this research, the width of the Gaussian radial basis kernel function that gave the highest correlation coefficient value and lowest MSE was determined iteratively.

Extreme learning machines

The Extreme Learning Machine (ELM) is a new learning algorithm for single-hidden layer feedforward neural networks (SLFNs) developed by Huang *et al*. (2006). Unlike the traditional learning algorithms such as the back-propagation which are iteratively used to tune the parameters of the network, the ELM randomly chooses hidden neurons based on Gaussian Probability Distribution and analytically determines the output weights of the SLFNs using generalised inverse method known as Moore-Penrose generalised pseudo inverse (Singh *et al*., 2012).

Given *N* arbitrary training samples (x_k, y_k) where input vector $x_k = [x_{k1}, x_{k2}, ..., x_{kn}]^\mathrm{T} \in R^n$, target vector $y_k = [y_{k1}, y_{k2}, ..., y_{kn}] \in R^m$, a SLFN with $\tilde{N}$ number of hidden neurons and activation function $g(x)$ for the training samples is mathematically modelled using Equation (4.53).

$$\sum_{i=1}^{\hat{N}} \beta_i g\left((w_i \cdot x_k) + b_i\right) = o_k, \forall = k = 1, 2, ..., N \tag{4.53}$$

where $w_i = (w_{k1}, w_{k2}, ..., w_{kn})$ is a weight vector connecting the ith hidden node and the input nodes, $\beta_i = (\beta_{k1}, \beta_{k2}, ..., \beta_{kn})$ is the output weight vector connecting the ith hidden node and the output nodes and b_i is the threshold of the ith hidden node. It is noteworthy that the weight vector w_i are randomly chosen.

The equations formed based on the *N* number of training samples can however be written as (Equation (4.54)):

$$\mathrm{H}\beta = \mathrm{Y} \tag{4.54}$$

where H (Equation (4.55)) is the hidden layer output matrix.

$$H=\begin{bmatrix} g\left(w_1 \cdot x_1 + b_1\right) & \cdots & g\left(w_{\hat{N}} \cdot x_1 + b_{\hat{N}}\right) \\ \vdots & \cdots & \vdots \\ g\left(w_1 \cdot x_N + b_1\right) & \cdots & g\left(w_{\hat{N}} \cdot x_N + b_{\hat{N}}\right) \end{bmatrix}_{N \times \hat{N}} \qquad (4.55)$$

According to Huang *et al*. (2006), if the number $\tilde{N}$ of hidden nodes is equal to the number N of distinct training samples that is $\tilde{N} = N$, then the matrix H becomes square and invertible when the input weight vectors w_i and the hidden biases b_i are randomly chosen. In such situations, SLFNs can approximate the training samples with zero error. In practical applications however, $\tilde{N}$ is usually much less than the number of N distinct training sample.

To train an SLFN with fixed input weights w_i and the hidden layer biases b_i is to find a least square solution $\hat{\beta}$ of the linear system (Equation (4.54). Applying the smallest norm least squares solution of Equation (4.54) the resulting $\hat{\beta}$ becomes Equation (4.56).

$$\hat{\beta} = H^{\dagger} Y \qquad (4.56)$$

where $H^{\dagger}$ is the Moore–Penrose generalized inverse of matrix H (Huang *et al*., 2006).

It is worth noting that, the adjustable parameters in the development of the ELM model are the number of hidden layer neurons and the activation function of neurons in the hidden layer (Jayaweera and Aziz, 2018). For the activation function, sigmoid activation function and sine activation function were considered in this research. For each of the training functions, the optimum number of hidden neurons was selected based on an experimental process. In this research, 1 to 40 neurons were investigated to ascertain the optimum ELM structure. Thus, in choosing the optimum ELM architecture, the number of hidden layer neurons and the activation function of neurons in the hidden layer that gave the least MSE, largest R for testing dataset was selected.

Gaussian process regression

A Gaussian process is a stochastic process (a collection of random variables), such that every finite collection of the random variables has a joint Gaussian distribution (Rasmussen and Williams, 2006). A Gaussian process $t(x)$ is parameterised by a mean function $m(x)$ and a covariance function (or kernel) $k(x, x')$ evaluated at points x and x'. These functions are defined in Equations (4.57) and (4.58) as:

$$m(x) = E(t(x)) \tag{4.57}$$

$$Cov(t(x), t(x')) = k(x, x'; \theta) = E((t(x) - m(x))(t(x') - m(x'))) \tag{4.58}$$

where θ denotes the set of hyperparameters. A gaussian process $t(x)$ is hence expressed in Equation (4.59) as:

$$t(x) \sim GP(m(x), k(x, x')) \tag{4.59}$$

where *GP* stands for Gaussian process. This means that the function *t(x)* is distributed as a Gaussian process with mean *m(x)* and covariance function $k(x, x')$.

Applying the Gaussian Process to solve regression problem is to model the dependence of a response variable *y* on some predictor variables x_i. Each response variable *y* can be related to an underlying arbitrary regression function *t(x)* with an additive independent identically distributed Gaussian noise (ε) which represents the noise component from the data. This is expressed in Equation (4.60).

$$y = t(x) + \varepsilon \tag{4.60}$$

The noise ε has zero mean and variance σ_n^2 that is $\varepsilon \sim N(0, \sigma_n^2)$. The Gaussian process represented in Equation (4.59) becomes Equation (4.61) (Li *et al.*, 2014).

$$t(x) \sim GP(m(x), k(x, x') + \sigma_n^2 I) \tag{4.61}$$

where I is the identity matrix. Based on the additive nature of the noise ε and the marginalization property of GPs, the joint distribution of the training output y at locations X and test outputs f_* at test points X_* is given in Equation (4.62) (Li *et al.*, 2014).

$$\begin{bmatrix} y \\ f_* \end{bmatrix} \sim N\left(\begin{bmatrix} m(X) \\ m(X_*) \end{bmatrix}, \begin{bmatrix} k(X, X + \sigma_n^2 I) & k(X, X_*) \\ k(X_*, X) & k(X_*, X_*) \end{bmatrix} \right) \tag{4.62}$$

Conditioning the joint Gaussian prior distribution based on X, y, and X_*, the predictive distribution is given in Equation (4.63).

$$p(y_* | X, y, X_*) \sim N(\bar{y}_*, \text{var}(y_*)) \tag{4.63}$$

where $\bar{y}_*$ (Equation (4.64)) is the predictive mean and $\text{var}(y_*)$ (Equation (4.65)) is the predictive variance (Li *et al.*, 2014).

$$\bar{y}_* = m(X_*) + k(X_*, X)\left[k(X, X) + \sigma_n^2 I \right]^{-1}(y - m(X)) \tag{4.64}$$

$$\text{var}(y_*) = k(X_*, X_*)\left[k(X, X) + \sigma_n^2 I \right]^{-1} k(X, X_*) \tag{4.65}$$

It is agreeable that covariance function is the central component in a Gaussian process regression model (GPR) (Rasmussen and Williams, 2006). Therefore, selecting the appropriate covariance function is crucial to the determination of the sample function being modelled. Given that the input points which are closely related are likely to have similar target values, likewise, test point near a training point should have a corresponding target value close to the training point. With this analogy, a test point's target value can be predicted. This measure of similarity is expressed by the covariance function (Kang *et al.*, 2015). There are a number of common covariance functions available in literature. Some of these include: Constant covariance function, Linear covariance function, Gaussian noise covariance function, Ornstein-Uhlenbeck covariance function, Squared exponential covariance function, Gamma exponential covariance function, Matérn Class of covariance function, Periodic covariance function, Rational quadratic covariance function and others

(Rasmussen and Williams, 2006). However, it is notable in literature that the squared exponential is the commonly used covariance function (Snelson, 2007).

Therefore, in the training of the GPR model, the parameters of the mean function and covariance (kernel) functions are called the hyperparameters of the Gaussian process (Kang *et al*., 2015). These hyperparameters define the behaviour of the GPR model. In order to train and formulate a GPR model, all the hyperparameters associated with the mean and covariance function must be learned. This can be done through either optimisation or sampling techniques. However, the widely used approach is to maximise the log marginal likelihood (Equation (4.66)) (Rasmussen and Williams, 2006).

$$\log p\left(y|X,\theta\right) = -\frac{1}{2}y^{\mathrm{T}}\left(K+\sigma_n^2 I\right)^{-1}y - \frac{1}{2}\log\left|K+\sigma_n^2 I\right| - \frac{n}{2}\log 2\pi \qquad (4.66)$$

where y^{T} is the transpose of vector y and θ is a vector containing all the hyperparameters.

To maximise the log marginal likelihood, the conjugate gradient method is an efficient gradient based optimisation algorithm that can be used (Moore *et al*., 2016).

In this study, a simple mean function with constant, c was used. For selecting the optimum covariance function for the proposed GPR model in this study, the following covariance functions as expressed in Equations (4.67) to (4.71) (Rasmussen and Williams, 2006) were tried and tested.

i. Squared Exponential Covariance Function

$$k\left(x_i, x_j\right) = \sigma_f^2 \exp\left[\frac{-d^2}{2\ell^2}\right] \qquad (4.67)$$

ii. Exponential Covariance Function

$$k\left(x_i, x_j\right) = \sigma_f^2 \exp\left[-\frac{d}{\ell}\right] \qquad (4.68)$$

iii. Rational Quadratic covariance function

$$k\left(x_i, x_j\right) = \sigma_f^2 \exp\left[1+\frac{d^2}{2\alpha\ell^2}\right]^{-\alpha} \qquad (4.69)$$

iv.   Matérn 3/2 Covariance Function

$$k\left(x_i, x_j\right) = \sigma_f^2 \left(1 + \frac{\sqrt{3}d}{\ell}\right) \exp\left(-\frac{\sqrt{3}d}{\ell}\right)$$

(4.70)

v.   Matérn 5/2 Covariance Function

$$k\left(x_i, x_j\right) = \sigma_f^2 \left(1 + \frac{\sqrt{5}d}{\ell} + \frac{5d^2}{3\ell^2}\right) \exp\left(-\frac{\sqrt{5}d}{\ell}\right)$$

(4.71)

where $d = \left\|x_i - x_j\right\|$ is the Euclidean distance between point x_i and x_j, σ_f^2 is the signal variance of function, α is the shape parameter for the rational quadratic covariance and ℓ is the length scale. Due to the mean function, covariance function and the noisy observations in data, the hyperparameters θ that were optimised in this study include: constant $(c), \sigma_f^2, \ell, \alpha, \sigma_n^2$. σ_n^2 is the noise variance.

4.2.2   Model Development Processes

Selection of input/ output parameters

In the development of the various AI models applied in this study for the ground vibration prediction, five parameters were utilised as the input layer neurons having one output neuron for the AI training. With this in mind, the input layer data consisted of the number of blast holes, cooperating charge (kg), distance between blasting point and monitoring station (m), hole depth (m) and powder factor. The PPV values for each blast were used as the output layer neurons. The burden and spacing were not considered because they were constant for each blast and thus did not have any significant influence on the model prediction results.

The input parameters that were selected for the air overpressure prediction modelling were the stemming length, the number of blast holes per blast, the cooperating charge and the distance between blasting point and monitoring station. The output parameter was the air overpressure values for each blast. Hence, four (4) inputs were used for the development of the AI models with the air overpressure as the output layer data.

Data normalisation

Since the data sets parameters have different values with different units, there is a need to ensure constant variability in the data set by normalising it into the range [-1, 1], [0, 1] or other scaling criteria. This data normalisation improves convergence speed and doing so reduces the chances of getting stuck in local minima (Ziggah *et al*., 2016). In this study, the input variables were normalised into the interval [-1, 1] using Equation (4.72)

$$y_i = y_{min} + \frac{(y_{max} - y_{min}) \times (x_i - x_{min})}{(x_{max} - x_{min})} \tag{4.72}$$

where, y_i is the normalised data, x_i represents the measured blast data, x_{max} and x_{min} represents the maximum and minimum values of the measured blast data with y_{max} and y_{min} values set at 1 and -1, respectively.

Network training and testing

The supervised learning technique was applied to develop the various predictive models. Thus, the data sets were first partitioned into two sets: training and testing based on the widely and successfully used hold-out cross-validation technique. Despite the fact that there is no universally accepted ratio for splitting the data, it is important that the training dataset be more than the testing data set in order to generate good prediction results. However, if the training data is more than enough it will cause overfitting whereby the model cannot perform well with independent data. In that regard, 130 out of the 210 blast data points (representing 62% of the entire blasting data) acquired from Ghana Manganese Company Limited were used as training data set to develop and train the various models for predicting ground vibration in this study. The remaining 80 blast data points were used as testing data set to independently validate the performance of the various developed models.

With regards to the air overpressure modelling, 98 data points out of the 171 (representing 57%) acquired from Newmont Golden Ridge Limited served as the training dataset. The remaining 73 data points were used to test the performance of the developed models.

The partitioning of the entire data sets was done with the aim of avoiding under- and overfitting of the models. To overcome such situations, the training data set was selected according to the rule of being well distributed across the whole data sets in the study area whereas blasting data excluded as training data of the study area were used as testing data set.

4.2.3   Empirical Methods

Ground vibration prediction

There are several empirical equations that are used in prediction of ground vibration (PPV) (Table 3.1). However, the empirical methods that were considered in this research to evaluate the performance of the AI techniques are the United State Bureau of Mines (USBM) model, Ambraseys-Hendron, model Langefors and Kilhstrom model and Indian Standard model (model (Duvall and Petkof, 1959; Langefors and Kihlstrom, 1963; Ambraseys and Hendron, 1968; Indian Standard Institute, 1973). These four empirical predictors were adopted because they have been found in literature (Khandelwal and Singh, 2006, Saadat *et al*., 2014, Mohammadnejad *et al*., 2012, Armaghani *et al*., 2014, Tiile 2016, Ragam and Nimaje, 2018 and references there in) to serve as benchmark methods over the years, when comparisons are being made with artificial intelligence methods applied to predict blast-induced ground vibration. Hence in this research, these aforementioned empirical methods were applied and compared to the various AI techniques. In addition to that, these four empirical predictors were applied because they are the techniques currently used in the Ghanaian mining industry for the prediction of blast-induced ground vibration. The same number of data sets used to train the AI models were also used to determine the site-specific constants of the empirical models (Equations (4.73) to (4.76)).

i.   United State Bureau of Mines (USBM)

$$PPV = k \left[\frac{D}{Q^{1/2}} \right]^{-\beta} \tag{4.73}$$

ii.   Indian Standard

$$PPV = k \left[\frac{Q}{D^{2/3}} \right]^{\beta} \tag{4.74}$$

97

iii. Ambrasey-Hendron

$$PPV = k\left[\frac{D}{Q^{1/3}}\right]^{-\beta}$$ (4.75)

iv. Langefors and Kihlstrom

$$PPV = k\left[\frac{Q^{1/2}}{D^{3/4}}\right]^{\beta}$$ (4.76)

In the above equations, D and Q denotes the distance between the blasting face and the monitoring point and cooperating charge respectively. The term in bracket in the above equations make up the scaled distance (SD). The site constant, k and β were obtained by linear regression analysis. This was done by plotting the PPV against the calculated scaled distance in an excel spreadsheet. The power trendline option was chosen to obtain the equation of the line in the form, $y = ax^b$, where y is the PPV, x is the scaled distance and a and b as the site constants.

Air overpressure

The air overpressure empirical models that were considered are the general predictor equation and the model that is used by Newmont Golden Ridge Limited, Akyem Mine for their prediction of air overpressure. The general predictor equation is expressed in the form of Equation (3.3) as:

$$Aop = H\left(\frac{D}{\sqrt[3]{Q}}\right)^{-\beta}$$

where, D is distance in meters, Q is the maximum instantaneous charge per delay, H and β are site constants.

The sites constants were obtained using the linear regression analysis procedure explained in the determination of the site constants of the ground vibration empirical models. The same data sets used to train the AI models for the air overpressure prediction were also used to determine the site constants of the General Predictor Equation.

The model used to predict air overpressure at Newmont Golden Ridge Limited is given in Equation (4.77) as:

$$AOp = 20 \times \log_{10}\left(\frac{3.3 \times \left(\dfrac{D}{Q^{1/3}} \right)^{-1.2}}{0.00000002} \right) \qquad (4.77)$$

where D is Distance in meters and Q is the Cooperating Charge in kg.

4.2.4 Model Performance Criteria

The prediction accuracies of each of the predictive models for ground vibration and air overpressure at Ghana Manganese Company and Newmont Golden Ridge Limited respectively, were assessed using statistical performance indicators of mean square error (MSE), root mean square error (RMSE), relative root mean square error (RRMSE), mean absolute error (MAE), coefficient of determination (R^2), correlation coefficient (R), Nash-Sutcliffe efficiency index (NASH) and variance accounted for (VAF). Equations (4.78) to (4.85) present their mathematical notations.

$$MSE = \frac{1}{n}\sum_{i=1}^{n}\left(o_i - p_i\right)^2 \qquad (4.78)$$

$$RMSE = \sqrt{MSE} = \sqrt{\frac{1}{n}\sum_{i=1}^{n}\left(o_i - p_i\right)^2} \qquad (4.79)$$

$$RRMSE = \frac{RMSE}{\overline{o}} = \frac{\sqrt{\dfrac{1}{n} \times \sum_{i=1}^{m}\left(o_i - p_i\right)^2}}{\overline{o}} \qquad (4.80)$$

$$MAE = \frac{1}{n}\sum_{i=1}^{n}\left|o_i - p_i\right| \qquad (4.81)$$

$$R^2 = \frac{\left(\sum_{i=1}^{n}\left(o_i - \overline{o}\right)\left(p_i - \overline{p}\right)\right)^2}{\sum_{i=1}^{n}\left(o_i - \overline{o}\right)^2 \times \sum_{i=1}^{n}\left(p_i - \overline{p}\right)^2} \qquad (4.82)$$

$$R = \left(\frac{\sum\limits_{i=1}^{n} (o_i - \bar{o})(p_i - \bar{p})}{\sqrt{\sum\limits_{i=1}^{n} (o_i - \bar{o})^2} \times \sqrt{\sum\limits_{i=1}^{n} (p_i - \bar{p})^2}} \right) \tag{4.83}$$

$$NASH = 1 - \frac{\sum\limits_{i=1}^{n} (o_i - p_i)^2}{\sum\limits_{i=1}^{n} (o_i - \bar{o})^2} \tag{4.84}$$

$$VAF = \left[1 - \frac{var(o_i - p_i)}{var(o_i)} \right] \times 100 \tag{4.85}$$

where *n* is the total number of test samples, o_i are the observed values, *p* are the predicted values $\bar{o}$ is the mean of the observed values and $\bar{p}$ is the mean of the predicted values.

Graphical comparison of the efficiency of the various models in predicting ground vibration was carried out. This was done by plotting the observed PPV against predicted PPV with a 1:1 line, a 95% confidence interval (CI) (Equation (4.86)) and 95% prediction interval (PI) (Equation (4.87)).

$$CI = \bar{p} \pm Z_{\alpha/2} \frac{\sigma}{\sqrt{n}} \tag{4.86}$$

where $\bar{p}$ is the mean of the predicted values, σ is the population standard deviation, $Z_{\alpha/2}$ is the Z value for the desired confidence level α and *n* is the number of predicted values. At a 95% Confidence Interval, $Z_{\alpha/2} = 1.96$.

$$PI = p_i \pm t_{(\alpha/2, n-2)} SD \sqrt{1 + \frac{1}{n} + \frac{(o_i - \bar{o})^2}{\sum (o_i - \bar{o})^2}} \tag{4.87}$$

where *n* is the total number of samples, O_i are the observed PPV values, P_i are the predicted PPV values, $\bar{O}$ is the mean of the observed PPV values, $t_{(\alpha/2, n-2)}$ is the α-level quantile of

a *t*-distribution with n – 2 degrees of freedom, *SD* is the standard deviation of the residuals (Equation (4.88)).

$$s = \sqrt{\frac{\sum(O_i - P_i)^2}{n - 2}}$$

(4.88)

4.2.5 Model Selection

As a means of selecting the most viable blast-induced ground vibration and air overpressure prediction model among the candidate models developed, the Akaike Information criterion (AIC) (Burnham and Anderson, 2002) was applied. The AIC is based on the number of parameters used in a particular model, residual sum of squares and the number of observations used. The model with the lowest calculated AIC value is chosen as the best for predicting ground vibration and air overpressure. The generic form of the AIC is given in Equation (4.89).

$$AIC = n \times \ln\left(\frac{RSS}{n}\right) + 2k$$

(4.89)

where *n* is the number of samples, *k* is the number of estimable parameters in the model, and *RSS* is the residual sum of squares. The residual sum of squares measures the overall difference between the observed values and the values predicted by the developed model.

4.2.6 AI-Based Software Development

After the selection of the most viable blast-induced ground vibration and air overpressure prediction model among the candidate models, a front-end, user-friendly, interactive application software was developed in the MATLAB environment to ask for and upload the data sets and generate the necessary results and graphs automatically. The essence of this AI-based software is to provide the mining engineer prior information about the efficiency of the blast design before blasting. That is, the blast design parameters can be fed into the software to estimate the ground vibration and air overpressure to be recorded if the current

blast is carried out per the design. Figure 4.7 shows the front-end diagram of the AI-based software.
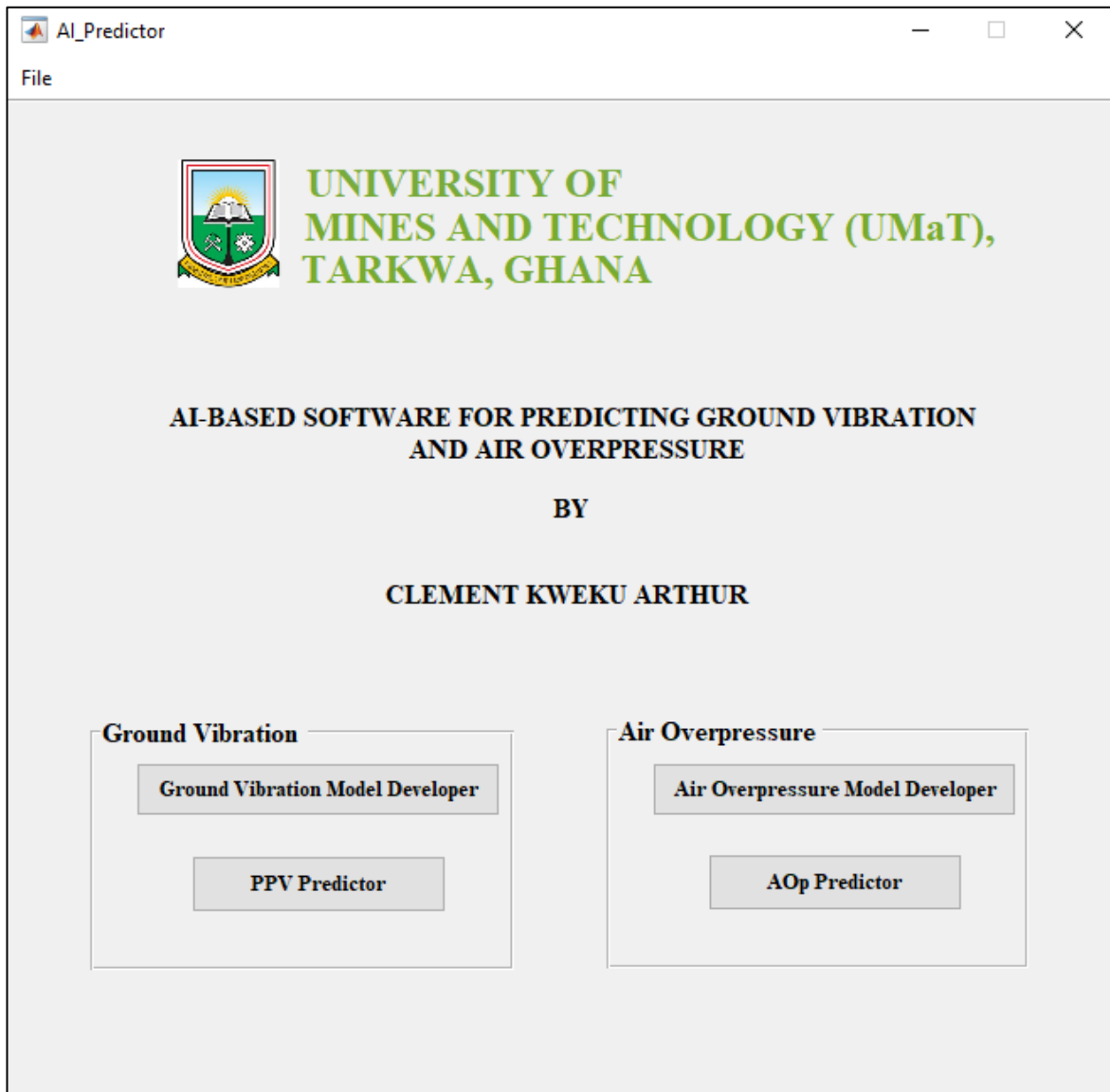
Figure 4.7 Front-end of AI-based Software

CHAPTER 5

INTERPRETATIONS OF BLAST-INDUCED GROUND VIBRATION PREDICTION

5.1 AI Models Developed for Blast-Induced Ground Vibration Prediction

5.1.1 BPNN Model for Blast-Induced Ground Vibration Prediction

Selection of the optimum number of hidden neurons and training function

In this study, different training algorithms were used in the BPNN model formulation. This was necessary because the BPNN is highly dependent on the fine tuning of the training algorithm parameters used to learn the data. Therefore, it was logical to apply and test the capability of different training functions. The results obtained by training the BPNN with different training algorithms and the number of hidden neurons used in the process are presented in Tables 5.1, 5.2 and 5.3 respectively.

Table 5.1 Results of Training and Testing with Levenberg-Marquardt Algorithm

Number of Hidden Neuron	Training		Testing	
	R	MSE	*R*	MSE
1	0.909001	0.020902	0.8537	0.021696
2	0.911621	0.020328	0.8445	0.023054
3	0.932809	0.015626	0.7927	0.029738
4	0.950299	0.011663	0.8031	0.031615
5	0.948547	0.012063	0.7753	0.034545
6	0.959839	0.00947	0.7428	0.040207
7	0.962816	0.008782	0.5732	0.101023
8	0.968806	0.007389	0.2788	4.500762
9	0.974224	0.006123	0.0934	1.107399
10	0.982438	0.004189	-0.19	9.474425
11	0.985522	0.003459	0.509	0.142711
12	0.9880567	0.0028569	0.0118042	1.21E+03

Table 5.2 Results of Training and Testing with Bayesian Regularisation Algorithm

Number of Hidden Neuron	Training		Testing	
	R	MSE	*R*	MSE
1	0.908928	0.020923	0.852883	0.02182
2	0.913343	0.019954	0.847394	0.02234
3	0.919223	0.018657	0.82894	0.02477
4	0.921331	0.018193	0.829543	0.02462
5	0.921282	0.018203	0.829663	0.0246
6	0.917295	0.019082	0.826446	0.02511
7	0.917265	0.019088	0.827089	0.02502
8	0.917236	0.019095	0.827613	0.02495
9	0.91721	0.019101	0.828041	0.02489
10	0.917187	0.019106	0.828394	0.0248
11	0.917167	0.01911	0.828688	0.0248
12	0.917163	0.019111	0.82867	0.0248

Table 5.3 Results of Training and Testing with Scaled Conjugate Gradient Algorithm

Number of Hidden Neuron	Training		Testing	
	R	MSE	R	MSE
1	0.909001	0.020902	0.8537	0.021696
2	0.922895	0.017839	0.8367	0.024232
3	0.924848	0.017405	0.7761	0.031499
4	0.943083	0.013307	0.8188	0.028453
5	0.941094	0.013758	0.78	0.033936
6	0.958204	0.009848	0.7842	0.033777
7	0.969562	0.007213	0.7316	0.055351
8	0.955671	0.010431	0.6154	0.071277
9	0.965633	0.008128	0.5536	0.143387
10	0.981101	0.004505	0.493	0.139806
11	0.984083	0.0038	0.445	0.258246
12	0.977391	0.005379	0.537	0.129354

In Table 5.1, it can be noticed that, for the Levenberg-Marquardt backpropagation algorithm, the optimum number of hidden neurons that gave the highest correlation coefficient (R) and the lowest mean squared error (MSE) for the testing data set was one. In the case of the Bayesian regularisation backpropagation algorithm (Table 5.2), the optimum number of hidden neurons was one. This is because it gave the largest R and the least MSE for the testing data set. From Table 5.3, it can be observed that the optimum neurons that produced the best testing results based on the MSE criterion and R for the scaled conjugate gradient backpropagation algorithm was also one.

A compilation of the optimum BPNN architectures from the various training algorithms applied are presented in Table 5.4. This was necessary to aid in selecting the optimum training function suitable for predicting ground vibration in the area of study. From Table 5.4, it can be noticed that, the Levenberg-Marquardt and the scaled conjugate backpropagation algorithms gave identical and best R and least MSE on the testing data set as compared with the Bayesian algorithm. The interpretation made here is that, the Levenberg-Marquardt and the scaled conjugate backpropagation algorithms were able to learn adequately on the training data and could generalise better on the testing data than the Bayesian technique. Hence, for ground vibration prediction both the Levenberg-Marquardt and scaled conjugate technique could be used. However, the Levenberg-Marquardt backpropagation algorithm was chosen for the study area because it has been used as a benchmark technique to train neural network system.

Optimal BPNN structure

The optimum BPNN structure consisted of three layers: input layer, hidden layer and output layer. The BPNN structure is made up of five inputs with a hyperbolic tangent hidden layer transfer function and a linear output layer transfer function. The network was trained for 8000 epochs using the Levenberg-Marquardt backpropagation algorithm with a learning rate of 0.03 and a momentum coefficient of 0.7. The optimum structure of the BPNN was [5 – 1 – 1] that is five inputs, one hidden neuron and one output.

Table 5.4 Identification of the Best Training Functions for BPNN

Training Function	Optimum Hidden Neurons	Training		Testing	
		R	**MSE**	**R**	**MSE**
Levenberg-Marquardt backpropagation algorithm	1	0.909001	0.020902	0.8537	0.021696
Bayesian Regularisation Backpropagation Algorithm	1	0.908928	0.020923	0.852883	0.02182
Scaled Conjugate Gradient Backpropagation Algorithm	1	0.909001	0.020902	0.8537	0.021696

5.1.2 RBFNN Model for Blast-Induced Ground Vibration Prediction

For the developed RBFNN model for blast-induced ground vibration prediction, the width parameter value and the maximum number of neurons that gave the highest R and the lowest MSE was 1.7 and 9, respectively. Hence, the optimum RBFNN structure selected for predicting ground vibration has five inputs with one hidden layer of 9 neurons and one output layer, that is, [5–9–1]. Table 5.5 present the optimal training and testing results based on the R and MSE criteria. All the width parameters and maximum number of neurons in the hidden layer that were used to arrive at the optimal results are presented in Table A1 of Appendix A.

Table 5.5 Optimal Training and Testing *R* and MSE Results for RBFNN

Width Parameter	Number of Neurons	Training		Testing	
		R	**MSE**	**R**	**MSE**
1.7	9	0.910429	0.020589	0.84764	0.022266

5.1.3 GRNN Model for Blast-Induced Ground Vibration Prediction

For the developed GRNN model for blast-induced ground vibration prediction, the width parameter value that gave the best R and the lowest MSE results is 0.40. Table 5.6 shows the optimal training and testing results. However, all the width parameters that were used to arrive at the optimal results are presented in Table B1 of Appendix B.

Table 5.6 Optimal Training and Testing R and MSE Results for GRNN

Width Parameter	Training		Testing	
	R	MSE	R	MSE
0.4	0.909774	0.023033	0.801213	0.030064

5.1.4 WNN Model for Blast-Induced Ground Vibration Prediction

The experimentation results revealed that, the WNN gave the highest R and the lowest MSE on the testing data set when three wavelons were used in the hidden layer. Thus, the structure of the optimum WNN is [5 – 3 – 1], that is five inputs, three wavelons in the hidden layer and one output. Table 5.7 shows the optimal training and testing results for the WNN technique based on the R and MSE criteria. All the wavelons in the hidden layer that were used to arrive at the optimal results are presented in Table C1 of Appendix C.

Table 5.7 Optimal Training and Testing R and MSE Results for WNN

Number of Wavelons	Training		Testing	
	R	MSE	R	MSE
3	0.9103	0.0206	0.8438	0.0227

5.1.5 GMDH Model for Blast-Induced Ground Vibration Prediction

The developed GMDH model with the lowest MSE and highest R value was found to have three parameters in input layer, one hidden layer with one neuron and a single value as model target at output layer. The corresponding polynomial equation representations of the developed GMDH for PPV prediction are shown in Equations (5.1) and (5.2). In fact, these equations revealed that the main contributing inputs among the entire inputs under

consideration are number of blast holes, the distance between blasting point and monitoring station (m) and the powder factor (kg/m^3). Table 5.8 shows the optimal training and testing results for the GMDH technique based on the R and MSE criteria.

Layer 1

$$x_6 = 0.8228 - 0.4542(x_3) + 0.361(x_1) - 0.06975(x_1)(x_3) \qquad (5.1)$$
$$+ 0.005446(x_3)^2 - 0.096(x_1)^2$$

Output layer

$$PPV = 0.08641 + 0.731(x_6) - 0.06422(x_5) + 0.6728(x_5)(x_6) \qquad (5.2)$$
$$- 0.07829(x_6)^2 - 0.04503(x_5)^2$$

where x_1 is the number of blast holes, x_3 is the distance between blasting point and monitoring station (m), x_5 is the powder factor (kg/m^3), x_6 is the resultant of layer 1.

Table 5.8 Optimal Training and Testing R and MSE Results for GMDH

Number of Neurons	Training		Testing	
	R	MSE	R	MSE
1	0.9049	0.0218	0.8270	0.0249

5.1.6   MARS Model for Blast-Induced Ground Vibration Prediction

The training and testing results of the three MARS models developed based on their order of interactions are presented in Table 5.9.

Table 5.9 Training and Testing Results for Each Order of Interaction

Order of Interaction	Training		Testing	
	R	MSE	R	MSE
Zero Order	0.91492	0.01960	0.84108	0.02330
First Order	0.92210	0.01802	0.80888	0.02896
Second Order	0.90360	0.02208	0.83008	0.02550

From Table 5.9, it can be observed that, the MARS model with zero order gave the lowest MSE and the highest *R* value for the testing phase. Hence, the final MARS model based on the zero order comprises of 5 out of the 20 basis functions used at the initial forward stage. Table 5.10 presents the corresponding equations for the selected basis functions.

Table 5.10 The Basis Functions (BF) and their Related Equations for MARS

Basis Function	Equations
BF2	max (0, 1100 - Distance from Blasting Point)
BF4	max (0, 0.828853 - Powder Factor)
BF5	max (0, Number of Blast Holes - 19)
BF7	max (0, 11 - Hole Depth)
BF8	max (0, Distance from Blasting Point - 1000)

The developed MARS model for predicting blast-induced ground vibration is given in Equation (5.3).

$$\text{PPV} = 0.577952 + 0.000764031 \times \text{BF2} - 0.731931 \times \text{BF4} + 0.00219317 \times \text{BF5} \qquad (5.3)$$
$$- 0.0486907 \times \text{BF7} - 0.000622675 \times \text{BF8}$$

5.1.7 SVM Model for Blast-Induced Ground Vibration Prediction

In this study, the optimum design values of ε and C was set at 0.00000001 and 50 respectively. The polynomial kernel of order one was the best kernel in this regard. Table 5.11 shows the optimal training and testing results.

Table 5.11 Optimal Training and Testing *R* and MSE Results for SVM

Training		Testing	
R	MSE	*R*	MSE
0.8931	0.0244	0.8441	0.023

5.1.8   LS-SVM Model for Blast-Induced Ground Vibration Prediction

In the development of the LS-SVM, the optimum design values of γ (Equation (4.27)) and σ^2 (Equation 4.33) that defined the optimum LS-SVM model are 19601.0969 and 25672.8908 respectively. Table 5.12 shows the optimal training and testing results.

Table 5.12 Optimal Training and Testing *R* and MSE Results for LS-SVM

Training		Testing	
R	MSE	*R*	MSE
0.90663	0.0214	0.85415	0.0215

5.1.9   RVM Model for Blast-Induced Ground Vibration Prediction

For the developed RVM model for ground vibration prediction, the optimum width parameter was found to be 0.1489. Table 5.13 shows the optimal training and testing results.

Table 5.13 Optimal Training and Testing *R* and MSE Results for RVM

Width Parameter	Training		Testing	
	R	MSE	*R*	MSE
0.1489	0.90627	0.08462	0.85312	0.09257

5.1.10 ELM Model for Blast-Induced Ground Vibration Prediction

Based on the experimental results, the optimum number of neurons for the developed ELM model was found to be 11 with a sigmoid activation function. Thus, the optimum ELM structure is [5 – 11 – 1] corresponding to five inputs with one hidden layer of 11 neurons and one output. Table 4 shows the optimal training and testing results for the ELM technique based on the *R* and MSE criteria. Table 5.14 shows the optimal training and testing results. All the neurons in the hidden layer that were used to arrive at the optimal results are presented in Table D1 of Appendix D.

Table 5.14 Optimal Training and Testing *R* and MSE Results for ELM

Number of Neurons	Training		Testing	
	R	MSE	*R*	MSE
11	0.907295	0.021274	0.853454	0.021662

5.1.11 GPR Model for Blast-Induced Ground Vibration Prediction

Using the MSE and *R* criteria, the comparative results obtained by the various covariance functions of the GPR using the testing data sets are presented in Table 5.15.

Table 5.15 Test Results of the Various Gaussian Process Regression Model

GPR Model Formed	Covariance Type	*R*	MSE
GPR-Squared exponential	Squared exponential	0.8300	0.0252
GPR-exponential	Exponential	0.8325	0.0245
GPR- Matérn 3/2	Matérn 3/2	0.8339	0.0246
GPR-Matérn 5/2	Matérn 5/2	0.8328	0.0248
GPR-Rational quadratic	Rational quadratic	0.8317	0.0250

From Table 5.15, it can be observed that, the various GPR models had very close *R* values in the range, 0.8300 to 0.8339 and MSE values falling in the range 0.0245 to 0.0252. These results confirm that the various GPR models can accurately predict blast-induced ground vibration levels. This is because they all gave *R* values close to 1 and MSE values close to 0, indicating good predictive capability. The results further indicated that the covariance functions (Table 5.15) utilised have similar predictive capabilities. However, in comparison, the GPR model with the Matérn 3/2 covariance function had the highest *R* value and the second least MSE to the exponential covariance function. The Matérn 3/2 was then selected as the optimum because from Table 5.15, it is noticeable that the MSE difference between the Matérn 3/2 and exponential covariance function is 0.0001 thus having very negligible influence on the GPR model outcome. By virtue of the results (Table 5.15), the selected proposed GPR model valid for blast-induced ground vibration prediction, has a constant mean function of 0.8812 and Matérn 3/2 covariance function with signal variance of 0.2760, a length scale of 0.33807 and a noise variance of 0.01568.

5.1.12 Empirical Models Developed for Blast-Induced Ground Vibration Prediction

Determination of site constants, k and β

The development of the empirical models for blast-induced ground vibration prediction involves the determination of site constants. The site constants (*k and β*) of the USBM, Indian Standard, Langefors-Kihlstrom and Ambrasey-Hendron equations were determined by plotting scaled distance against PPV values. The results are presented in Figures 5.1, 5.2, 5.3 and 5.4, respectively.

The figure shows a scatter plot of PPV (mm/s) on the y-axis (ranging from 0 to 1.8) versus D/(Q^(1/2)) on the x-axis (ranging from 50 to 300), with a fitted trend line and the equation:

$$y = 300.7x^{-1.319}$$
$$R^2 = 0.655$$
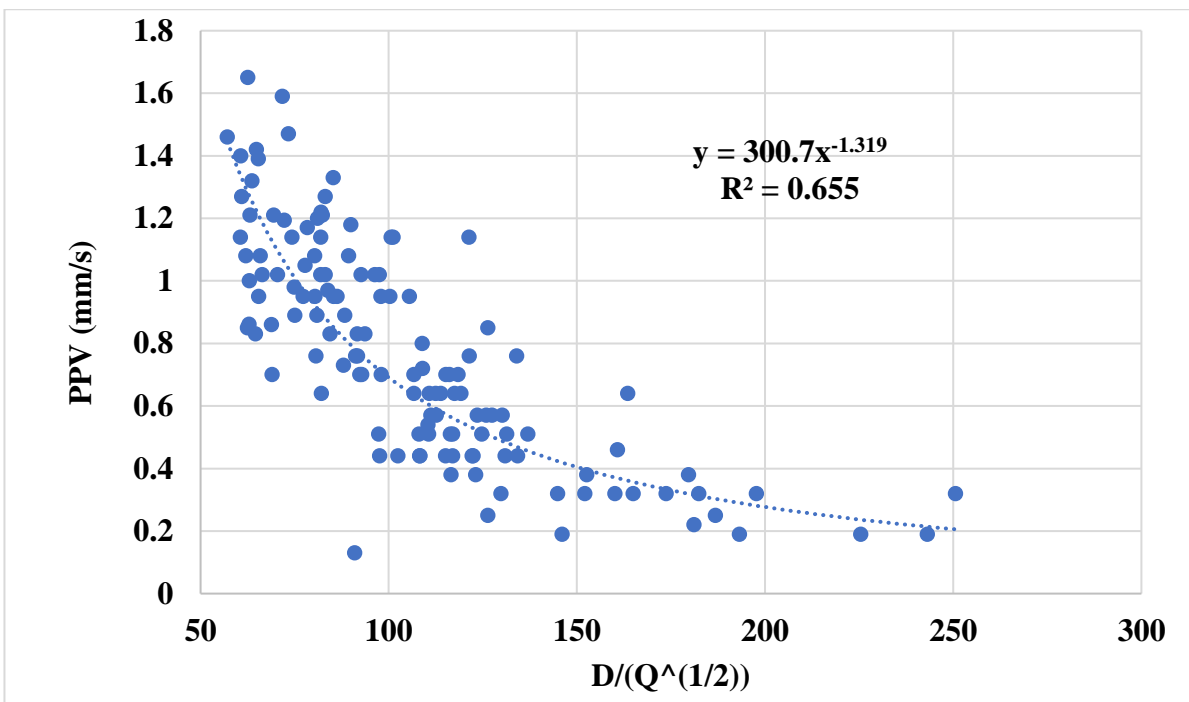
Figure 5.1 Resultant PPV Versus Scaled Distance Relationship for USBM Equation
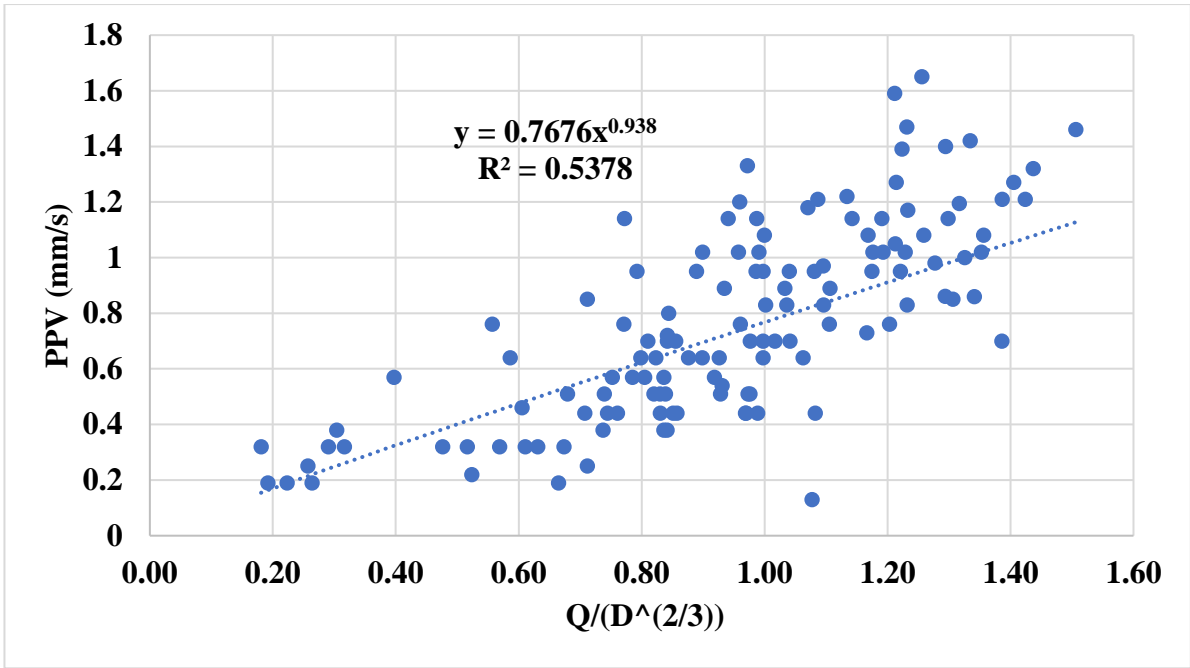
Figure 5.2 Resultant PPV Versus Scaled Distance Relationship for Indian Standard Equation
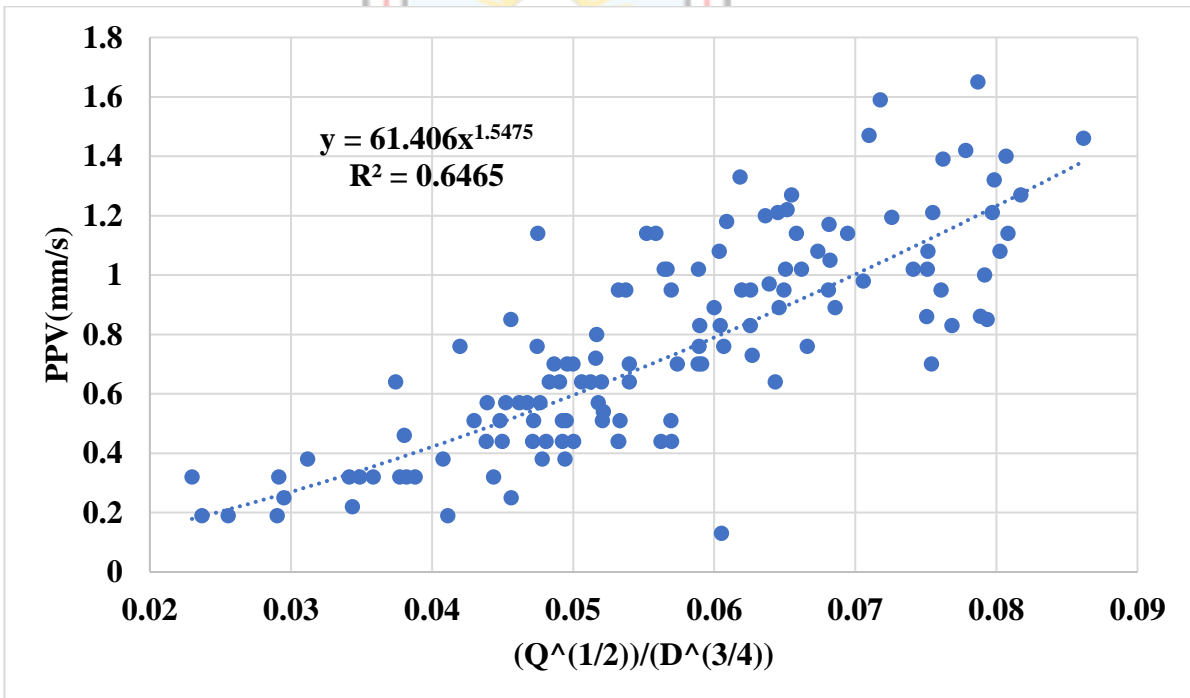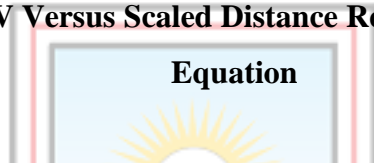
Figure 5.3 Resultant PPV Versus Scaled Distance Relationship for Langefors-Kihlstrom Equation
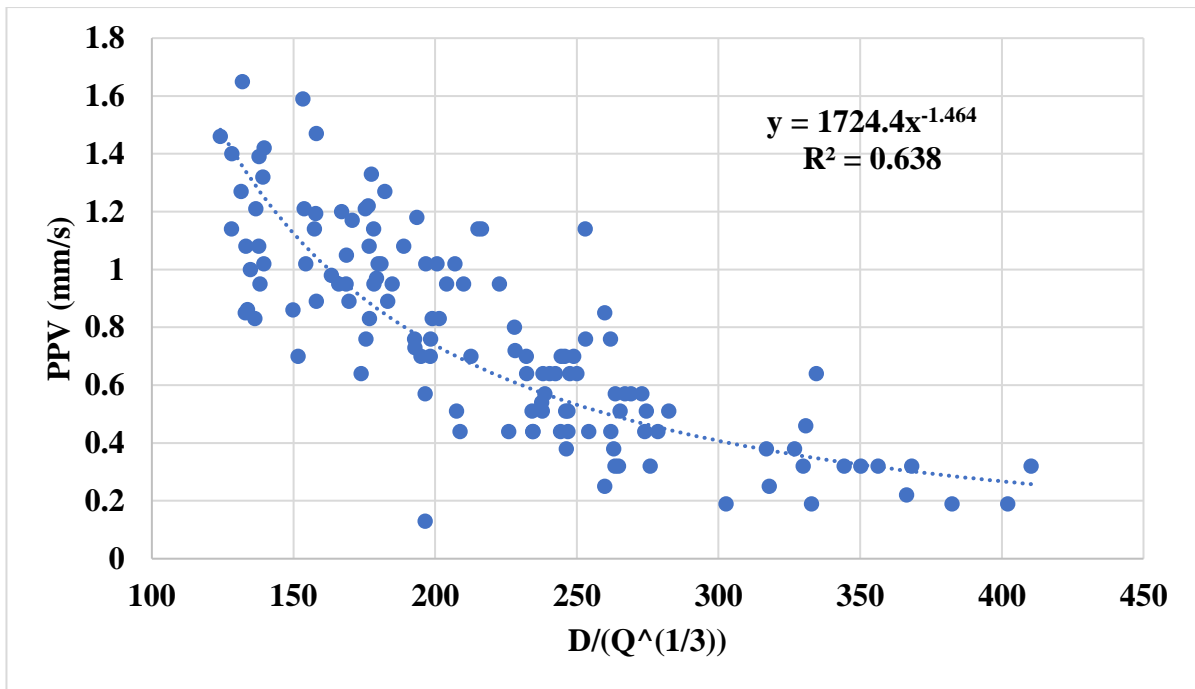
Figure 5.4 Resultant PPV Versus Scaled Distance Relationship for Ambrasey-Hendron Equation

Table 5.16 presents the summary of the k and b values of the empirical equations used in this research. Table 5.17 presents the developed empirical predictor models.

Table 5.16 Summary of the k and b Values of the Various Empirical Equation

Equation	k	β
USBM	300.7	-1.319
Indian Standard	0.7676	0.938
Ambrasey-Hendron	1724.4	-1.464
Langefors-Kihlstrom	61.406	1.5475

Table 5.17 Formulated Models of the Empirical Equations

Empirical Methods	Equations
USBM	$PPV = 300.7\left[D/(Q)^{1/2}\right]^{-1.319}$
Indian Standard	$PPV = 0.7676\left[Q/D^{2/3}\right]^{0.938}$
Ambrasey-Hendron	$PPV = 1724.4\left[D/(Q)^{1/3}\right]^{-1.464}$
Langefors and Kihlstrom	$PPV = 61.406\left[Q^{1/2}/D^{3/4}\right]^{1.5475}$

114

5.2 PPV Predictions from the Various Techniques Implemented

The PPV predicted values of the testing data produced by the various AI and the empirical methods are presented in Table E1 of Appendix E.

5.3 Comparison of the AI Methods and the Empirical Methods for Blast-Induced Ground Vibration Prediction

The statistical results based on the testing data for each of the techniques applied are presented in Table 5.18.

Table 5.18 Models Performance Criteria Results

Various Models	Performance Criteria							
	MSE	MAE	RMSE	RRMSE	R	R^2	η	VAF (%)
BPNN	0.0217	0.1216	0.1473	0.1813	0.8537	0.7288	72.4927	72.8248
RBFNN	0.0223	0.1213	0.1492	0.1837	0.8476	0.7185	71.8333	65.3360
GRNN	0.0301	0.1458	0.1734	0.2134	0.8012	0.6419	0.6188	62.5572
WNN	0.0227	0.1240	0.1508	0.1856	0.8438	0.7120	0.7117	71.2005
GMDH	0.0249	0.1305	0.1579	0.1943	0.8289	0.6870	0.6840	68.6065
MARS	0.0233	0.1265	0.1526	0.1879	0.8411	0.7074	0.7046	70.5868
GPR	0.0245	0.1302	0.1568	0.1930	0.8338	0.6593	0.6883	68.8718
LS-SVM	0.0215	0.1231	0.1467	0.1805	0.8542	0.7296	0.7273	72.9508
SVM	0.0230	0.1288	0.1516	0.1866	0.8441	0.7125	0.7087	71.0200
RVM	0.0926	0.2690	0.3043	0.3745	0.8531	0.7278	-0.1736	72.7590
ELM	0.0217	0.1218	0.1472	0.1811	0.8532	0.7280	0.7254	72.7792
USBM	0.0561	0.1818	0.2369	0.2916	0.7622	0.5810	0.2883	39.3169
Ambrasey-Hendron	0.0659	0.2009	0.2566	0.3159	0.7466	0.5574	0.1649	28.0240
Indian Standard	0.0342	0.1504	0.1849	0.2276	0.7554	0.5707	0.5665	56.9673
Langefors-Kihlstrom	0.0456	0.1630	0.2136	0.2629	0.7833	0.6136	0.4216	49.4308

This study assessed the capability of new AI techniques of LS-SVM, MARS, RVM, GPR and WNN as alternative ground vibration prediction tool to the benchmark AI methods of

BPNN, RBFNN, GRNN, ELM and SVM. The motive was to ascertain whether those proposed new techniques could produce comparable and satisfactory ground vibration predictions. Considering the dimensioned error statistic indicators (MSE, RMSE, RRMSE and MAE), it was found that the proposed LS-SVM produced the lowest MSE, RMSE and RRMSE values of 0.0215, 0.1467 and 0.1805 mm/s respectively (Table 5.18). That is, the LS-SVM was the best among all the candidate models. This was however, closely followed by the BPNN and ELM approach. These results indicate that comparatively, the proposed LS-SVM has strong calibration or learning power and was able to generalise well across the entire testing data more adequately than the other techniques considered in this study. This assertion is in line with the rule of thumb that, the closer the values of MSE, RMSE and MAE are to zero, the better the prediction capability of the developed model. However, a careful study of Table 5.18 indicates that comparatively, the other three proposed novel methods of WNN, MARS and GPR performed fairly well and thus their MSE, RMSE and MAE results deviate only marginally from the best performing AI methods considered in this research. Clearly, it can be stated that the proposed WNN, MARS and GPR can produce very comparable and closely related ground vibration prediction results. In comparison to the empirical models, the proposed AI methods outperformed them. Conversely, the proposed RVM technique could not produce acceptable results as it could not generalise well across the entire testing dataset. A visual confirmation of the predictive strength of the LS-SVM, WNN, MARS and GPR methods can additionally be viewed in Figures 5.5, 5.6, 5.7 and 5.8.

The R^2 results presented in Table 5.18 provide quantitative evidence on how close the predicted ground vibration values from the various techniques are to the least squares line of best fit. With reference to Table 5.19, it can be seen that the proposed AI techniques (LS-SVM, WNN, MARS, RVM and GPR) had high R^2 values. This means they can appropriately explain the variability in the observed PPV data around its mean. However, in comparison with the other AI techniques, it can be observed that the LS-SVM had the highest R^2 value of 0.7296. The other proposed methods (WNN, MARS, RVM and GPR) could produce comparable results as their R^2 values were marginally different from the benchmark AI methods (BPNN, RBFNN, ELM, SVM, GRNN, GMDH) between the range of 0.687 to 0.7296. The empirical predictors on the other hand had lower R^2 values as they predicted less than 62% of the variation in the observed PPV data. Figure 5.9 provides a graphical illustration of the R^2 results.
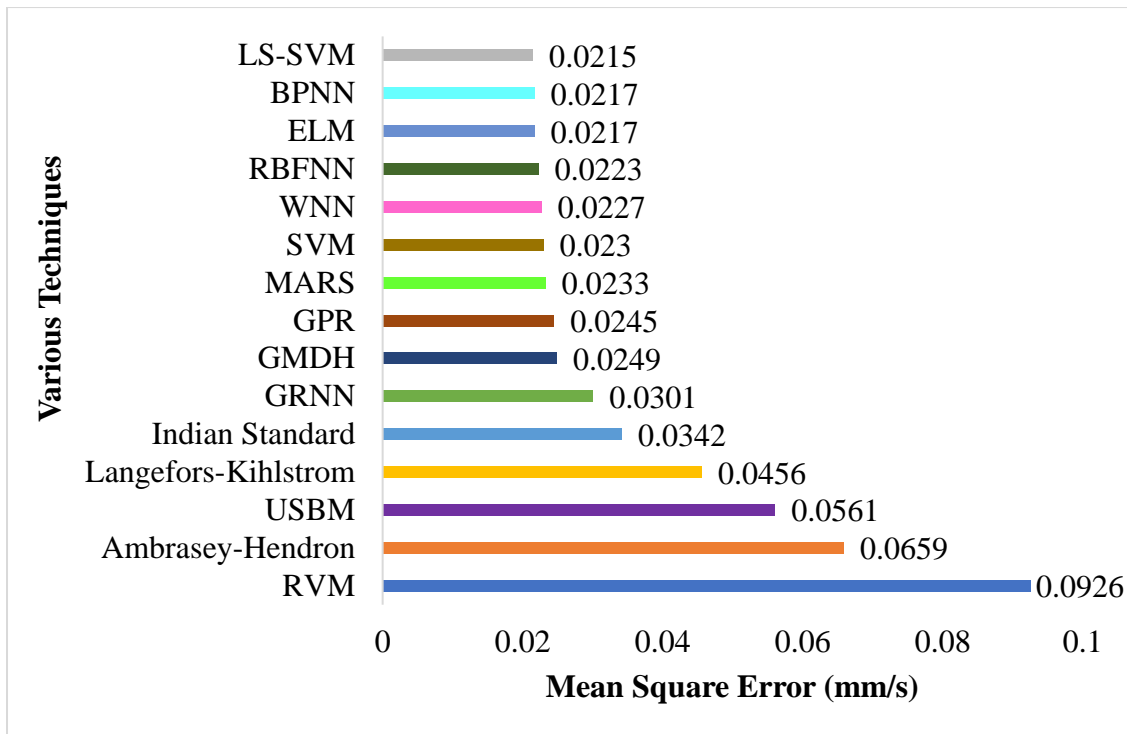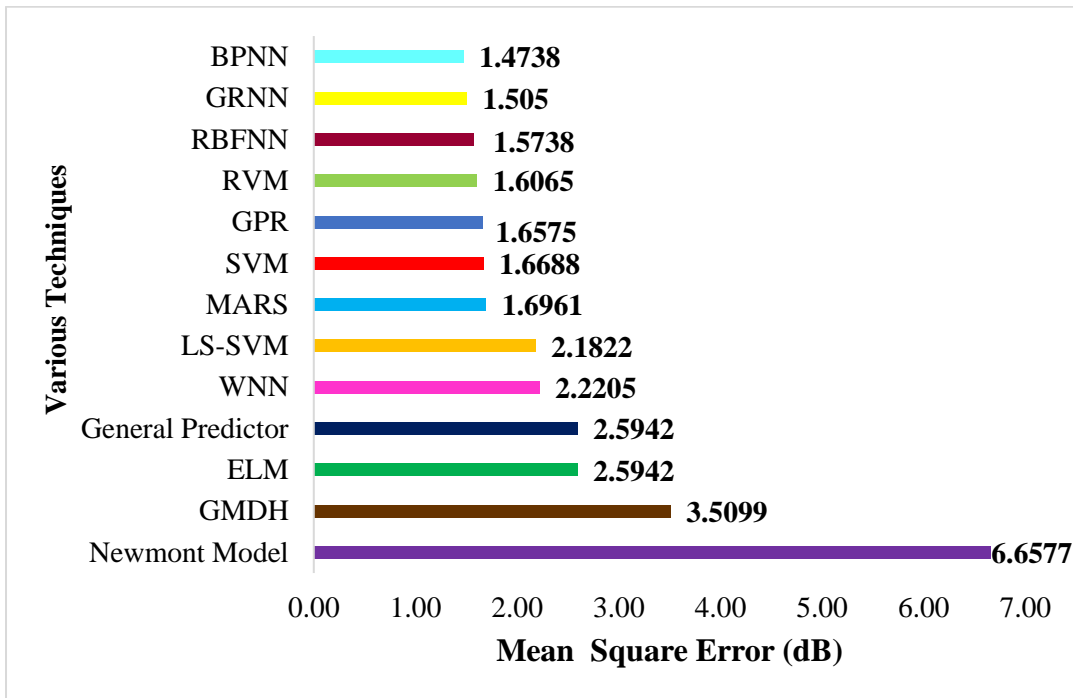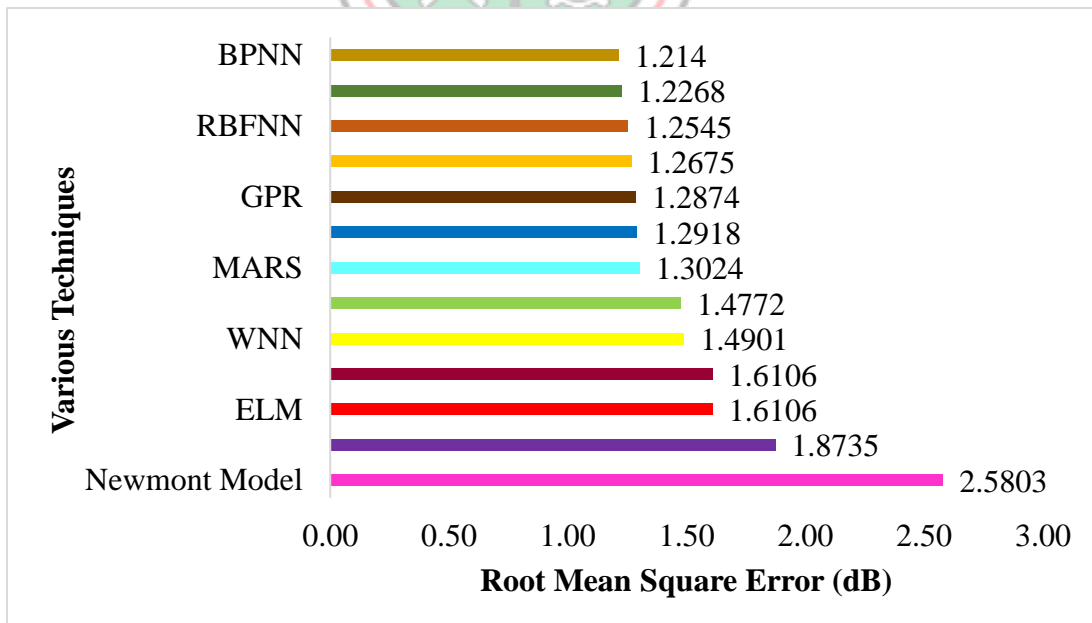
Figure 5.5 Performance of Various Models for Predicting PPV Using Mean Square Error (MSE)
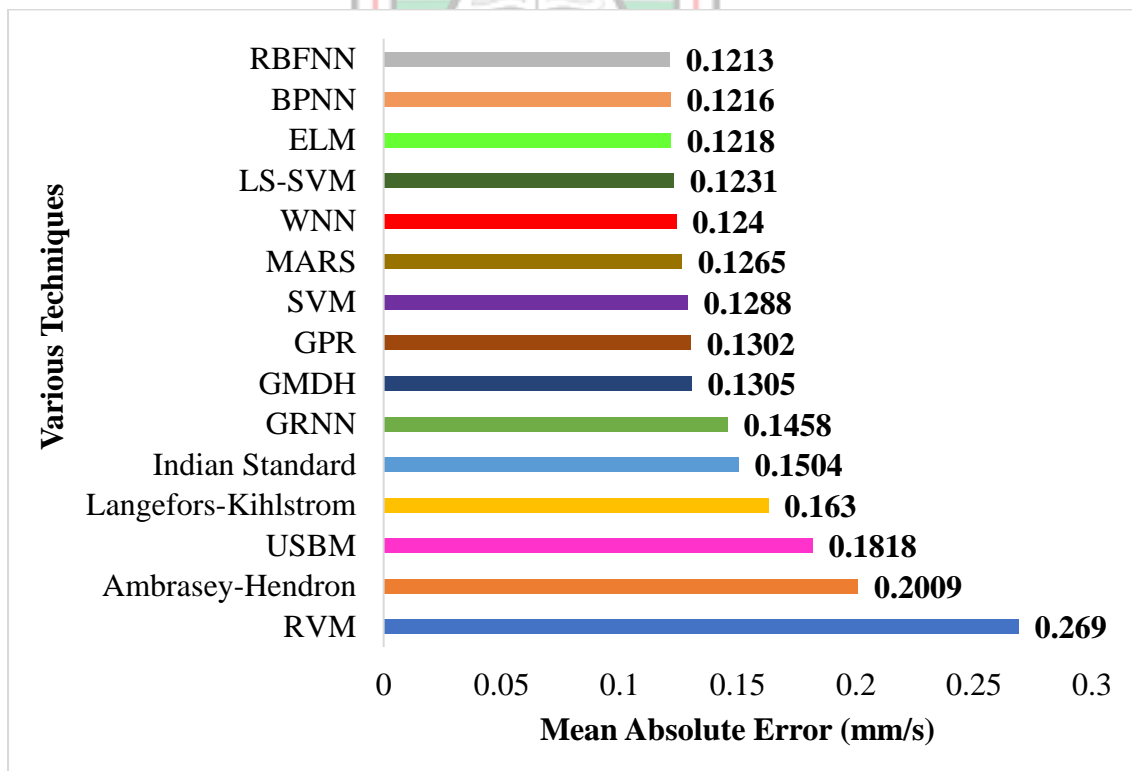
Figure 5.6 Performance of Various Models for Predicting PPV Using Mean Absolute Error (MAE)
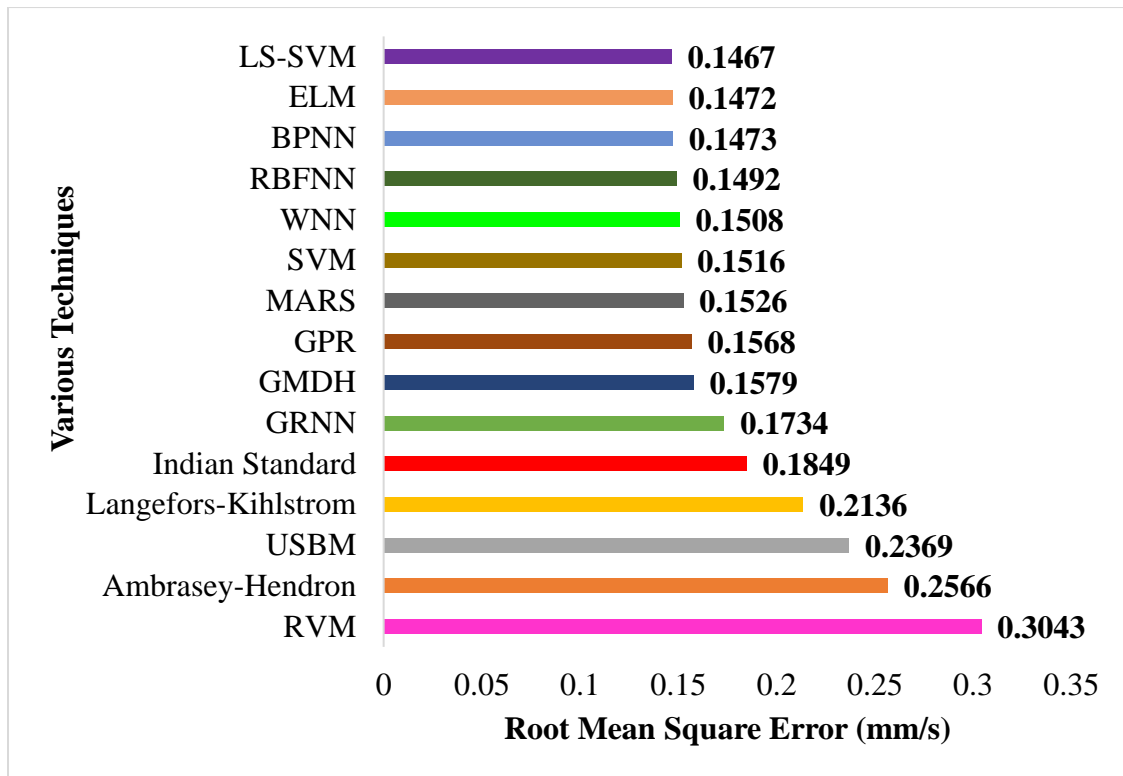
Figure 5.7 Performance of Various Models for Predicting PPV Using Root Mean Square Error (RMSE)
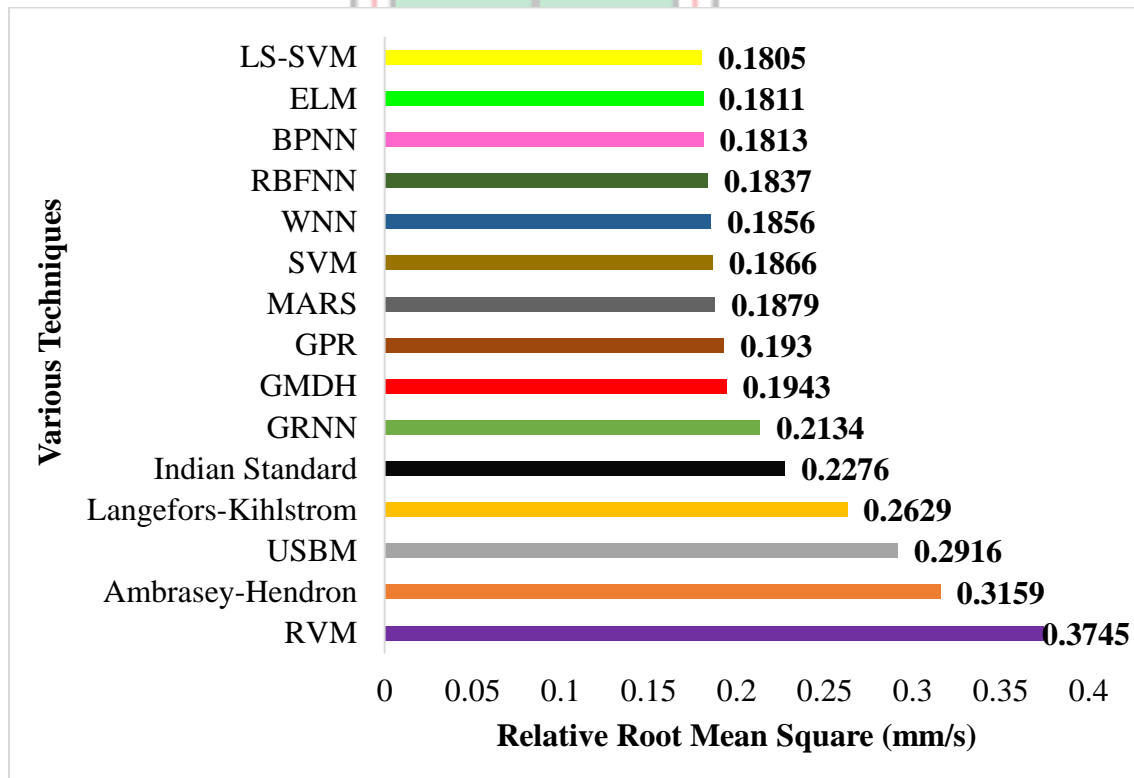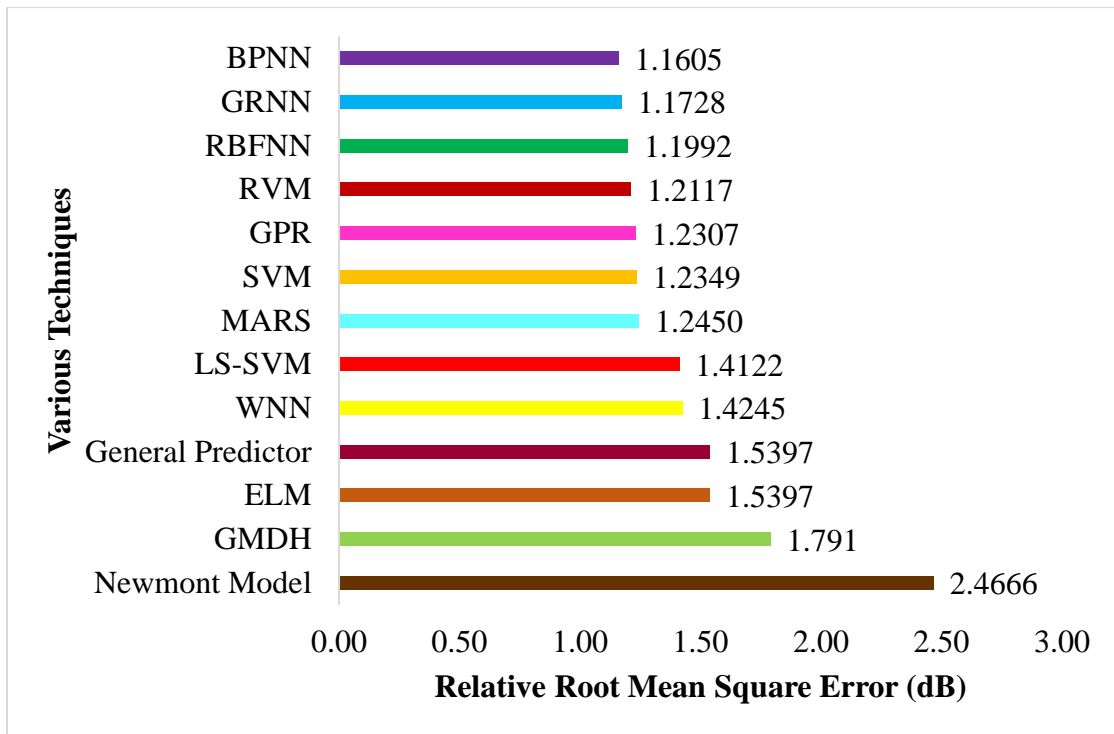

Figure 5.8 Performance of Various Models for Predicting PPV Using Relative Root Mean Square Error (RRMSE)
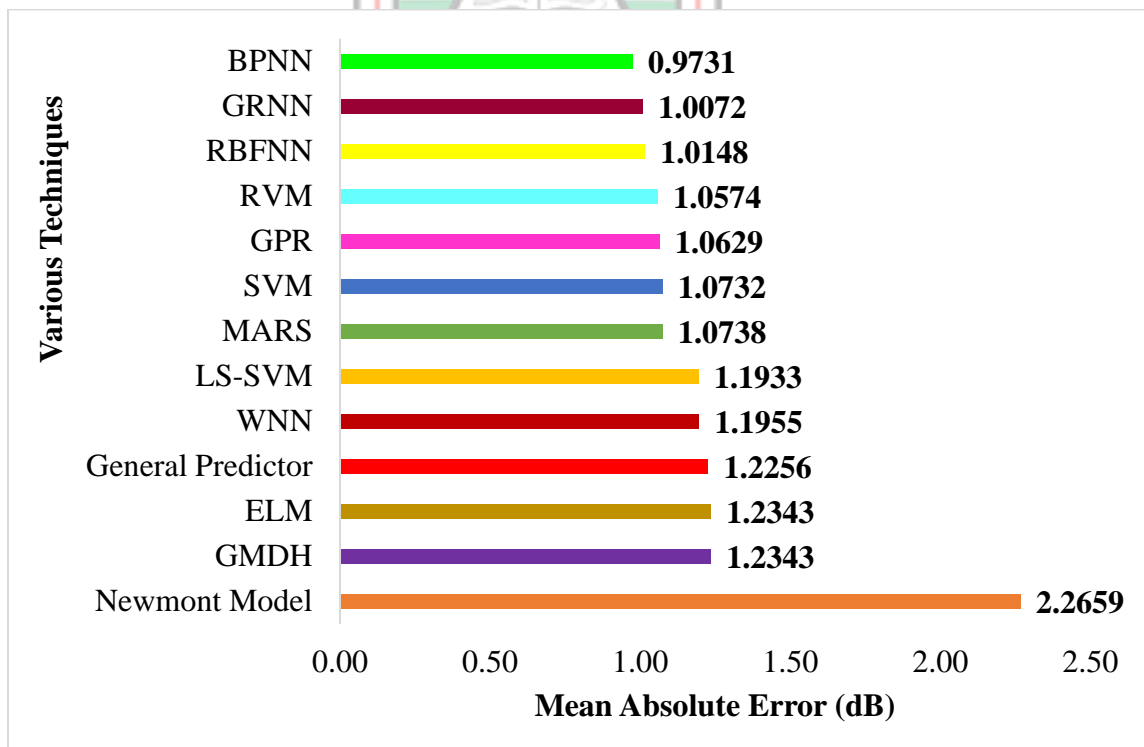
118
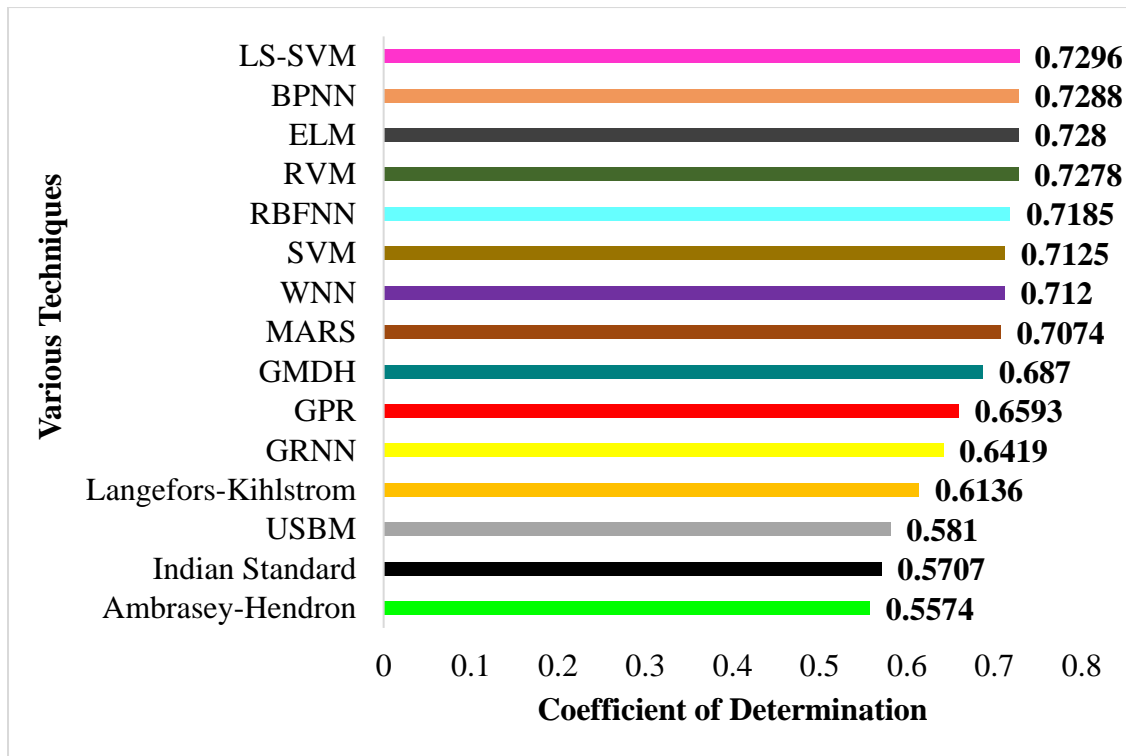
Figure 5.9 Performance of Various Models for Predicting PPV Using Coefficient of Determination

The correlation coefficient, R which ranges from -1 to +1 with the strength of the relationship increasing towards the extremes was also used. The essence is to ascertain the strength of the relationship between the measured PPV values and the predicted results. In Table 5.18, it can be seen that all the proposed AI techniques (LS-SVM, WNN, MARS, RVM and GPR) had R values greater than 0.8. This reveals a high strength of linear dependency between the measured and predicted PPV by these proposed AI techniques. In comparing the performance of the proposed AI techniques on the basis of the R values to the benchmark AI techniques, it can be realised that, the LS-SVM had the highest R value of 0.8542. The other proposed methods had very comparable results to the benchmark AI techniques. The overall analysis indicates that the empirical models performed poorly by obtaining R values less than 0.8. The interpretation made here is that, the artificial intelligent techniques could predict to an accuracy above 80% as compared to the empirical models. This assertion can additionally be viewed in Figure 5.10.
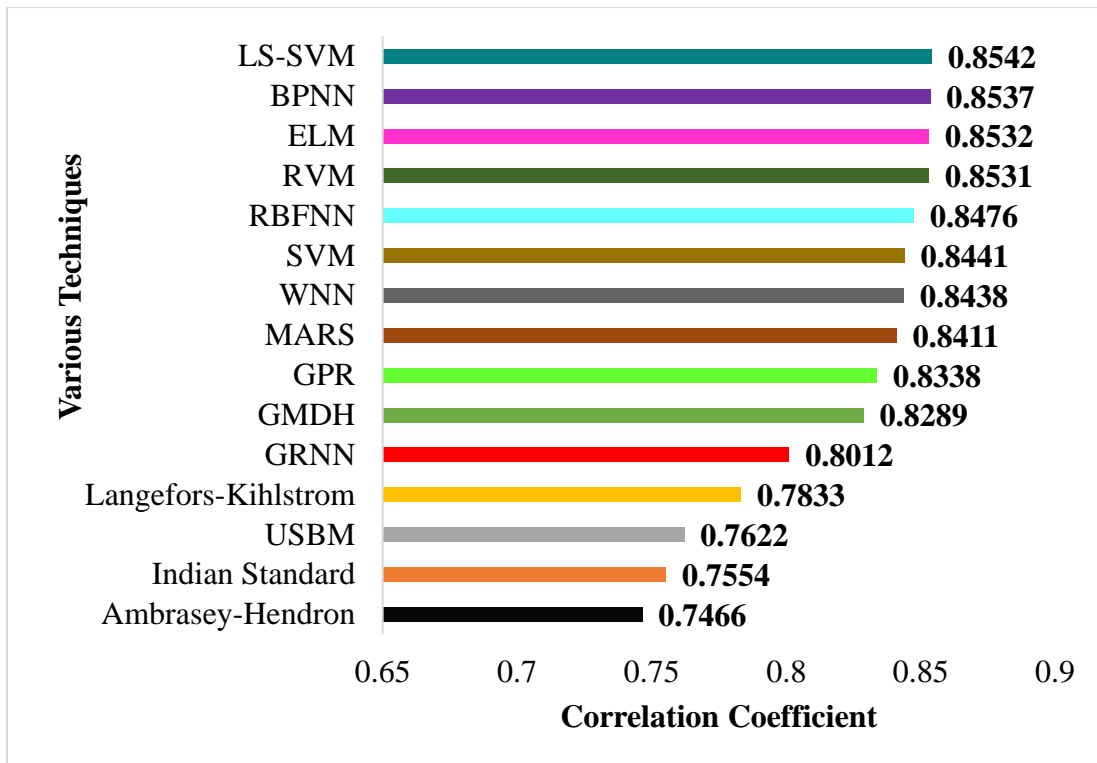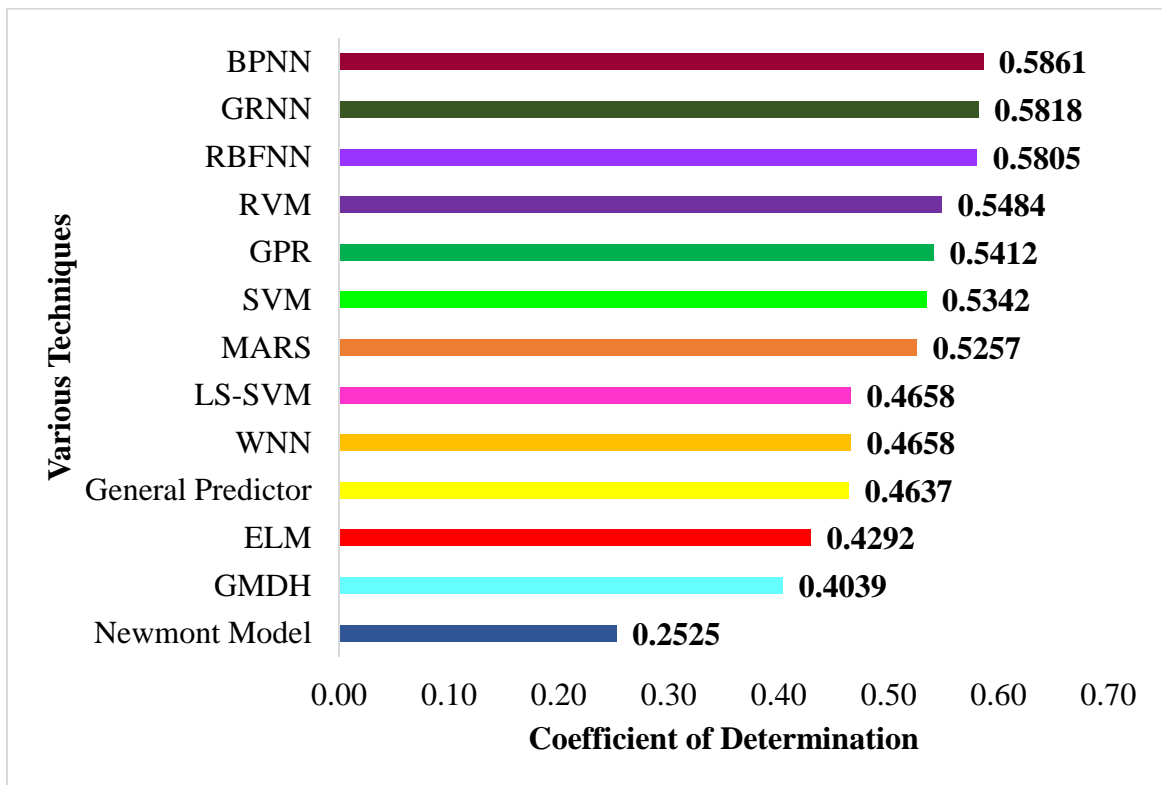
Figure 5.10 Performance of Various Models for Predicting PPV Using Correlation Coefficient

The NASH (Equation (4.79)) is a model efficiency-based indicator. It takes values of -∞ to 1 with improved model performance approaching one. The NASH provides the degree to which the model predictions are error free, by evaluating the accuracy of the predicted PPV value with respect to the observed PPV data. Based on the computed NASH values (Table 5.18), it was found that the proposed AI techniques (LS-SVM, WNN MARS and GPR) could explain more than 68% of the potential error.

Conversely, the proposed RVM technique could not adequately explain the potential error in its prediction as it got a very low NASH value of -0.1736. In comparing the performance of the proposed to benchmark AI techniques, it can be seen that the LS-SVM had the highest NASH value of 0.7273. It can also be seen that, the NASH results as produced by the other proposed AI techniques (WNN, MARS and GPR) are comparable to those produced by the benchmark AI techniques. It can however be observed that, collectively, the AI models outperformed the empirical models in their entirety on account of the NASH evaluator. Figure 5.11 provides a graphical illustration of the NASH results.
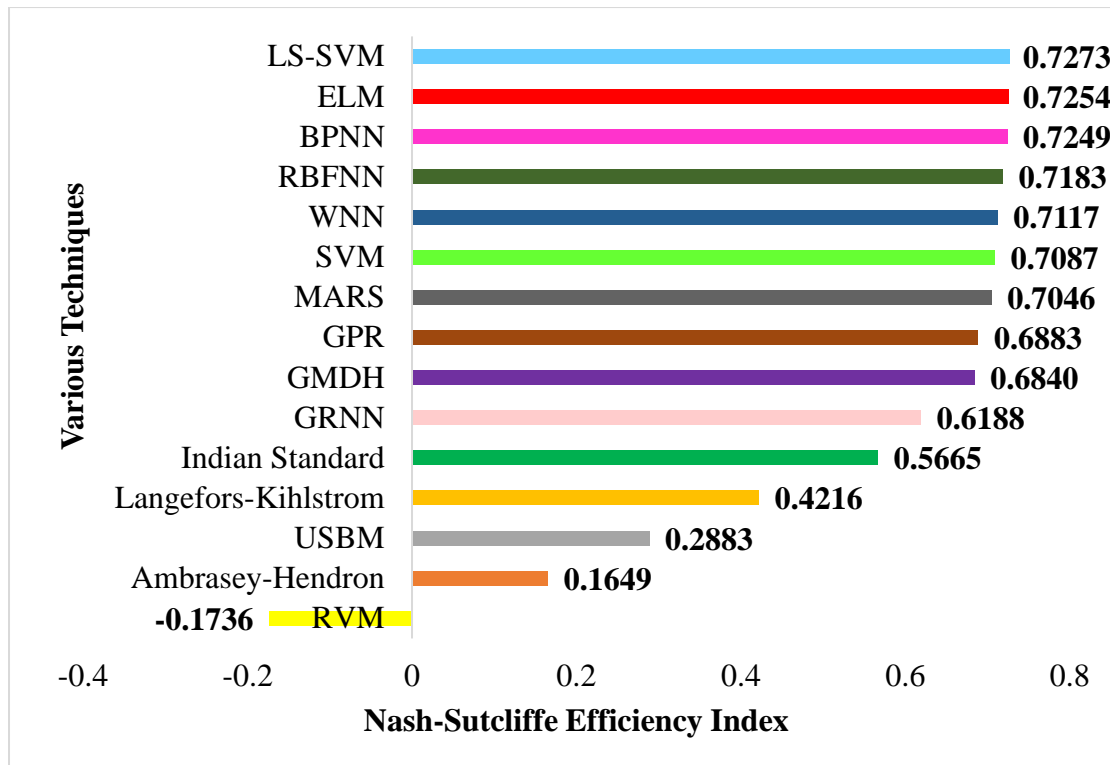
Figure 5.11 Performance of Various Models for Predicting PPV Using Nash-Sutcliffe Efficiency Index

In this study, the VAF was also used to verify the correctness of the models and how well they could approximate the unseen dataset (Delis *et al*., 2013). That is, a model with a VAF value closest to 100% is the most accurate among candidate models. It can thus be inferred from Table 5.18 that, the proposed AI models (LS-SVM, RVM, WNN, MARS and GPR) produced high VAF values of above 68%. This indicates that the proposed AI methods can effectively approximate unseen data. Furthermore, when compared to the benchmark AI techniques, the proposed LS-SVM had the highest VAF value of 72.95%. The strength of the LS-SVM approach could be attributed to its intrinsic ability to adopt equality constraints and a linear Karush-Kuhn-Tucker system, which has a more powerful computational ability in solving the nonlinear and small sample problem (Du *et al*., 2016). The other proposed AI techniques (WNN, RVM, MARS and GPR) had very comparable VAF values to the benchmark AI techniques. The empirical models on the other hand, had VAF values lower than 57% making them inaccurate in predicting blast-induced ground vibration compared to the AI methods. Figure 5.12 provides a graphical illustration of the VAF results.

121
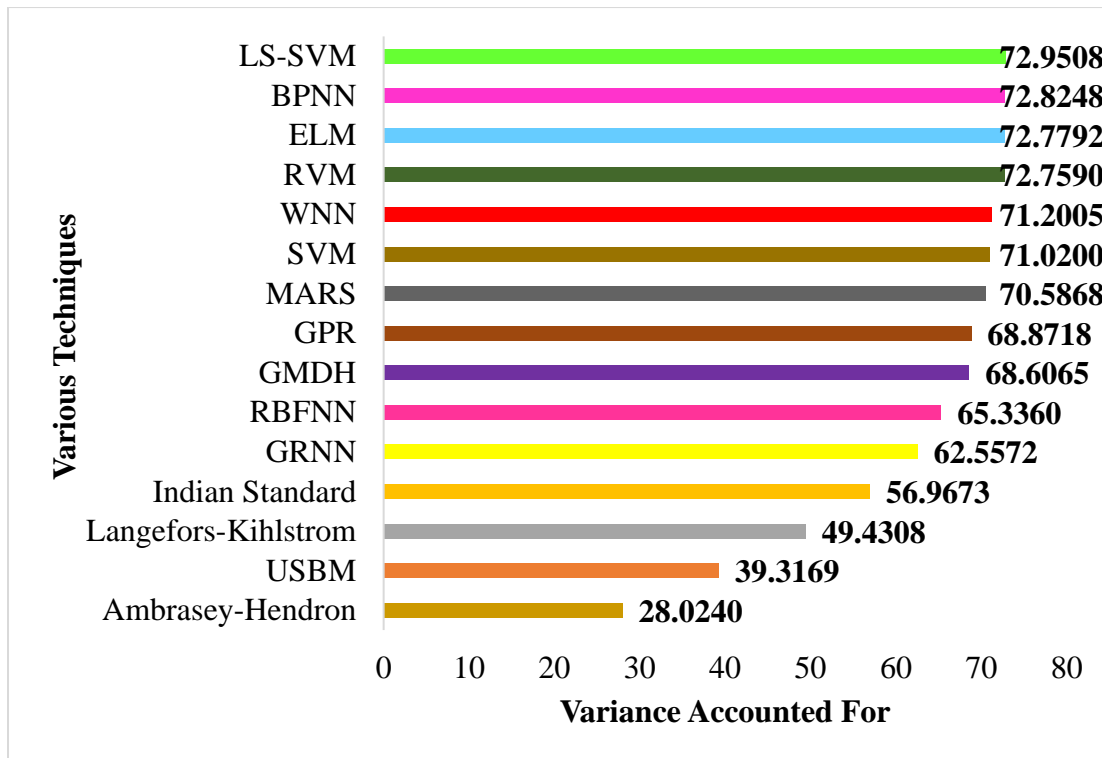
Figure 5.12 Performance of Various Models for Predicting PPV Using Variance Accounted For

Based on obtained results of performance indices, it was found out that four out of the five proposed AI techniques (LS-SVM, WNN, MARS and GPR) produced comparable and satisfactory results as the benchmark techniques of BPNN, RBFNN, ELM, SVM. Hence LS-SVM, WNN, MARS and GPR are proposed to be used as suitable alternative tools to predict blast-induced ground vibration.

Scatter plots along with the regression line, 95% PI and CI for the various models are presented in Figures 5.13 to 5.27. A critical look at the figures shows that the 1:1 line for each model fell in between the 95% CI lines. This means that, there is a 95% probability that the true best-fit line for the population data lies within the CI. It can also be observed that at least 96% of the predicted PPV values fell within the 95% PI lines for all the models. This indicates that when these models are used to predict new PPV values, there is a 95% probability that, at least 96% of the predicted PPV values will fall into the prediction interval. Overall, visual inspection of the various scatter plots revealed that the predictions produced by AI techniques had a narrower prediction interval band width than USBM, Ambrasey-Hendron, Langefors-Kihlstrom and Indian standard model. The comparative

results showed that the AI techniques are superior to the empirical techniques used in this study and are the suitable tools for modelling and predicting blast-induced ground vibration.
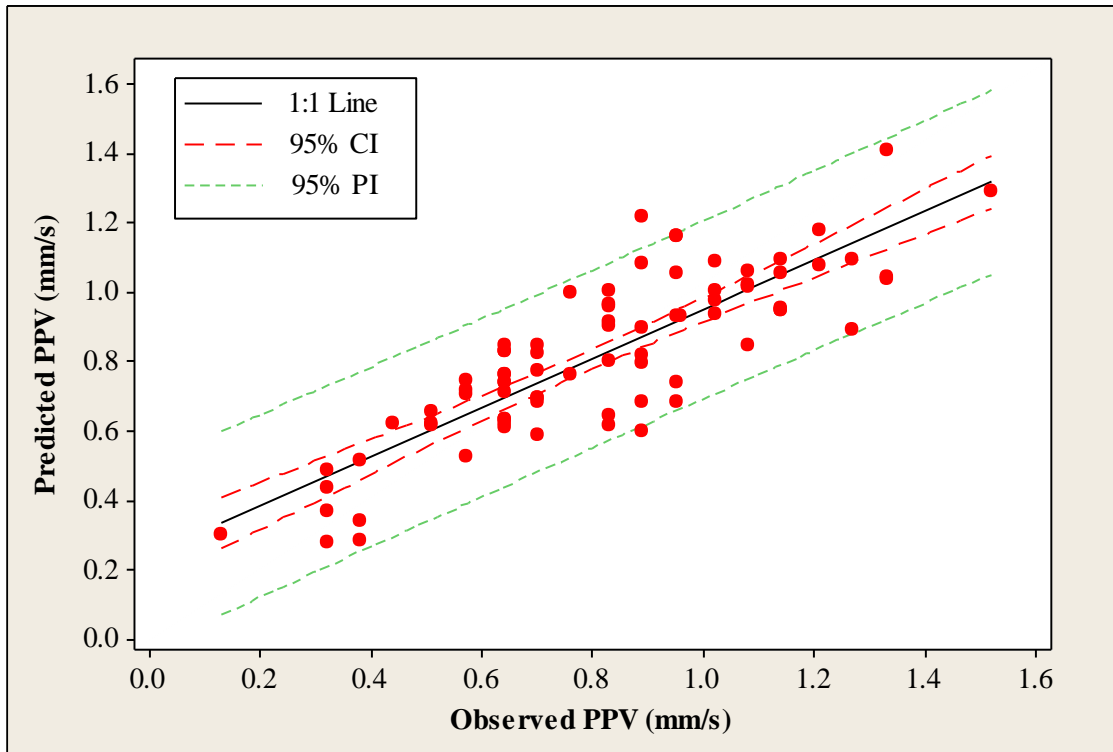
Figure 5.13 Observed PPV Versus Predicted PPV by WNN
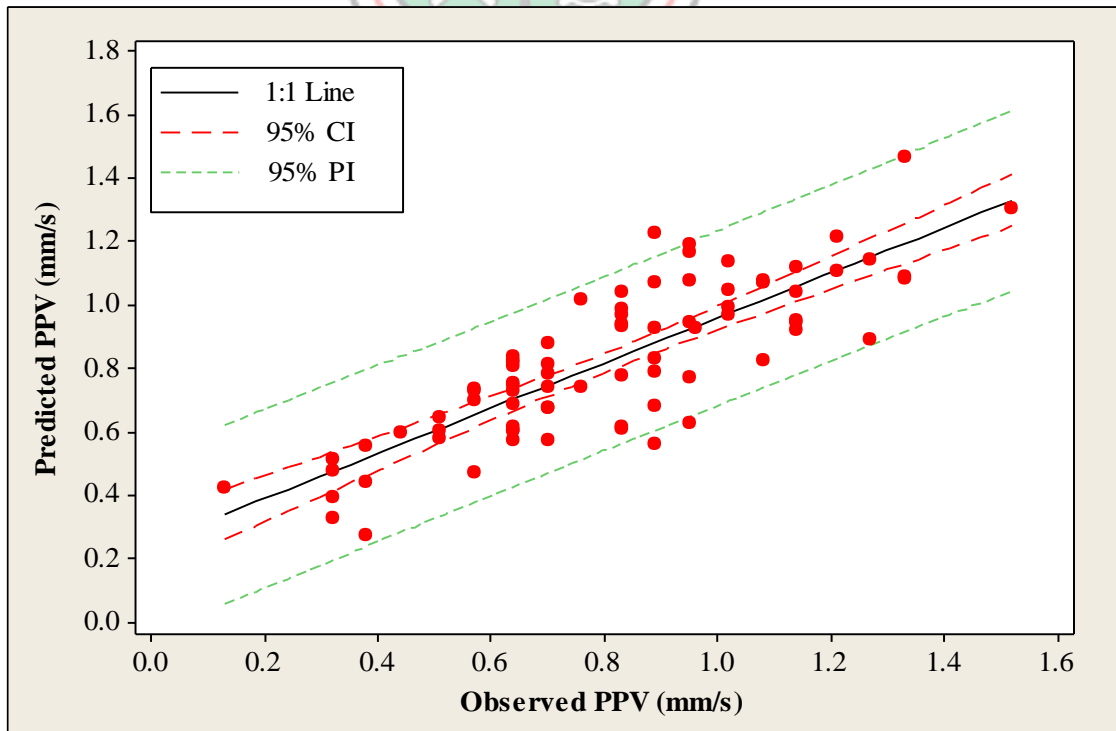
Figure 5.14 Observed PPV Versus Predicted PPV by GMDH
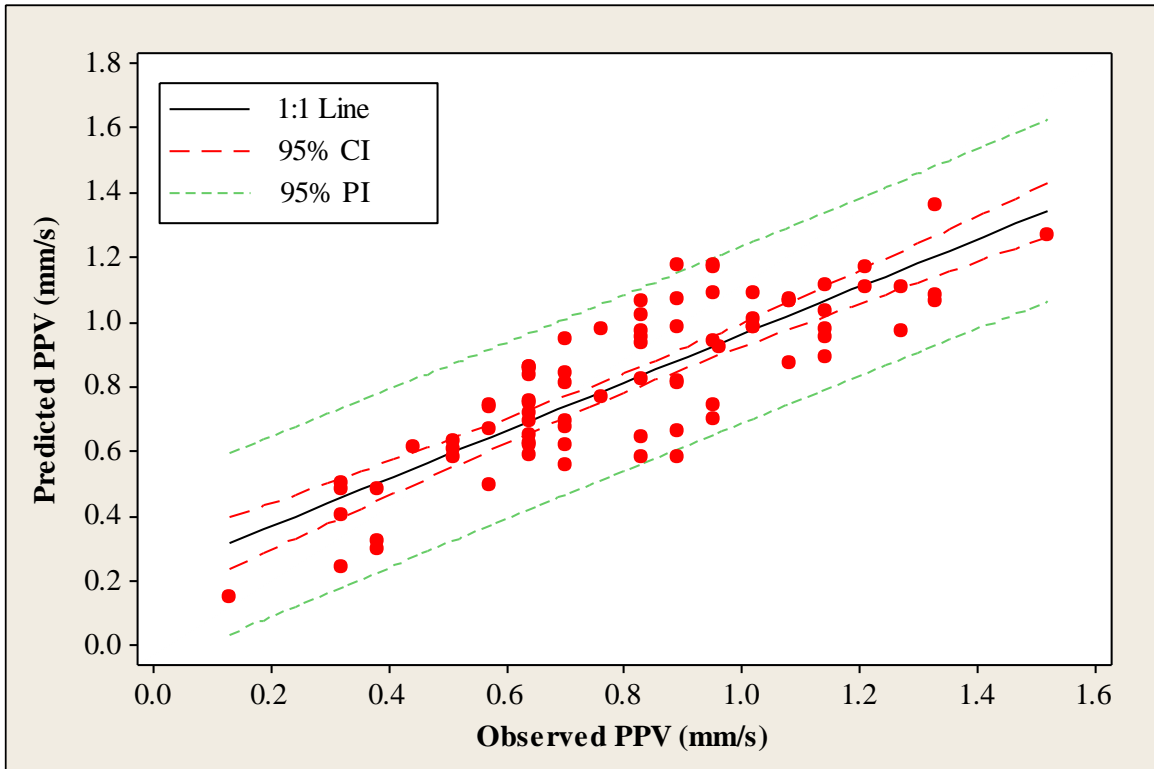
Figure 5.15 Observed PPV Versus Predicted PPV by MARS
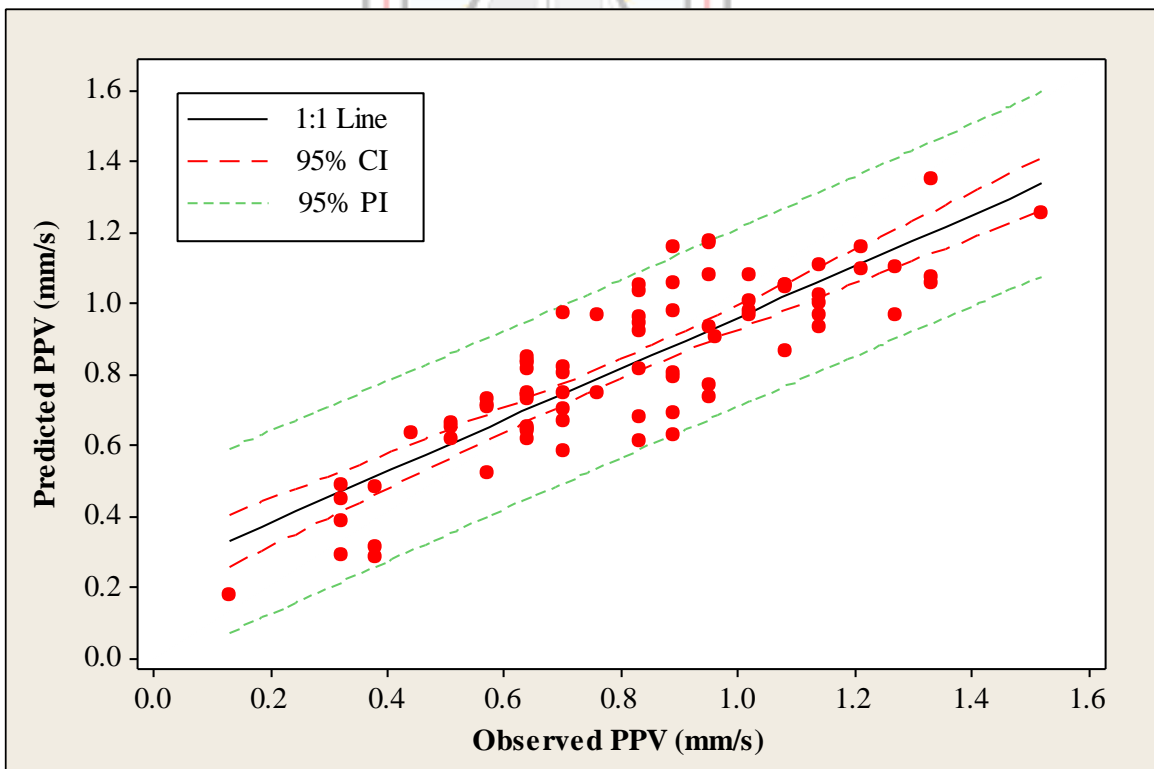
Figure 5.16 Observed PPV Versus Predicted PPV by LS-SVM

124
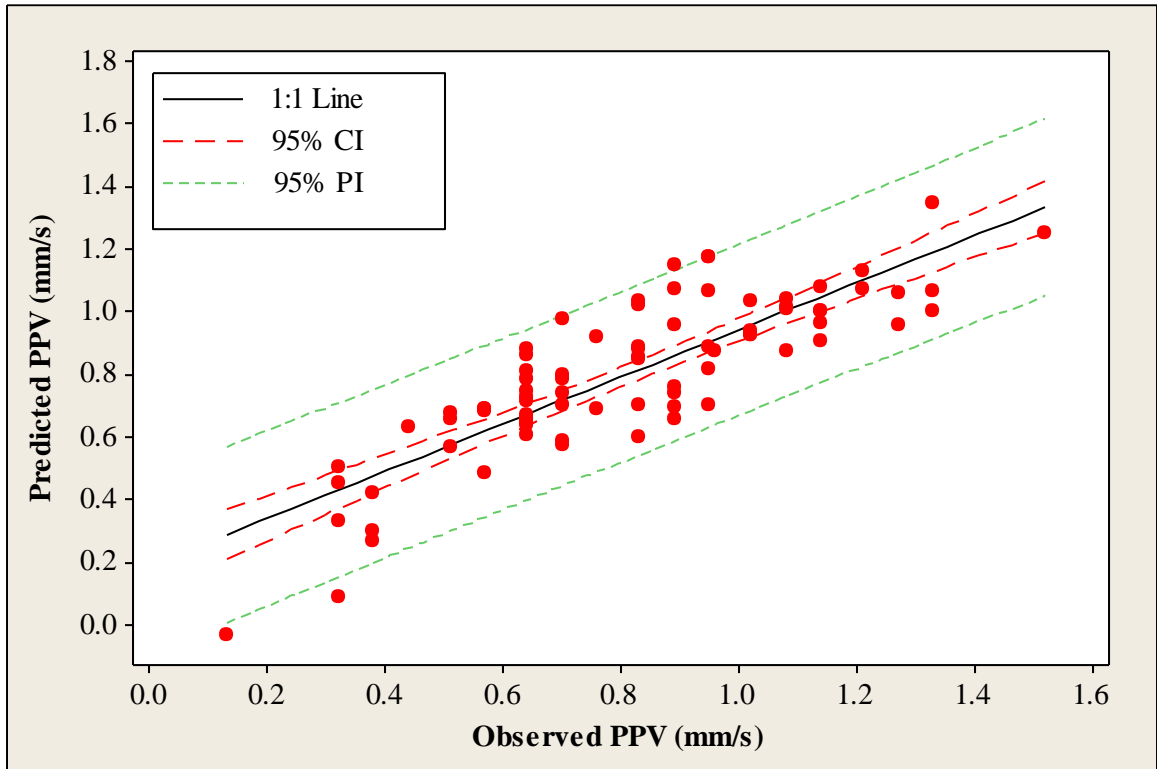
Figure 5.17 Observed PPV Versus Predicted PPV by SVM
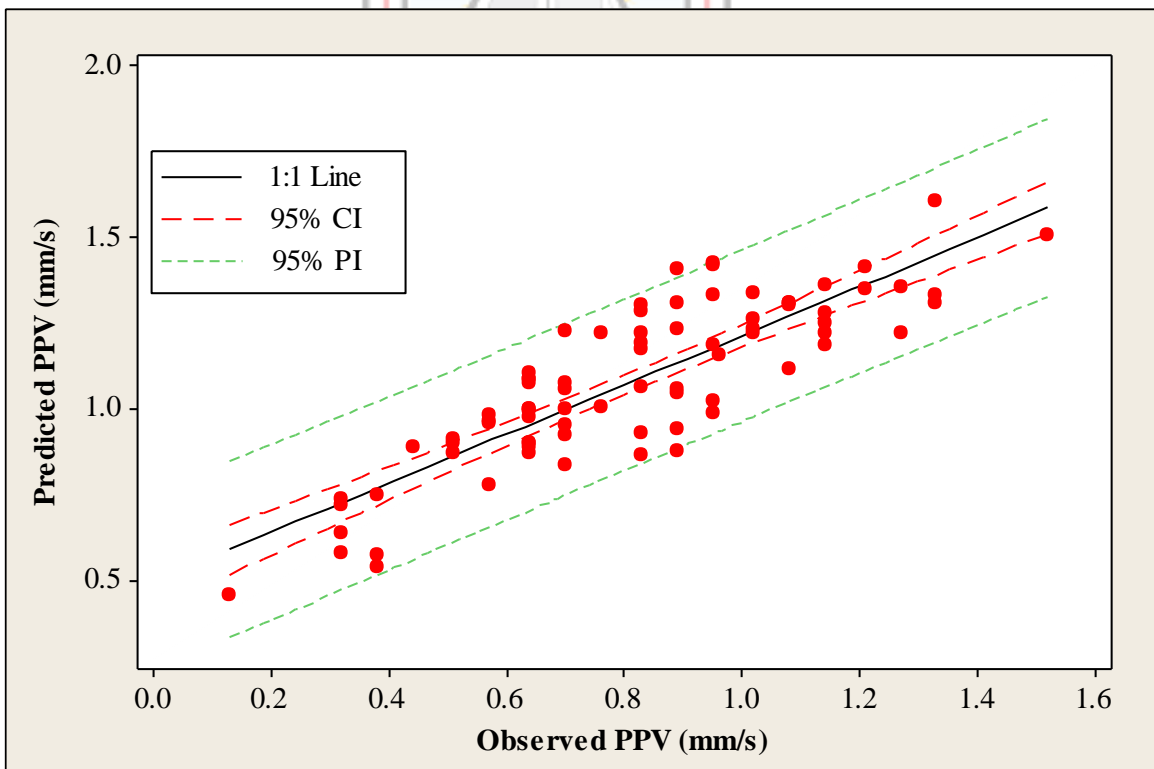
Figure 5.18 Observed PPV Versus Predicted PPV by RVM
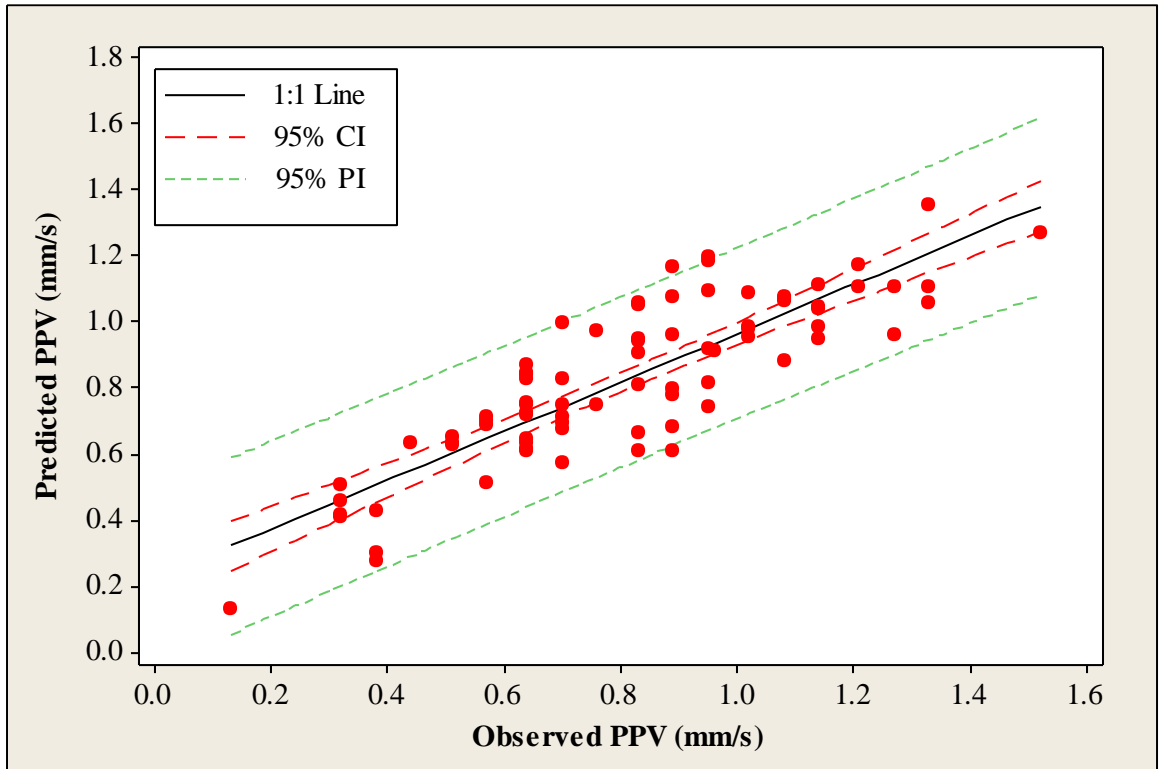
Figure 5.19 Observed PPV Versus Predicted PPV by ELM
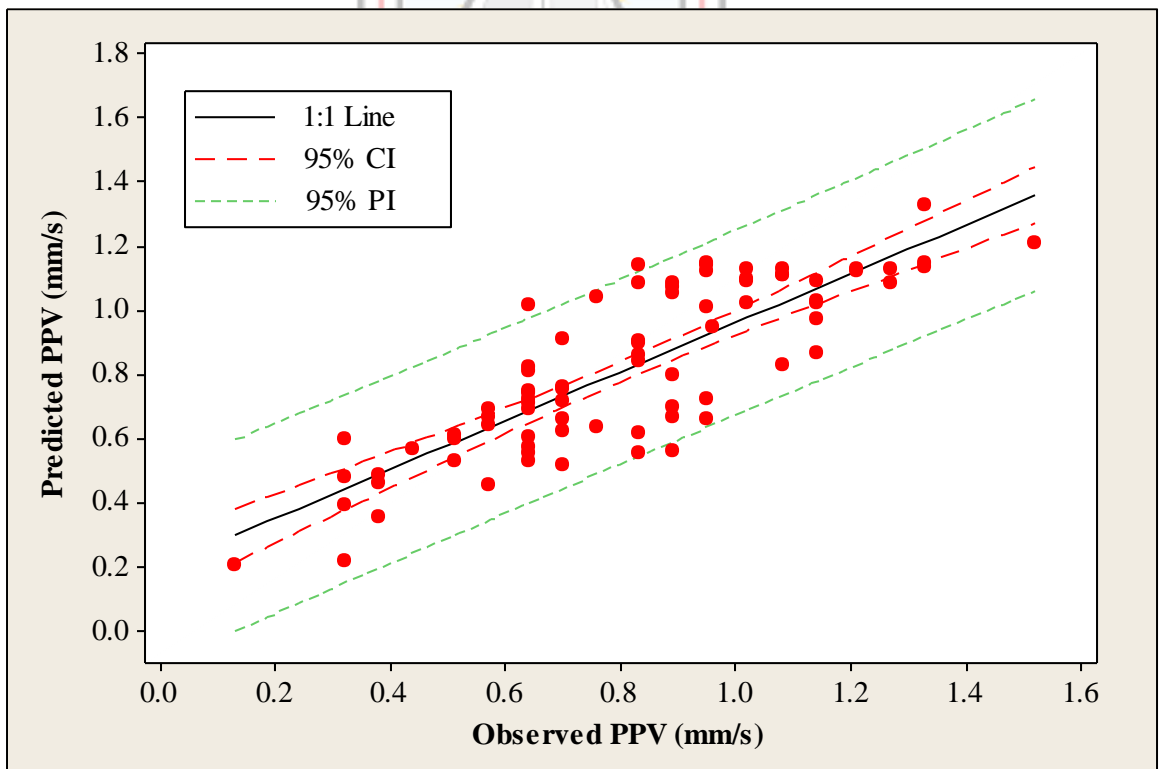
Figure 5.20 Observed PPV Versus Predicted PPV by GPR-Matérn 3/2
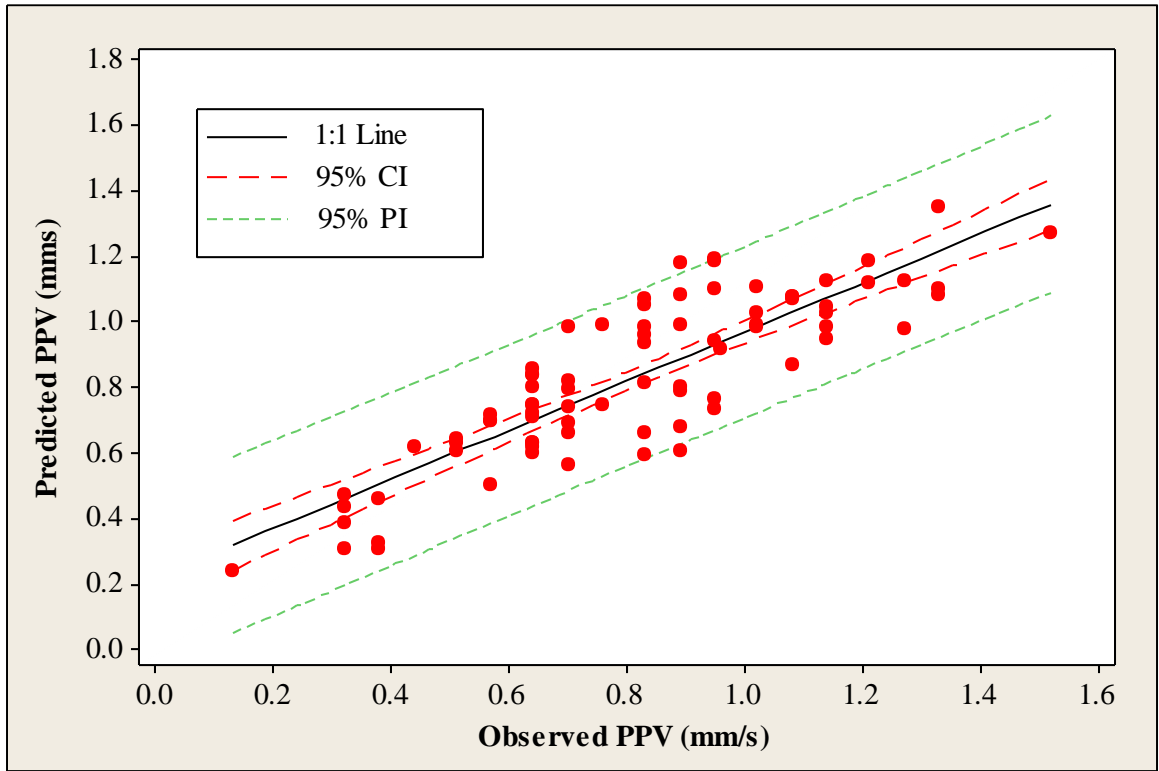
Figure 5.21 Observed PPV Versus Predicted PPV by BPNN
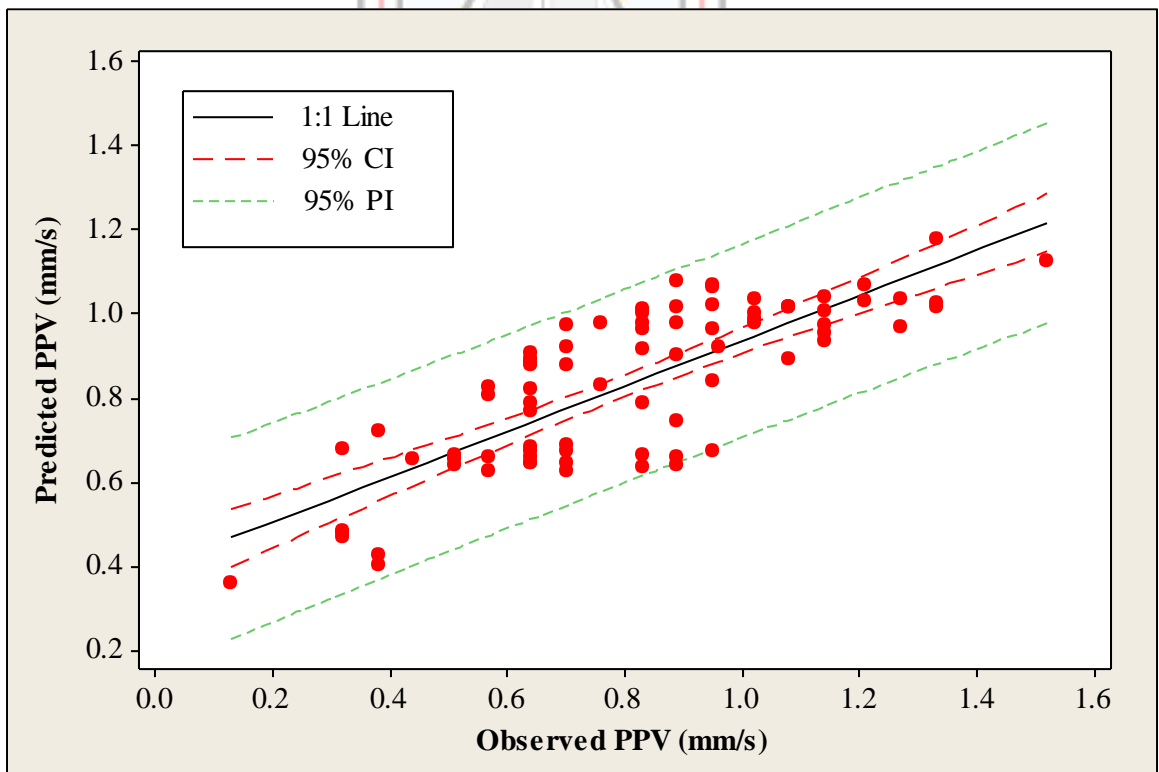
Figure 5.22 Observed PPV Versus Predicted PPV by GRNN
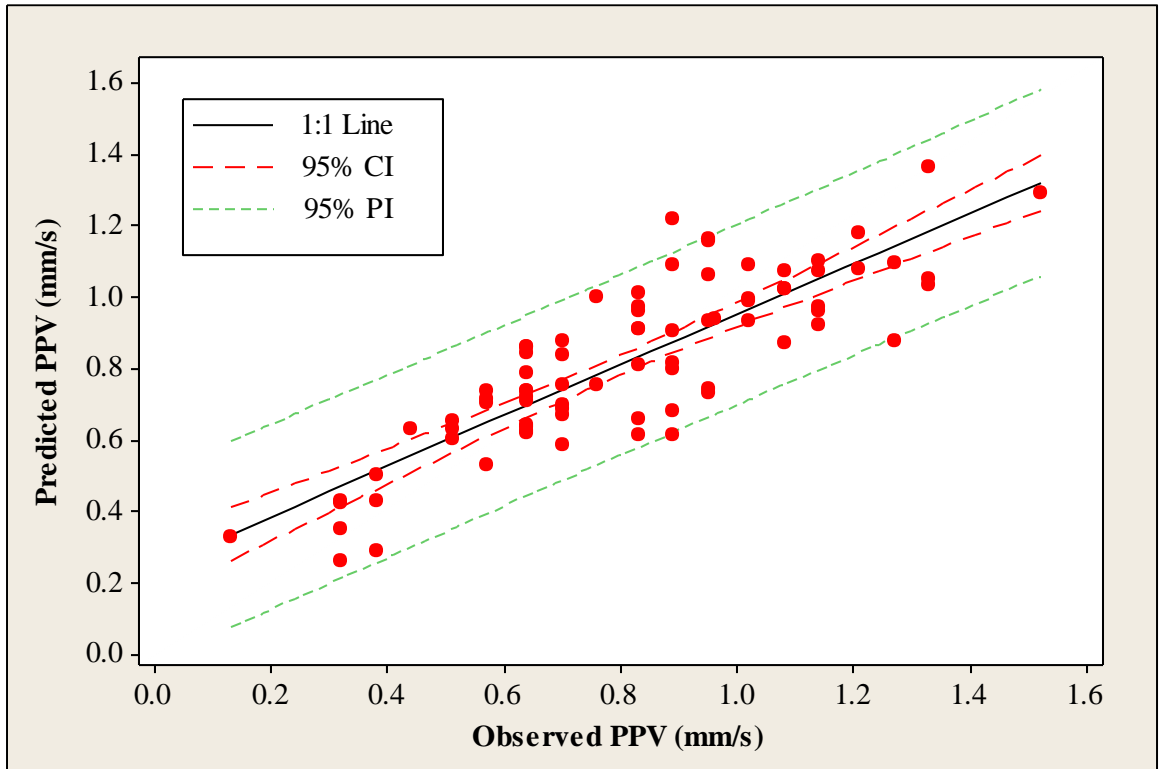
Figure 5.23 Observed PPV Versus Predicted PPV by RBFNN
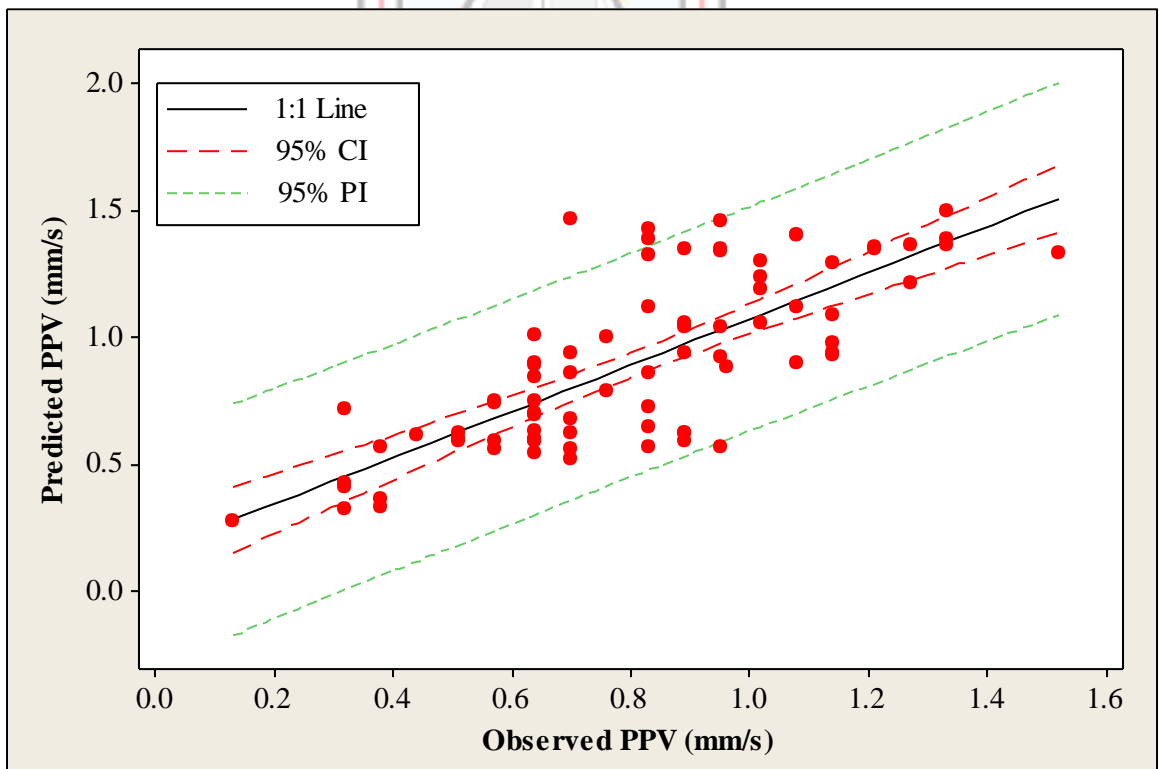
Figure 5.24 Observed PPV Versus Predicted PPV by USBM
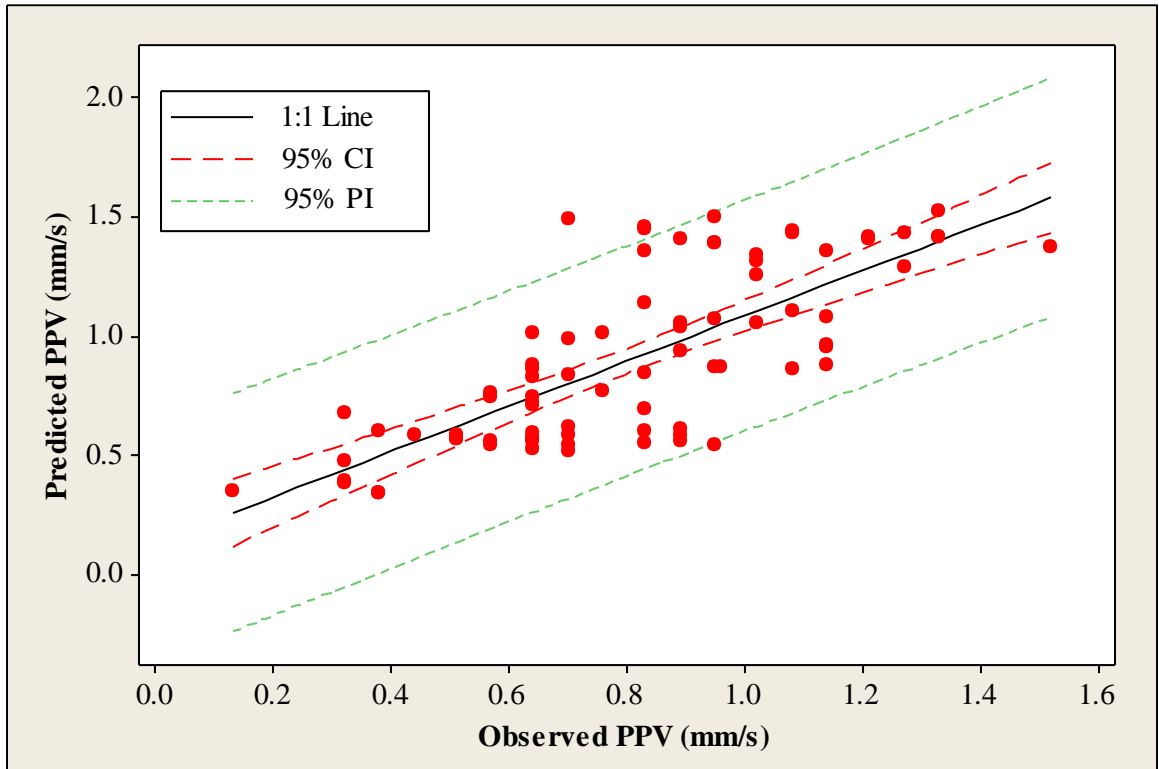
Figure 5.25 Observed PPV Versus Predicted PPV by Ambrasey-Hendron
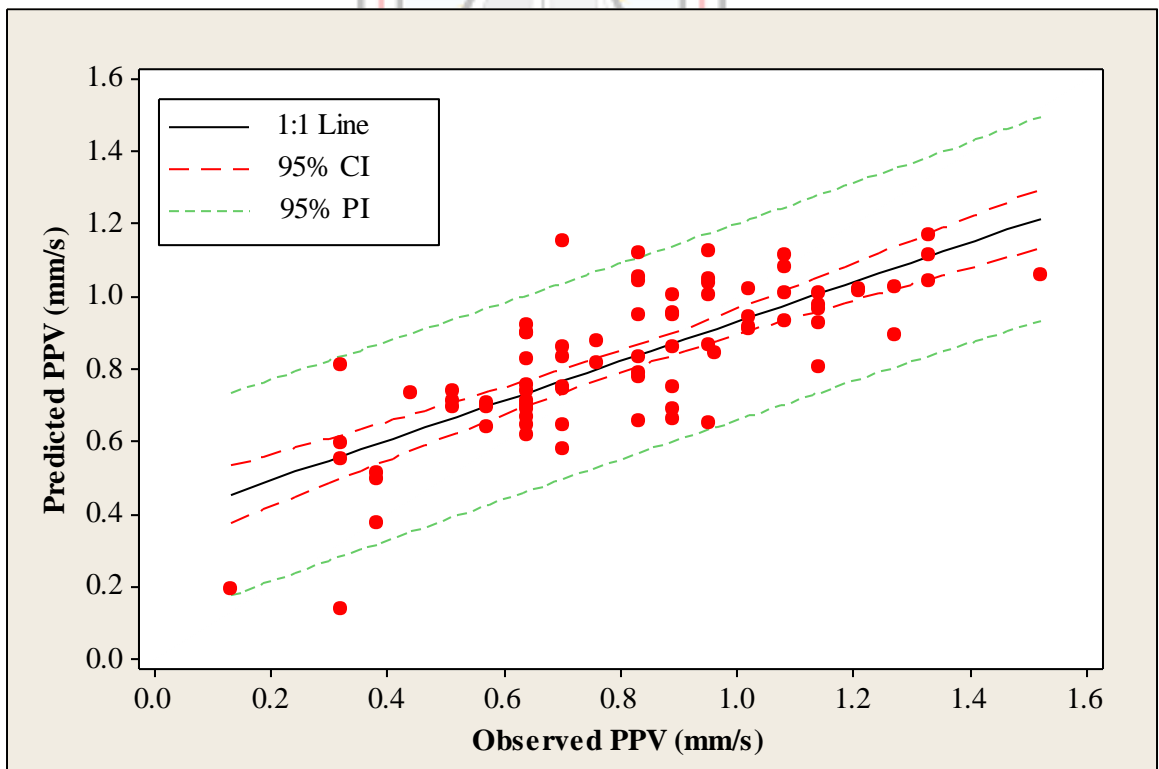
Figure 5.26 Observed PPV Versus Predicted PPV by Indian Standard
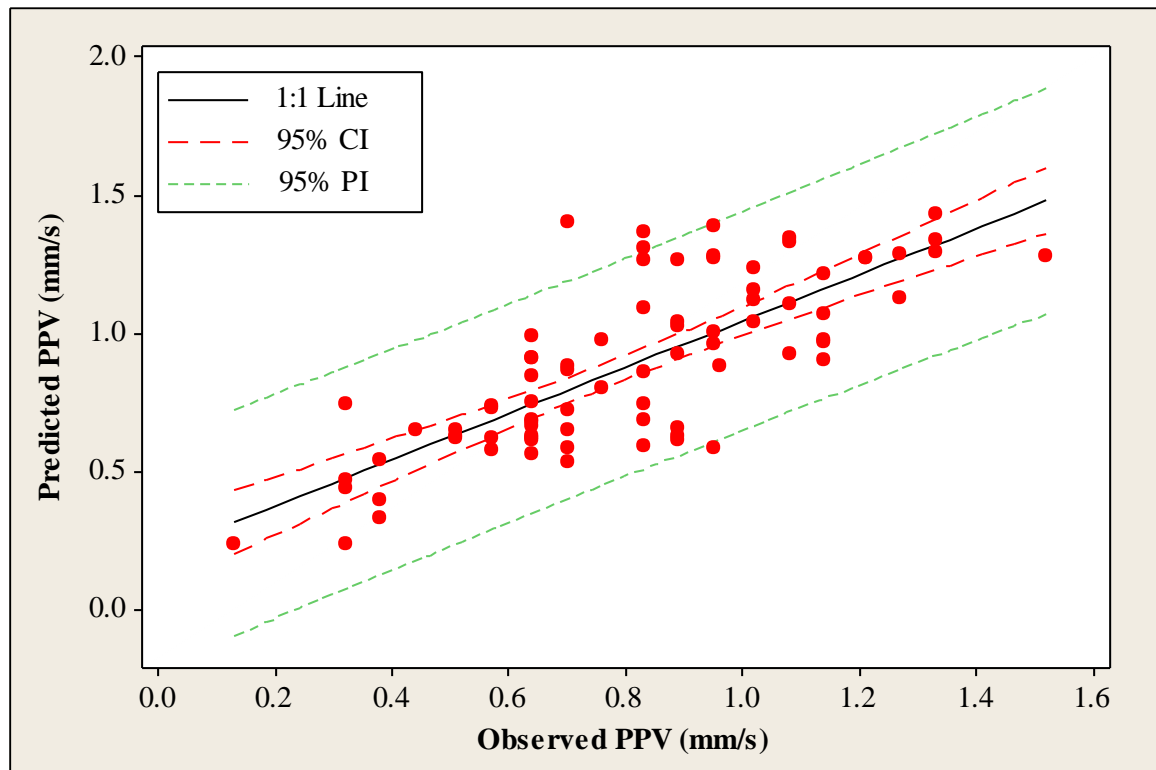
Figure 5.27 Observed PPV Versus Predicted PPV by Langefors-Kihlstrom

5.4   Blast-Induced Ground Vibration Prediction Model Selection

The AIC technique is a model selection criterion. This was utilised in this study to select the best model among the candidate models applied. When AIC values are made up of both negative and positive values, the most negative is the smallest and hence the model with that value is the selected model. The computed AIC values (Table 5.19) showed that the proposed LS-SVM approach had a better capability of producing reliable results than the other investigated techniques. This is because, among the methods, the LS-SVM had the least AIC value (Table 5.19) and thus was selected as the best technique over the other AI methods and the empirical methods considered. The obtained results also revealed that the other proposed AI methods (WNN, MARS and GPR) produced comparable and satisfactory prediction results. This affirms the assertion made that, the proposed AI models can suitably be used to predict blast-induced ground vibration. A graphical illustration of the AIC results is shown in Figure 5.28.

Therefore, on the basis of the quantitative analyses presented in this study, it can logically be stated that the potential of LS-SVM, WNN, MARS and GPR in the blast-induced ground vibration prediction for the Ghana Manganese Limited has been duly investigated.

Table 5.19 AIC Values for the Various Methods

Various Methods	AIC Values
LS-SVM	-70.111
ELM	-69.568
BPNN	-69.42
RBFNN	-67.347
WNN	-65.65
SVM	-64.833
MARS	-63.718
GPR	-59.41
GMDH	-58.314
GRNN	-43.323
Indian Standard	-39.035
Langefors-Kihlstrom	-15.968
USBM	0.6315
Ambrasey-Hendron	13.4178
RVM	46.6458
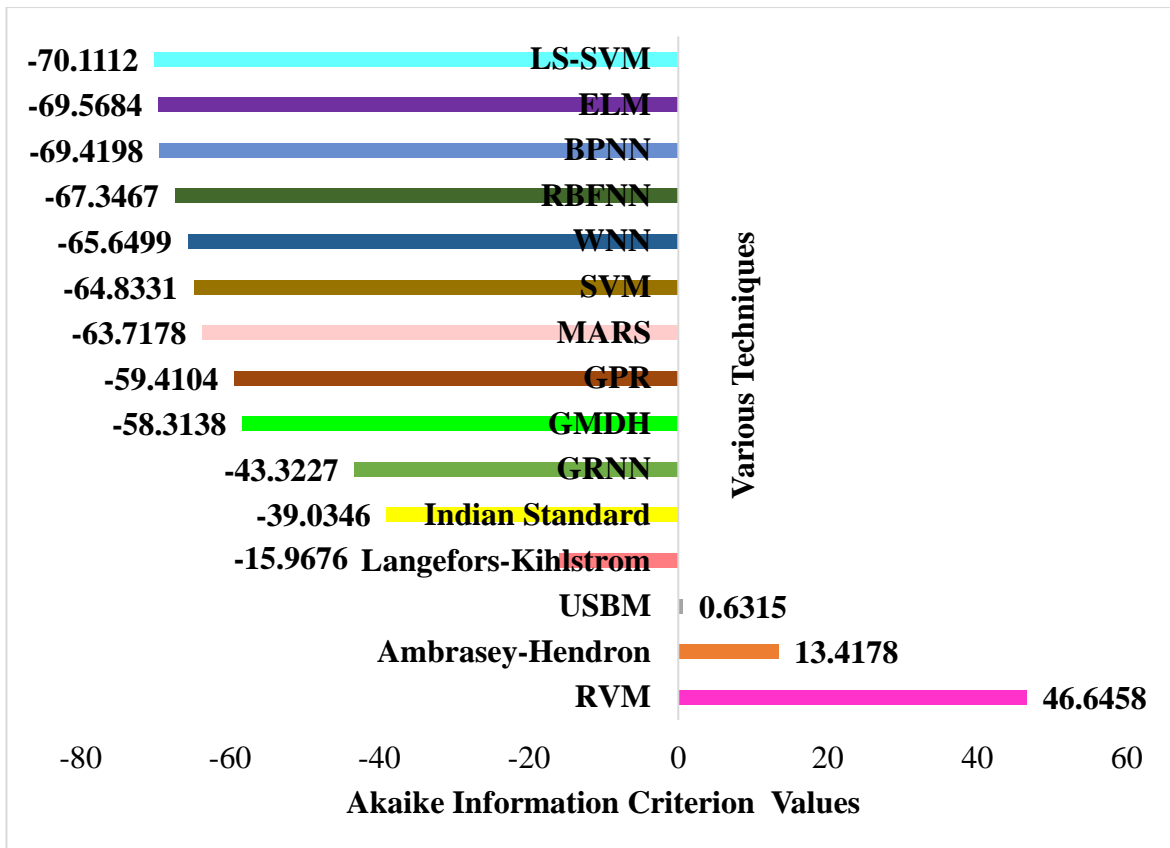
Figure 5.28 AIC Values of the Various Blast-Induced Ground Vibration Models

CHAPTER 6

INTERPRETATIONS OF AIR OVERPRESSURE PREDICTION

6.1 AI Models Developed for Air Overpressure Prediction

6.1.1 RBFNN Model for Air Overpressure Prediction

After experimenting on the width parameter value and the maximum number of neurons in the hidden layer, to obtain the optimum RBFNN structure to predict air overpressure at NGRL, a width parameter value of 1.4 and a maximum number of 13 neurons in the hidden layer gave the highest R and lowest MSE for both the training and testing data sets. Hence, the optimum RBFNN structure selected for predicting air overpressure is [4 – 13 – 1]. That is, four inputs with one hidden layer of 13 neurons and one output layer. Table 6.1 presents the optimal training and testing results based on the R and MSE criteria. All the width parameter and maximum number of neurons in the hidden layer that were used to arrive at the optimal results are presented in Table F1 of Appendix F.

Table 6.1 Optimal Training and Testing R and MSE Results for the RBFNN Model

Width Parameter	Number of Neurons	Training		Testing	
		R	MSE	R	MSE
1.4	13	0.757403	1.765968	0.76556	1.573762

6.1.2 GRNN Model for Air Overpressure Prediction

For the developed GRNN model for air overpressure prediction, the width parameter value that gave the highest R and the lowest MSE is 0.33. Table 6.2 shows the optimal training and testing results. However, all the width parameters that were used to arrive at the optimal results are presented in Table G1 of Appendix G.

Table 6.2 Optimal Training and Testing R and MSE Results for the GRNN Model

Width Parameter	Training		Testing	
	R	MSE	R	MSE
0.33	0.8167	1.4683	0.7619	1.5050

6.1.3 BPNN Model for Air Overpressure Prediction

Selection of the optimum training function and number of hidden neurons

The results obtained by training and testing the BPNN for air overpressure prediction with the scaled conjugate gradient, Levenberg-Marquardt and Bayesian regularisation algorithms including the different number of neurons applied in the hidden layer are presented in Tables 6.3, 6.4 and 6.5 respectively.

Table 6.3 Scaled Conjugate Gradient Backpropagation Algorithm

Numbers of Neurons	Training		Testing	
	R	MSE	*R*	MSE
1	0.643764	2.425514	0.751499	1.529449
2	0.801971	1.478096	0.60997	2.514451
3	0.845982	1.177672	0.661453	2.392507
4	0.86045	1.075407	0.463342	11.9177
5	0.889023	0.868356	0.422787	5.027626
6	0.916653	0.661696	0.535021	5.077056
7	0.917788	0.653072	0.426872	7.414732
8	0.937206	0.503875	0.304976	8.903666
9	0.945267	0.441013	0.407616	22.97268
10	0.940015	0.482033	-0.02687	24.35303
11	0.956656	0.351289	0.203257	37.16648
12	0.964665	0.287555	0.034378	56.0914

From Table 6.3, it was observed that, using the scaled conjugate gradient, the number of neurons in the hidden layer that gave the best *R* and the lowest MSE for the testing data set is 1. It can also be realised that as the number of hidden neurons increased the *R* and the MSE of training became better while that of the testing became worse. That is, from a hidden layer of 4 upwards, there was overfitting. Here, the backpropagation could not learn the relationship between the input parameters and the target values. Hence, when new input data sets were introduced into the system, the air overpressure could not be properly predicted.

From Table 6.4, it can be observed that, using the Levenberg-Marquardt algorithm, the number of neurons in the hidden layer that gave the best R and the lowest MSE for the testing data set is 1. It can also be realised that as the number of neurons in the hidden layer increased, the R and the MSE of training became better while that of the testing became worse. That is from the hidden layer of 6 upwards, there was overfitting.

Table 6.4 Levenberg-Marquardt Backpropagation Algorithm

Numbers of Neurons	Training		Testing	
	R	MSE	R	MSE
1	0.64378	2.425428	0.750613	1.535101
2	0.74093	1.868186	0.615317	2.487786
3	0.68527	2.19699	0.619682	2.230534
4	0.86466	1.045275	0.714371	2.21146
5	0.84404	1.191212	0.622374	2.866
6	0.90438	0.754229	0.588765	4.109689
7	0.925	0.597974	0.585553	4.251269
8	0.92822	0.573271	0.521987	5.132623
9	0.94545	0.439543	0.095905	28758.09
10	0.9555	0.36018	0.22841	9.896274
11	0.9582	0.339039	0.087962	793.0012
12	0.9651	0.284074	0.189766	61.45825

From Table 6.5, it was observed that, using the Bayesian regularisation backpropagation algorithm, the number of neurons in the hidden layer that gave the best R and the lowest MSE for the testing data set is also 1. It was also realised that, as the number of neurons in the hidden layer increased, the MSE of the testing data increased at a corresponding value as the number of neurons.

The best results from Tables 6.3, 6.4 and 6.5 were selected and presented in Table 6.6. With reference to Table 6.6, the training function selected for the training of BPNN for the prediction of air overpressure at NGRL is the Bayesian regularisation backpropagation algorithm. This is because it gave the highest R value and lowest MSE for the testing data set.

Table 6.5 Bayesian Regularisation Backpropagation Algorithm

Number of Neurons	Training		Testing	
	R	MSE	*R*	MSE
1	0.640157	2.448225	0.762784	1.473757
2	0.757645	1.766464	0.762235	2.508773
3	0.779699	1.628184	0.745949	3.576965
4	0.784913	1.595108	0.758454	4.517133
5	0.784994	1.594571	0.758129	5.522484
6	0.785002	1.594515	0.757801	6.525853
7	0.785006	1.594484	0.757583	7.528027
8	0.781204	1.618605	0.745442	8.611742
9	0.781202	1.618616	0.744025	9.623944
10	0.781213	1.618547	0.743056	10.63229
11	0.781211	1.618555	0.742018	11.64129
12	0.781215	1.618529	0.741552	12.64534

Table 6.6 Selection of the Best Training Function for Backpropagation Algorithm

Training Function	Optimum Hidden Neurons	Training		Testing	
		R	MSE	*R*	MSE
Levenberg-Marquardt backpropagation algorithm	1	0.64378	2.425428	0.750613	1.535101
Bayesian regularisation backpropagation algorithm	1	0.640157	2.448225	0.762784	1.473757
Scaled conjugate gradient backpropagation algorithm	1	0.643764	2.425514	0.751499	1.529449

Optimal BPNN structure

The optimum structure of the BPNN for air overpressure prediction consists of three layers: input layer, hidden layer and the output layer. The BPNN structure is made up of four inputs with a hyperbolic tangent hidden layer transfer function and a linear output layer transfer function. The network was trained for 8000 epochs using the Bayesian regularisation backpropagation algorithm. The optimum structure of the BPNN was [4 – 1 – 1] that is four inputs, one hidden neuron and one output.

6.1.4   WNN Model for Air Overpressure Prediction

In the development of the WNN model for air overpressure prediction, it was found out based on the experimental results that when two wavelons were used in the hidden layer, the highest R and the lowest MSE were obtained on the testing data set. Thus, the structure of the optimum WNN is [4 – 2 – 1], that is four inputs, two wavelons in the hidden layer and one output. Table 6.7 shows the optimal training and testing results for the WNN technique based on the R and MSE criteria. All the wavelons in the hidden layer that were used to arrive at the optimal results are presented in Table H1 of Appendix H.

Table 6.7 Optimal Training and Testing *R* and MSE Results for WNN

Number of wavelons	Training		Testing	
	R	MSE	R	MSE
2	0.8292	1.3045	0.6551	2.2205

6.1.5   GMDH Model for Air Overpressure Prediction

The developed GMDH model for air overpressure prediction having the lowest MSE and highest R value was found to have two parameters in input layer, one hidden layer with one neuron and an output layer. The corresponding polynomial equation representations of the developed GMDH for air overpressure prediction are shown Equations (6.1) and (6.2). These equations revealed that the main contributing input relative to the training and testing data sets are the number of blast holes, stemming length (m) and distance between the monitoring station and the blast point (m) to the entire inputs variables under consideration

Table 6.8 shows the optimal training and testing results for the GMDH technique based on the R and MSE criteria.

Layer 1

$$x_5 = 9.960 - 0.0555(x_4) + 87.51(x_2) + 0.01342(x_2)(x_4)$$
$$+ 1.736 \times 10^{-6}(x_4)^2 - 16.44(x_2)^2$$

(6.1)

Output layer

$$y = -645.7 + 13.82(x_5) - 0.1628(x_1) + 0.001387(x_1)(x_5)$$
$$- 0.06331(x_5)^2 + 2.66 \times 10^{-5}(x_1)^2$$

(6.2)

where x_1 is the number of blast holes, x_2 is the stemming length, x_4 is the distance from the blasting point to the monitoring station (m), x_5 is the resultant of layer 1.

Table 6.8 Optimal Training and Testing R and MSE Results for GMDH

Number of Neurons	Training		Testing	
	R	MSE	R	MSE
1	0.73067	1.9306	0.5025	3.5099

6.1.6 MARS Model for Air Overpressure Prediction

The training and testing results of the three MARS models developed based on their order of interactions are presented in Table 6.9.

Table 6.9 Training and Testing Results for Each Order of Interaction

Order of Interaction	Training		Testing	
	R	MSE	R	MSE
First Order	0.5487	2.8951	0.7117	1.6961
Second Order	0.7423	1.8595	0.6774	1.8597
Third Order	0.6606	2.3343	0.6658	1.9132

From Table 6.9, it can be observed that, the MARS model with zero order gave the lowest MSE and the highest R value for the testing phase. Hence, the final MARS model based on the zero order comprises of 2 out of the 20 basis functions used at the initial forward stage. Table 6.10 presents the corresponding equations for the selected basis functions.

Table 6.10 The Basis Functions (BF) and their Related Equations

Basis Functions	Equations
BF9	max (0, Number of blast holes – 186)
BF11	max (0, Distance – 1713)

The developed MARS model for predicting blast-induced air overpressure is given in Equation (6.3).

$$\text{AOp} = 106.156 - 0.0106961 \times \text{BF9} - 0.00238971 \times \text{BF11} \qquad (6.3)$$

6.1.7   SVM Model for Air Overpressure Prediction

In this study, the optimum design values of ε and C was set at 0.00000001 and 50 respectively. The polynomial kernel of order one was the best kernel in this regard. Table 6.11 shows the optimal training and testing results.

Table 6.11 Optimal Training and Testing R and MSE Results for SVM

Training		Testing	
R	MSE	R	MSE
0.6082	2.6338	0.7357	1.6688

6.1.8   LS-SVM Model for Air Overpressure Prediction

In the development of the LS-SVM, the optimum design values of γ (Equation (4.27)) and σ^2 (Equation 4.33) that produced the best predicted air overpressure values are 3.6459 and 0.7239. Table 6.12 shows the optimal training and testing results.

Table 6.12 Optimal Training and Testing *R* and MSE Results for LS-SVM

Training		Testing	
R	MSE	*R*	MSE
0.92375	0.64267	0.63553	2.18221

6.1.9 RVM Model for Air Overpressure Prediction

For the developed RVM model for air overpressure prediction, the optimum width parameter was found to be 1.6294. Table 6.13 shows the optimal training and testing results.

Table 6.13 Optimal Training and Testing *R* and MSE Results for RVM

Width Parameter	Training		Testing	
	R	MSE	*R*	MSE
1.6294	0.62993	2.50169	0.74057	1.60649

6.1.10 ELM Model for Air Overpressure Prediction

For the developed ELM model for air overpressure prediction, the optimum number of neurons that gave the highest *R* and MSE is 18 having the sigmoid activation function. Therefore, the optimum ELM structure is [4 – 18 – 1] which equates to four inputs with one hidden layer of 18 neurons and one output. Table 6.14 shows the optimal training and testing results for the ELM technique based on the *R* and MSE criteria. All the neurons in the hidden layer that were used to arrive at the optimal results are presented in Table I1 of Appendix I.

Table 6.14 Optimal Training and Testing *R* and MSE Results for ELM

Number of Neurons	Training		Testing	
	R	MSE	*R*	MSE
18	0.78213	1.60832	0.68251	2.59418

6.1.11 GPR Model for Air Overpressure Prediction

Using the *R* and MSE criteria, the comparative results obtained by the various GPR models using the testing data sets are presented in Table 6.15.

Table 6.15 Test Results of the Various Gaussian Process Regression Model

GPR Model	Covariance Function	*R*	MSE
GPR- Squared exponential	Squared exponential	0.5430	2.4980
GPR- Exponential	Exponential	0.7059	1.7473
GPR- Matérn 3/2	Matérn 3/2	0.65508	1.99573
GPR- Matérn 5/2	Matérn 5/2	0.54681	4.03049
GPR- Rational quadratic	Rational quadratic	0.73091	1.6575

From Table 6.15, it can be noticed that, the Rational Quadratic covariance function gave the highest *R* of 0.73091 and lowest MSE of 1.6575, relative to the other candidate covariance functions applied in this study. The selected proposed GPR model valid for air overpressure prediction has a mean function of constant 0.4536 and Rational quadratic covariance function with a signal variance of 44275.3144, a length scale of 8.8753 and noise variance of 4.23573×10^{-10}.

6.1.12 Empirical Models Developed for Air Overpressure Prediction

Determination of the site constants of the General Predictor equation

The site constants of the general predictor equation which was determined by plotting the air overpressure (AOp) values against the scaled distance of $D/\sqrt[3]{Q}$ is presented in Figure 6.1.

$$y = 133.46x^{-0.041}$$
$$R^2 = 0.214$$
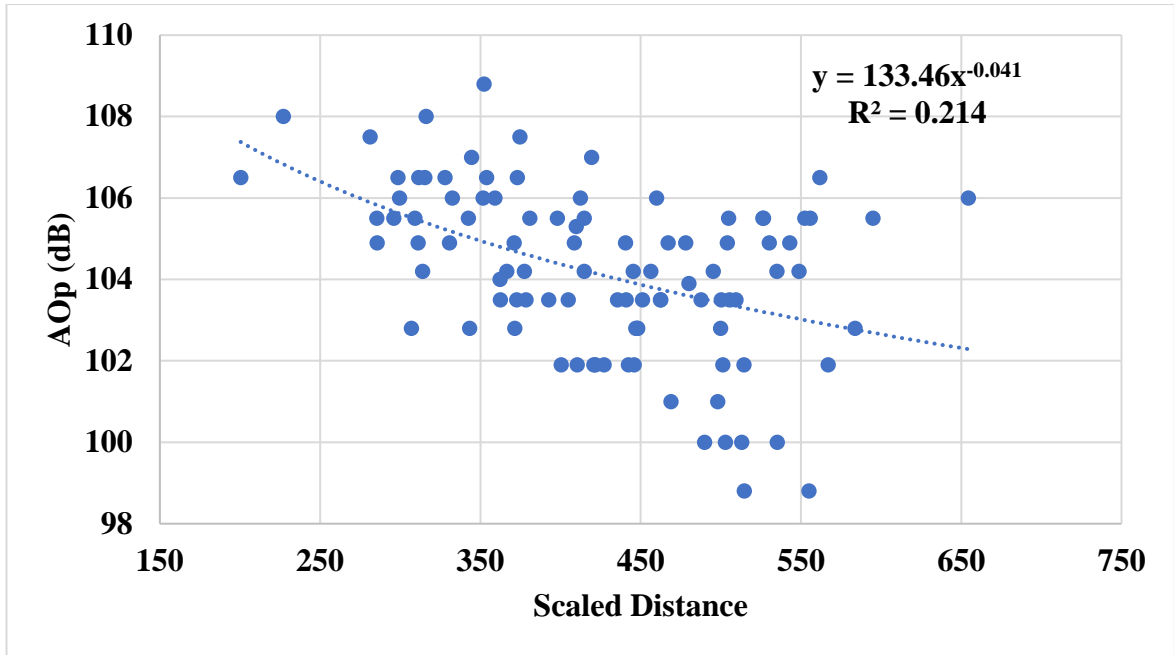
Figure 6.1 Resultant AOp Versus Scaled Distance Relationship for General Predictor Equation
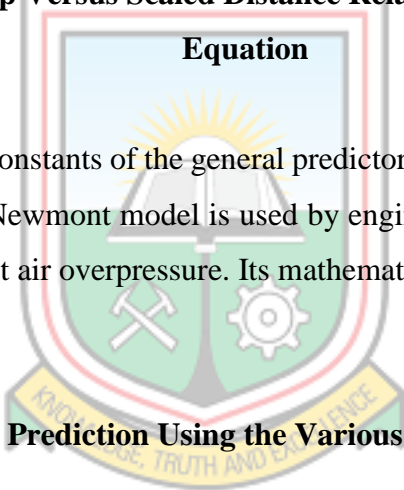
From Figure 6.1, the site constants of the general predictor equation, k and β are 133.46 and -0.041 respectively. The Newmont model is used by engineers at Newmont Golden Ridge Limited (NGRL) to predict air overpressure. Its mathematical notation is given in Equation (4.73).

6.2   Air Overpressure Prediction Using the Various Models

The AOp predicted values of the testing data using the various AI and empirical models are presented in Table J1 of Appendix J.

6.3   Comparison of the AI Methods and the Empirical Methods for Air Overpressure Prediction

The statistical results based on the testing data for each of the techniques applied are presented in Table 6.16.

Table 6.16 Models Performance Criteria Results

Various Techniques	Performance Indicators							
	MSE	RMSE	RRMSE (%)	MAE	R	R^2	NASH	VAF (%)
BPNN	1.4738	1.214	1.1605	0.9731	0.7628	0.5818	0.5712	57.938
GRNN	1.505	1.2268	1.1728	1.0072	0.7619	0.5805	0.5621	56.831
RBFNN	1.5738	1.2545	1.1992	1.0574	0.7656	0.5861	0.5421	58.352
GMDH	3.5099	1.8735	1.791	1.2256	0.5025	0.2525	-0.0213	-2.1175
WNN	2.2205	1.4901	1.4245	1.1955	0.6551	0.4292	0.3539	37.546
SVM	1.6688	1.2918	1.2349	1.0629	0.7357	0.5412	0.5144	53.284
LS-SVM	2.1822	1.4772	1.4122	1.1933	0.6355	0.4039	0.365	38.466
RVM	1.6065	1.2675	1.2117	1.0148	0.7405	0.5484	0.5326	54.762
ELM	2.5942	1.6106	1.5397	1.2343	0.6825	0.4658	0.2452	24.881
GPR	1.6575	1.2874	1.2307	1.0732	0.7309	0.5342	0.5177	52.027
MARS	1.6961	1.3024	1.2450	1.0738	0.7251	0.5257	0.5065	50.7183
General Predictor	2.5942	1.6106	1.5397	1.2343	0.6825	0.4658	0.2452	24.881
Newmont Model	6.6577	2.5803	2.4666	2.2659	0.681	0.4637	-0.9372	-16.671

From Table 6.16 it can be observed that the BPNN model had the lowest MSE, RMSE, RRMSE and MAE values of 1.471, 1.2129, 1.1594 and 0.9843 dB respectively These statistical results indicate that the developed BPNN model for AOp predictions marginally deviated from the observed PPV. The reason being that the closer the statistical error indicator (MSE, RMSE, RRMSE and MAE) is to zero, the better the model could approximate closely the observed data. It can also be observed that the proposed AI techniques of GRNN, RBFNN, RVM, and MARS produced comparable results to benchmark techniques of BPNN, GPR and SVM. However, the other proposed and tested AI techniques of LS-SVM, WNN and ELM could not adequately generalise well on the test data and hence failed to produce comparable results. This was directly followed by the General Predictor, GMDH and Newmont model in a decreasing order of performance. A visual confirmation of the predictive strength of the BPNN and the proposed AI techniques

(GRNN, RBFNN, RVM and MARS) can additionally be viewed in Figures 6.2, 6.3, 6.4 and 6.5.

Figure 6.2 Performance of Various Models for Predicting AOp Using Mean Square Error (MSE)

Figure 6.3 Performance of Various Models for Predicting AOp Using Root Mean Square Error (RMSE)

Figure 6.4 Performance of Various Models for Predicting AOp Using Relative Root Mean Square Error (RRMSE)

Figure 6.5 Performance of Various Models for Predicting AOp Using Mean Absolute Error (MAE)

In Table 6.16, it is clear that the benchmark techniques of BPNN, GPR and SVM as well as the proposed and tested AI techniques of GRNN, RBFNN, MARS and RVM had R values greater than 0.7. This reveals a slightly high strength of linear correlation between the measured and predicted AOp. This is because the correlation coefficient, R which ranges from -1 to +1 with the strength of the relationship increasing towards the extremes, is used to ascertain the strength of the models' prediction performance by comparing the relationship between the observed and the predicted AOp values.

The analysis of the results presented in Table 6.16 further revealed that the other new AI techniques (LS-SVM, ELM and WNN) tested, the benchmark technique of GMDH and empirical models of General predictor and Newmont Model performed poorly and could not adequately model the test data. The reason being that, these models had R values less than 0.7. Comparatively, the AI techniques of RBFNN, GRNN and BPNN had the high R values, with RBFNN having the highest, indicating the strongest strength of correlation. This assertion can additionally be viewed in Figure 6.6.
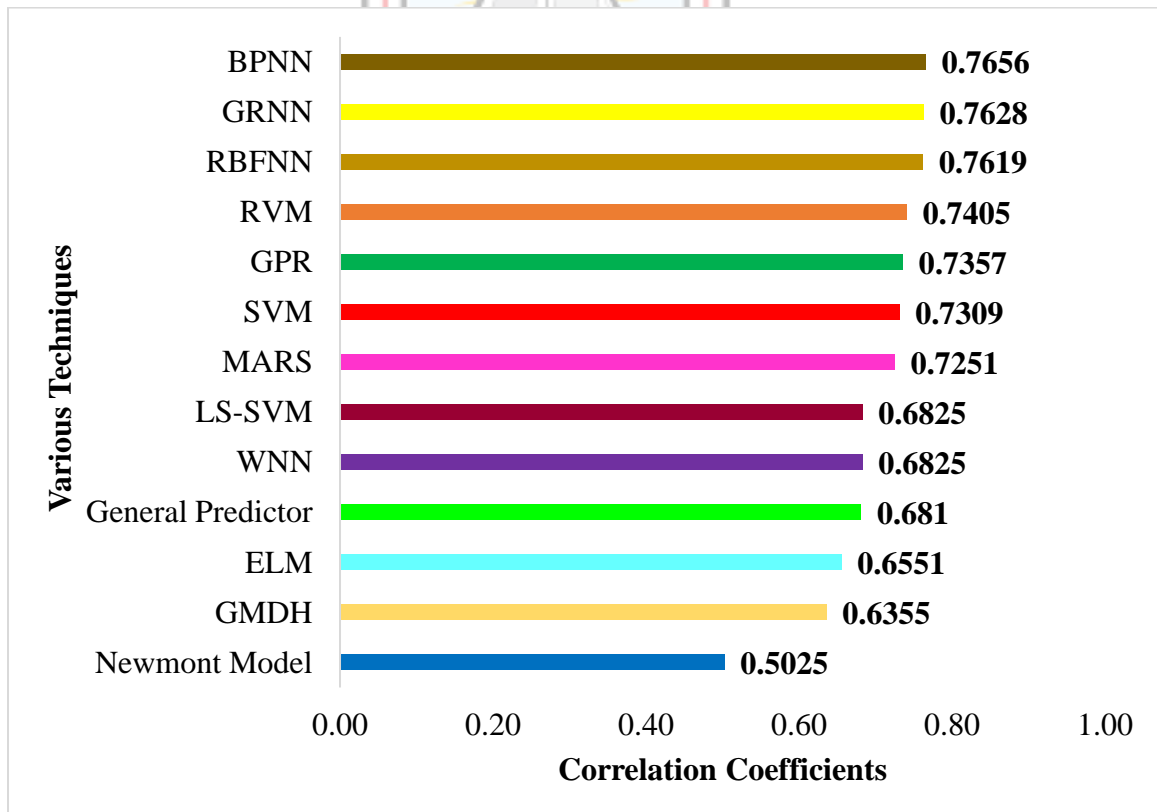
Figure 6.6 Performance of Various Models for Predicting AOp Using Correlation Coefficient

The R^2 results presented in Table 6.16 provide quantitative evidence on how close the predicted air overpressure values using the various techniques are to the least squares line of best fit. Hence with reference to Table 6.16, it is evident that the benchmark techniques of BPNN, GPR, SVM as well as the newly tested AI techniques of GRNN, RBFNN, MARS and RVM were able to predict a little more than 50% of the variation in the observed AOp data. However, the other AI techniques of GMDH, LS-SVM, ELM, WNN together with the empirical models of General predictor and Newmont Model were able to predict less than 50% of the variation in the observed AOp data. This means that the developed BPNN, GRNN, RBFNN, MARS, SVM, RVM and GPR models could appropriately explain the variability in the observed AOp data around its mean more effectively than the other AI and empirical methods. Figure 6.7 provides a graphical illustration of the R^2 results.

Figure 6.7 Performance of Various Models for Predicting AOp Using Coefficient of Determination

The NASH (Equation (4.79)) is a model efficiency-based indicator. It takes values of $-\infty$ to 1 with improved model performance approaching one. The NASH evaluates how well the plot of the observed and the predicted data fits the 1:1 line. It also explains the degree to which model predictions are error free. Hence, on the basis of the computed NASH values

147

(Table 6.16), it was found that 57.12% of the potential error has been explained by the BPNN model developed for predicting air overpressure. This was however, closely followed by the GRNN approach, with a NASH value of 56.12%. The rest of the models, RBFNN, RVM, GPR, SVM, MARS, LS-SVM, WNN, ELM, General Predictor, GMDH and Newmont Model performed in that decreasing order. Furthermore, it can be stated based on graphical evidence (Figure 6.8) that among the fifteen methods applied, the BPNN, GPR, SVM and the proposed AI techniques of GRNN, RBFNN, MARS and RVM approaches have comparatively demonstrated better capabilities of producing satisfactory air overpressure prediction results than the other methods utilised in this study.
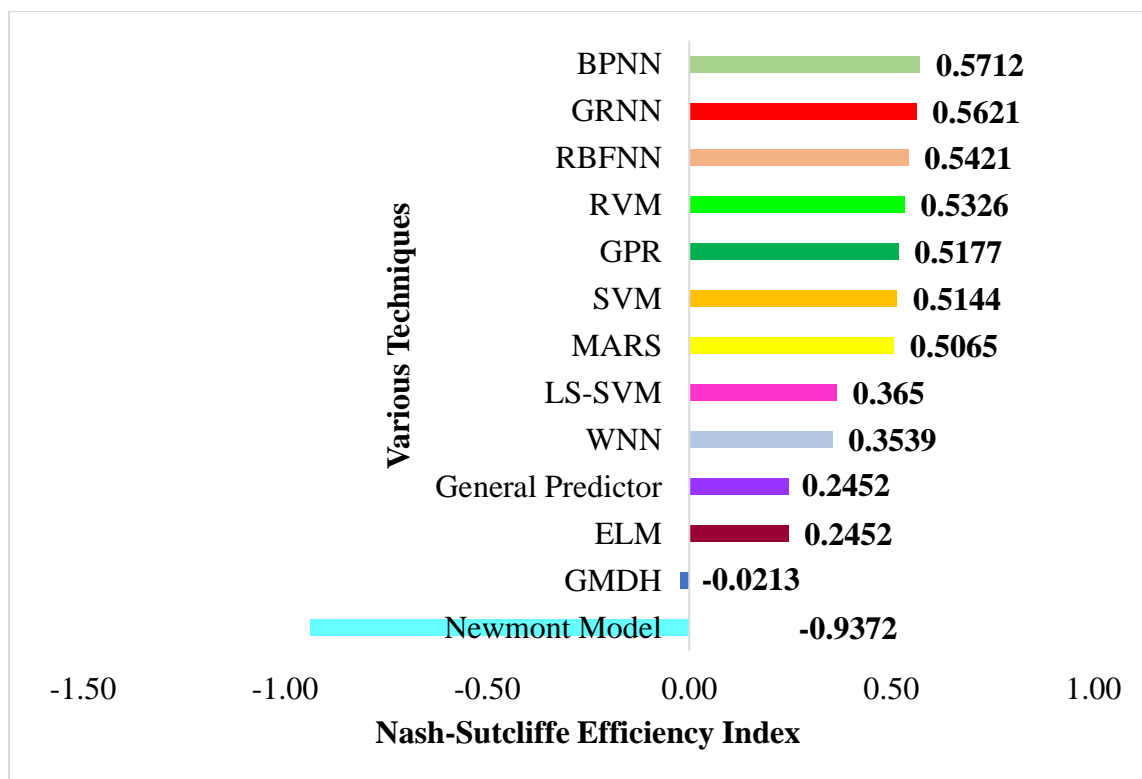
Figure 6.8 Performance of Various Models for Predicting AOp Using Nash-Sutcliffe Efficiency Index

The VAF as described by Delis *et al*. (2013) is used to verify the correctness of the models and how well they could estimate the unseen dataset. A model with a VAF value closest to 100% is said to be the most accurate among candidate models. Thus, from Table 6.16 it is evident that the newly tested AI techniques of GRNN, RBFNN, MARS and RVM were able to explain a little more than 50% of the potential errors in the prediction results as well as the benchmark techniques of BPNN, GPR and SVM. Furthermore, in comparing the

performance of these aforementioned newly tested AI techniques to the benchmark techniques of BPNN, GPR and SVM on the basis of the VAF values (Table 6.16), it can be observed that the RBFNN was most able to explain the potential error as it had the highest VAF value of 58.352%. The other had very comparable VAF values.

The analysis of the results presented in Table 6.16 further revealed that the other new AI techniques (LS-SVM, ELM and WNN) tested, the benchmark technique of GMDH and empirical models of General predictor and Newmont Model were able to predict less than 39% of the variation in the observed AOp data. They therefore performed poorly and could not adequately model the test data as they had.
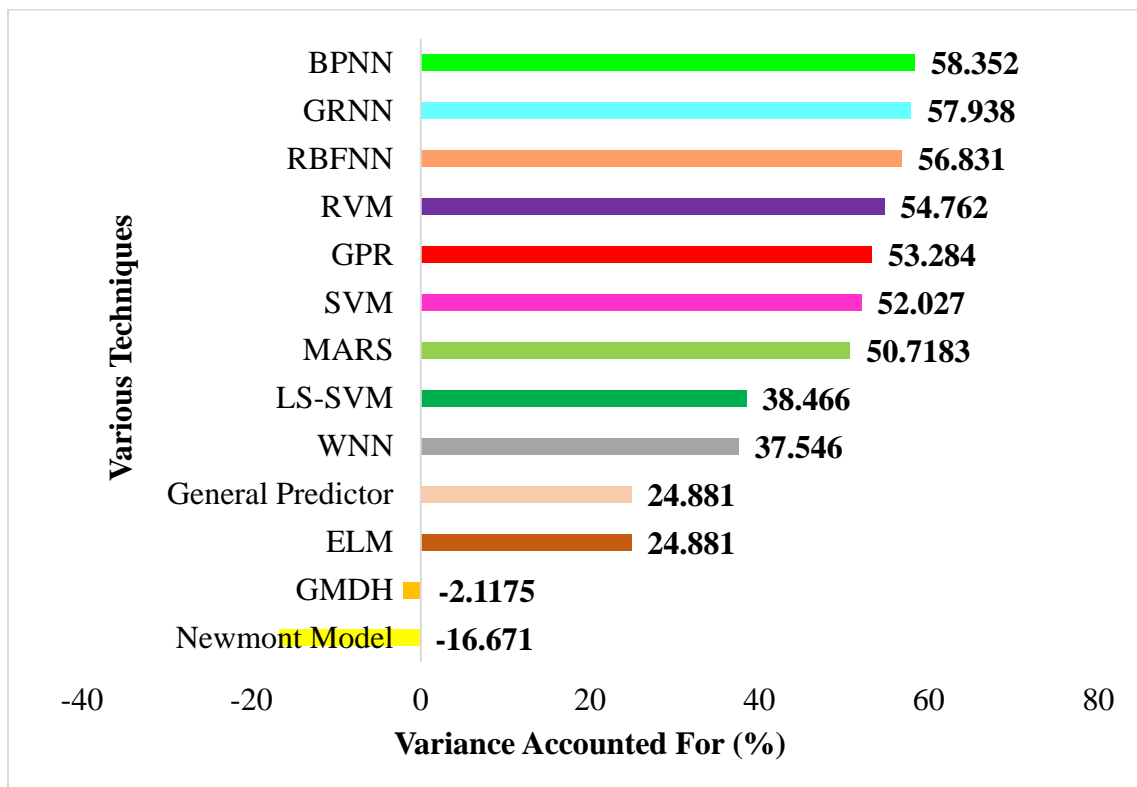
Figure 6.9 Performance of Various Models for Predicting PPV Using Variance Accounted For

Based on the obtained results (Table 6.16), it was found that four out of the seven newly tested AI techniques (GRNN, RBFNN, RVM and MARS) in this study produced comparable and satisfactory results as the widely used BPNN, GPR and SVM. Hence the proposed GRNN, RBFNN, RVM and MARS are proposed as suitable alternatives to the prediction of air overpressure.

149

Scatter plots along with the regression line, 95% PI and CI for the various models are presented in Figures 6.10 to 6.22. A critical look at the figures shows that the 1:1 line for each model fell in between the 95% CI lines. This means that, there is a 95% probability that the true best-fit line for the population data lies within the CI. It can also be observed that at least 93% of the predicted AOp values fell within the 95% PI lines for all the models. This indicates that when these models are used to predict new PPV values, there is a 93% probability that, at least 96% of the predicted AOp values will fall into the prediction interval. Comparatively, the proposed GRNN had the highest value of 100%. This was keenly followed by BPNN, with value of about 99%. The empirical models of General Predictor and Newmont Model had the lowest value of about 93%. The comparative results showed that the GRNN and BPNN models are superior to the other predictive techniques used in this study and is a promising tool for modelling and predicting air overpressure.
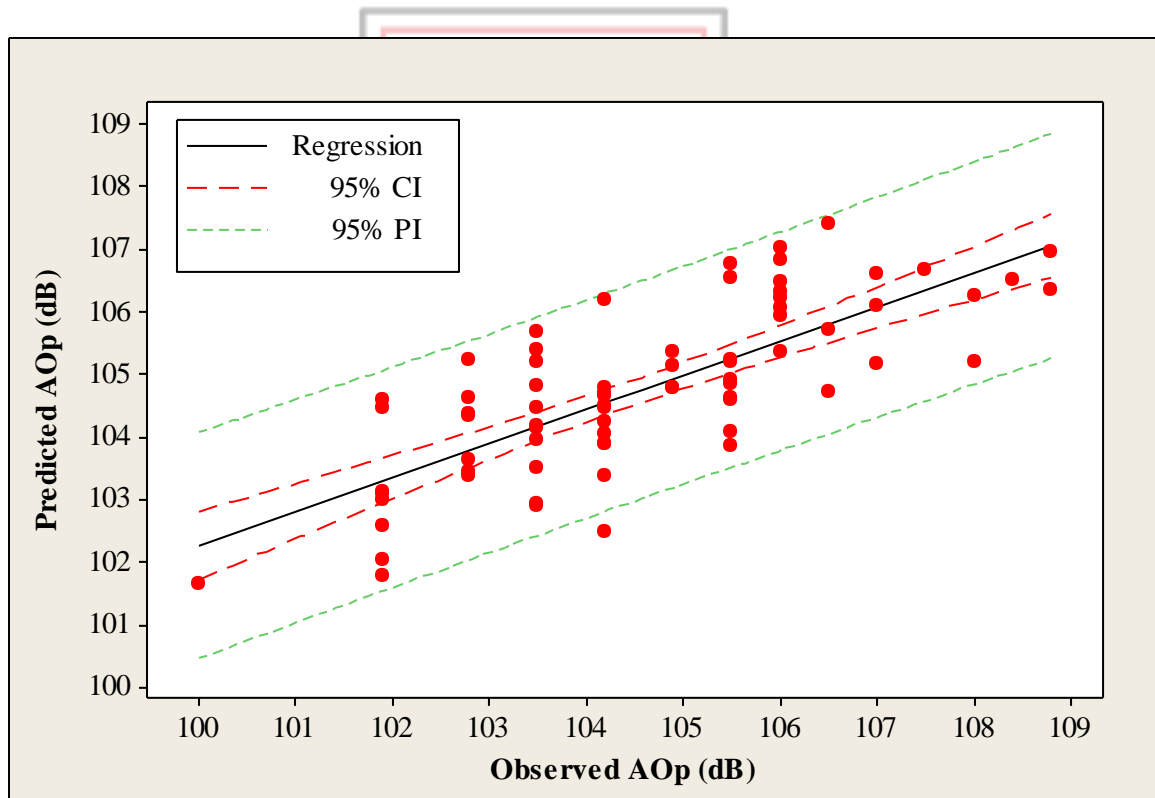
Figure 6.10 Observed AOp Versus Predicted AOp by BPNN
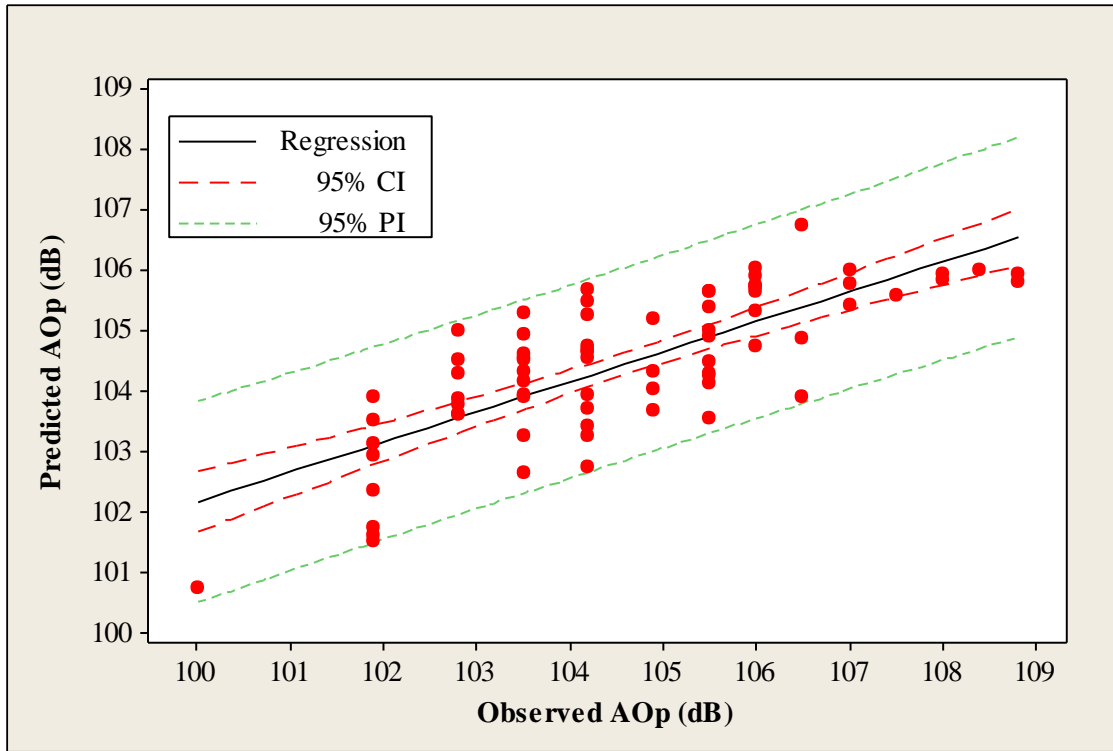
Figure 6.11 Observed AOp Versus Predicted AOp by GRNN
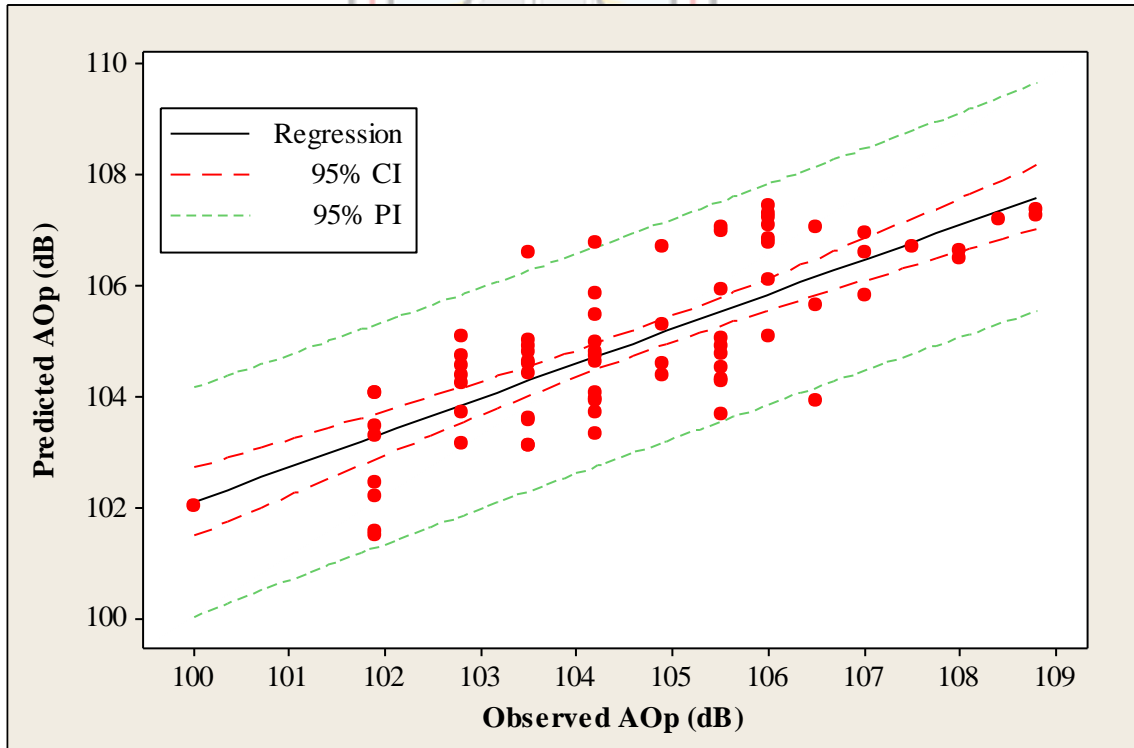
Figure 6.12 Observed AOp Versus Predicted AOp by RBFNN

151
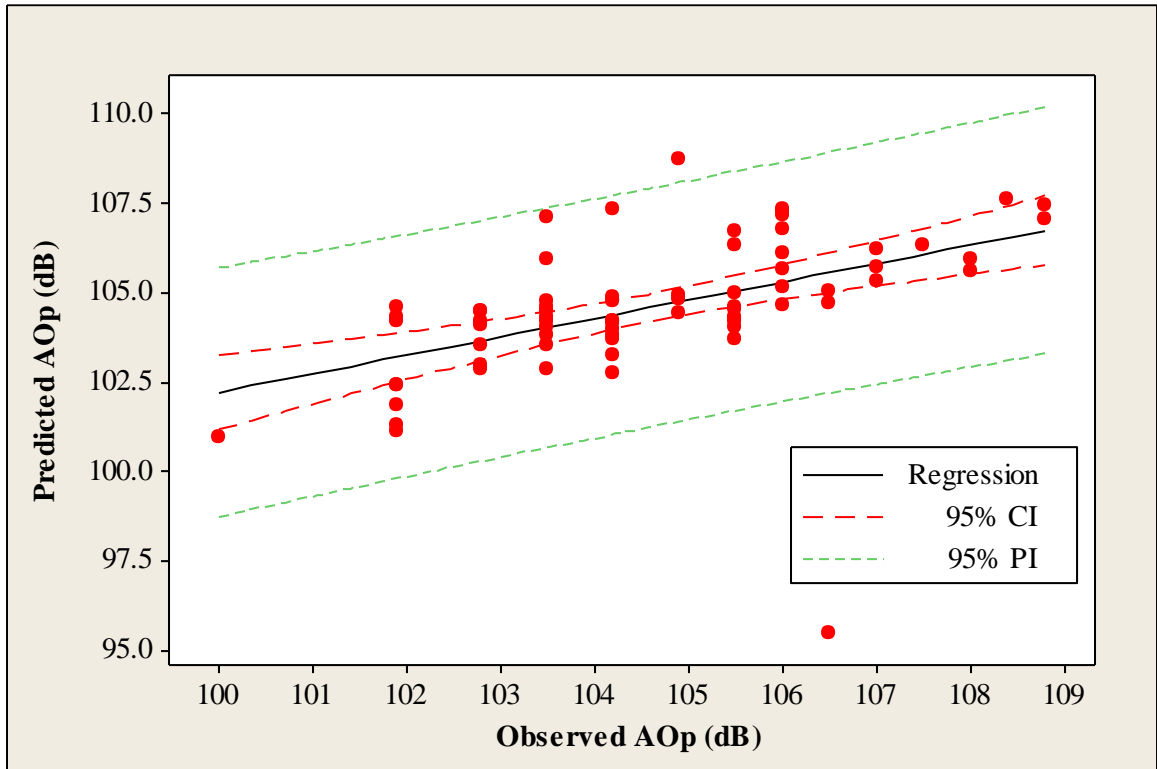
Figure 6.13 Observed AOp Versus Predicted AOp by GMDH
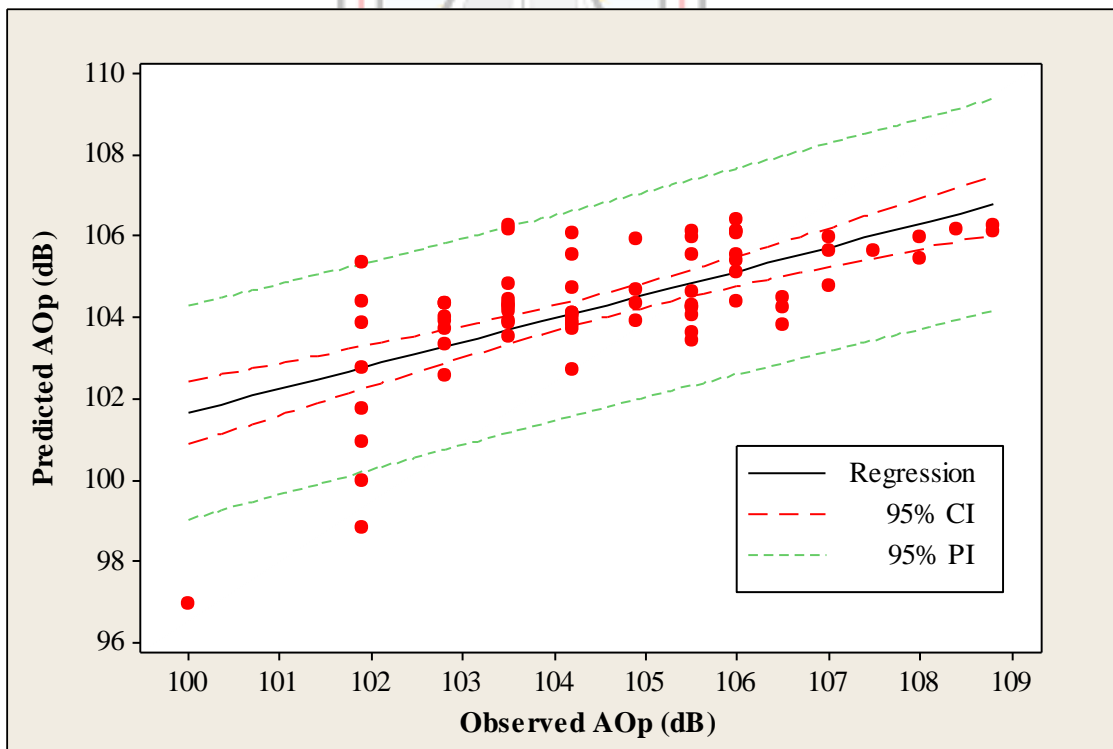
Figure 6.14 Observed AOp Versus Predicted AOp by WNN

152
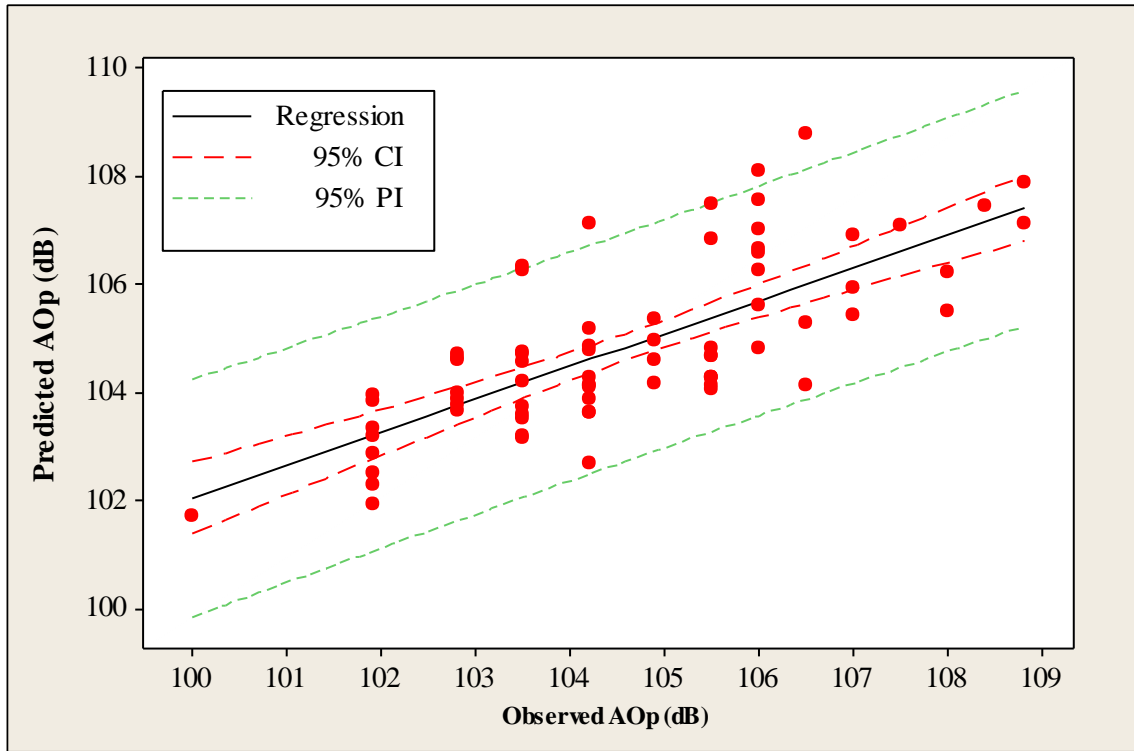
Figure 6.15 Observed AOp Versus Predicted AOp by SVM
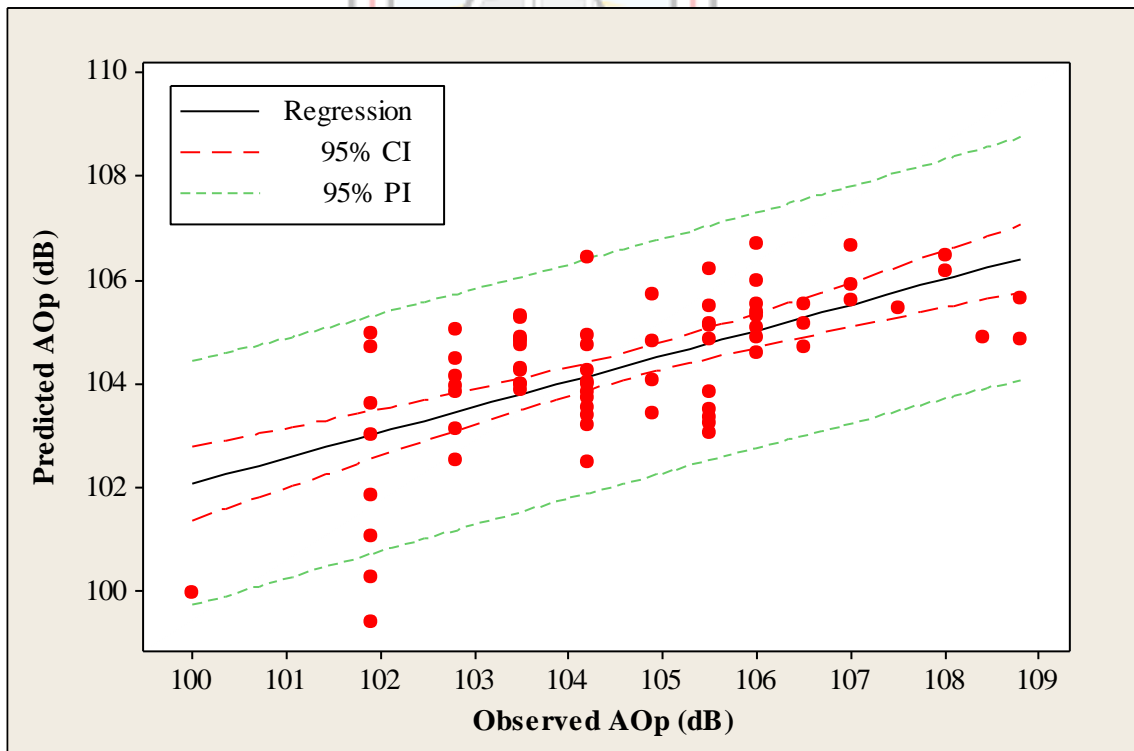
Figure 6.16 Observed AOp Versus Predicted AOp by LS-SVM
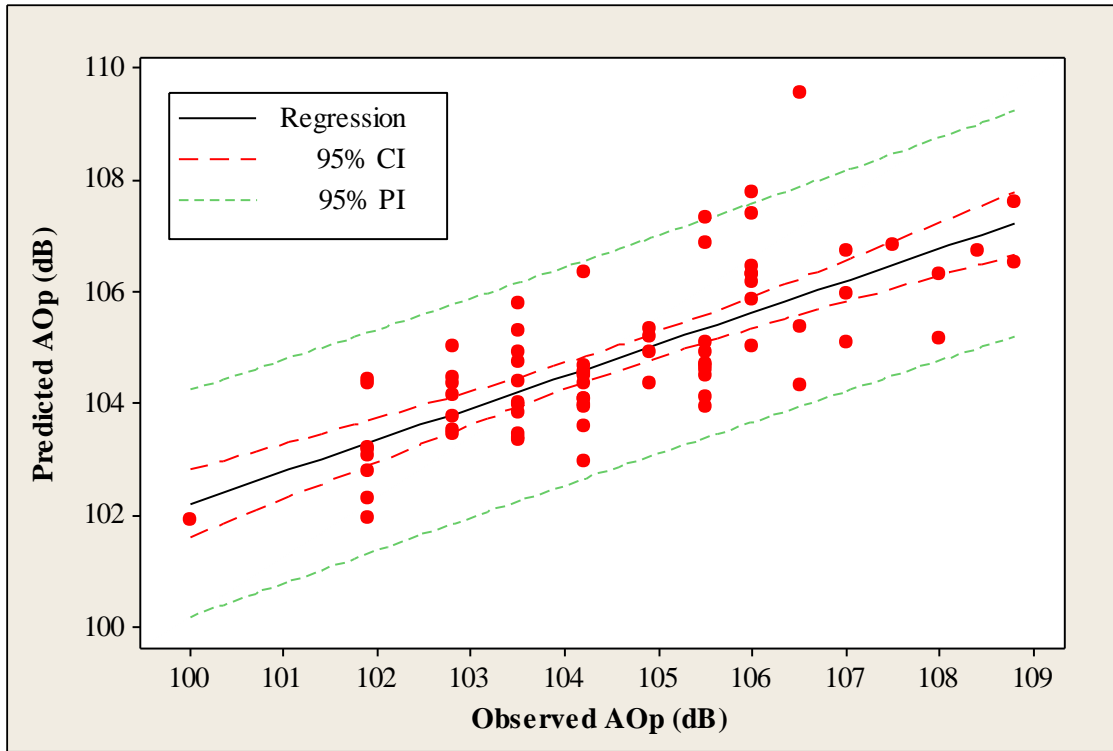
Figure 6.17 Observed AOp Versus Predicted AOp by RVM
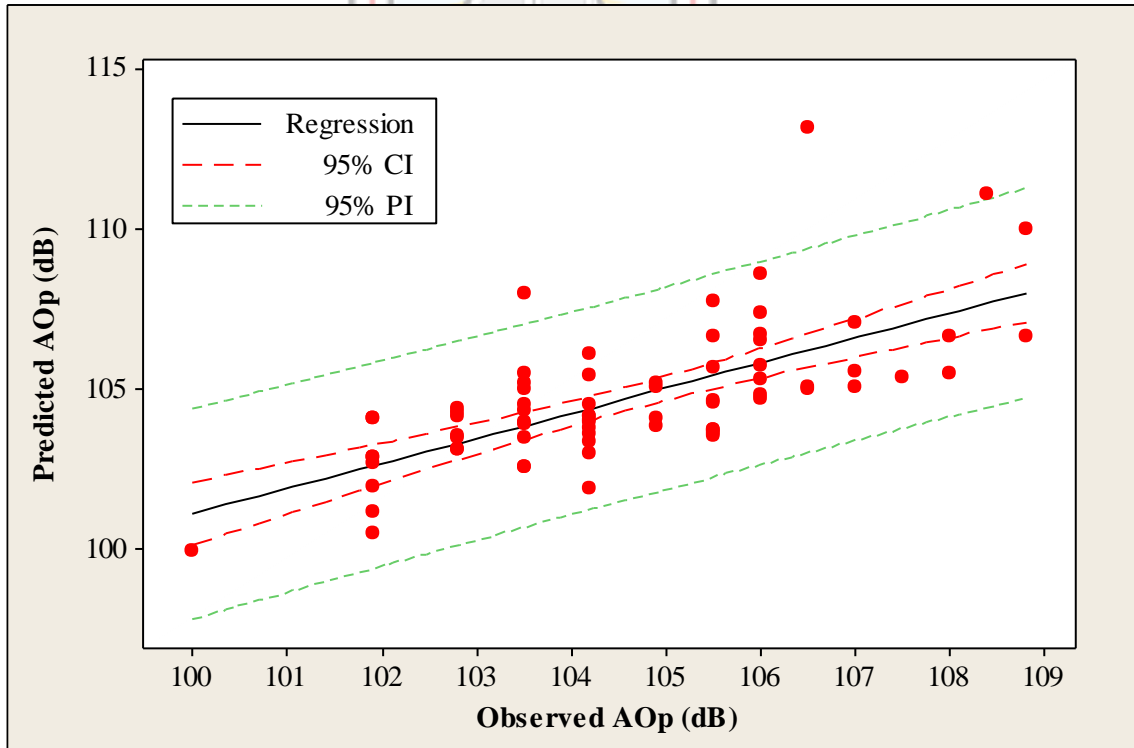
Figure 6.18 Observed AOp Versus Predicted AOp by ELM
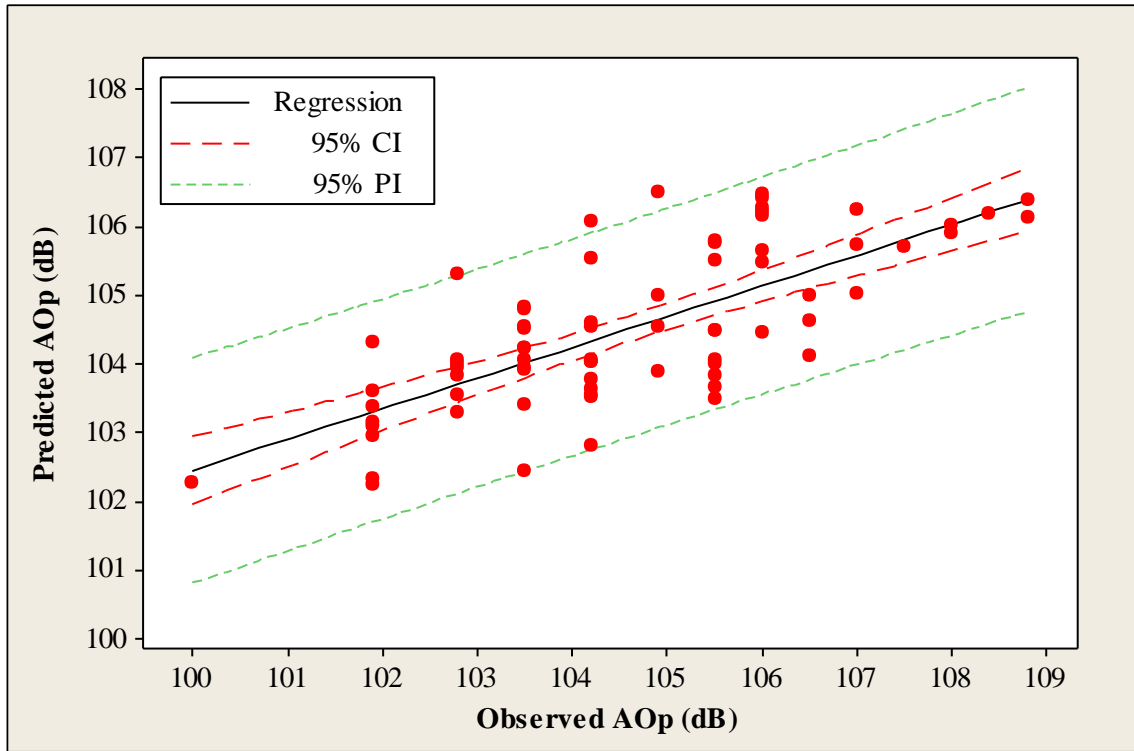
Figure 6.19 Observed AOp Versus Predicted AOp by GPR
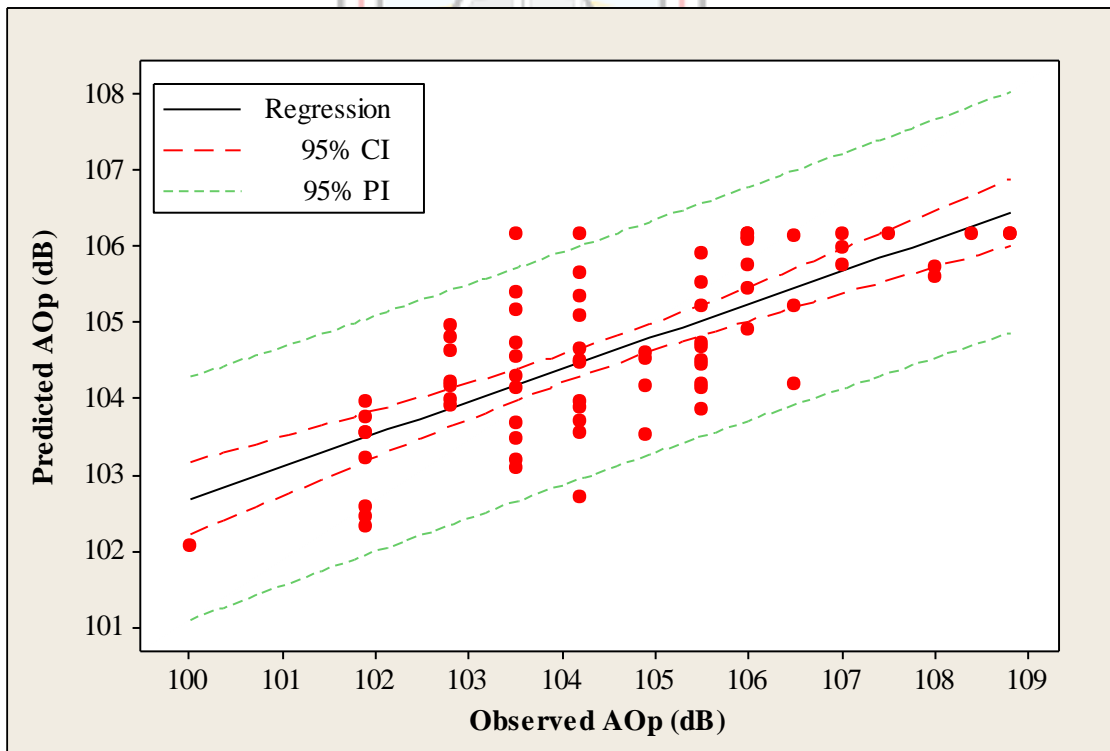
Figure 6.20 Observed AOp Versus Predicted AOp by MARS
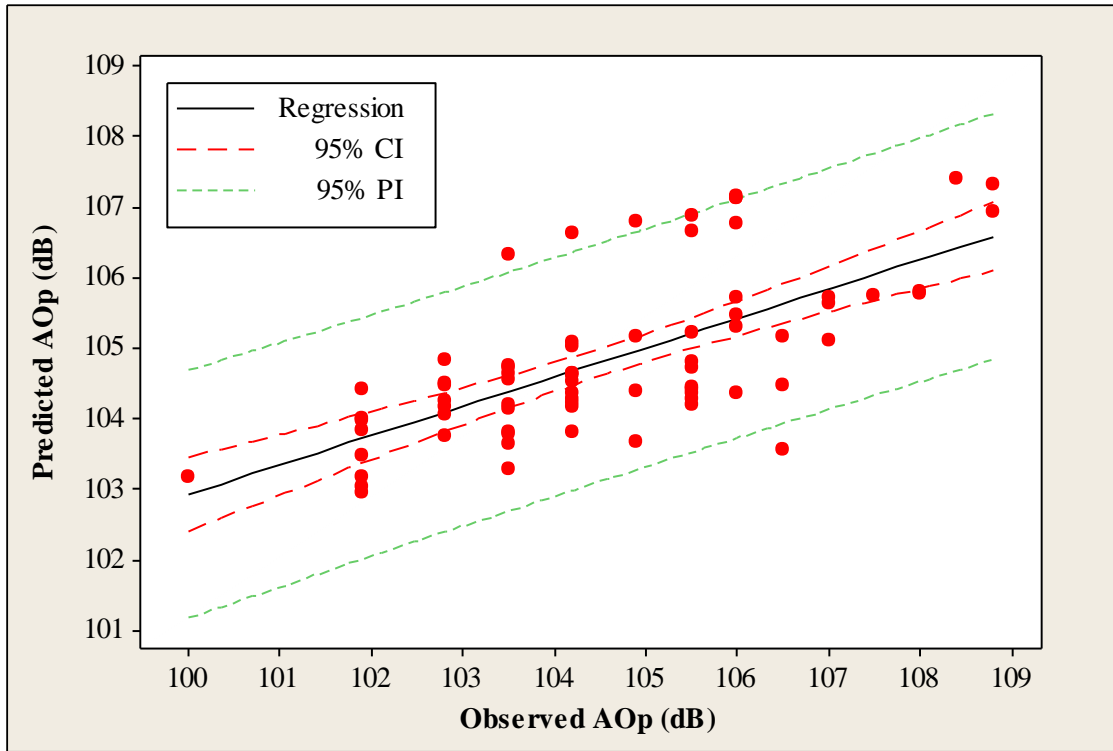
Figure 6.21 Observed AOp Versus Predicted AOp by General Predicted
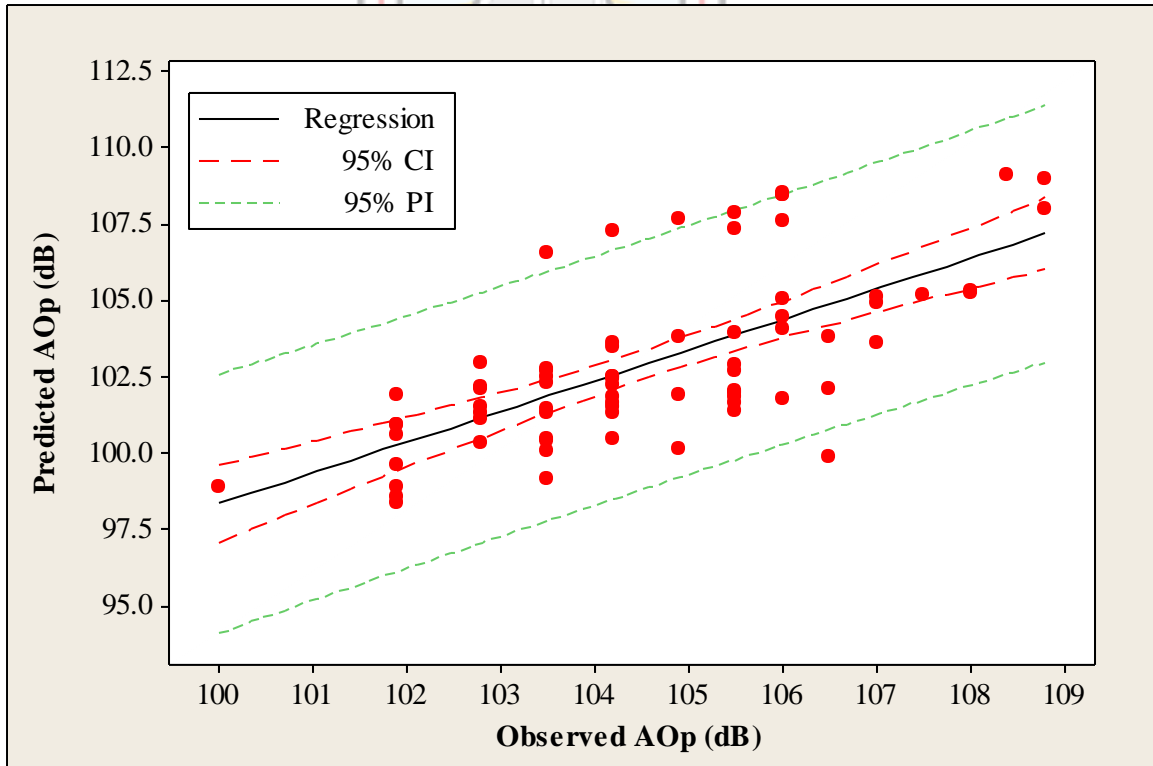
Figure 6.22 Observed AOp Versus Predicted AOp by Newmont Model

156

6.4   Air Overpressure Prediction Model Selection

The calculated AIC values for the different air over pressure prediction models presented in this research are shown in Table 6.17 and graphically illustrated in Figure 6.23.

From Table 6.17 and Figure 6.23, it can be observed that BPNN model had the lowest AIC value of 36.3105 is the best model among the candidate investigated models. This because in relation to the AIC computations, models with the lowest AIC values are the best and should be the selected model. Nevertheless, it can also be observed that the proposed AI techniques of GRNN, RBFNN, MARS and RVM produced relatively lower AIC values and hence can be said to produce comparable results to the BPNN. Conversely, the Newmont model had the highest AIC value and hence the most unsuitable model for predicting air overpressure among the other investigated techniques. Thus, the BPNN model is the most recommended approach to predict air overpressure at Newmont Golden Ridge Limited. This confirms the superiority of the AI techniques as the optimum models in predicting air overpressure over the popularly used empirical models (general predictor and Newmont model).

Table 6.17 The Various Models' AIC Values

Various Techniques	AIC
BPNN	36.3105
GRNN	37.8414
RBFNN	41.1032
RVM	42.6057
GPR	44.8873
SVM	45.3831
MARS	46.5698
General Predictor	51.5905
LS-SVM	64.9647
WNN	66.2334
ELM	77.5889
GMDH	99.6587
Newmont Model	142.391

Therefore, on the basis of the quantitative analyses presented in this study, it can logically be stated that the potential of GRNN, RBFNN, MARS and RVM in the air overpressure prediction for the Newmont Golden Ridge Limited has been duly investigated.
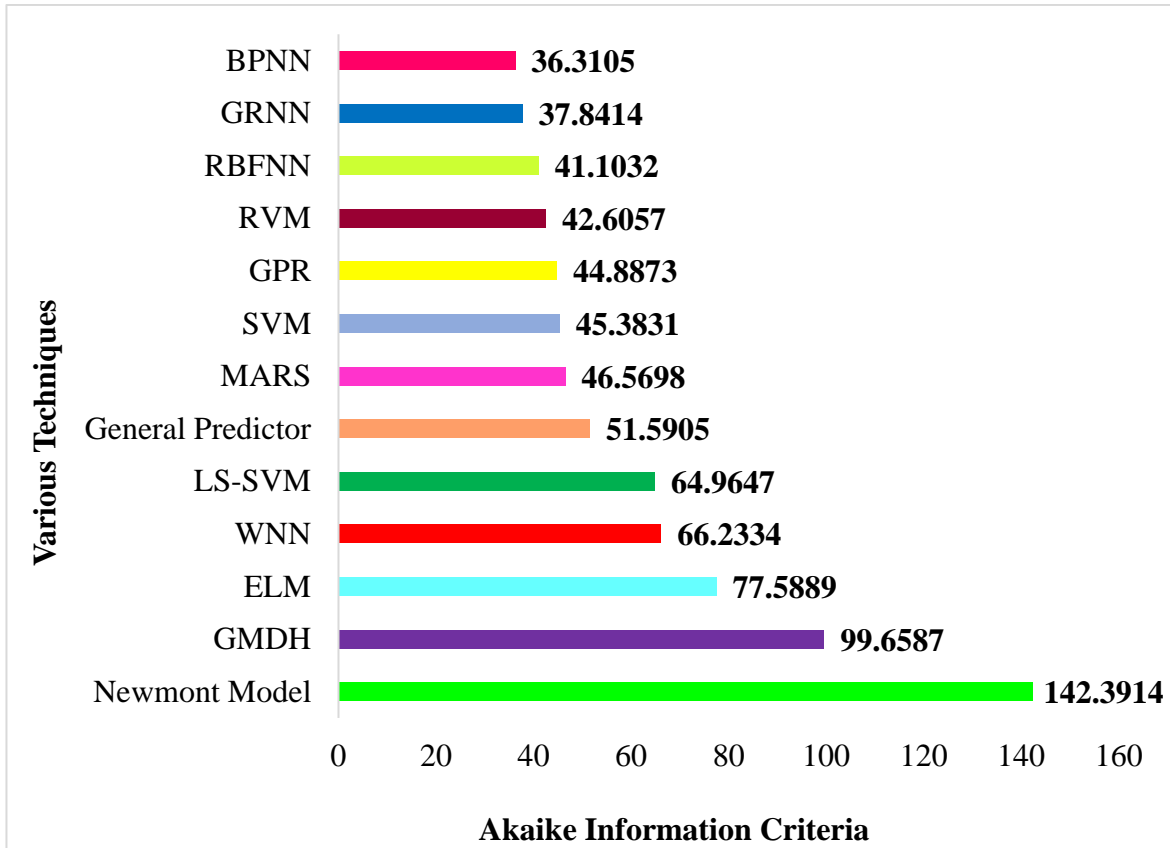
Figure 6.23 AIC Values of the Various Air Overpressure Prediction Models

CHAPTER 7

CONCLUSIONS AND RECOMMENDATIONS

7.1   Conclusions

In the present study, blast-induced ground vibration and air overpressure prediction using AI techniques were investigated. In the case of blast-induced ground vibration prediction, five novel AI techniques of LS-SVM, WNN, RVM, MARS and GPR have been proposed and tested as new adaptive computational alternative tool for PPV prediction. To provide a comprehensive performance evaluation of these novel techniques, six benchmark methods namely BPNN, GRNN, RBFNN, GMDH, SVM, and ELM and four empirical methods of USBM, Indian Standard, Ambrasey-Hendron and Langefors-Kihlstrom were applied to assess the suitability of the proposed LS-SVM, WNN, MARS, RVM and GPR approaches.

To achieve this aim, a total of 210 blast event data sets acquired from Ghana Manganese Company (GMC) were used to develop the various predictive models. Out of the 210 blast data, 130 was used in the model construction stage. The remaining 80 blast data sets were used to independently assess the models' adequacy. To formulate the AI models, the number of blast holes, cooperating charge (kg), distance between blasting point and monitoring station (m), hole depth (m), powder factor were the input parameters while the PPV value was used as the output parameter.

Statistical performance criteria of mean square error (MSE), root mean square error (RMSE), relative root mean square error (RRMSE), mean absolute error (MAE), coefficient of determination (R^2), correlation coefficient (R), Nash-Sutcliffe efficiency index and variance accounted for (VAF) were used as the basis for evaluating the performance of the techniques employed in this research. The Akaike Information Criterion (AIC) approach was further used in selecting the best model among the candidate techniques considered in this research.

Based on the obtained statistical results, it was found out that four out of the five proposed AI techniques (LS-SVM, WNN, MARS and GPR) could produce good ground vibration predictions. Hence LS-SVM, WNN, MARS and GPR were proposed to be used as suitable

alternative tools to predict blast-induced ground vibration. However, taking into account all the methods, the LS-SVM model had the highest performance capacity and was the best selected model based on the AIC approach for the prediction of blast-induced ground vibration for Ghana Manganese Company Limited. The overall analysis indicates that the proposed LS-SVM, WNN, MARS and GPR models have demonstrated their suitability to serve as alternatives AI prediction tools due to strong calibration power and good generalisation capabilities. Therefore, the proposed LS-SVM, WNN, MARS and GPR models could be replicated and applied in the mining and civil engineering industries where blast operation is still relevant as a source of rock fragmentation.

In the case of air-overpressure prediction, the predictive capability of the novel methods of GRNN, RBFNN, LS-SVM, ELM, WNN, RVM and MARS were investigated. To indicate the performance of those aforementioned techniques, benchmark techniques of BPNN, GMDH, GPR, SVM and two empirical models (General predictor and Newmont model) were developed. In that regard, a total of 171 blast event data sets acquired from Newmont Golden Ridge Limited (NGRL) were used in the air overpressure prediction modelling. Out of the 171 blast data sets, 98 were used in the model development stage. The remaining 73 blast data sets were used to independently assess the performance of the various predictive models. To develop the AI models, number of blast holes, stemming height (m), cooperating charge (kg), distance between blasting point and monitoring station (m), were considered as input parameters while the AOp value was the output parameter. Based on the obtained statistical results, it was found that four out of the seven novel methods (GRNN, RBFNN, RVM, and MARS) tested, produced comparable and satisfactory results as the widely used BPNN, GPR and SVM. By virtue of that, the GRNN, RBFNN, RVM and MARS methods proposed could serve as suitable alternatives to the prediction of air overpressure. However, based on the obtained AIC values, the BPNN was the selected model for the prediction of air overpressure at Newmont Golden Ridge Limited (NGRL).

The statistical analyses confirmed the superiority of applying AI techniques to the empirical techniques in predicting ground vibration and air overpressure. To this end, it is clear that the computational adaptive strategy of the AI techniques applied in this research enabled the correct calibration and generalisation to the data set.

Finally, a front-end, user-friendly, interactive application software was developed in the MATLAB program environment which enables the user to upload the data sets and generate the necessary results and graphs automatically. The essence of this AI-based software is to provide the mining engineer prior information about the efficiency of the blast design before blasting. In that regard, the blast design parameters can be fed into the software to estimate the ground vibration and air overpressure to be recorded if the current blast is carried out per the design.

7.2   Recommendations

It is recommended that:

i.   The selected artificial intelligent techniques for predicting blast-induced ground vibration and air overpressure should be adopted and used in Ghana Manganese Company Limited and Newmont Golden Ridge Limited since only the empirical predictors are being used. The AI-based software could be used for this purpose.

ii. Previous studies reviewed have shown that little has been done in the area of applying evolutionary optimisation methods to automate the artificial intelligent system. This optimisation will minimise the human interferences that are usually encountered in majority of the artificial intelligent model development process, improve the computational speed as well as realising global optimum. This is because most artificial intelligent methods are based on fine tuning iterative parameters, slow convergence due to the gradient descent training algorithms used and possibility of not realising global optimisation but rather local minima.

iii. The application of dimensionality reduction methods in ground vibration induced by blasting and air overpressure prediction is one area that is yet to be explored. The essence of applying those methods is to reduce the dimension of input data that are being used to create the model. The reason is that, it is not all the input parameters that contribute equally to the prediction of the output (vibration and air overpressure). Hence, to reduce the complexity of the model, check the relevance of each input parameter there is the need to move in such direction of research. This will further enhance the predictive strength of the artificial intelligent models.

iv. For future research works, denoising techniques such as discrete wavelet transforms (DWT) may be applied to remove any white noise in the data before applying the artificial intelligent techniques. Elimination of the noise and uncertainty in the data can lead to enhancement in the AI model prediction results.

REFERENCES

Akeil, S. (2004), "Comparative Study on Ground Vibrations Prediction by Statistical and Neural Networks Approaches at Tunçbilek Coal Mine, Panel BYH", *Unpublished MSc Thesis Report*, Middle East Technical University, 113 pp.

Alexandridis, A. K. and Zapranis, A. D. (2013) "Wavelet Neural Networks: A Practical Guide", *Neural Networks*, Vol. 42 1–27.

Álvarez-Vigil, A. E., González-Nicieza, C., López Gayarre, F. and Álvarez- Fernández, M. I. (2012), "Predicting Blasting Propagation Velocity and Vibration Frequency Using Artificial Neural Networks", *International Journal of Rock Mechanics & Mining Sciences*, Vol. 55, pp. 108 – 116.

Ambraseys, N. R. and Hendron, A. J. (1968), "Dynamic Behavior of Rock Masses: Rock Mechanics in Engineering Practices", *Rock mechanics in Engineering Practices*, In: Stagg K, Wiley J, (eds), Wiley London, pp. 203 – 207.

Amegbey, N. and Afum, B. O. (2015), "Blast Impact Prediction Studies at Ghana Manganese Company (GMC) Ltd", Nsuta, Ghana", *Ghana Mining Journal*, Vol. 15, No. 1, pp. 73 - 77.

Amegbey, N., Afum, B. O., Ndur, S. and Coffie-Anum, E. (2016), "Impact Assessment of Atmospheric Pollutants Emissions from Mining Operations at Ghana Manganese Company Ltd.", *Ghana Mining Journal*, Vol. 16, No. 2, pp. 65 – 72.

AminShokravi, A., Eskandar, H., Derakhsh, A.M., Rad, H.N. and Ghanadi, A. (2018), "The Potential Application of Particle Swarm Optimization Algorithm for Forecasting the Air-Overpressure Induced by Mine Blasting", *Engineering with Computers*, Vol. 34, No. 2, pp.277-285.

Amiri, M., Amnieh, H. B., Hasanipanah, M. and Khanli, L. M. (2016), "A New Combination of Artificial Neural Network and K-Nearest Neighbors Models to Predict Blast-Induced Ground Vibration and Air-Overpressure", *Engineering with Computers*, Vol. 32, No. 4, pp. 631-644.

Amnieh, B. H., Mozdianfard, M. R. and Siamaki, A. (2010), "Predicting of Blasting Vibrations in Sarcheshmeh Copper Mine by Neural Network", *Safety Science*, Vol. 38, No. 3, pp. 319 – 325.

ANN and Empirical Geomechanical Relationships", *REM-International Engineering Journal*, Vol. 71, No. 1, pp. 89–95.

Anon. (2014), "Computing Distance", *www.iris.edu/hq/Wiki/Computing_Distance*, Accessed: October 12, 2017.

Anon. (2015), "Akyem Gold Mine, Ghana", *www.mining-technology.com*, Accessed: January 2, 2017.

Anon. (2017a), "Open-pit Mining and Ore Processing at Akyem", *www.miningtechnology.com/projects/akyem-gold-mine/*, Accessed: December 13, 2017.

Anon. (2017b), "Seismic Wave", *http://www.colorado.edu/physics/phys2900/homepages/ Marianne.Hogan/waves.html*, Accessed: October 10, 2017.

Anon. (2018a), "Controlling the Adverse Effects of Blasting", *https://www.osmre.gov/.../ blasting/.../WYBlasterCertModules/8AdverseEffectsBlasting, Accessed: March 16, 2018.*

Apalangya, P. A. (2014), "An Assessment of the Blast Practices at Pit C of Ghana Manganese Company Limited", *Unpublished MSc Thesis Report*, University of Mines and Technology, Tarkwa, 88 pp.

Appianing, E. J. A. (2013), "A Review of Waste Dump Reclamation Practices at GMC Nsuta", *Unpublished BSc Project Report*, University of Mines and Technology, Tarkwa, 35 pp.

Armaghani, D. J., Hajihassani, M., Marto, A., Faradonbeh, R. S. and Mohamad, E. T. (2015c), "Prediction of Blast-Induced Air Overpressure: A Hybrid AI-Based Predictive Model", *Environmental Monitoring and Assessment*, Vol. 187, No. 11, p.666 – 679.

Armaghani, D. J., Hajihassani, M., Mohamad, E. T., Marto, A. and Noorani, S. A. (2014), "Blasting-Induced Flyrock and Ground Vibration Prediction Through an Expert Artificial Neural Network Based on Particle Swarm Optimization", *Arabian Journal of Geosciences*, Vol. 7, No. 12, pp. 5383-5396.

Armaghani, D. J., Hajihassani, M., Sohaei, H., Mohamad, E. T., Marto, A., Motaghedi, H. and Moghaddam, M. R. (2015b), "Neuro-Fuzzy Technique to Predict AirOverpressure Induced by Blasting", *Arabian Journal of Geosciences*, Vol. 8, No. 12, pp. 10937-10950.

Armaghani, D. J., Hasanipanah, M. and Mohamad, E. T. (2016), "A Combination of the ICA-ANN Model to Predict Air-Overpressure Resulting from Blasting", *Engineering with Computers*, Vol. 32, No. 1, pp.155-171.

Armaghani, D. J., Hasanipanah, M., Amnieh, H. B. and Mohamad, E. T. (2018), "Feasibility of ICA in Approximating Ground Vibration Resulting from Mine Blasting", *Neural Computing and Applications*, Vol. 29, No. 9, pp. 457–465.

Armaghani, D. J., Momeni, E. Abad, S. V. A. N. and Khandelwal, M. (2015a), "Feasibility of ANFIS Model for Prediction of Ground Vibrations Resulting from Quarry Blasting", *Environmental Earth Sciences*, Vol. 74, pp. 2845–2860.

Arthur, C. K. (2015), "Determination of the Achieved Navigation Accuracy when JIGSAW is Used in Drilling", *Unpublished BSc Project Report*, University of Mines and Technology, Tarkwa, 25 pp.

Assaleh, K., Shanableh, T., Kheil, Y. A. (2013), "Group Method of Data Handling for Modeling Magnetorheological Dampers", *Intelligent Control and Automation*, Vol. 4, No. 1, pp. 70 - 79.

Ataei, M. and Kamali, M. (2013), "Prediction of Blast-Induced Vibration by Adaptive Neuro-Fuzzy Inference System in Karoun 3 Power Plant and Dam", *Journal of Vibration and Control*, Vol. 19, No. 12, pp. 1906–1914.

Bansah, K. J., Arko-Gyimah, K., Kansake, B. A. and Dumakor-Dupey, N. K. (2016), "Mitigating Blast Vibration Impact", *4th UMaT Biennial International Mining and Mineral Conference*, pp. MP 30-36.

Baughman, D. R. and Liu, Y. A. (2014), *Neural Networks in Bioprocessing and Chemical Engineering*, Academic Press, Cambridge, 399 pp.

Bhandari, S. (1997), *Engineering Rock Blasting Operations*, A. A. Balkema, Rotterdam, 375 pp.

Bui, X.N., Nguyen, H., Le, H.A., Bui, H.B. and Do, N.H. (2019), "Prediction of Blast-Induced Air Over-pressure in Open-Pit Mine: Assessment of Different Artificial Intelligence Techniques", *Natural Resources Research*, pp.1-21.

Burnham, K. P. and Anderson, D. R. (2002), *Model Selection and Multimodel Inference: A Practical Information – Theoretic Approach*, Springer-Verlag, New York, 488 pp.

Chandar, K. R., Sastry, V. R. and Hegde, C. (2017), "A Critical Comparison of Regression Models and Artificial Neural Networks to Predict Ground Vibrations", *Geotechnical and Geological Engineering*, Vol. 35, No. 2, pp. 573–583.

Davies, B., Farmer, I. W. and Attewell, P. B. (1964), "Ground Vibration from Shallow SubSurface Blasts", *Engineer*, Vol. 217, pp. 553 – 559.

Dehghani, H. and Ataee-Pour, M. (2011), "Development of a Model to Predict Peak Particle Velocity in a Blasting Operation", *International Journal of Rock Mechanics and Mining Sciences*, Vol. 48, No. 1, pp. 51–58.

Delis, I., Panzeri, S., Pozzo, T. and Berret, B. (2013), "A Unifying Model of Concurrent Spatial and Temporal Modularity in Muscle Activity", *Journal of Neurophysiology*, Vol. 111, No. 3, 675 – 693.

Dindarloo, S. R. (2015), "Prediction of Blast-Induced Ground Vibrations via Genetic Programming", *International Journal of Mining Science and Technology*, Vol. 25, No. 6, pp.1011 – 1015.

Dorofki, M., Elshafie, A. H., Jaafar, O., Karim, O. A. and Mastura, S. (2012), "Comparison of Artificial Neural Network Transfer Functions Abilities to Simulate Extreme Runoff Data", *International Proceedings of Chemical, Biological and Environmental Engineering*, Vol. 33, pp. 39 – 44.

Du, D., Jia, X. and Hao, C. (2016), "A New Least Squares Support Vector Machines Ensemble Model for Aero Engine Performance Parameter Chaotic Prediction", *Mathematical Problems in Engineering*, pp. 1 – 8.

Duvall, W. I. and Petkof, B. (1959), *Spherical Propagation of Explosion Generated Strain Pulses in Rock (No. BM-RI-5483)*, Bureau of Mines, Washington DC, USA, 24 pp.

Elevli, B. and Arpaz, E. (2010), "Evaluation of Parameters Affected on the Blast Induced Ground Vibration (BIGV) by Using Relation Diagram Method (RDM)", *Acta Montanistica Slovaca*, Vol. 15, No. 4, pp. 261 – 268.

Faradonbeh, R. S. and Monjezi, M. (2017), "Prediction and Minimization of Blast-Induced Ground Vibration Using Two Robust Meta-Heuristic Algorithms", *Engineering with Computers*, Vol. 33, No. 4, pp. 835–851.

Faradonbeh, R. S., Armaghani, D. J., Majid, M. Z. A., Tahir, M. M. Murlidhar, B. R., Monjezi, M. and Wong, H, M. (2016), "Prediction of Ground Vibration due to Quarry Blasting Based on Gene Expression Programming: A New Model for Peak Particle Velocity Prediction", *International Journal of Environmental Science and Technology*, Vol. 13, No. 6 pp. 1453–1464.

Faradonbeh, R.S., Hasanipanah, M., Amnieh, H.B., Armaghani, D.J. and Monjezi, M. (2018), "Development of GP and GEP Models to Estimate an Environmental Issue Induced by Blasting Operation", *Environmental Monitoring and Assessment*, Vol. 190, No. 6, pp. 351 – 366.

Fişne, A., Kuzu, C. and Hüdaverdi, T. (2011), "Prediction of Environmental Impacts of Quarry Blasting Operation Using Fuzzy Logic", *Environmental Monitoring and Assessment*, Vol. 174, No. 1–4, pp. 461–470.

Foresee, F. D. and Hagan, M. T. (1997), "Gauss-Newton approximation to Bayesian learning", *Proceedings of International Conference on Neural Networks (ICNN'97)*, IEEE, Vol. 3, pp. 1930-1935.

Fouladgar, N., Hasanipanah, M. and Amnieh, H. B. (2017), "Application of Cuckoo Search Algorithm to Estimate Peak Particle Velocity in Mine Blasting", *Engineering with Computers*, Vol. 33, No. 2, pp.181-189.

Friedman, J. H. (1991), "Multivariate Adaptive Regression Splines", *The Annals of Statistics*, Vol. 19, No. 1, pp. 1 – 67.

Gao, W., Alqahtani, A. S., Mubarakali, A. and Mavaluru, D. (2019), "Developing an Innovative Soft Computing Scheme for Prediction of Air Overpressure Resulting from Mine Blasting Using GMDH Optimized by GA", *Engineering with Computers*, pp.1-8.

Ghasemi, E., Ataei, M. and Hashemolhosseini, H. (2013), "Development of a Fuzzy Model for Predicting Ground Vibration Caused by Rock Blasting in Surface Mining", *Journal of Vibration and Control*, Vol. 19, No. 5, pp. 755 – 770.

Ghoraba, S. Monjezi, M., Talebi1, N., Jahed Armaghani, D. and Moghaddam, M. R. (2016), "Estimation of Ground Vibration Produced by Blasting Operations Through Intelligent and Empirical Models", *Environmental Earth Sciences*, Vol. 75, pp. 1 – 9.

Ghosh, A and Daemen, J. K. (1983), "A Simple New Blast Vibration Predictor (Based on Wave Propagation Laws)", *Proceedings of the 24th US Symposium on Rock Mechanics*, Texas, USA, pp. 151 – 161.

Gokhale, B. V. (2011), *Rotary Drilling and Blasting in Large Surface Mines*, CRC Press/Balkema, Leiden, The Netherlands, 744 pp.

Görgülü, K., Arpaz, E., Demirci, A., Koçaslan, A., Dilmaç, M. K. and Yüksek, A. G. (2013), "Investigation of Blast-Induced Ground Vibrations in the Tülü Boron Open Pit Mine", *Bulletin of Engineering Geology and the Environment*, Vol. 72, No. 3-4, pp.555 – 564.

Görgülü, K., Arpaz, E., Uysa, Ö., Durutürk, A. G., Yüksek, A. G., Koçaslan, A. and Dilmaç, M. K. (2015), "Investigation of the Effects of Blasting Design Parameters and Rock Properties on Blast-Induced Ground Vibrations", *Arabian Journal of Geosciences*, Vol. 8, pp.4269 – 4278.

Gupta, A. (2013), "The Top 10 Gold Producing Countries", *www.mining-technology.com/ features/feature-ten-largest-gold-producing-countries-china's*, Accessed: March 14, 2018.

Gupta, R. N, Roy, P. P. and Singh, B. (1987), "On a Blast Induced Blast Vibration Predictor for Efficient Blasting", *Proceedings of the 22nd International Conference on Safety in Mines Research Institute*, Beijing, China, pp.1015 – 1021.

Hagan, M. T., Demuth, H. B., Beale, M. H. and De Jesús, O. (1996), *Neural Network Design*, PWS Publishing Company, Boston, 1012 pp.

Hajihassani, M., Armaghani, D. J., Monjezi, M. and Mohamad, E. T. (2015), "Blast-induced air and ground vibration prediction: a particle swarm optimization-based artificial neural network approach", *Environmental Earth Sciences*, Vol. 74, No. 4, pp. 2799–2817.

Hajihassani, M., Armaghani, D. J., Sohaei, H., Mohamad, E. T. and Marto, A. (2014), "Prediction of Airblast-Overpressure Induced by Blasting Using a Hybrid Artificial Neural Network and Particle Swarm Optimization", *Applied Acoustics*, Vol. 80, pp.57-67.

Hasanipanah, M., Amnieh, H. B., Khamesi, H., Armaghani, D. J., Golzar, S. B. and Shahnazar, A. (2018), "Prediction of an Environmental Issue of Mine Blasting: An Imperialistic Competitive Algorithm-Based Fuzzy System", *International Journal of Environmental Science and Technology*, Vol. 15, No. 3, pp.551-560.

Hasanipanah, M., Armaghani, D. J., Amnieh, H. B., Majid, M. Z. A. and Tahir, M. M. (2017a), "Application of PSO to Develop a Powerful Equation for Prediction of Flyrock Due to Blasting", *Neural Computing and Applications*, Vol. 28, No. 1, pp.1043-1050.

Hasanipanah, M., Armaghani, D. J., Khamesi, H., Amnieh, H. B. and Ghoraba, S. (2016a), "Several Non-Linear Models in Estimating Air-Overpressure Resulting from Mine Blasting", *Engineering with Computers*, Vol. 32, No. 3, pp. 441–455.

Hasanipanah, M., Faradonbeh, R. S., Amnieh, H. B., Armaghani, D. J. and Monjezi, M. (2017c), "Forecasting Blast-Induced Ground Vibration Developing a CART Model", *Engineering with Computers*, Vol. 33, No. 2, pp. 307-316.

Hasanipanah, M., Faradonbeh, R.S., Armaghani, D.J., Amnieh, H.B. and Khandelwal, M. (2017b), "Development of a Precise Model for Prediction of Blast-Induced Flyrock Using Regression Tree Technique", *Environmental Earth Sciences*, Vol. 76, No. 1, p.27.

Hasanipanah, M., Monjezi, M., Shahnazar, A., Armaghani, D. J. and Farazmand, A. (2015), "Feasibility of Indirect Determination of Blast Induced Ground Vibration Based on Support Vector Machine", *Measurement*, Vol. 75, pp.289-297.

Hasanipanah, M., Naderi, R., Kashir, J., Noorani, S. A. and Qaleh, A. Z. A. (2017d), "Prediction of Blast-Produced Ground Vibration Using Particle Swarm Optimization", *Engineering with Computers*, Vol. 33, No. 2, pp. 173–179.

Hasanipanah, M., Noorian-Bidgoli, M., Armaghani, D. J. and Khamesi, H. (2016b), "Feasibility of PSO-ANN Model for Predicting Surface Settlement Caused by Tunnelling", *Engineering with Computers*, Vol. 32, No. 4, pp. 705–715.

Hasanipanah, M., Shahnazar, A., Amnieh, H. B. and Armaghani, D. J. (2017e), "Prediction of Air-Overpressure Caused by Mine Blasting Using A New Hybrid PSO–SVR model", *Engineering with Computers*, Vol. 33, No. 1, pp.23-31.

Holmberg, R. and Persson, P. A. (1979), "Design of Tunnel Perimeter Blasthole Patterns to Prevent Rock Damage", *Proceedings of IMM Tunnelling'79 Conference, London*, pp. 280 – 283.

Hornik, K., Stinchcombe, M. and White, H. (1989), "Multilayer Feed Forward Networks are Universal Approximators", *Neural Network*, Vol. 2, No. 5, pp. 359 – 366.

Hu, J. and Tse, P. W. (2013), "A Relevance Vector Machine-Based Approach with Application to Oil Sand Pump Prognostics", *Sensors*, Vol. 13, no. 9, pp. 12663 – 12686.

Huang, G. B., Zhu, Q. Y., Siew, C. K. (2006), "Extreme Learning Machine: Theory and Applications", *Neurocomputing*, Vol. 70, No. 1-3, pp. 489 – 501.

Indian Standard Institute (1973), *Criteria for Safety and Design of Structures Subject to Underground Blasts*, Bureau of Indian Standard, New Delhi, India, 9 pp.

Iphar, M., Yavuz, M. and Ak, H. (2008), "Prediction of Ground Vibrations Resulting from The Blasting Operations in An Open-Pit Mine by Adaptive Neuro-Fuzzy Inference System", *Environmental Geology*, Vol. 56, No. 1, pp. 97–107.

Iramina, W. S., Sansone, E. C., Wichers, M., Wahyudi, S., Eston, S. M. D., Shimada, H. and Sasaoka, T. (2018), "Comparing Blast-Induced Ground Vibration Models Using

Ivakhnenko, A. G. (1970), "Heuristic Self-Organization in Problems of Engineering Cybernetics", *Automatica*, Vol. 6, No. 2, pp. 207 – 219.

Jayaweera, C. D. and Aziz, N, (2018), "Development and Comparison of Extreme Learning Machine and Multi-Layer Perceptron Neural Network Models for Predicting Optimum Coagulant Dosage for Water Treatment", *Journal of Physics: Conference Series*, Vol. 1123, No. 1, pp. 1 – 8.

Jiang, W., Arslan, C. A., Tehrani, M. S., Khorami, M. and Hasanipanah, M. (2018), "Simulating the Peak Particle Velocity in Rock Blasting Projects Using a Neuro-Fuzzy Inference System", *Engineering with Computers*, pp.1-9.

Jiang, X. and Adeli, H. (2005), "Dynamic Wavelet Neural Network Model for Traffic Flow Forecasting", *Journal of Transportation Engineering*, Vol. 131, No. 10, pp. 771 – 779.

Kaba, F. A. (2013), "Student Internship Technical Report on Newmont Golden Ridge Limited, Akyem", *Unpublished Technical Report*, University of Mines and Technology, Tarkwa, 27 pp.

Kamali, M. and Ataei, M. (2010) "Prediction of Blast Induced Ground Vibrations in Karoun III Power Plant and Dam: A Neural Network", *The Journal of The Southern African Institute of Mining and Metallurgy*, Vol. 110, No. 8, pp. 481 – 490.

Kamara, A. A. (2014), "An Assessment of the Performance of Blend Emulsion Explosives in Blasting at Ghana Manganese Company Limited, Nsuta- Wassaw", *Unpublished MSc Thesis Report*, University of Mines and Technology, Tarkwa, 68 pp.

Kang, F., Han, S., Salgado, R. and Li, J. (2015), "System Probabilistic Stability Analysis of Soil Slopes Using Gaussian Process Regression with Latin Hypercube Sampling", *Computers and Geotechnics*, Vol. 63, pp.13-25.

Khandelwal, M. (2010), "Evaluation and Prediction of Blast-Induced Ground Vibration Using Support Vector Machine", *International Journal of Rock Mechanics & Mining Sciences*, Vol. 47, pp. 509–516.

Khandelwal, M. (2011), "Blast-induced Ground Vibration Prediction Using Support Vector Machines", *Engineering with Computers*", Vol. 27, pp. 193 – 200.

Khandelwal, M. and Kankar, P. K. (2011), "Prediction of Blast-Induced Air Overpressure Using Support Vector Machine", *Arabian Journal of Geosciences*, Vol. 4, No. (34), pp.427-433.

Khandelwal, M. and Singh, T. N. (2006), "Prediction of Blast Induced Ground Vibrations and Frequency in Opencast Mine: A Neural Network Approach", *Journal of Sound and Vibration*, Vol. 289, pp. 711 – 725.

Khandelwal, M. and Singh, T. N. (2007), "Evaluation of Blast-Induced Ground Vibration Predictors", *Soil Dynamics and Earthquake Engineering*, Vol. 27, No. 2, pp. 116 – 125.

Khandelwal, M. and Singh, T. N. (2009), "Prediction of Blast-Induced Ground Vibration Using Artificial Neural Network", *International Journal of Rock Mechanics and Mining Sciences*, Vol. 46, No. 7, pp. 1214–1222.

Khandelwal, M. and Singh, T.N. (2005), "Prediction of Blast Induced Air Overpressure in Opencast Mine", *Noise & Vibration Worldwide*, Vol. 36, No. 2, pp.7-16.

Khandelwal, M., Kankar, P. K. and Harsha, S. P. (2010), "Evaluation and Prediction of Blast Induced Ground Vibration Using Support Vector Machine", *Mining Science and Technology (China)*, Vol. 20, No. 1, pp.64-70.

Khandelwal, M., Kumar, D. L. and Yellishetty, M. (2011), "Application of Soft Computing to Predict Blast-induced Ground Vibration, *Engineering with Computers*, Vol. 27, No. 2, pp. 117 – 125.

Kostić, S., Perc, M., Vasović, N. and Trajković, S. (2013), "Predictions of Experimentally Observed Stochastic Ground Vibrations Induced by Blasting", *PLoS one*, Vol. 8, No. 12, pp. 1–13.

Langefors, U. and Kilstrom, B. (1963), *The Modern Technique of Rock Blasting*, John Wiley and Sons, New York, 405 pp.

Lapčević, R., Kostić, S., Pantović, R. and Vasović, N. (2014), "Prediction of Blast-Induced Ground Motion in a Copper Mine", *International Journal of Rock Mechanics & Mining Sciences*, Vol. 69, pp. 19 – 25.

Li, J. J., Jutzeler, A., Faltings, B., Winter, S. and Rizos, C. (2014), "Estimating Urban Ultrafine Particle Distributions with Gaussian Process Models", *Research@ Locate14*, pp.145-153.

Malakar, P., Mukherjee, A. and Sarkar, S. (2018), "Potential Application of Advanced Computational Techniques in Prediction of Groundwater Resource of India", *Groundwater of South Asia*, Springer, Mukherjee, A. (ed.), pp. 643-655.

Mohamad, E. T., Armaghani, D. J., Hasanipanah, M., Murlidhar, B. R. and Alel, M. N. A. (2016), "Estimation of Air-Overpressure Produced by Blasting Operation through a Neuro-Genetic Technique", *Environmental Earth Sciences*, Vol. 75, No. 2, p.174 – 189.

Mohamad, E. T., Noorani, S. A., Armghani, D. J. and Saad, R. (2012), "Simulation of Blasting Induced Ground Vibration by Using Artificial Neural Network", *The Electronic Journal of Geotechnical Engineering*, Vol. 17, pp. 2571 – 2584.

Mohamadnejad, M., Gholami, R. and Ataei, M. (2012), "Comparison of Intelligence Science Techniques and Empirical Methods for Prediction of Blasting Vibrations", *Tunnelling and Underground Space Technology*, Vol. 28, pp. 238–244.

Mohamed, M. T. (2009), "Artificial Neural Network for Prediction and Control of Blasting Vibrations in Assiut (Egypt) Limestone Quarry", *International Journal of Rock Mechanics and Mining Sciences*, Vol. 46, No. 2, pp. 426–431.

Mohamed, M. T. (2011), "Performance of Fuzzy Logic and Artificial Neural Network in Prediction of Ground and Air Vibrations", *Journal of Engineering Sciences*, Vol. 39, No. 2, pp. 425 – 440.

Mohammadnejad, M., Gholami, R., Ramezanzadeh, A. and Jalali, M. E. (2012), "Prediction of blast-induced vibrations in limestone quarries using Support Vector Machine", *Journal of Vibration and Control*, Vol. 18, No. 9, pp. 1322 – 1329.

Mojtahedi, S. F. F., Ebtehaj, I., Hasanipanah, M., Bonakdari, H. and Amnieh, H. B. (2019), "Proposing a Novel Hybrid Intelligent Model for The Simulation of Particle Size Distribution Resulting from Blasting", *Engineering with Computers*, Vol. 35, No. 1, pp.47-56.

Mokfi, T., Shahnazar, A., Bakhshayeshi, I., Derakhsh, A. M. and Tabrizi, O. (2018), "Proposing of a New Soft Computing-Based Model to Predict Peak Particle Velocity Induced by Blasting", *Engineering with Computers*, Vol. 34, No. 4, pp. 881-888.

Møller, M. F. (1993), "A Scaled Conjugate Gradient Algorithm for Fast Supervised Learning", *Neural Networks*, Vol. 6, No. 4, pp. 525-533.

Monjezi, M., Ahmadi, M., Sheikhan, M., Bahrami, A. and Salimi, A. R. (2010b), "Predicting Blast-Induced Ground Vibration Using Various Types of Neural Networks", *Soil Dynamics and Earthquake Engineering*, Vol. 30, No. 11, pp. 1233 – 1236.

Monjezi, M., Baghestani, M., Faradonbeh, R. S., Saghand, M. P. and Armaghani, D. J. (2016), "Modification and Prediction of Blast-Induced Ground Vibrations Based on Both Empirical and Computational Techniques", *Engineering with Computers*, Vol. 32, No. 4, pp. 717–728.

Monjezi, M., Ghafurikalajahi, M. and Bahrami, A. (2011), "Prediction of Blast-Induced Ground Vibration Using Artificial Neural Networks", *Tunnelling and Underground Space Technology*, Vol. 26, No. 1, pp. 46–50

Monjezi, M., Hasanipanah, M. and Khandelwal, M. (2013), "Evaluation and Prediction of Blast-Induced Ground Vibration at Shur River Dam, Iran, by Artificial Neural Network", *Neural Computing and Applications*, Vol. 22, No. 7-8, pp.1637-1643.

Monjezi, M., Rezaei, M. and Yazdian, A. (2010a), "Prediction of Backbreak in Open-Pit Blasting Using Fuzzy Set Theory", *Expert Systems with Applications*, Vol. 37, No. 3, pp. 2637–2643.

Moore, C. J., Chua, A. J., Berry, C. P. and Gair, J. R. (2016), "Fast Methods for Training Gaussian Processes on Large Datasets", *Royal Society Open Science*, Vol. 3, No. 5, pp. 1 – 10.

Murmu, S., Maheshwari, P. and Verma, H. K. (2018), "Empirical and Probabilistic Analysis of Blast-Induced Ground Vibrations", *International Journal of Rock Mechanics and Mining Sciences*, Vol. 103, pp. 267–274.

NAASRA (1983), *Explosives in Roadworks - A User Guide*, National Association of Australian State Road Authorities, Sydney, 242 pp.

Najah, A., El-Shafie, A., Karim, O. A., Jaafar, O. and El-Shafie, A. H. (2011), "An Application of Different Artificial Intelligences Techniques for Water Quality Prediction", *International Journal of the Physical Sciences*, Vol. 6, No. 22, pp. 52985308.

Nanda, M. A., Seminar, K. B., Nandika, D. and Maddu, A. (2018), "A Comparison Study of Kernel Functions in the Support Vector Machine and Its Application for Termite Detection", *Information*, Vol. 9, No. 1, pp. 1 – 14.

Nguyen, H. and Bui, X. N. (2018), "Predicting Blast-Induced Air Overpressure: A Robust Artificial Intelligence System Based on Artificial Neural Networks and Random Forest", *Natural Resources Research*, pp.1-15.

Nguyen, H., Bui, X. N., Bui, H. B. and Mai, N. L. (2018), "A Comparative Study of Artificial Neural Networks in Predicting Blast-Induced Air-Blast Overpressure at Deo Nai Open-Pit Coal Mine, Vietnam", *Neural Computing and Applications*, pp.1-17.

Nicholson, R. F. (2005), "Determination of Blast Vibrations using Peak Particle Velocity at Bengal Quarry, in St Ann, Jamiaca", *Unpublished MSc Thesis Report*, Luleå University of Technology, Sweden, 65 pp.

Nyame, F. K. (2011), "Texture and Compositional Evidence for Epigenetic Alteration in Mn Carbonate Protore at the Palaeo-Proterozoic Nsuta Manganese Deposit, Western Ghana", *Ghana Mining Journal,* Vol. 13, No. 1, pp. 15 – 23.

Olofsson, S. O. (1990), *Applied Explosives Technology for Construction and Mining*, APPLEX. Sweden, 3014 pp.

Parida, A. and Mishra, M. K. (2015), "Blast Vibration Analysis by Different Predictor Approaches – A Comparison", *Procedia Earth and Planetary Science*, Vol. 11, pp. 337 – 345.

Persson, P. A., Holmberg R. and Jaimin, L. (1994), *Rock and Explosives Engineering*, CRC Press LLC, New York, USA, 560 pp.

Poulos, M. Belesiotis, V. S. and Alexandris, N. (2010), "A Classroom Observation Model Fitted to Stochastic and Probabilistic Decision Systems", *Proceedings of IFIP International Conference on Artificial Intelligence Applications and Innovations*, Papadopoulos, H., Andreou, A. S., Bramer, M. (eds.), Larnaca, Cyprus, pp. 30 – 36.

Ragam, P. and Nimaje, D. S. (2018), "Evaluation and Prediction of Blast-Induced Peak Particle Velocity Using Artificial Neural Network: A Case Study", *Noise & Vibration Worldwide*, Vol. 49, pp. 111 – 119.

Rai, R. and Singh, T. N. (2004), "A New Predictor for Ground Vibration Prediction and its Comparison with Other Predictors", *Indian Journal of Engineering and Materials Sciences*, Vol. 11, pp. 178 – 184.

Rasmussen, C. E. and Williams, C. K. I. (2006), *Gaussian Processes for Machine Learning*, The MIT Press, Cambridge, 247 pp.

Richards, A. B. and Moore, A. J. (2012), *Blast Vibration Course: Measurement, Assessment, Control*, Terrock Consulting Engineers (Terrock Pty Ltd), Australia, 87 pp.

Roy, P. P. (1991), "Vibration Control in an Opencast Mine Based on Improved Blast Vibration Predictors", *Mining Science and Technology*, Vol. 12, pp. 157 – 165.

Saadat, M., Khandelwal, M. and Monjezi, M. (2014), "An ANN-Based Approach to Predict Blast-Induced Ground Vibration of Gol-E-Gohar Iron Ore Mine, Iran", *Journal of Rock Mechanics and Geotechnical Engineering*, Vol. 6, No. 1, pp. 67 – 76.

Sawmliana, C., Roy, P. P., Singh, R. K. and Singh, T. N. (2007), "Blast Induced Air Overpressure and Its Prediction Using Artificial Neural Network", *Mining Technology*, Vol. 116, No. 2, pp. 41 – 48.

Shahnazar, A., Rad, H. N., Hasanipanah, M., Tahir, M. M., Armaghani, D. J. and Ghoroqi, M. (2017), "A New Developed Approach for The Prediction of Ground Vibration Using a Hybrid PSO-Optimized ANFIS-Based Model", *Environmental Earth Sciences*, Vol. 76, No. 15, pp. 527.

Shahri, A. A. and Asheghi, A. (2018), "Optimized Developed Artificial Neural NetworkBased Models to Predict the Blast-Induced Ground Vibration", *Innovative Infrastructure Solutions*, Vol. 3, pp. 1–10.

Sheykhi, H., Bagherpour, R., Ghasemi, E. and Kalhori, H. (2018), "Forecasting Ground Vibration Due to Rock Blasting: A Hybrid Intelligent Approach Using Support Vector Regression and Fuzzy C-Means Clustering", *Engineering with Computers*, Vol. 34, No. 2, pp. 357–365.

Shin, M. and Park, C. (2000), "A Radial Basis Function Approach to Pattern Recognition and Its Applications", *ETRI Journal*, Vol. 22, No. 2, pp. 1 – 10.

Shuran, L. and Shujin, L. (2011), "Applying BP Neural Network Model to Forecast Peak Velocity of Blasting Ground Vibration", *Procedia Engineering*, Vol. 26, pp. 257 – 263.

Singh, L., Chetty, G. and Sharma, D. (2012), "A Novel Approach to Protein Structure Prediction Using PCA or LDA Based Extreme Learning Machines", *Neural Information Processing*, Vol. 7666, pp. 492 – 499.

Singh, T. N. (2004), "Artificial Neural Network Approach for Prediction and Control of Ground Vibrations in Mines", *Mining Technology*, Vol. 113, No. 4, pp. 251–256.

Singh, T. N. and Singh, V. (2005), "An Intelligent Approach to Prediction and Control Ground Vibration in Mines", *Geotechnical and Geological Engineering*, Vol. 23, pp. 249–262.

Singla, P., Subbarao, K. and Junkins, J. L. (2007), "Direction-Dependent Learning Approach for Radial Basis Function Networks", *IEEE Transactions on Neural Networks*, Vol. 18, No. 1, pp. 203 – 222.

Snelson, E. L. (2007), "Flexible and Efficient Gaussian Process Models for Machine Learning", *Published Thesis Report*, University of London, London, 135 pp.

Specht, D. F. (1991), "A General Regression Neural Network", *IEEE Transactions on Neural Network*, Vol. 2, No. 6, pp. 568 – 576.

Surmenok, P. (2017), "Estimating an Optimal Learning Rate for a Deep Neural Network", *https://towardsdatascience.com/estimating-optimal-learning-rate-for-a-deepneural-network-ce32f2556ce0*, Accessed: January 26, 2018.

Suykens, J. A. and Vandewalle, J. (1999), "Least Squares Support Vector Machine Classifiers", *Neural Processing Letters*, Vol. 9, No. 3, pp.293-300.

Suykens, J. A., De Brabanter, J., Lukas, L. and Vandewalle, J. (2002), "Weighted least squares support vector machines: robustness and sparse approximation", *Neurocomputing*, Vol. 48, No. 1-4, pp.85-105.

Taheri, K., Hasanipanah, M., Golzar, S. B. and Majid, M. Z. A. (2017), "A Hybrid Artificial Bee Colony Algorithm-Artificial Neural Network for Forecasting the Blast-Produced Ground Vibration", *Engineering with Computers*, Vol. 33, No. 3, pp.689700.

Thomas, C. and Goldfarb, J. (2005) "Air Blast: Fundamentals, Effects and Controls", *Optimization of Blasting Operations Course*, Queen's University, Kingston, Ontario, 50 pp.

Tiile, R. N. (2016), "Artificial Neural Network Approach to Predict Blast-Induced Ground Vibration, Airblast and Rock Fragmentation" *Published MSc Thesis Report*, Missouri University of Science and Technology, Rolla, 89 pp.

Vasović, D., Kostić, S., Ravilić, M. and Trajković, S. (2014), "Environmental Impact of Blasting at Drenovac Limestone Quarry (Serbia), *Environmental Earth Sciences*, Vol. 72, No. 10, pp. 3915–3928.

Verma, A. K. and Singh, T. N. (2011), "Intelligent Systems for Ground Vibration Measurement: A Comparative Study", *Engineering with Computers*, Vol. 27, No. 3, pp. 225–233.

Wang, G., Guo, L. and Duan, H. (2013), "Wavelet Neural Network Using Multiple Wavelet Functions in Target Threat Assessment", *The Scientific World Journal*, Vol. 2013, pp. 1 – 7.

Xue, X. and Yang, X. (2014), "Predicting Blast-Induced Ground Vibration Using General Regression Neural Network", *Journal of Vibration and Control*, Vol. 20, No. 10, pp.1512–1519.

Xue, X., Yang, X. and Li, P. (2017), "Evaluation of Ground Vibration Due to Blasting Using Fuzzy Logic", *Geotechnical and Geological Engineering*, Vol. 35, No. 3, pp. 1231–1237.

Yegnanarayana, B. (2005), *Artificial Neural Networks*, Prentice-Hall of India Private Limited, New Delhi, 461 pp.

Zadeh, L.A. (1994), "Fuzzy Logic, Neural Networks, and Soft Computing", *Communications of the ACM*, Vol. 37, No. 3, pp.77-85.

Zhang, Q. and Benvenite, A (1992), "Wavelet Networks", *IEEE Transactions on Neural Networks*, Vol. 3, No. 6, pp. 889 – 898.

Zhongya, Z. and Xiaoguang, J. (2018), "Prediction of Peak Velocity of Blasting Vibration Based on Artificial Neural Network Optimized by Dimensionality Reduction of FAMIV", *Mathematical Problems in Engineering*, Vol. 2018, pp. 1–12.

Ziggah, Y. Y., Youjian, H., Yu, X. and Basommi, L. P. (2016), "Capability of Artificial Neural Network for Forward Conversion of Geodetic Coordinates (ϕ, λ, h) to Cartesian Coordinates (X, Y, Z)", *Mathematical Geosciences*, Vol. 48, No. 6. pp. 687 – 721.
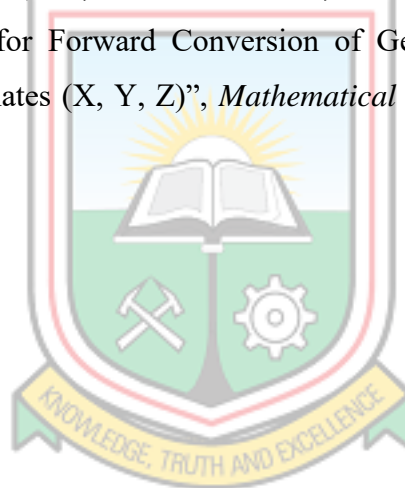
APPENDICES

APPENDIX A

EXPERIMENTATION RESULTS OF THE WIDTH PARAMETER AND MAXIMUM NUMBER OF NEURONS FOR DEVELOPMENT OF RBFNN MODEL FOR BLAST-INDUCED GROUND VIBRATION PREDICTION

Table A1 Training and Testing R and MSE Results for RBFNN Blast-Induced Ground Vibration Prediction Model

Width Parameter	Number of Neurons	Training		Testing	
		R	MSE	R	MSE
0.1	1	0.275726	0.111173	0.283751	0.081774
0.1	2	0.319904	0.108007	0.211568	0.081862
0.1	3	0.363352	0.104435	0.217865	0.082933
0.1	4	0.422694	0.098823	0.217854	0.083946
0.1	5	0.443424	0.096662	0.236904	0.084755
0.1	6	0.482657	0.092291	0.356354	0.084584
0.1	7	0.518667	0.087952	0.356335	0.08571
0.1	8	0.543294	0.084806	0.351216	0.085979
0.1	9	0.570436	0.081168	0.41106	0.084089
0.1	10	0.589657	0.078485	0.442657	0.081618
0.1	11	0.611084	0.07539	0.442663	0.082696
0.1	12	0.62603	0.073165	0.443316	0.083686
0.1	13	0.634537	0.071875	0.442485	0.084488
0.1	14	0.648811	0.069671	0.525773	0.082059
0.1	15	0.656471	0.068468	0.526114	0.082995
0.1	16	0.671006	0.066146	0.526142	0.084132
0.1	17	0.684702	0.063912	0.526202	0.085329
0.1	18	0.698628	0.061594	0.533183	0.086269
0.1	19	0.711081	0.059482	0.533205	0.087519
0.1	20	0.721833	0.057628	0.533159	0.088752

Table A1 Continued

0.2	1	0.248319	0.112901	0.10499	0.081979
0.2	2	0.425948	0.09849	0.359088	0.071537
0.2	3	0.434543	0.097601	0.346203	0.073066
0.2	4	0.547208	0.084292	0.341011	0.075794
0.2	5	0.583052	0.079417	0.538258	0.057927
0.2	6	0.589983	0.078439	0.5337	0.05831
0.2	7	0.606154	0.076112	0.54257	0.058091
0.2	8	0.629439	0.07265	0.539881	0.059196
0.2	9	0.654266	0.068816	0.658913	0.045289
0.2	10	0.688761	0.063241	0.660202	0.045584
0.2	11	0.712994	0.059154	0.661193	0.046026
0.2	12	0.741503	0.054165	0.661857	0.046516
0.2	13	0.74419	0.053685	0.661903	0.046807
0.2	14	0.761554	0.050539	0.664749	0.046877
0.2	15	0.768439	0.049271	0.661138	0.047573
0.2	16	0.782248	0.046695	0.661386	0.048229
0.2	17	0.794304	0.044408	0.655762	0.049647
0.2	18	0.80527	0.042297	0.641298	0.052536
0.2	19	0.811629	0.04106	0.64755	0.052281
0.2	20	0.819363	0.039543	0.644535	0.05333
0.3	1	0.397247	0.101333	0.313717	0.074817
0.3	2	0.630005	0.072564	0.338138	0.078556
0.3	3	0.634705	0.071849	0.357289	0.077405
0.3	4	0.685314	0.063811	0.407987	0.07416
0.3	5	0.742982	0.053901	0.586002	0.056733
0.3	6	0.763735	0.050139	0.585113	0.058355
0.3	7	0.767985	0.049355	0.579566	0.059014
0.3	8	0.782899	0.046572	0.576328	0.060483
0.3	9	0.802845	0.042767	0.574744	0.061677
0.3	10	0.812337	0.040922	0.553548	0.064747
0.3	11	0.821804	0.039061	0.566973	0.062306

179

Table A1 Continued

0.3	12	0.831128	0.037206	0.645307	0.050092
0.3	13	0.852706	0.032835	0.643252	0.050937
0.3	14	0.871751	0.028883	0.650709	0.050832
0.3	15	0.871752	0.028883	0.65072	0.050817
0.3	16	0.881148	0.026901	0.651075	0.050921
0.3	17	0.890561	0.024894	0.649629	0.05195
0.3	18	0.89515	0.023909	0.646363	0.052868
0.3	19	0.901366	0.022565	0.665281	0.049965
0.3	20	0.901371	0.022564	0.665092	0.050023
0.4	1	0.518658	0.087953	0.432733	0.067549
0.4	2	0.770304	0.048926	0.490162	0.068111
0.4	3	0.772622	0.048496	0.502774	0.066529
0.4	4	0.812153	0.040958	0.555656	0.061092
0.4	5	0.834398	0.036551	0.555476	0.063558
0.4	6	0.849099	0.033573	0.662187	0.048943
0.4	7	0.853458	0.03268	0.642186	0.051379
0.4	8	0.857729	0.031801	0.635743	0.052198
0.4	9	0.857748	0.031797	0.635168	0.052366
0.4	10	0.860805	0.031165	0.634441	0.051629
0.4	11	0.872646	0.028695	0.651038	0.050553
0.4	12	0.888703	0.025292	0.651777	0.051361
0.4	13	0.894703	0.024005	0.650989	0.050717
0.4	14	0.896192	0.023684	0.646553	0.051666
0.4	15	0.897848	0.023326	0.652059	0.049727
0.4	16	0.901806	0.022469	0.688968	0.044926
0.4	17	0.910203	0.020639	0.717808	0.040524
0.4	18	0.921074	0.018243	0.714576	0.041238
0.4	19	0.925677	0.01722	0.714948	0.041447
0.4	20	0.926012	0.017146	0.712428	0.041875
0.5	1	0.578427	0.080064	0.504486	0.061103
0.5	2	0.815808	0.040242	0.581805	0.057751

Table A1 Continued

0.5	3	0.816562	0.040094	0.587587	0.056334
0.5	4	0.843352	0.034743	0.591508	0.056076
0.5	5	0.859317	0.031473	0.586983	0.057928
0.5	6	0.861138	0.031096	0.568268	0.060346
0.5	7	0.878426	0.027477	0.704586	0.043135
0.5	8	0.884992	0.026084	0.725471	0.039804
0.5	9	0.890943	0.024812	0.71877	0.040665
0.5	10	0.893525	0.024258	0.711656	0.041816
0.5	11	0.893634	0.024235	0.713519	0.041327
0.5	12	0.901148	0.022612	0.710175	0.042603
0.5	13	0.901149	0.022612	0.709997	0.042633
0.5	14	0.904621	0.021858	0.706552	0.043053
0.5	15	0.913317	0.019955	0.719822	0.041486
0.5	16	0.917321	0.019074	0.71305	0.04238
0.5	17	0.919925	0.018498	0.710304	0.043076
0.5	18	0.922245	0.017984	0.710308	0.043218
0.5	19	0.925612	0.017235	0.715811	0.04319
0.5	20	0.928823	0.016519	0.739703	0.039474
0.6	1	0.734168	0.055467	0.573759	0.0596
0.6	2	0.744408	0.053646	0.612852	0.051894
0.6	3	0.842341	0.034948	0.639486	0.048471
0.6	4	0.842687	0.034878	0.643083	0.047867
0.6	5	0.860616	0.031204	0.672754	0.044429
0.6	6	0.866006	0.030084	0.655288	0.046187
0.6	7	0.889472	0.025128	0.695239	0.042458
0.6	8	0.902431	0.022334	0.70253	0.041843
0.6	9	0.902507	0.022317	0.703871	0.041459
0.6	10	0.904314	0.021924	0.69283	0.043322
0.6	11	0.904319	0.021923	0.692266	0.043398
0.6	12	0.909819	0.020723	0.71386	0.041059
0.6	13	0.917128	0.019116	0.722182	0.03977

Table A1 Continued

0.6	14	0.91847	0.01882	0.712045	0.040985
0.6	15	0.921021	0.018255	0.718791	0.039853
0.6	16	0.921277	0.018198	0.71566	0.040483
0.6	17	0.923363	0.017735	0.710659	0.041069
0.6	18	0.924775	0.017421	0.716765	0.040621
0.6	19	0.926868	0.016955	0.73533	0.038391
0.6	20	0.932512	0.015692	0.73116	0.040066
0.7	1	0.762787	0.050313	0.614573	0.0538
0.7	2	0.764887	0.049927	0.633267	0.051503
0.7	3	0.811792	0.041029	0.742456	0.036888
0.7	4	0.86725	0.029825	0.730679	0.039473
0.7	5	0.889361	0.025151	0.736593	0.037032
0.7	6	0.88937	0.025149	0.736782	0.037029
0.7	7	0.890946	0.024812	0.729187	0.037984
0.7	8	0.891211	0.024755	0.732297	0.03734
0.7	9	0.899088	0.023058	0.740596	0.036851
0.7	10	0.905228	0.021725	0.744188	0.036963
0.7	11	0.909064	0.020888	0.74362	0.036139
0.7	12	0.913729	0.019865	0.770347	0.032663
0.7	13	0.917645	0.019002	0.766056	0.033075
0.7	14	0.918102	0.018901	0.763545	0.033416
0.7	15	0.921254	0.018203	0.783513	0.030897
0.7	16	0.923595	0.017684	0.780298	0.03131
0.7	17	0.926086	0.017129	0.762931	0.033553
0.7	18	0.927111	0.016901	0.756182	0.034536
0.7	19	0.931051	0.01602	0.726945	0.038859
0.7	20	0.932484	0.015699	0.723575	0.039419
0.8	1	0.772562	0.048507	0.6386	0.049833
0.8	2	0.836114	0.036206	0.650382	0.053662
0.8	3	0.866127	0.030059	0.653457	0.047417
0.8	4	0.866274	0.030028	0.656314	0.04688

Table A1 Continued

0.8	5	0.884681	0.02615	0.723456	0.038169
0.8	6	0.884906	0.026102	0.727057	0.03765
0.8	7	0.888832	0.025265	0.705532	0.040285
0.8	8	0.898313	0.023226	0.746577	0.035236
0.8	9	0.902456	0.022328	0.756183	0.03401
0.8	10	0.90707	0.021324	0.784709	0.030558
0.8	11	0.911341	0.020389	0.789842	0.02989
0.8	12	0.912601	0.020113	0.791183	0.029984
0.8	13	0.914602	0.019673	0.787297	0.031075
0.8	14	0.915905	0.019386	0.791674	0.030208
0.8	15	0.91704	0.019135	0.796276	0.02969
0.8	16	0.920179	0.018442	0.794338	0.030086
0.8	17	0.923849	0.017627	0.795691	0.029774
0.8	18	0.925863	0.017179	0.79135	0.029939
0.8	19	0.928447	0.016603	0.7853	0.030942
0.8	20	0.931218	0.015983	0.792938	0.030618
0.9	1	0.825541	0.03832	0.719555	0.038673
0.9	2	0.825755	0.038277	0.718024	0.039046
0.9	3	0.865717	0.030144	0.712697	0.042437
0.9	4	0.887838	0.025477	0.759339	0.033884
0.9	5	0.889213	0.025183	0.745479	0.035526
0.9	6	0.900765	0.022695	0.77883	0.031234
0.9	7	0.907058	0.021326	0.797109	0.028821
0.9	8	0.908439	0.021025	0.788838	0.029832
0.9	9	0.909037	0.020894	0.788439	0.029928
0.9	10	0.912189	0.020203	0.791936	0.029622
0.9	11	0.912662	0.020099	0.791481	0.029819
0.9	12	0.916203	0.01932	0.782076	0.031472
0.9	13	0.918196	0.01888	0.776077	0.032417
0.9	14	0.926477	0.017042	0.751842	0.036105
0.9	15	0.927995	0.016704	0.755569	0.035021

Table A1 Continued

0.9	16	0.928314	0.016632	0.751721	0.035421
0.9	17	0.929383	0.016393	0.761292	0.034486
0.9	18	0.931144	0.015999	0.771834	0.03287
0.9	19	0.931811	0.015849	0.767963	0.033608
0.9	20	0.932074	0.015791	0.762981	0.034315
1	1	0.85597	0.032163	0.791319	0.0304
1	2	0.859871	0.031358	0.780062	0.03153
1	3	0.86371	0.030562	0.762469	0.033641
1	4	0.879537	0.027242	0.785182	0.031003
1	5	0.87959	0.027231	0.783996	0.03125
1	6	0.892074	0.02457	0.78448	0.030714
1	7	0.904887	0.0218	0.791338	0.03009
1	8	0.906378	0.021475	0.79375	0.030504
1	9	0.910386	0.020599	0.804669	0.028217
1	10	0.913655	0.019881	0.808195	0.027506
1	11	0.916528	0.019248	0.814868	0.026595
1	12	0.917758	0.018977	0.812589	0.026944
1	13	0.919496	0.018593	0.808947	0.02739
1	14	0.922579	0.017909	0.793882	0.029227
1	15	0.923626	0.017677	0.800969	0.028392
1	16	0.924511	0.01748	0.790029	0.029872
1	17	0.925246	0.017317	0.780722	0.031249
1	18	0.926448	0.017049	0.792992	0.02965
1	19	0.928657	0.016556	0.801662	0.029123
1	20	0.930085	0.016236	0.814045	0.027598
1.1	1	0.851214	0.03314	0.713811	0.041201
1.1	2	0.856546	0.032045	0.736104	0.037015
1.1	3	0.883989	0.026298	0.760324	0.034126
1.1	4	0.892012	0.024583	0.74156	0.036016
1.1	5	0.902203	0.022383	0.771674	0.032008
1.1	6	0.902302	0.022362	0.769604	0.03225

Table A1 Continued

1.1	7	0.907125	0.021312	0.782743	0.030766
1.1	8	0.907379	0.021256	0.776961	0.031594
1.1	9	0.913381	0.019941	0.797006	0.029289
1.1	10	0.914653	0.019662	0.792853	0.029599
1.1	11	0.915253	0.019529	0.793874	0.029393
1.1	12	0.916492	0.019256	0.79389	0.029274
1.1	13	0.918181	0.018884	0.801862	0.028334
1.1	14	0.920053	0.01847	0.811386	0.027193
1.1	15	0.922273	0.017977	0.819307	0.02645
1.1	16	0.92371	0.017658	0.804466	0.028342
1.1	17	0.924993	0.017373	0.793743	0.029771
1.1	18	0.925873	0.017177	0.784824	0.030974
1.1	19	0.926971	0.016932	0.779037	0.031832
1.1	20	0.92819	0.01666	0.790546	0.030057
1.2	1	0.84881	0.033632	0.713341	0.04084
1.2	2	0.87737	0.0277	0.762568	0.033325
1.2	3	0.878663	0.027427	0.757477	0.034326
1.2	4	0.880439	0.027051	0.745772	0.035713
1.2	5	0.888748	0.025282	0.742078	0.035793
1.2	6	0.902887	0.022235	0.786539	0.030208
1.2	7	0.90661	0.021424	0.782238	0.031421
1.2	8	0.906623	0.021421	0.780839	0.031631
1.2	9	0.909353	0.020825	0.796038	0.029488
1.2	10	0.909897	0.020706	0.799259	0.029183
1.2	11	0.910976	0.020469	0.795649	0.029352
1.2	12	0.913838	0.019841	0.812781	0.027156
1.2	13	0.913999	0.019805	0.812465	0.027205
1.2	14	0.914344	0.01973	0.819008	0.02624
1.2	15	0.916943	0.019157	0.814872	0.026672
1.2	16	0.91794	0.018937	0.818745	0.026177
1.2	17	0.918941	0.018716	0.817868	0.026385

Table A1 Continued

Table A1 Continued

1.2	18	0.920773	0.01831	0.818943	0.026108
1.2	19	0.924112	0.017569	0.816174	0.026472
1.2	20	0.928312	0.016633	0.815975	0.027112
1.3	1	0.866475	0.029986	0.813181	0.027491
1.3	2	0.884188	0.026255	0.797461	0.0293
1.3	3	0.890251	0.024961	0.783616	0.030789
1.3	4	0.90105	0.022633	0.810029	0.027123
1.3	5	0.902174	0.02239	0.804217	0.027912
1.3	6	0.904096	0.021972	0.803199	0.028196
1.3	7	0.905546	0.021656	0.805505	0.028181
1.3	8	0.911776	0.020294	0.818808	0.026227
1.3	9	0.914234	0.019754	0.834202	0.024499
1.3	10	0.91495	0.019596	0.834247	0.024387
1.3	11	0.915379	0.019502	0.83384	0.024374
1.3	12	0.916345	0.019289	0.829727	0.025079
1.3	13	0.917225	0.019095	0.822193	0.02628
1.3	14	0.920288	0.018417	0.830766	0.024997
1.3	15	0.920434	0.018385	0.832653	0.024762
1.3	16	0.924909	0.017392	0.805338	0.028581
1.3	17	0.924919	0.017389	0.805472	0.028542
1.3	18	0.924925	0.017388	0.804	0.028724
1.3	19	0.925395	0.017283	0.802276	0.028835
1.3	20	0.926193	0.017105	0.798342	0.029099
1.4	1	0.861492	0.031022	0.809724	0.027926
1.4	2	0.880008	0.027143	0.791952	0.029974
1.4	3	0.88716	0.025622	0.778312	0.031406
1.4	4	0.901865	0.022457	0.812138	0.026876
1.4	5	0.903118	0.022184	0.809573	0.027229
1.4	6	0.90884	0.020937	0.81581	0.026657
1.4	7	0.908856	0.020933	0.816457	0.026583
1.4	8	0.910045	0.020673	0.824975	0.025379

Table A1 Continued

1.4	9	0.910845	0.020498	0.828122	0.025088
1.4	10	0.911929	0.02026	0.830148	0.024835
1.4	11	0.912963	0.020033	0.824101	0.02554
1.4	12	0.913566	0.019901	0.819127	0.026282
1.4	13	0.914276	0.019744	0.812772	0.027332
1.4	14	0.916131	0.019336	0.814631	0.026762
1.4	15	0.917701	0.01899	0.824866	0.02528
1.4	16	0.917843	0.018958	0.827347	0.024948
1.4	17	0.919389	0.018616	0.826022	0.025058
1.4	18	0.920857	0.018291	0.824439	0.025363
1.4	19	0.921771	0.018089	0.814192	0.026768
1.4	20	0.924658	0.017447	0.806207	0.028172
1.5	1	0.866303	0.030022	0.761079	0.035104
1.5	2	0.883929	0.02631	0.784067	0.031643
1.5	3	0.896801	0.023552	0.799523	0.028461
1.5	4	0.897307	0.023443	0.794502	0.029174
1.5	5	0.903337	0.022137	0.824989	0.025202
1.5	6	0.905059	0.021762	0.819372	0.025983
1.5	7	0.906454	0.021458	0.820251	0.025908
1.5	8	0.909837	0.020719	0.830855	0.02463
1.5	9	0.911508	0.020353	0.821648	0.025793
1.5	10	0.91228	0.020183	0.821994	0.025779
1.5	11	0.912724	0.020086	0.821035	0.025914
1.5	12	0.914901	0.019607	0.812572	0.027072
1.5	13	0.916016	0.019361	0.81934	0.026301
1.5	14	0.916683	0.019214	0.823066	0.025635
1.5	15	0.917111	0.01912	0.826967	0.025103
1.5	16	0.918023	0.018918	0.829655	0.024838
1.5	17	0.918576	0.018796	0.823569	0.025706
1.5	18	0.918641	0.018782	0.822864	0.02578
1.5	19	0.920759	0.018313	0.805849	0.027888

Table A1 Continued

1.5	20	0.924573	0.017466	0.788852	0.030136
1.6	1	0.865906	0.030105	0.759345	0.035191
1.6	2	0.903936	0.022006	0.835968	0.023972
1.6	3	0.904419	0.021901	0.83786	0.023836
1.6	4	0.906532	0.021441	0.826556	0.025405
1.6	5	0.907562	0.021216	0.834783	0.024078
1.6	6	0.908027	0.021115	0.835566	0.023901
1.6	7	0.908311	0.021053	0.834751	0.023997
1.6	8	0.909048	0.020891	0.839544	0.023324
1.6	9	0.911728	0.020304	0.827654	0.024891
1.6	10	0.912936	0.020039	0.823934	0.025556
1.6	11	0.916198	0.019321	0.840059	0.023402
1.6	12	0.916566	0.01924	0.840538	0.023314
1.6	13	0.916807	0.019187	0.840578	0.023283
1.6	14	0.918563	0.018799	0.830877	0.02453
1.6	15	0.919549	0.018581	0.823239	0.025604
1.6	16	0.920214	0.018434	0.817827	0.026292
1.6	17	0.920894	0.018283	0.816352	0.026645
1.6	18	0.921638	0.018118	0.818281	0.026385
1.6	19	0.922929	0.017832	0.813966	0.027013
1.6	20	0.92591	0.017169	0.779284	0.032031
1.7	1	0.864804	0.030335	0.757032	0.035408
1.7	2	0.90507	0.02176	0.838789	0.023662
1.7	3	0.905272	0.021716	0.836078	0.024075
1.7	4	0.905631	0.021638	0.834995	0.024186
1.7	5	0.905864	0.021587	0.832131	0.02446
1.7	6	0.90665	0.021415	0.830246	0.024761
1.7	7	0.908775	0.020951	0.837868	0.023597
1.7	8	0.910115	0.020658	0.845947	0.022554
1.7	9	0.910429	0.020589	0.84764	0.022266
1.7	10	0.912468	0.020142	0.838781	0.02372

188

Table A1 Continued

1.7	11	0.912995	0.020026	0.834457	0.024176
1.7	12	0.914497	0.019696	0.825305	0.025384
1.7	13	0.914638	0.019665	0.826002	0.025285
1.7	14	0.915966	0.019372	0.838659	0.023506
1.7	15	0.91658	0.019237	0.839088	0.023687
1.7	16	0.917924	0.01894	0.833836	0.024334
1.7	17	0.91898	0.018707	0.835529	0.024207
1.7	18	0.921408	0.018169	0.83169	0.024696
1.7	19	0.922059	0.018025	0.832978	0.024627
1.7	20	0.923889	0.017618	0.822959	0.025889
1.8	1	0.863307	0.030646	0.754401	0.035707
1.8	2	0.905689	0.021625	0.840967	0.023444
1.8	3	0.905848	0.02159	0.838718	0.023793
1.8	4	0.906458	0.021457	0.836206	0.023984
1.8	5	0.906971	0.021345	0.837065	0.023763
1.8	6	0.907167	0.021302	0.837406	0.023764
1.8	7	0.907624	0.021203	0.834811	0.024074
1.8	8	0.908018	0.021117	0.836419	0.023865
1.8	9	0.909127	0.020874	0.832199	0.024522
1.8	10	0.912285	0.020182	0.83149	0.02447
1.8	11	0.913229	0.019975	0.828953	0.024794
1.8	12	0.914195	0.019762	0.83504	0.02395
1.8	13	0.915991	0.019367	0.83233	0.024405
1.8	14	0.91671	0.019208	0.830193	0.024803
1.8	15	0.918023	0.018919	0.823699	0.025494
1.8	16	0.919016	0.018699	0.824142	0.025566
1.8	17	0.920078	0.018464	0.82418	0.025672
1.8	18	0.920601	0.018348	0.819512	0.026313
1.8	19	0.921017	0.018256	0.825312	0.025709
1.8	20	0.921954	0.018048	0.821585	0.026177
1.9	1	0.861614	0.030997	0.751628	0.036052

Table A1 Continued

1.9	2	0.905966	0.021564	0.842651	0.023292
1.9	3	0.906741	0.021395	0.841014	0.023363
1.9	4	0.907123	0.021312	0.84149	0.023252
1.9	5	0.907133	0.02131	0.840677	0.023354
1.9	6	0.907844	0.021155	0.839303	0.02345
1.9	7	0.907955	0.02113	0.837012	0.023777
1.9	8	0.909111	0.020878	0.837226	0.023648
1.9	9	0.909323	0.020831	0.836561	0.023727
1.9	10	0.913294	0.01996	0.837298	0.024048
1.9	11	0.913839	0.019841	0.833532	0.024501
1.9	12	0.914461	0.019704	0.833113	0.024464
1.9	13	0.91476	0.019638	0.828629	0.024969
1.9	14	0.915433	0.01949	0.823931	0.025659
1.9	15	0.91684	0.01918	0.835555	0.02403
1.9	16	0.91937	0.018621	0.829625	0.024713
1.9	17	0.921055	0.018247	0.81218	0.027011
1.9	18	0.92161	0.018124	0.806322	0.027775
1.9	19	0.923266	0.017757	0.792429	0.029632
1.9	20	0.92426	0.017536	0.792656	0.029669
2	1	0.85985	0.031362	0.748832	0.036419
2	2	0.906019	0.021553	0.843956	0.023188
2	3	0.907065	0.021325	0.842039	0.023281
2	4	0.907728	0.02118	0.844226	0.022839
2	5	0.908049	0.02111	0.839257	0.023482
2	6	0.908175	0.021082	0.839556	0.023459
2	7	0.909187	0.020861	0.837095	0.023702
2	8	0.911158	0.020429	0.834405	0.024046
2	9	0.911267	0.020405	0.832623	0.024273
2	10	0.912589	0.020115	0.834028	0.024185
2	11	0.913517	0.019911	0.834517	0.024053
2	12	0.914204	0.01976	0.828941	0.024908

Table A1 Continued

2	13	0.915995	0.019366	0.828925	0.024997
2	14	0.916914	0.019163	0.822923	0.025614
2	15	0.917356	0.019066	0.817212	0.026389
2	16	0.918033	0.018916	0.821073	0.02586
2	17	0.918887	0.018727	0.82666	0.025311
2	18	0.919306	0.018635	0.826193	0.025377
2	19	0.920522	0.018366	0.805839	0.028045
2	20	0.921432	0.018164	0.803194	0.028511

APPENDIX B

EXPERIMENTATION RESULTS OF THE WIDTH PARAMETER FOR DEVELOPMENT OF GRNN MODEL FOR BLAST-INDUCED GROUND VIBRATION PREDICTION

Table B1 Training and Testing R and MSE Results for GRFNN Blast-Induced Ground Vibration Prediction Model

Width Parameter	Training		Testing	
	R	MSE	R	MSE
0.10	0.99377	0.0015	0.73665	0.0395
0.11	0.99255	0.0018	0.74581	0.03795
0.12	0.99097	0.00219	0.75328	0.03666
0.13	0.98899	0.00268	0.75918	0.03564
0.14	0.98655	0.00329	0.76376	0.03482
0.15	0.98365	0.004	0.76735	0.03416
0.16	0.98029	0.00483	0.77018	0.03362
0.17	0.97657	0.00575	0.77248	0.03317
0.18	0.97258	0.00672	0.77438	0.03279
0.19	0.96845	0.00773	0.77598	0.03246
0.20	0.96428	0.00873	0.77735	0.03218
0.21	0.96015	0.00973	0.77857	0.03194
0.22	0.95612	0.0107	0.77967	0.03172
0.23	0.95223	0.01163	0.7807	0.03153
0.24	0.9485	0.01253	0.78169	0.03135
0.25	0.94494	0.01339	0.78267	0.0312
0.26	0.94156	0.01421	0.78366	0.03105
0.27	0.93835	0.015	0.78467	0.03092
0.28	0.93531	0.01575	0.78571	0.0308
0.29	0.93244	0.01646	0.7868	0.03069
0.30	0.92973	0.01715	0.78793	0.03059
0.31	0.92718	0.01781	0.78913	0.0305
0.32	0.92478	0.01845	0.79037	0.03041

Table B1 Continued

0.33	0.92252	0.01906	0.79167	0.03033
0.34	0.9204	0.01966	0.79302	0.03026
0.35	0.91839	0.02024	0.7944	0.03019
0.36	0.91649	0.02081	0.79579	0.03014
0.37	0.91469	0.02137	0.79718	0.0301
0.38	0.91298	0.02193	0.79856	0.03007
0.39	0.91134	0.02248	0.79991	0.03006
0.40	0.90977	0.02303	0.80121	0.03006
0.41	0.90827	0.02359	0.80247	0.03009
0.42	0.90681	0.02414	0.80366	0.03013
0.43	0.90541	0.0247	0.80479	0.03019
0.44	0.90405	0.02527	0.80585	0.03026
0.45	0.90273	0.02584	0.80684	0.03036
0.46	0.90144	0.02642	0.80778	0.03047
0.47	0.90019	0.02701	0.80864	0.03059
0.48	0.89896	0.02761	0.80944	0.03074
0.49	0.89775	0.02822	0.81019	0.0309
0.50	0.89655	0.02885	0.81087	0.03107
0.51	0.89537	0.02949	0.8115	0.03126
0.52	0.89418	0.03014	0.81208	0.03146
0.53	0.89299	0.03081	0.8126	0.03168
0.54	0.89179	0.03149	0.81308	0.0319
0.55	0.89058	0.03218	0.8135	0.03214
0.56	0.88936	0.03289	0.81389	0.03239
0.57	0.88813	0.03361	0.81423	0.03264
0.58	0.88689	0.03434	0.81453	0.03291
0.59	0.88565	0.03508	0.81479	0.03318
0.60	0.88441	0.03583	0.815	0.03347
0.61	0.88317	0.03659	0.81519	0.03376
0.62	0.88195	0.03735	0.81533	0.03405
0.63	0.88075	0.03812	0.81544	0.03435

Table B1 Continued

0.64	0.87957	0.0389	0.81552	0.03466
0.65	0.87843	0.03968	0.81556	0.03498
0.66	0.87733	0.04046	0.81557	0.03529
0.67	0.87628	0.04125	0.81555	0.03562
0.68	0.87529	0.04203	0.8155	0.03594
0.69	0.87435	0.04282	0.81542	0.03627
0.70	0.87347	0.04361	0.81531	0.0366
0.71	0.87266	0.0444	0.81518	0.03694
0.72	0.87192	0.0452	0.81502	0.03728
0.73	0.87125	0.04599	0.81484	0.03762
0.74	0.87066	0.04678	0.81464	0.03797
0.75	0.87014	0.04757	0.81443	0.03831
0.76	0.86969	0.04837	0.81419	0.03866
0.77	0.86932	0.04916	0.81395	0.03901
0.78	0.86901	0.04995	0.8137	0.03937
0.79	0.86877	0.05074	0.81344	0.03972
0.80	0.8686	0.05153	0.81318	0.04008
0.81	0.86849	0.05232	0.81291	0.04044
0.82	0.86843	0.0531	0.81265	0.04079
0.83	0.86842	0.05388	0.8124	0.04115
0.84	0.86846	0.05466	0.81216	0.04151
0.85	0.86855	0.05544	0.81193	0.04187
0.86	0.86867	0.05621	0.81171	0.04224
0.87	0.86883	0.05698	0.81152	0.0426
0.88	0.86901	0.05775	0.81135	0.04296
0.89	0.86922	0.05851	0.8112	0.04332
0.90	0.86945	0.05927	0.81109	0.04369
0.91	0.8697	0.06002	0.811	0.04405
0.92	0.86996	0.06076	0.81094	0.04441
0.93	0.87023	0.0615	0.81091	0.04477
0.94	0.87052	0.06223	0.81092	0.04513

Table B1 Continued

0.95	0.8708	0.06295	0.81096	0.04549
0.96	0.87109	0.06367	0.81104	0.04585
0.97	0.87139	0.06438	0.81115	0.04621
0.98	0.87168	0.06508	0.81129	0.04656
0.99	0.87197	0.06578	0.81146	0.04692
1.00	0.87226	0.06646	0.81166	0.04727

EXPERIMENTATION RESULTS OF THE NUMBER OF NEURONS FOR DEVELOPMENT OF WNN MODEL FOR BLAST-INDUCED GROUND VIBRATION PREDICTION

Table C1 Training and Testing R and MSE Results for WNN Blast-Induced Ground Vibration Prediction Model

Number of Neurons	Training		Testing	
	R	MSE	R	MSE
1	0.910723	0.020543	0.835420	0.023908
2	0.912838	0.020064	0.831450	0.024362
3	0.910333	0.020611	0.843820	0.022743
4	0.910855	0.020502	0.831400	0.024399
5	0.928962	0.016539	0.826180	0.025312
6	0.925149	0.017341	0.827010	0.024963
7	0.924545	0.017475	0.825730	0.025272
8	0.928443	0.016606	0.818080	0.026119
9	0.923828	0.017633	0.818290	0.026136
10	0.93949	0.014133	0.783500	0.032367
11	0.910195	0.020641	0.840700	0.023205
12	0.931072	0.016016	0.787700	0.031071
13	0.929103	0.016474	0.818000	0.026451
14	0.937403	0.014616	0.807600	0.027562
15	0.945905	0.012695	0.787100	0.030984
16	0.93915	0.014247	0.810200	0.027879
17	0.935792	0.014962	0.826900	0.024948
18	0.932929	0.015605	0.771200	0.032453
19	0.936154	0.014878	0.796100	0.029589
20	0.589495	0.157951	-0.167096	0.360049

EXPERIMENTATION RESULTS OF THE NUMBER OF NEURONS FOR DEVELOPMENT OF ELM MODEL FOR BLAST-INDUCED GROUND VIBRATION PREDICTION

Table D1 Training and Testing R and MSE Results for ELM Blast-Induced Ground Vibration Prediction Model

Number of Neurons	Training		Testing	
	R	MSE	R	MSE
1	-0.0706	0.15176	0.14181	0.09356
2	0.71715	0.05874	0.43175	0.06793
3	0.84352	0.03495	0.75881	0.03565
4	0.67371	0.0658	0.42293	0.07281
5	0.8289	0.03811	0.70246	0.04021
6	0.89338	0.02429	0.83211	0.02547
7	0.90801	0.02112	0.85127	0.02217
8	0.90488	0.0218	0.84269	0.02301
9	0.91034	0.02061	0.84545	0.02274
10	0.90929	0.02084	0.84847	0.02228
11	0.9073	0.02127	0.85345	0.02166
12	0.91298	0.02003	0.84061	0.02384
13	0.91011	0.02066	0.85218	0.02194
14	0.91164	0.02032	0.83472	0.02509
15	0.90873	0.02096	0.84699	0.02267
16	0.91177	0.0203	0.85141	0.02197
17	0.91333	0.01995	0.84736	0.02225
18	0.91337	0.01994	0.83395	0.02498
19	0.91603	0.01936	0.78481	0.0309
20	0.91711	0.01912	0.82404	0.0271
21	0.91975	0.01854	0.82253	0.02623
22	0.91277	0.02008	0.82975	0.02464
23	0.92087	0.01829	0.81324	0.02743

Table D1 Continued

24	0.91382	0.01985	0.85199	0.02222
25	0.91786	0.01896	0.74118	0.03774
26	0.91839	0.01884	0.81993	0.02587
27	0.91569	0.01943	0.81619	0.02721
28	0.91589	0.01939	0.83289	0.02492
29	0.92233	0.01797	0.82059	0.02793
30	0.91914	0.01867	0.77993	0.036
31	0.9316	0.0159	0.75489	0.04051
32	0.92308	0.0178	0.59133	0.06877
33	0.9254	0.01728	0.74866	0.04079
34	0.93003	0.01625	0.74141	0.04627
35	0.93098	0.01604	0.62483	0.12564
36	0.93318	0.01554	0.75911	0.03658
37	0.92691	0.01695	0.71959	0.04218
38	0.92983	0.01629	0.65194	0.13931
39	0.9307	0.0161	0.7136	0.05566
40	0.93217	0.01577	0.74003	0.04474
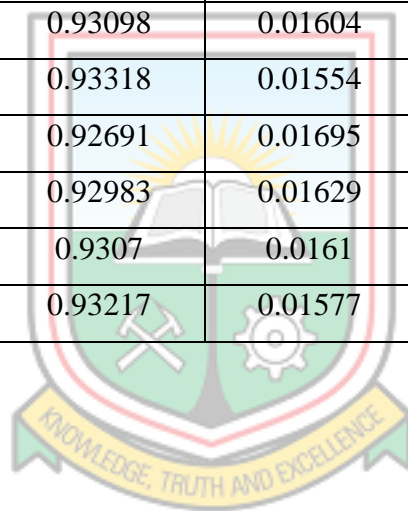
PREDICTED PPV VALUES ON THE TESTING DATA SETS BY THE VARIOUS PREDICTION TECHNIQUES

Table E1 Observed and Predicted PPV for the Various Models

Observed PPV (mm/s)	Predicted PPV (mm/s)														
	BPNN	GRNN	RBFNN	MARS	WNN	GMDH	LSSVM	RVM	SVM	ELM	GPR	USBM	Ambrasey-Hendron	Indian Standard	Langefors-Kihlstrom
1.14	1.03	0.94	0.92	0.89	0.95	0.92	1.00	1.25	1.00	1.04	0.87	0.94	0.88	1.01	0.97
0.83	0.59	0.64	0.62	0.58	0.62	0.61	0.62	0.87	0.60	0.61	0.55	0.57	0.55	0.66	0.59
0.13	0.24	0.36	0.33	0.15	0.30	0.42	0.18	0.46	-0.03	0.13	0.20	0.28	0.35	0.19	0.24
0.64	0.63	0.66	0.64	0.63	0.63	0.60	0.65	0.90	0.64	0.65	0.58	0.63	0.59	0.76	0.66
0.7	0.69	0.67	0.69	0.68	0.69	0.68	0.70	0.95	0.70	0.69	0.66	0.62	0.58	0.74	0.65
0.7	0.74	0.69	0.70	0.69	0.69	0.67	0.75	1.00	0.80	0.71	0.72	0.68	0.62	0.83	0.72
0.83	0.96	0.92	0.96	0.96	0.97	0.94	0.94	1.19	0.89	0.95	0.86	0.86	0.85	0.84	0.86
0.64	0.60	0.64	0.62	0.59	0.62	0.60	0.62	0.87	0.61	0.61	0.55	0.59	0.56	0.69	0.61
0.51	0.63	0.64	0.63	0.61	0.62	0.60	0.65	0.90	0.68	0.63	0.60	0.60	0.57	0.71	0.63
0.64	0.62	0.77	0.63	0.65	0.61	0.57	0.64	0.89	0.64	0.61	0.53	0.75	0.74	0.74	0.75
0.89	0.61	0.64	0.61	0.58	0.60	0.56	0.63	0.88	0.66	0.61	0.56	0.62	0.59	0.75	0.66
0.64	0.71	0.79	0.71	0.75	0.72	0.69	0.73	0.98	0.73	0.72	0.69	0.70	0.71	0.67	0.69
0.64	0.74	0.68	0.73	0.72	0.74	0.75	0.75	1.00	0.75	0.75	0.74	0.60	0.57	0.70	0.62
0.51	0.64	0.65	0.65	0.63	0.66	0.65	0.66	0.91	0.65	0.65	0.61	0.59	0.56	0.70	0.62
0.83	0.66	0.67	0.66	0.64	0.65	0.62	0.68	0.93	0.70	0.67	0.62	0.65	0.60	0.79	0.69

Table E1 Continued

0.57	0.50	0.63	0.53	0.49	0.53	0.47	0.52	0.78	0.49	0.51	0.46	0.59	0.56	0.69	0.62
0.7	0.56	0.62	0.59	0.56	0.59	0.57	0.58	0.83	0.58	0.57	0.52	0.56	0.54	0.65	0.58
0.51	0.61	0.67	0.60	0.58	0.62	0.58	0.62	0.87	0.57	0.63	0.53	0.62	0.58	0.74	0.65
0.64	0.84	0.89	0.84	0.86	0.83	0.82	0.83	1.09	0.79	0.85	0.75	0.90	0.87	0.90	0.91
0.57	0.70	0.66	0.71	0.67	0.71	0.73	0.71	0.96	0.69	0.71	0.69	0.56	0.54	0.64	0.58
0.89	0.80	0.90	0.80	0.82	0.80	0.79	0.80	1.06	0.74	0.78	0.70	0.94	0.93	0.86	0.92
0.32	0.39	0.49	0.35	0.40	0.37	0.33	0.39	0.64	0.33	0.41	0.39	0.43	0.39	0.59	0.47
0.7	0.82	0.88	0.84	0.84	0.83	0.81	0.82	1.07	0.79	0.83	0.76	0.86	0.84	0.86	0.87
0.57	0.72	0.83	0.74	0.75	0.74	0.73	0.73	0.98	0.68	0.70	0.67	0.75	0.76	0.70	0.74
0.32	0.47	0.47	0.42	0.50	0.43	0.48	0.49	0.74	0.45	0.50	0.48	0.41	0.38	0.55	0.44
0.83	0.81	0.79	0.81	0.83	0.80	0.78	0.82	1.07	0.85	0.81	0.84	0.72	0.70	0.78	0.74
0.64	0.63	0.65	0.64	0.62	0.63	0.62	0.65	0.90	0.67	0.64	0.60	0.60	0.57	0.71	0.63
0.89	0.68	0.66	0.68	0.67	0.68	0.68	0.69	0.94	0.70	0.68	0.67	0.59	0.56	0.69	0.62
0.44	0.62	0.65	0.63	0.61	0.62	0.60	0.64	0.89	0.63	0.63	0.57	0.62	0.58	0.74	0.65
0.7	0.66	0.64	0.67	0.62	0.70	0.74	0.67	0.92	0.59	0.67	0.62	0.52	0.51	0.58	0.53
0.64	0.74	0.67	0.72	0.69	0.76	0.82	0.74	1.00	0.66	0.76	0.71	0.55	0.53	0.62	0.56
0.95	0.94	0.96	0.94	0.94	0.93	0.95	0.93	1.19	0.89	0.92	1.01	1.04	1.07	0.87	1.00
0.95	0.76	0.84	0.74	0.74	0.69	0.63	0.77	1.02	0.81	0.81	0.66	0.93	0.87	1.00	0.96
0.95	0.73	0.67	0.73	0.70	0.74	0.77	0.74	0.99	0.70	0.74	0.72	0.57	0.54	0.65	0.59
1.08	1.07	1.01	1.07	1.07	1.06	1.07	1.05	1.30	1.04	1.07	1.11	1.12	1.11	1.01	1.11
0.32	0.43	0.68	0.43	0.48	0.49	0.51	0.45	0.72	0.50	0.46	0.60	0.72	0.68	0.81	0.75
0.38	0.32	0.42	0.43	0.30	0.34	0.44	0.32	0.58	0.30	0.28	0.46	0.33	0.34	0.38	0.33
0.76	0.99	0.98	1.00	0.98	1.00	1.02	0.97	1.22	0.92	0.97	1.04	1.00	1.01	0.88	0.98

Table E1 Continued

0.89	0.79	0.75	0.82	0.81	0.82	0.83	0.79	1.04	0.76	0.80	0.80	0.62	0.61	0.66	0.63
0.7	0.79	0.92	0.75	0.81	0.77	0.78	0.80	1.06	0.74	0.75	0.76	0.94	0.99	0.75	0.88
0.96	0.91	0.92	0.94	0.92	0.93	0.93	0.90	1.16	0.88	0.91	0.95	0.88	0.87	0.85	0.88
0.83	0.93	0.96	0.91	0.93	0.91	0.93	0.92	1.18	0.86	0.91	0.90	1.12	1.14	0.95	1.09
1.08	0.87	0.89	0.87	0.87	0.85	0.82	0.87	1.12	0.88	0.88	0.83	0.90	0.86	0.93	0.92
0.83	1.05	1.00	0.97	1.02	0.96	0.99	1.03	1.29	1.03	1.06	1.08	1.43	1.46	1.12	1.37
0.64	0.85	0.88	0.86	0.86	0.83	0.81	0.85	1.10	0.86	0.87	0.81	0.90	0.86	0.92	0.91
0.7	0.98	0.98	0.88	0.95	0.85	0.88	0.97	1.23	0.98	0.99	0.91	1.47	1.49	1.15	1.40
0.38	0.46	0.72	0.50	0.48	0.52	0.56	0.48	0.75	0.42	0.43	0.49	0.57	0.60	0.50	0.54
0.38	0.31	0.40	0.29	0.32	0.28	0.27	0.29	0.54	0.27	0.30	0.35	0.37	0.34	0.52	0.40
0.64	0.72	0.82	0.74	0.76	0.74	0.73	0.74	0.99	0.72	0.72	0.72	0.70	0.72	0.64	0.68
0.83	1.07	1.01	1.01	1.06	1.00	1.04	1.05	1.30	1.02	1.05	1.14	1.39	1.45	1.04	1.31
0.57	0.70	0.81	0.72	0.74	0.72	0.70	0.72	0.97	0.69	0.69	0.64	0.74	0.74	0.71	0.73
1.27	1.12	1.04	1.09	1.11	1.09	1.14	1.10	1.36	1.06	1.10	1.13	1.37	1.43	1.03	1.29
1.27	0.98	0.97	0.88	0.97	0.89	0.89	0.97	1.22	0.96	0.96	1.08	1.21	1.29	0.89	1.13
1.08	1.08	1.02	1.03	1.07	1.02	1.08	1.05	1.31	1.01	1.07	1.11	1.40	1.43	1.11	1.35
1.02	0.99	0.99	0.93	0.98	0.94	0.97	0.98	1.23	0.93	0.95	1.09	1.24	1.31	0.92	1.16
1.33	1.10	1.03	1.05	1.08	1.04	1.08	1.08	1.33	1.06	1.10	1.15	1.39	1.41	1.11	1.34
1.02	1.03	1.00	0.99	1.01	1.00	1.04	1.01	1.26	0.94	0.99	1.09	1.19	1.25	0.91	1.12
1.02	1.11	1.03	1.09	1.09	1.09	1.14	1.08	1.34	1.03	1.09	1.13	1.30	1.34	1.02	1.24
1.02	0.98	0.98	0.99	0.98	0.98	0.99	0.96	1.22	0.93	0.98	1.02	1.05	1.05	0.94	1.04
1.14	0.98	0.97	0.97	0.98	0.95	0.95	0.97	1.22	0.97	0.98	1.03	1.09	1.08	0.98	1.07
1.08	1.08	1.02	1.02	1.07	1.02	1.07	1.05	1.31	1.01	1.06	1.13	1.40	1.44	1.08	1.33

Table E1 Continued

0.89	0.99	0.98	0.90	0.98	0.90	0.92	0.98	1.23	0.96	0.96	1.05	1.35	1.41	1.00	1.26
1.52	1.27	1.13	1.29	1.27	1.29	1.31	1.25	1.51	1.25	1.27	1.21	1.34	1.37	1.06	1.28
0.89	1.08	1.02	1.09	1.07	1.08	1.07	1.06	1.31	1.07	1.07	1.09	1.04	1.03	0.95	1.03
0.64	0.80	0.91	0.79	0.84	0.76	0.75	0.82	1.07	0.88	0.82	1.02	1.01	1.01	0.90	0.99
1.14	0.95	0.95	0.96	0.96	0.95	0.95	0.93	1.19	0.91	0.95	0.97	0.98	0.96	0.93	0.98
0.76	0.75	0.83	0.75	0.77	0.76	0.74	0.75	1.01	0.69	0.75	0.64	0.79	0.77	0.82	0.80
0.95	1.19	1.06	1.16	1.17	1.16	1.17	1.17	1.42	1.17	1.19	1.12	1.35	1.39	1.05	1.28
1.21	1.12	1.03	1.08	1.11	1.08	1.10	1.10	1.35	1.07	1.10	1.13	1.35	1.41	1.02	1.28
0.32	0.31	0.48	0.26	0.25	0.28	0.40	0.29	0.58	0.09	0.41	0.22	0.32	0.48	0.14	0.24
1.14	1.04	1.00	1.07	1.04	1.06	1.04	1.02	1.28	1.00	1.04	1.02	0.93	0.95	0.81	0.90
1.21	1.18	1.07	1.18	1.17	1.18	1.21	1.16	1.42	1.13	1.17	1.12	1.35	1.41	1.02	1.27
0.95	1.10	1.02	1.06	1.09	1.05	1.08	1.08	1.33	1.07	1.09	1.14	1.34	1.39	1.04	1.28
0.89	1.18	1.08	1.22	1.17	1.22	1.22	1.16	1.41	1.15	1.17	1.07	1.06	1.05	0.95	1.04
0.83	0.98	0.98	0.91	0.97	0.91	0.97	0.96	1.22	0.88	0.94	0.91	1.32	1.36	1.05	1.27
0.95	1.19	1.07	1.16	1.18	1.16	1.19	1.17	1.43	1.17	1.20	1.15	1.46	1.50	1.12	1.39
1.33	1.35	1.18	1.37	1.36	1.41	1.46	1.35	1.60	1.35	1.35	1.33	1.50	1.53	1.17	1.43
1.33	1.08	1.02	1.04	1.07	1.04	1.09	1.06	1.31	1.00	1.05	1.14	1.36	1.41	1.04	1.29
0.64	0.84	0.88	0.86	0.86	0.85	0.83	0.84	1.09	0.81	0.84	0.82	0.84	0.83	0.83	0.84
1.14	1.13	1.04	1.10	1.11	1.10	1.12	1.11	1.36	1.08	1.11	1.09	1.29	1.36	0.97	1.21

**EXPERIMENTATION RESULTS OF THE WIDTH PARAMETER AND
MAXIMUM NUMBER OF NEURONS FOR DEVELOPMENT OF RBFNN
MODEL FOR AIR OVERPRESSURE PREDICTION**

**Table F1 Training and Testing R and MSE Results for RBFNN Air Overpressure
Prediction Model**

Width Parameter	Maximum Number of Neurons	Training		Testing	
		R	MSE	R	MSE
0.1	1	0.166848	4.026843	-0.02868	3.650764
0.1	2	0.175126	4.015117	-0.02868	3.627714
0.1	3	0.214011	3.952439	-0.0289	3.577931
0.1	4	0.434651	3.359613	0.204703	3.465466
0.1	5	0.438106	3.347122	0.223	3.456109
0.1	6	0.453229	3.291288	0.23412	3.442062
0.1	7	0.457840	3.273885	0.233635	3.437853
0.1	8	0.460982	3.261928	0.233229	3.435711
0.1	9	0.496435	3.121331	-0.03269	3.479245
0.1	10	0.506847	3.078058	-0.0325	3.472474
0.1	11	0.510414	3.063028	-0.0323	3.470052
0.1	12	0.512792	3.052951	-0.0433	3.477137
0.1	13	0.526274	2.994924	-0.0439	3.484637
0.1	14	0.530704	2.975529	-0.0443	3.490873
0.1	15	0.535416	2.954719	-0.0447	3.499039
0.1	16	0.537081	2.947325	-0.0449	3.504049
0.1	17	0.582302	2.73765	-0.046	3.541599
0.1	19	0.587776	2.711119	-0.0462	3.541665
0.1	20	0.591329	2.693766	-0.0458	3.555809
0.2	1	0.316611	3.726934	-0.08856	3.954509
0.2	2	0.383943	3.531548	-0.02504	3.693904

Table F1 Continued

0.2	3	0.399508	3.481039	-0.013	3.589052
0.2	4	0.602303	2.639509	0.219256	3.273481
0.2	5	0.602773	2.637161	0.217282	3.275216
0.2	6	0.668269	2.292334	0.195888	3.345498
0.2	7	0.669541	2.285287	0.191579	3.366934
0.2	8	0.690624	2.166506	0.190796	3.326245
0.2	9	0.690955	2.164611	0.192522	3.320512
0.2	10	0.691202	2.163195	0.19101	3.325484
0.2	11	0.691218	2.163106	0.18945	3.328381
0.2	12	0.709458	2.05728	0.20388	3.348785
0.2	13	0.713938	2.030868	0.21123	3.31291
0.2	14	0.713949	2.030802	0.2112	3.314097
0.2	15	0.719308	1.998988	0.21439	3.289152
0.2	16	0.751184	1.80483	0.28653	3.16054
0.2	17	0.752611	1.795942	0.28422	3.164284
0.2	18	0.759781	1.751025	0.14519	3.638146
0.2	19	0.779177	1.627381	0.12408	3.710847
0.2	20	0.780092	1.621472	0.11196	3.748493
0.3	1	0.055990	4.129168	-0.15974	3.654667
0.3	2	0.098022	4.102354	-0.15974	3.559928
0.3	3	0.410081	3.445584	0.405523	2.930589
0.3	4	0.412791	3.436346	0.408098	2.930149
0.3	5	0.494019	3.131241	0.398621	2.990194
0.3	6	0.557818	2.853279	0.414215	3.182617
0.3	7	0.568492	2.80348	0.397906	3.35905
0.3	8	0.604004	2.631012	0.429378	3.063432
0.3	9	0.605482	2.623602	0.398675	3.130127
0.3	10	0.606063	2.620691	0.39342	3.16148
0.3	11	0.635136	2.471216	0.34407	3.447228
0.3	12	0.646906	2.408713	0.29859	3.705978

Table F1 Continued

0.3	13	0.766591	1.707971	0.4407	2.873698
0.3	14	0.770502	1.683065	0.43008	2.967437
0.3	15	0.774292	1.658818	0.45299	2.844459
0.3	16	0.776016	1.647748	0.46033	2.783915
0.3	17	0.782124	1.608322	0.44522	2.9121
0.3	18	0.782892	1.603348	0.43802	2.976259
0.3	19	0.824116	1.328939	0.41216	2.920385
0.3	20	0.826211	1.314615	0.42475	2.954236
0.4	1	0.093978	4.10557	0.237536	3.448153
0.4	2	0.153967	4.04396	0.237547	3.326492
0.4	3	0.627061	2.513437	0.529291	2.685733
0.4	4	0.653424	2.373608	0.528492	2.529751
0.4	5	0.654531	2.367611	0.530193	2.554042
0.4	6	0.712498	2.039374	0.558932	2.363511
0.4	7	0.712814	2.037512	0.562682	2.350095
0.4	8	0.722012	1.982841	0.552383	2.41344
0.4	9	0.765119	1.717307	0.585643	2.378778
0.4	10	0.774617	1.65673	0.57696	2.332132
0.4	11	0.775018	1.65416	0.57913	2.333922
0.4	12	0.775018	1.654159	0.57911	2.333883
0.4	13	0.777563	1.637791	0.57094	2.345018
0.4	14	0.781092	1.615006	0.58187	2.342773
0.4	15	0.786196	1.581873	0.60616	2.413115
0.4	16	0.788896	1.564257	0.59906	2.298591
0.4	17	0.789088	1.563001	0.5941	2.295528
0.4	18	0.791408	1.547809	0.5836	2.296524
0.4	19	0.793327	1.535217	0.56688	2.373925
0.4	20	0.810138	1.42356	0.48497	3.095134
0.5	1	0.232959	3.917359	0.37432	3.161819
0.5	2	0.314676	3.731993	0.374471	2.965067

Table F1 Continued

0.5	3	0.374952	3.559812	0.382141	3.026305
0.5	4	0.590335	2.698634	0.513653	2.749792
0.5	5	0.656333	2.357827	0.61734	2.248562
0.5	6	0.660216	2.336653	0.611754	2.284066
0.5	7	0.665891	2.305479	0.596734	2.392617
0.5	8	0.697247	2.12843	0.636238	2.216
0.5	9	0.697258	2.128371	0.636905	2.212518
0.5	10	0.706797	2.072893	0.61723	2.302155
0.5	11	0.712420	2.039833	0.58455	2.483617
0.5	12	0.712521	2.03924	0.59092	2.44768
0.5	13	0.720565	1.991489	0.53104	2.790543
0.5	14	0.729136	1.940023	0.45098	3.276322
0.5	15	0.730161	1.933824	0.41348	3.521654
0.5	16	0.737767	1.88758	0.28384	4.533923
0.5	17	0.752122	1.798986	0.13308	6.461002
0.5	18	0.752582	1.796123	0.16391	5.979463
0.5	19	0.755058	1.780657	0.25421	4.741599
0.5	20	0.768997	1.692664	0.11212	7.726998
0.6	1	0.241265	3.901044	0.421693	3.128468
0.6	2	0.337599	3.67006	0.422279	2.836417
0.6	3	0.382512	3.536092	0.424553	2.918041
0.6	4	0.407974	3.45272	0.491889	2.693294
0.6	5	0.421036	3.407869	0.489316	2.796348
0.6	6	0.648530	2.399999	0.544857	2.796273
0.6	7	0.740064	1.873519	0.666387	2.034421
0.6	8	0.743480	1.852526	0.658697	2.053993
0.6	9	0.747042	1.830537	0.644146	2.134969
0.6	10	0.751221	1.804597	0.62184	2.271359
0.6	11	0.754227	1.785854	0.57206	2.574412
0.6	12	0.754335	1.78518	0.58274	2.509874

Table F1 Continued

0.6	13	0.761082	1.742829	0.66573	2.087836
0.6	14	0.763305	1.728791	0.61993	2.300608
0.6	15	0.769205	1.691341	0.67732	2.041976
0.6	16	0.770963	1.680125	0.61629	2.29377
0.6	17	0.812167	1.409923	0.15963	7.288368
0.6	18	0.812186	1.409797	0.14742	7.42662
0.6	19	0.825082	1.322338	0.36444	4.297613
0.6	20	0.839051	1.226049	0.62715	2.109617
0.7	1	0.248076	3.887239	0.451894	3.134555
0.7	2	0.355834	3.617684	0.452239	2.742419
0.7	3	0.389756	3.512919	0.451653	2.842812
0.7	4	0.403070	3.469198	0.446057	2.955296
0.7	5	0.424226	3.396699	0.41126	3.212896
0.7	6	0.446647	3.31582	0.490982	2.89436
0.7	7	0.646764	2.409477	0.406499	3.919043
0.7	8	0.746026	1.836818	0.694909	1.923381
0.7	9	0.746735	1.832436	0.693995	1.904804
0.7	10	0.748330	1.822555	0.68989	1.907085
0.7	11	0.749335	1.816324	0.69523	1.907598
0.7	12	0.764657	1.720234	0.65988	1.997409
0.7	13	0.776242	1.646291	0.71004	2.285803
0.7	14	0.782384	1.606638	0.73093	2.740783
0.7	15	0.782390	1.606602	0.73036	2.716876
0.7	16	0.788091	1.569515	0.74025	3.731281
0.7	17	0.790501	1.553754	0.729	2.613777
0.7	18	0.795468	1.521128	0.61966	2.340981
0.7	19	0.796721	1.51286	0.54934	2.4835
0.7	20	0.796954	1.511322	0.5173	2.609501
0.8	1	0.254321	3.874242	0.470126	3.165597
0.8	2	0.370448	3.573718	0.467661	2.687207

Table F1 Continued

0.8	3	0.396960	3.489445	0.467764	2.795771
0.8	4	0.441019	3.336515	0.505721	2.64348
0.8	5	0.445346	3.320628	0.502808	2.694928
0.8	6	0.450919	3.299939	0.489465	2.831412
0.8	7	0.658785	2.344471	0.464339	3.486763
0.8	8	0.750884	1.806697	0.71254	1.979437
0.8	9	0.750967	1.80618	0.712905	1.957342
0.8	10	0.751845	1.800716	0.71183	1.860894
0.8	11	0.751855	1.800653	0.71167	1.851744
0.8	12	0.764469	1.721426	0.68074	1.978188
0.8	13	0.764717	1.719853	0.68555	1.989474
0.8	14	0.765094	1.717468	0.67452	1.978327
0.8	15	0.771332	1.67777	0.70903	2.271829
0.8	16	0.782422	1.606394	0.59364	2.320285
0.8	17	0.791251	1.548839	0.72987	2.393356
0.8	18	0.814355	1.395183	0.38562	3.972979
0.8	19	0.816429	1.381173	0.32147	5.127931
0.8	20	0.818743	1.365503	0.1672	6.585819
0.9	1	0.260697	3.86064	0.480621	3.207786
0.9	2	0.382614	3.53577	0.471561	2.673272
0.9	3	0.404373	3.464839	0.475627	2.77394
0.9	4	0.452961	3.292291	0.494095	2.731424
0.9	5	0.652345	2.379445	0.553742	2.671167
0.9	6	0.754644	1.783246	0.716119	2.072167
0.9	7	0.754664	1.783121	0.716113	2.082469
0.9	8	0.754665	1.783119	0.716118	2.078989
0.9	9	0.754886	1.781733	0.715665	2.024391
0.9	10	0.754928	1.781475	0.71621	1.977551
0.9	11	0.764033	1.724184	0.70786	2.139127
0.9	12	0.764036	1.724167	0.70805	2.143792

Table F1 Continued

0.9	13	0.771995	1.673525	0.71734	2.704551
0.9	14	0.776860	1.642317	0.70711	2.056213
0.9	15	0.778238	1.633438	0.69726	1.989812
0.9	16	0.778328	1.632859	0.7031	2.013717
0.9	17	0.778332	1.632832	0.70243	2.009036
0.9	18	0.789771	1.558535	0.75146	3.395284
0.9	19	0.811302	1.415745	0.56692	2.895903
0.9	20	0.813062	1.403902	0.49893	3.324575
1.0	1	0.290435	3.792751	0.510259	3.199509
1.0	2	0.434322	3.360796	0.485382	2.63484
1.0	3	0.442070	3.33267	0.493368	2.620059
1.0	4	0.443732	3.326572	0.501259	2.585019
1.0	5	0.446751	3.315435	0.494433	2.639769
1.0	6	0.717580	2.009271	0.614738	4.237895
1.0	7	0.741085	1.867255	0.681306	3.708964
1.0	8	0.744716	1.844906	0.703143	3.205198
1.0	9	0.758045	1.761939	0.735849	2.294176
1.0	10	0.772474	1.670467	0.75258	3.374856
1.0	11	0.773581	1.663376	0.75048	3.231331
1.0	12	0.786529	1.579702	0.68816	2.191566
1.0	13	0.788643	1.565908	0.65734	2.220657
1.0	14	0.798530	1.500907	0.543	3.448117
1.0	15	0.798958	1.49808	0.56198	3.406213
1.0	16	0.803679	1.46674	0.42101	4.082587
1.0	17	0.811086	1.417191	0.1942	6.536784
1.0	18	0.816890	1.378059	0.08734	9.182863
1.0	19	0.817790	1.371961	0.0382	10.802929
1.0	20	0.819759	1.358609	-0.0517	13.148749
1.1	1	0.293886	3.784399	0.51237	3.248248
1.1	2	0.438593	3.345355	0.473256	2.684376

Table F1 Continued

1.1	3	0.443323	3.328073	0.478232	2.673885
1.1	4	0.451040	3.299487	0.485556	2.670371
1.1	5	0.451648	3.297213	0.477355	2.713102
1.1	6	0.452116	3.295459	0.471072	2.746987
1.1	7	0.480524	3.185716	0.509086	2.804409
1.1	8	0.738926	1.880491	0.568483	4.191074
1.1	9	0.751718	1.801505	0.659141	3.569435
1.1	10	0.753863	1.788128	0.68661	3.090196
1.1	11	0.782034	1.608909	0.71921	2.190164
1.1	12	0.782660	1.604849	0.7379	2.33153
1.1	13	0.785159	1.588621	0.72263	2.26208
1.1	14	0.786011	1.583075	0.73732	2.321713
1.1	15	0.792054	1.543573	0.56938	2.686022
1.1	16	0.808529	1.434349	0.3185	5.778833
1.1	17	0.811329	1.41556	0.23555	7.006707
1.1	18	0.819083	1.363194	0.12626	10.289813
1.1	19	0.820829	1.351334	0.05412	13.214115
1.1	20	0.832462	1.271669	-0.1717	22.355155
1.2	1	0.298474	3.773142	0.515173	3.269297
1.2	2	0.438562	3.345466	0.454469	2.73455
1.2	3	0.447467	3.312785	0.469806	2.705064
1.2	4	0.447901	3.311174	0.470393	2.706269
1.2	5	0.462473	3.256224	0.511865	2.54846
1.2	6	0.462774	3.255072	0.509144	2.564518
1.2	7	0.466613	3.240293	0.516127	2.574195
1.2	8	0.726322	1.956988	0.699452	2.097935
1.2	9	0.739652	1.876044	0.70476	1.857138
1.2	10	0.759276	1.754199	0.74683	1.953703
1.2	11	0.775818	1.649018	0.74664	2.299254
1.2	12	0.781781	1.610544	0.73014	4.39289

Table F1 Continued

1.2	13	0.781998	1.609139	0.72861	4.324867
1.2	14	0.782987	1.602728	0.73394	4.179534
1.2	15	0.783193	1.601394	0.73726	4.078539
1.2	16	0.789285	1.561713	0.70748	4.624343
1.2	17	0.789602	1.559641	0.7243	4.268069
1.2	18	0.822807	1.337868	0.14166	4.795021
1.2	19	0.833827	1.262248	0.02396	6.212741
1.2	20	0.833921	1.261599	0.0477	5.952323
1.3	1	0.301650	3.765248	0.515014	3.304409
1.3	2	0.441679	3.334102	0.440337	2.793448
1.3	3	0.452239	3.295001	0.465272	2.738125
1.3	4	0.452304	3.294758	0.464876	2.742707
1.3	5	0.491986	3.139542	0.540453	2.433857
1.3	6	0.495549	3.124969	0.564981	2.344479
1.3	7	0.503223	3.093221	0.614913	2.193645
1.3	8	0.509254	3.06793	0.608448	2.382667
1.3	9	0.536014	2.952065	0.538913	2.617259
1.3	10	0.616204	2.569347	0.40359	3.142282
1.3	11	0.757564	1.764955	0.68205	2.872181
1.3	12	0.762819	1.731864	0.71391	2.944984
1.3	13	0.765019	1.717941	0.72442	2.791019
1.3	14	0.767374	1.702995	0.74156	2.586511
1.3	15	0.775346	1.652053	0.78216	2.058031
1.3	16	0.783071	1.602183	0.74508	2.307346
1.3	17	0.791159	1.549442	0.61043	3.518352
1.3	18	0.791758	1.54552	0.68441	2.959306
1.3	19	0.806311	1.449186	0.33935	7.766053
1.3	20	0.828102	1.301657	-0.0081	21.846609
1.4	1	0.304764	3.757426	0.513588	3.334968
1.4	2	0.444222	3.32477	0.427091	2.860896

Table F1 Continued

1.4	3	0.457324	3.27584	0.464292	2.765997
1.4	4	0.457397	3.275563	0.465523	2.757295
1.4	5	0.507392	3.07577	0.554956	2.378932
1.4	6	0.507392	3.07577	0.555013	2.37871
1.4	7	0.510344	3.063324	0.55536	2.379172
1.4	8	0.510724	3.061718	0.561378	2.360507
1.4	9	0.740707	1.869572	0.719193	2.243893
1.4	10	0.745783	1.838318	0.71121	1.986148
1.4	11	0.747224	1.829406	0.70771	2.056128
1.4	12	0.757254	1.766906	0.76035	1.598571
1.4	13	0.757403	1.765968	0.76556	1.573762
1.4	14	0.772570	1.669849	0.78059	1.934464
1.4	15	0.772648	1.669351	0.7816	1.979519
1.4	16	0.785452	1.586712	0.69643	2.685672
1.4	17	0.796344	1.515349	0.55422	5.947606
1.4	18	0.816440	1.381102	0.1508	16.065747
1.4	19	0.837187	1.238993	-0.0115	55.640623
1.4	20	0.848639	1.159021	-0.0226	60.370569
1.5	1	0.291237	3.790821	0.338389	3.636047
1.5	2	0.293987	3.784153	0.291134	3.622302
1.5	3	0.316096	3.728284	0.433059	3.604485
1.5	4	0.382078	3.537468	0.467445	2.859242
1.5	5	0.384936	3.528387	0.461411	3.05282
1.5	6	0.566178	2.814356	0.428196	4.277868
1.5	7	0.587373	2.713081	0.47737	3.933314
1.5	8	0.588668	2.706774	0.4735	3.823123
1.5	9	0.613673	2.582239	0.451699	3.574857
1.5	10	0.634036	2.477003	0.36433	3.813929
1.5	11	0.697333	2.127934	0.55638	4.893531
1.5	12	0.774638	1.656596	0.7558	3.048669

Table F1 Continued

1.5	13	0.774809	1.655497	0.74927	2.92465
1.5	14	0.776519	1.644513	0.71675	3.105895
1.5	15	0.777191	1.640186	0.65755	3.581872
1.5	16	0.781450	1.612688	0.70439	3.16755
1.5	17	0.781458	1.612636	0.69792	3.217646
1.5	18	0.789085	1.56302	0.77763	2.900455
1.5	19	0.789478	1.560448	0.78424	2.821531
1.5	20	0.819401	1.36104	0.50606	13.300112
1.6	1	0.293131	3.786234	0.33593	3.656439
1.6	2	0.294712	3.782385	0.294337	3.652377
1.6	3	0.314564	3.732286	0.435719	3.615651
1.6	4	0.391911	3.505941	0.462099	2.911702
1.6	5	0.394114	3.49877	0.453533	3.116193
1.6	6	0.580515	2.74626	0.444688	4.079601
1.6	7	0.594732	2.677049	0.48512	3.751641
1.6	8	0.594802	2.676705	0.484457	3.716466
1.6	9	0.627207	2.512678	0.459342	3.504597
1.6	10	0.650738	2.388116	0.3559	4.111687
1.6	11	0.710389	2.051804	0.57173	4.834368
1.6	12	0.773267	1.665385	0.75816	3.209768
1.6	13	0.773338	1.664929	0.75354	3.091139
1.6	14	0.774748	1.655889	0.72365	3.172279
1.6	15	0.775299	1.65235	0.65837	3.611907
1.6	16	0.786879	1.577421	0.75073	6.970177
1.6	17	0.787551	1.573038	0.74341	6.325772
1.6	18	0.837029	1.240088	0.29333	6.423051
1.6	19	0.844566	1.187589	0.27171	6.750205
1.6	20	0.844568	1.187579	0.27181	6.746178
1.7	1	0.294778	3.782225	0.333582	3.673696
1.7	2	0.295543	3.780354	0.300935	3.674769

Table F1 Continued

1.7	3	0.313321	3.735517	0.438003	3.625238
1.7	4	0.404543	3.464269	0.459634	2.977153
1.7	5	0.406048	3.459215	0.450379	3.170798
1.7	6	0.406049	3.459214	0.450571	3.170838
1.7	7	0.610786	2.596882	0.500838	4.273409
1.7	8	0.616471	2.567984	0.531516	3.909108
1.7	9	0.642383	2.432871	0.557834	3.856681
1.7	10	0.642499	2.432251	0.55889	3.874305
1.7	11	0.643019	2.429485	0.55413	3.727743
1.7	12	0.664918	2.31084	0.57651	4.149611
1.7	13	0.714627	2.026789	0.60074	8.486882
1.7	14	0.768202	1.697728	0.72673	5.098855
1.7	15	0.769427	1.689923	0.65877	4.638945
1.7	16	0.771462	1.676933	0.71562	5.488587
1.7	17	0.821430	1.347245	0.15812	6.572002
1.7	18	0.825610	1.318727	-0.0166	10.39976
1.7	19	0.826423	1.313169	0.01608	10.867553
1.7	20	0.830167	1.287476	0.14233	8.510365
1.8	1	0.188338	3.995225	0.215804	3.647832
1.8	2	0.328704	3.694609	0.184098	3.888375
1.8	3	0.421597	3.405912	0.391355	3.485699
1.8	4	0.553176	2.874637	0.517893	3.416552
1.8	5	0.658535	2.345832	0.580426	4.10142
1.8	6	0.659210	2.34215	0.566144	4.140312
1.8	7	0.745541	1.839813	0.690633	3.978612
1.8	8	0.746042	1.836717	0.696758	3.96739
1.8	9	0.753439	1.790773	0.728362	3.29201
1.8	10	0.755926	1.775226	0.70587	3.644004
1.8	11	0.757233	1.767035	0.74389	3.463451
1.8	12	0.758221	1.76083	0.75966	3.521689

Table F1 Continued

1.8	13	0.768435	1.696244	0.77268	4.213573
1.8	14	0.768752	1.694223	0.77785	3.609577
1.8	15	0.772246	1.671924	0.69698	8.492686
1.8	16	0.772260	1.671835	0.68767	8.702444
1.8	17	0.784258	1.594478	0.46249	15.079678
1.8	18	0.789603	1.559636	0.37475	28.734067
1.8	19	0.829219	1.293991	0.17148	13.05611
1.8	20	0.836650	1.242717	0.13389	15.690801
1.9	1	0.193229	3.987496	0.216165	3.645896
1.9	2	0.327629	3.697531	0.178657	3.917748
1.9	3	0.425070	3.393731	0.401891	3.462882
1.9	4	0.549438	2.89171	0.516223	3.404381
1.9	5	0.657816	2.349754	0.583471	4.016319
1.9	6	0.658737	2.344728	0.565113	4.056505
1.9	7	0.742446	1.858889	0.688913	4.023735
1.9	8	0.742637	1.857713	0.692597	4.017532
1.9	9	0.751919	1.800253	0.72995	3.309086
1.9	10	0.755318	1.779032	0.70038	3.787624
1.9	11	0.756498	1.771643	0.74199	3.585878
1.9	12	0.757640	1.764482	0.76041	3.652902
1.9	13	0.775005	1.654243	0.78292	4.990304
1.9	14	0.775005	1.654242	0.78311	4.970796
1.9	15	0.775709	1.649717	0.74218	7.315046
1.9	16	0.777723	1.636762	0.72803	9.178786
1.9	17	0.783234	1.601124	0.51034	15.357574
1.9	18	0.788521	1.566705	0.40305	33.424024
1.9	19	0.824532	1.326101	0.2395	11.523879
1.9	20	0.835722	1.249141	0.16965	17.224176
2.0	1	0.197457	3.980654	0.216437	3.644195
2.0	2	0.326668	3.700137	0.174354	3.94088

Table F1 Continued

2.0	3	0.428259	3.382458	0.410775	3.441355
2.0	4	0.545997	2.907325	0.515626	3.372395
2.0	5	0.656941	2.354519	0.5874	3.906952
2.0	6	0.658111	2.348147	0.564964	3.946591
2.0	7	0.739274	1.87836	0.687733	4.036837
2.0	8	0.753557	1.790037	0.713635	4.128283
2.0	9	0.758942	1.756301	0.692848	4.041943
2.0	10	0.759851	1.750581	0.67076	4.571312
2.0	11	0.768513	1.695747	0.66546	4.663459
2.0	12	0.768594	1.695232	0.65944	4.833385
2.0	13	0.769170	1.691562	0.69522	4.128475
2.0	14	0.769640	1.688569	0.75369	3.717277
2.0	15	0.803448	1.468271	0.77006	8.761943
2.0	16	0.823067	1.336095	0.60241	9.323572
2.0	17	0.823117	1.335756	0.59855	9.717422
2.0	18	0.848001	1.163511	0.28806	22.957803
2.0	19	0.853813	1.122541	0.25254	33.011151
2.0	20	0.856576	1.10296	0.24967	25.43816
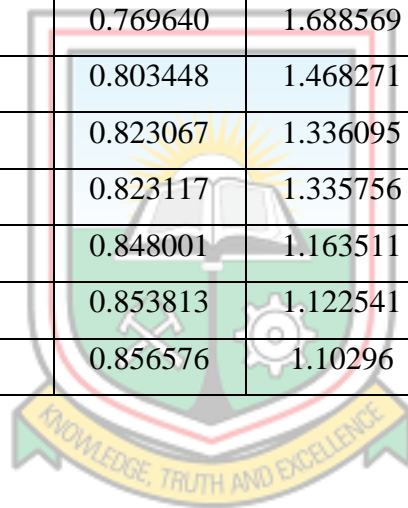
APPENDIX G

EXPERIMENTATION RESULTS OF THE WIDTH PARAMETER FOR DEVELOPMENT OF GRNN MODEL FOR AIR OVERPRESSURE PREDICTION

Table G1 Training and Testing R and MSE Results for GRNN Air Overpressure Prediction Model

Width Parameter	Training		Testing	
	R	MSE	R	MSE
0.10	0.961792	0.317504	0.48684	3.314226
0.11	0.955984	0.366098	0.50234	3.156089
0.12	0.950333	0.413955	0.51811	3.001924
0.13	0.944599	0.462861	0.53432	2.852437
0.14	0.938511	0.514602	0.55125	2.707097
0.15	0.931878	0.570173	0.56903	2.565811
0.16	0.924665	0.629414	0.58748	2.429729
0.17	0.916985	0.691228	0.6062	2.300922
0.18	0.909035	0.754089	0.62465	2.181511
0.19	0.901029	0.816513	0.64234	2.073003
0.20	0.893154	0.877316	0.65892	1.976088
0.21	0.885543	0.935719	0.67415	1.890775
0.22	0.878276	0.991332	0.68794	1.816608
0.23	0.871381	1.044085	0.70026	1.752847
0.24	0.864851	1.094137	0.71118	1.69861
0.25	0.858654	1.141774	0.72077	1.652958
0.26	0.852746	1.187328	0.72914	1.61497
0.27	0.847086	1.231112	0.73641	1.583795
0.28	0.841637	1.27339	0.74269	1.558686
0.29	0.836371	1.314374	0.74806	1.539006
0.30	0.831265	1.354231	0.7526	1.524222
0.31	0.826303	1.393096	0.75637	1.513884
0.32	0.821468	1.431085	0.75945	1.507594
0.33	0.816747	1.468303	0.76187	1.504989

Table G1 Continued

0.34	0.812126	1.504843	0.76371	1.505725
0.35	0.807592	1.540789	0.765	1.509467
0.36	0.803132	1.57621	0.76583	1.515894
0.37	0.798736	1.61116	0.76623	1.524697
0.38	0.794398	1.645679	0.76628	1.535591
0.39	0.790111	1.679789	0.76602	1.548311
0.40	0.785875	1.713503	0.7655	1.562622
0.41	0.781686	1.746821	0.76477	1.578315
0.42	0.777548	1.77974	0.76386	1.595206
0.43	0.77346	1.812251	0.76281	1.613138
0.44	0.769425	1.844346	0.76164	1.631973
0.45	0.765445	1.876017	0.76038	1.651594
0.46	0.761522	1.907254	0.75905	1.671899
0.47	0.757655	1.938054	0.75766	1.692801
0.48	0.753847	1.96841	0.75622	1.714222
0.49	0.750097	1.998319	0.75475	1.736094
0.50	0.746406	2.027779	0.75325	1.758358
0.51	0.742773	2.056789	0.75174	1.78096
0.52	0.739199	2.085346	0.75021	1.803852
0.53	0.735682	2.113451	0.74868	1.826988
0.54	0.732222	2.141105	0.74714	1.850327
0.55	0.72882	2.168309	0.74561	1.873833
0.56	0.725475	2.195065	0.74408	1.897469
0.57	0.722186	2.221376	0.74256	1.921203
0.58	0.718953	2.247245	0.74104	1.945003
0.59	0.715776	2.272679	0.73955	1.96884
0.60	0.712655	2.297683	0.73807	1.992686
0.61	0.709589	2.322263	0.7366	2.016517
0.62	0.706578	2.346429	0.73516	2.040306
0.63	0.703621	2.370188	0.73375	2.064032
0.64	0.700719	2.393551	0.73236	2.087672

Table G1 Continued

0.65	0.69787	2.416527	0.731	2.111206
0.66	0.695074	2.439127	0.72967	2.134616
0.67	0.692331	2.461361	0.72838	2.157883
0.68	0.689639	2.483242	0.72712	2.180992
0.69	0.686998	2.50478	0.72591	2.203927
0.70	0.684407	2.525987	0.72473	2.226674
0.71	0.681864	2.546873	0.7236	2.24922
0.72	0.679369	2.567451	0.72251	2.271554
0.73	0.676919	2.58773	0.72146	2.293664
0.74	0.674514	2.607721	0.72046	2.315541
0.75	0.672152	2.627434	0.71951	2.337176
0.76	0.669831	2.646878	0.71861	2.358561
0.77	0.667549	2.666062	0.71776	2.379689
0.78	0.665306	2.684994	0.71695	2.400554
0.79	0.663099	2.703681	0.7162	2.421149
0.80	0.660925	2.722131	0.71549	2.44147
0.81	0.658785	2.740351	0.71483	2.461512
0.82	0.656675	2.758344	0.71422	2.481271
0.83	0.654593	2.776118	0.71365	2.500744
0.84	0.65254	2.793675	0.71313	2.519928
0.85	0.650511	2.811021	0.71265	2.538821
0.86	0.648507	2.828158	0.71222	2.55742
0.87	0.646525	2.845089	0.71182	2.575725
0.88	0.644565	2.861818	0.71147	2.593733
0.89	0.642624	2.878345	0.71115	2.611444
0.90	0.640702	2.894673	0.71086	2.628858
0.91	0.638798	2.910803	0.71061	2.645974
0.92	0.636911	2.926736	0.71039	2.662793
0.93	0.635039	2.942473	0.7102	2.679315
0.94	0.633182	2.958014	0.71003	2.69554
0.95	0.63134	2.973361	0.70989	2.71147

Table G1 Continued

0.96	0.629512	2.988513	0.70978	2.727105
0.97	0.627698	3.00347	0.70968	2.742448
0.98	0.625897	3.018233	0.70961	2.7575
0.99	0.624109	3.032802	0.70955	2.772263
1.00	0.622333	3.047177	0.70951	2.786739

APPENDIX H

EXPERIMENTATION RESULTS OF THE NUMBER OF NEURONS FOR DEVELOPMENT OF WNN MODEL FOR AIR OVERPRESSURE PREDICTION

Table H1 Training and Testing R and MSE Results for WNN Air Overpressure Prediction Model

Number of wavelons	Training		Testing	
	R	MSE	R	MSE
1	0.662424	2.393671	0.416895	3.349886
2	0.829222	1.304473	0.655149	2.220467
3	0.865855	1.037036	0.126214	44.277157
4	0.840528	1.216792	0.245651	38.882232
5	0.855197	1.113297	0.600602	2.555487
6	0.885915	0.89121	0.613846	2.490908
7	0.895546	0.820739	0.503404	3.442285
8	0.904324	0.755851	0.212029	13.601103
9	0.911602	0.703535	0.588081	2.895814
10	0.920941	0.629497	0.527007	2.994557
11	0.897545	0.809023	0.533309	2.785099
12	0.925107	0.598168	0.458044	4.778487
13	0.941914	0.474367	0.49239	3.89988
14	0.920611	0.632634	0.424708	7.285348
15	0.918916	0.647115	0.532564	3.228061
16	0.923326	0.611634	0.583772	2.715249
17	0.929370	0.569123	0.349354	5.234822
18	0.951174	0.394928	0.168478	10.674106
19	0.935638	0.518238	0.084647	14.193746
20	0.929775	0.563313	0.551053	5.171826

EXPERIMENTATION RESULTS OF THE NUMBER OF NEURONS FOR DEVELOPMENT OF ELM MODEL FOR AIR OVERPRESSURE PREDICTION

Table I1 Training and Testing R and MSE Results for ELM Air Overpressure Prediction Model

Number of Neurons	Training		Testing	
	R	MSE	R	MSE
1	-0.308042	1280.59283	-0.381013	1830.083913
2	0.285687	49.762514	0.469775	50.910363
3	0.269833	8.335737	-0.156645	12.188697
4	0.144991	9.386551	-0.233652	11.926608
5	-0.430779	234.267516	-0.476217	277.584165
6	0.440006	4.088657	0.533459	4.23514
7	0.649211	2.399635	0.304497	6.22982
8	0.672977	2.274472	0.397278	5.964566
9	0.689639	2.183468	0.225106	10.835281
10	0.756416	1.773126	0.271383	11.013166
11	0.686103	2.199696	0.46459	4.675781
12	0.655315	2.372119	0.589382	2.992013
13	0.739202	1.879033	0.605862	3.864762
14	0.772167	1.67288	0.132864	28.584665
15	0.728739	1.945187	0.495288	6.249487
16	0.747264	1.830395	0.4222	4.699861
17	0.767746	1.700628	0.374074	13.267117
18	0.782129	1.608317	0.682514	2.594184
19	0.786761	1.578526	0.380538	32.38551
20	0.798097	1.503774	-0.05641	186.507465
21	0.792719	1.539549	0.209277	243.809467
22	0.783539	1.599295	0.325998	50.335294
23	0.810577	1.42094	0.303136	13.743804
24	0.840147	1.218435	0.155257	1222.242569

Table I1 Continued

25	0.809454	1.42817	0.167893	32.308697
26	0.816537	1.380454	0.019404	147.725434
27	0.841311	1.210335	-0.080776	345.888
28	0.846939	1.170981	0.192223	253.928187
29	0.847936	1.163963	-0.083973	847.274617
30	0.84553	1.180844	0.195546	123.944314
31	0.870427	1.003877	0.299927	12.086098
32	0.847935	1.163973	-0.117216	2073.549334
33	0.858011	1.092777	0.3904	8.591206
34	0.862569	1.060286	0.142293	5594.504399
35	0.874575	0.973898	0.226044	111.748952
36	0.871058	0.999331	0.127562	25187.40149
37	0.876392	0.960718	0.138423	8432.889395
38	0.874622	0.973556	0.139481	2221.804237
39	0.899578	0.790156	0.115582	84851.47808
40	0.879552	0.937735	0.13288	9027.058671
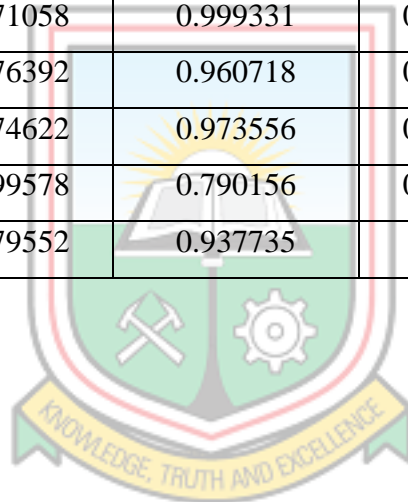
PREDICTED AIR OVERPRESSURE VALUES ON THE TESTING DATA SETS BY THE VARIOUS PREDICTION TECHNIQUES

Table J1 Observed and Predicted AOp for the Various Models

Observed Aop (dB)	Predicted AOp (dB)											General Predicted	Newmont Model
	BPNN	GRNN	RBFNN	GMDH	WNN	SVM	LS-SVM	RVM	ELM	GPR	MARS		
104.2	103.9	104.6	104.6	103.7	103.9	104.1	104.0	104.0	104.0	104.0	104.5	104.5	102.2
101.9	102.0	101.5	101.5	101.3	98.8	102.3	99.4	102.3	101.2	102.3	102.6	103.2	98.9
102.8	103.4	103.6	103.7	103.0	102.6	103.7	102.5	103.5	103.1	103.6	104.0	104.2	101.3
105.5	104.9	104.3	104.5	104.3	104.3	104.3	103.8	104.7	103.7	104.1	104.2	104.4	102.0
103.5	104.2	103.9	103.6	104.8	104.8	103.6	105.3	103.9	105.2	104.8	103.7	103.3	99.2
101.9	103.0	102.9	103.5	102.4	101.8	103.2	101.9	103.2	102.7	103.6	103.6	104.0	100.9
103.5	105.4	104.6	104.9	106.0	106.3	106.3	104.8	105.3	108.0	104.1	106.2	104.1	101.3
102.8	103.6	104.3	104.4	103.5	103.3	103.9	103.1	103.8	103.5	103.8	104.2	104.5	102.1
104.9	104.8	103.7	106.7	108.8	105.9	105.3	104.8	105.2	105.1	106.5	103.5	106.8	107.7
105.5	105.2	104.9	104.9	104.5	104.2	104.7	103.3	105.1	103.7	104.5	104.5	104.8	102.9
101.9	104.6	103.5	104.1	104.3	104.4	104.0	104.7	104.4	104.1	103.4	104.0	104.0	100.9
101.9	102.6	102.3	102.2	101.9	100.9	102.9	101.1	102.8	101.9	102.2	103.2	103.5	99.6

Table J1 Continued

103.5	104.1	102.6	103.1	104.2	104.2	103.5	104.0	104.0	104.0	102.4	103.5	103.6	100.1
102.8	104.6	103.8	104.2	104.2	104.4	104.0	103.9	104.5	103.5	103.9	103.9	104.2	101.5
104.2	104.3	102.7	103.3	104.2	104.1	103.6	103.9	104.1	103.8	102.8	103.5	103.8	100.5
108.8	106.4	105.9	107.4	107.5	106.3	107.1	104.8	106.5	110.0	106.4	106.2	107.3	109.0
101.9	103.1	103.1	103.3	102.4	102.7	103.3	103.0	103.2	102.8	103.0	103.8	103.8	100.6
103.5	105.7	105.3	106.6	107.1	106.2	106.3	104.8	105.8	105.5	104.8	105.4	106.3	106.5
104.2	104.8	104.6	105.0	104.9	104.0	105.2	103.5	104.7	104.1	103.5	105.7	104.6	102.5
108	105.2	105.9	106.7	105.9	106.0	105.5	106.5	105.2	106.7	106.0	105.6	105.8	105.2
106	106.5	105.3	106.9	106.1	105.4	106.6	105.3	106.4	105.3	105.5	106.1	105.3	104.1
103.5	104.8	103.3	103.1	104.3	104.3	104.6	104.8	104.7	105.0	104.0	104.1	103.8	100.5
106	107.0	105.7	107.2	107.2	106.1	108.1	105.5	107.8	106.7	106.1	106.2	107.1	108.5
107	105.2	106.0	106.6	105.7	106.0	105.5	106.7	105.1	107.1	106.2	105.8	105.6	104.9
106	105.9	105.7	106.1	105.2	105.1	105.6	105.1	105.9	104.8	105.6	105.4	105.5	104.5
105.5	106.8	105.4	107.0	106.7	106.1	107.5	105.1	107.3	107.7	105.8	105.9	106.9	107.9
108	106.3	105.8	106.5	105.6	105.4	106.2	106.2	106.3	105.5	105.9	105.7	105.8	105.3
105.5	106.6	105.7	107.1	106.3	106.0	106.8	105.5	106.9	106.6	105.8	105.5	106.7	107.4
104.2	104.6	105.7	105.9	104.8	105.6	104.9	106.4	104.6	106.1	105.5	105.3	105.1	103.6
106	106.3	106.0	106.8	105.6	105.6	106.3	106.7	106.3	105.7	106.2	106.1	105.7	105.1
106	106.8	105.7	107.3	106.8	106.1	107.5	106.0	107.4	107.4	106.5	106.1	107.1	108.4

Table J1 Continued

103.5	102.9	104.5	104.8	104.0	103.5	103.2	104.3	103.4	102.6	104.6	103.1	104.7	102.7
106	106.1	105.9	107.5	107.4	106.4	106.7	104.9	106.2	108.6	106.3	105.8	107.2	108.5
101.9	103.1	101.7	102.5	104.6	105.3	102.5	105.0	103.1	104.1	103.1	102.5	103.0	98.6
103.5	102.9	104.3	104.6	103.5	104.2	103.2	104.0	103.4	102.6	104.5	103.2	104.6	102.5
105.5	104.1	105.0	105.1	104.0	104.6	104.3	104.8	104.1	104.6	104.5	104.7	104.7	102.7
105.5	104.9	104.1	104.3	104.3	104.0	104.3	103.5	104.7	103.7	103.8	104.1	104.4	101.9
104.2	102.5	103.3	104.0	102.8	103.7	102.7	103.7	103.0	101.9	104.5	102.7	104.3	101.6
105.5	104.6	105.6	105.9	105.0	105.5	104.8	106.2	104.6	105.7	105.5	105.2	105.2	103.9
104.2	104.7	103.7	103.9	104.2	103.9	104.1	103.4	104.5	103.6	103.6	104.0	104.2	101.5
101.9	104.5	103.9	104.1	104.2	103.9	103.9	103.6	104.4	102.9	104.3	103.6	104.4	101.9
104.2	104.5	103.4	103.7	104.1	103.8	103.9	103.2	104.4	103.4	103.5	103.7	104.2	101.3
104.9	105.4	105.2	105.3	104.9	104.3	105.0	103.4	105.3	103.8	104.5	104.6	105.2	103.8
107	106.6	105.8	107.0	106.2	105.7	106.9	105.6	106.7	105.6	105.7	106.2	105.7	105.1
104.9	104.8	104.0	104.6	104.8	104.7	104.2	105.7	104.4	105.2	105.0	104.2	103.7	100.1
103.5	103.5	103.9	103.6	102.9	104.4	103.7	105.3	103.5	103.5	104.2	104.3	103.8	100.4
108.4	106.5	106.0	107.2	107.6	106.2	107.4	104.9	106.7	111.1	106.2	106.2	107.4	109.1
105.5	104.6	103.6	103.7	104.2	103.6	104.0	103.1	104.5	103.5	103.5	103.9	104.2	101.4
108.8	107.0	105.8	107.3	107.1	106.1	107.9	105.7	107.6	106.6	106.1	106.2	106.9	108.0
107.5	106.7	105.6	106.7	106.3	105.6	107.1	105.4	106.8	105.4	105.7	106.2	105.7	105.2

Table J1 Continued

104.2	104.5	105.3	105.5	104.8	104.7	104.8	104.9	104.5	104.5	104.6	105.1	105.0	103.5
106.5	104.7	103.9	103.9	104.7	104.2	104.2	105.2	104.3	105.0	104.6	104.2	103.6	99.9
102.8	104.3	105.0	105.1	104.5	104.4	104.6	104.5	104.4	104.3	104.1	105.0	104.8	102.9
103.5	104.5	104.9	105.0	104.5	104.3	104.8	104.3	104.4	104.4	104.2	105.2	104.7	102.7
102.8	103.4	103.6	103.2	102.8	103.7	103.8	103.8	103.5	103.1	103.3	104.2	103.7	100.3
107	106.1	105.4	105.8	105.3	104.8	106.0	105.9	106.0	105.0	105.0	106.0	105.1	103.6
104.2	104.0	104.7	104.8	104.0	104.1	104.3	104.3	104.1	104.1	104.1	104.7	104.6	102.5
103.5	103.9	104.6	104.6	103.8	103.9	104.2	103.9	104.0	103.9	103.9	104.5	104.5	102.3
106.5	105.7	104.9	105.7	105.1	104.5	105.3	105.5	105.4	105.0	105.0	105.2	104.5	102.1
104.9	105.1	104.3	104.4	104.4	103.9	104.6	104.1	104.9	104.1	103.9	104.5	104.4	101.9
102.8	105.2	104.5	104.6	104.5	104.0	104.7	104.1	105.0	104.1	104.0	104.6	104.5	102.1
103.5	105.2	104.2	104.4	104.6	103.9	104.7	104.9	104.9	104.5	103.4	104.7	104.2	101.4
106.5	107.4	106.8	107.1	95.5	103.8	108.8	104.7	109.6	113.2	104.1	106.1	105.2	103.8
105.5	105.2	104.5	104.8	104.6	104.2	104.7	105.2	104.9	104.5	104.0	104.7	104.3	101.6
106	106.2	105.7	107.1	107.3	106.1	107.0	104.6	106.3	106.5	106.4	106.2	106.8	107.6
104.2	106.2	105.5	106.8	107.3	106.1	107.1	104.8	106.3	105.4	106.1	106.2	106.6	107.3
105.5	103.8	104.3	104.3	103.7	103.4	104.1	103.3	103.9	103.6	103.7	104.5	104.4	102.0
104.2	103.4	103.9	104.1	103.2	102.7	103.6	102.5	103.6	103.0	103.8	103.9	104.4	101.8
104.2	103.9	104.7	104.7	103.8	104.0	104.1	104.0	104.0	104.0	104.0	104.5	104.6	102.4

Table J1 Continued

106	105.3	104.8	105.1	104.7	104.4	104.8	105.4	105.0	104.7	104.4	104.9	104.4	101.8
102.8	104.4	103.9	104.7	104.1	103.9	104.6	105.0	104.1	104.4	105.3	104.8	104.1	101.1
101.9	101.8	101.6	101.6	101.1	100.0	101.9	100.3	102.0	100.5	103.2	102.3	103.0	98.4
100	101.7	100.7	102.0	100.9	96.9	101.7	100.0	101.9	100.0	102.3	102.1	103.2	98.9

INDEX

232

233

238

241

252

254

257